CRWR Online Report 05–05

Drifter Modeling and Error Assessment in Wind Driven Currents

by

Jordan E. Furnans, B.S.E., M.S.E.
Graduate Research Assistant

Ben R. Hodges, Ph.D.
Co-Principal Investigator

and

Jörg Imberger, Ph.D.
Co-Principal Investigator

The University of Texas at Austin
December 15, 2005

This document is available online via World Wide Web at
http://www.crwr.utexas.edu/online.html

Drifter Modeling and Error Assessment in Wind Driven Currents

Abstract

As hydrodynamic models are used to predict the transport of contaminants, it follows that model validation should involve assessments of the model's ability to predict observed Lagrangian transport pathways. Existing validation methods, however, often only involve comparisons of Eulerian field and model data, from which Lagrangian transport pathways are not always discernible. This research explores the use of drifters and particle tracking in assessing a hydrodynamic model's ability to predict Lagrangian transport. The significant advances resulting from this research are the development of the Generalized Acceleration-Based Inertia and Forcing (GABI-F) model for predicting drifter transport, and the development of the Circle Assessment method for comparing sets of drifter paths. The advantages of the these advances were demonstrated while assessing the ability of the Estuary and Lake Computer Model (ELCOM) to reproduce drifter paths observed in Marmion Marine Park, Western Australia. The analyses indicated the ELCOM model was successful at reproducing the larger-scale features of the observed drifter movement to the degree that predicting movement was computationally achievable given the input data available. Through the Circle Assessment analyses of GABI-F drifter results, possible ELCOM model deficiencies were also identified.

The GABI-F drifter model predicts drifter movement by determining the forces acting on the drifter by the surrounding fluids. The model incorporates the influence of winds and inertia on drifter motion. Existing drifter models assumed drifters moved in perfect accord with the surrounding currents or with velocities offset from the current velocities by some small fraction of the wind velocity. Such simplistic models are adequate for predicting larger-scale characteristics of waterbody circulation, but are too imprecise to accurately reproduce drifter paths over the shorter time and length scales.

The Circle Assessment method for analyzing drifter data quantifies the model's ability to reproduce the field drifter motion over both short and long time and length scales. The method also provides diagnostic information regarding model performance, which may suggest avenues for model improvement by changing the hydrodynamic model algorithms or setup. Existing assessment methods are only applicable over larger time and length scales, are qualitative, and do not provide diagnostic information regarding model behavior.

TABLE OF CONTENTS

1. Introduction

1.1. Motivation

The fate and transport of nutrients and pollutants entering inland and coastal waters is closely linked to water circulation patterns, which are predictable with hydrodynamic models (Aldridge et al, 2003; Siddorn et al, 2003; Marti and Imberger, 2004; Hughes et al, 2004). In the past decade, there has been increasing emphasis on developing Total Maximum Daily Load (TMDL) standards for nutrients and pollutants in waterways listed as out of compliance with section 303(d) of the U.S. Clean Water Act (Bergeson, 2001; Borsuk et al, 2004;). There have been a few high profile TMDL studies with extensive hydrodynamic modeling of water circulation (e.g., Neuse River Estuary – See Bowen, 2003; Borsuk et al, 2003; Wool et al, 2003, Stow et al, 2003), while many more TMDL's have used relatively simplistic approaches (e.g., Pickett, 1997; Havens and Walker, 2002; Mankin et al, 2003). The use of simple models has relatively little consequence when the costs of cleanup are low and easily partitioned between stakeholders in the watershed. However, as cleanup costs rise, stakeholders are increasingly likely to turn to litigation to try to limit their financial exposure (e.g., the CERCLA litigation between US EPA and G.E. regarding Hudson River PCB contamination – US EPA #1).

As the required modeling complexity increases with the complexity of the system (and arguably with the potential liability of the stakeholders), there is a greater need to have accepted means of testing and validating the skill with which hydrodynamic models predict transport. In particular, surface water hydrodynamic models predict the time-varying Eulerian velocity field, but the transport of contaminants is inherently a Lagrangian path integral through the velocity field. Traditional hydrodynamic measures of model skill, namely agreement with tidal height (Umgiesser and Zampato, 2001), single-point velocity (Hillmer and Imberger, 2005; Roulund et al, 2005), temperature (Caissie et al, 2005) and/or salinity fields (Holt et al, 2005) cannot conclusively demonstrate that a model's Eulerian field will correctly reproduce the Lagrangian transport. It follows that when circulation model results are used to apportion cleanup costs, the parties can become mired in a courtroom battle of expert witnesses over the model validity.

To further expound on the above idea, Figure 1.1 illustrates how surface water hydrodynamic models represent velocities and fluid properties on a fixed mesh, and their relationship to the Lagrangian particle path. Clearly, the visual differences between Figure 1.1A and 1.1B are minor, and a model that captures the velocity field within ±5% would generally be hailed as excellent. And yet, from Figure 1.1C it is clear that the path integral of a particle through the two fields is substantially different. The error bias introduced in Figure 1.1B is integrated through the Lagrangian path, and leads to large separations in predicted particle positions

While visualization and analysis of such Eulerian velocity fields may lead to insight into the fluid dynamics of a system (e.g., Jiang et al, 2001; Pan et al, 2002;), the transport of particle contaminants is more difficult to directly assess (Zhenquan, 2002) as each particle follows a path in space-time through the temporally-varying flow field (i.e., a Lagrangian view). This issue has been addressed through development of

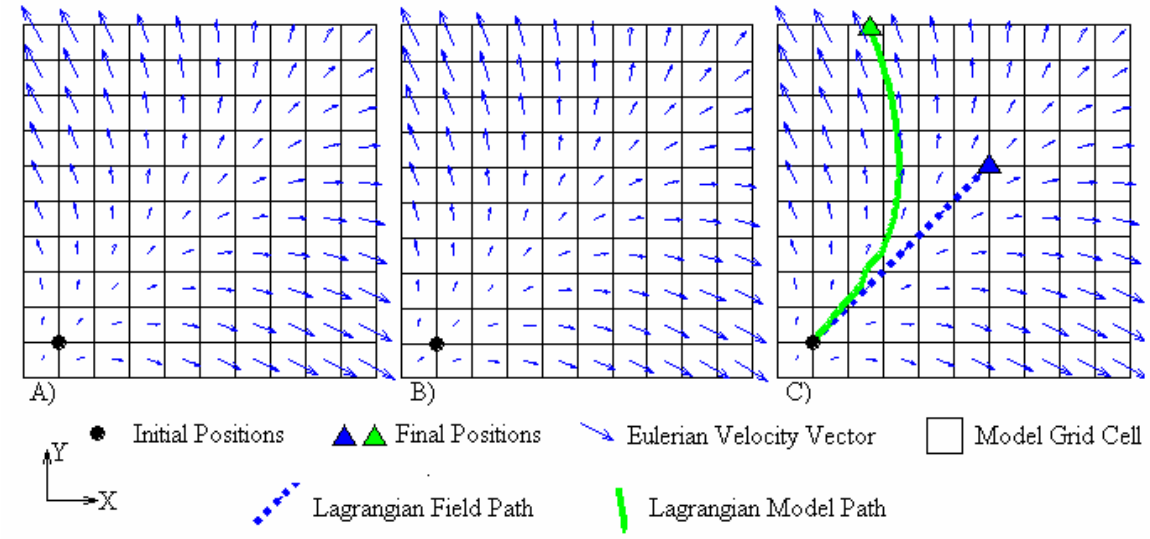

Figure 1.1 – Sample error integration in particle tracking – A) Temporally constant "field" Eulerian velocity vectors indicating a divergent flow, B) Modeled representation of flow in A), with velocities equal to 95% and 105% of the field velocities in the X,Y component directions, respectively, C) Lagrangian paths resulting from the field and model Eulerian velocities. Small errors in the modeled velocity field produce large separations in Lagrangian paths over time.

Lagrangian particle tracking, defined as the determination of transport paths of objects immersed within the flow field (Yeung and Pope, 1988). Lagrangian particle tracks, computed from the modeled Eulerian velocity field, have been used to infer patterns of scalar transport (Simpson and Gobat, 1994; Carey and Shen, 1995; Fuentes and Marinone, 1999; Tambasco and Steinman, 2002; Chen et al, 2003). However, as shown in Figure 1.1, a simply-modeled Lagrangian path will integrate model error forward in time, and will always diverge from a real particle track over a sufficiently long time in a sufficiently complex flow field. Indeed, it can be argued that relatively minor errors in a relatively good Eulerian velocity field may accumulate into significant errors in the Lagrangian track, making it difficult to claim a model is skillful. As a perfect model of hydrodynamic circulation is likely to remain out of reach for the foreseeable future, modeling efforts will continue to have some uncertainty in their predictive skill for particle contaminant transport.

The present state-of-science in validating numerical models has focused principally on validation with Eulerian data (e.g., Johnson et al, 1993; Umgiesser and Zampato, 2001), arguably because scientists think and work most readily in an Eulerian frame of reference. Lagrangian field drifters, which attempt to follow Lagrangian particle paths in a real fluid flow, have been extensively employed to provide insight into ocean circulation (Freeland et al., 1975; Colin de Verdiere, 1983; Krauss and Bfoning, 1987; Poulain and Niiler, 1989; Paduan and Niiler, 1993; Sanderson, 1995; Poulain et al, 1996; Richez, 1998;), but have principally been linked with models to qualitatively show general agreement (see § 2.4) rather than quantitatively demonstrating model skill. The emphasis on Eulerian validation leaves supporters of model results (e.g. regulatory authorities) arguing by hand-waving that a good representation of the Eulerian field implies a good representation of contaminated particle transport. As illustrated in Figure 1.1, this contention can be readily countered by visual presentations that are readily understood by non-

experts. In a courtroom setting, such intuitive arguments may be more compelling than more complicated analyses understood principally by experts. Arguably, to support modeling conclusions in an adversarial setting requires two significant advances: 1) new quantitative methods for evaluating model skill based on predicted Lagrangian paths (i.e., error measures with direct relevance to contaminant transport) that are recognized as state-of-science techniques, and 2) new methods for assessing the end-of-simulation uncertainty in predicted contaminant transport using the quantified model skill. The first of these issues can be rewritten as the underlying research question for this work:

> *Can particle tracking be used to improve model validation?*

The answer, as developed and demonstrated herein for surface drifters in a coastal ocean environment, is affirmative. The second issue, quantitatively assessing model uncertainty, remains an outstanding research question that can be addressed by building on the newly-developed quantitative validation methods.

1.2. Background

Validation of hydrodynamic models for lakes, estuaries and coastal oceans involves assessing the model results in comparison to field data (Johnson et al, 1993). Traditional model validation requires sensitive equipment to record time-histories of temperature, pressure, atmospheric forcing parameters, salinity, and water velocity (Johnson et al, 1993). These Eulerian point measurements are generally compared to the Eulerian model results to assess model validity. Financial constraints usually limit the practical number of field sampling stations, while issues such as high levels of ship traffic, established fisheries, or private property rights may further restrict station placement. Therefore, traditional model validation typically depends upon limited point measurements, which may not capture the large-scale circulation patterns or property variations.

Whereas traditional model validation involves point measurements, displays of circulation patterns, transport pathways, and mixing properties of fluid flow have typically been created through particle tracking (Yvergniaux and Chollet, 1989; Simpson and Gobat, 1994; Carey and Shen, 1995; Fuentes and Marinone, 1999; Garraffo et al, 2001; Tambasco and Steinman, 2002; Thorpe et al, 2004). A non-traditional, alternative approach to model validation is applying particle tracking within hydrodynamic models to assess how the model captures the observed properties of a fluid flow (Toner et al, 2001; Thompson et al, 2003; Thorpe et al 2004). As field drifter motion is indicative of the circulation in an ocean, lake or estuary, it stands to reason that agreement between observed drifter paths and those modeled through particle tracking implies the model correctly reproduces the circulation (Bennett and Clites, 1987; Yeung and Pope, 1988, Toner et al, 2001; Thompson et al, 2003).

When compared to field drifter data, particle tracking results may be considered to indicate model validity all along the drifter tracks, therefore covering a larger area than practical with Eulerian measurements. To contrast the two approaches toward model validation, particle tracking provides data for numerous locations at single points in time, whereas Eulerian methods provide numerous time data at single points in space. The debate as to which approach is "better" should hinge on the model's purpose. For contaminant transport predictions, particle tracking is arguably a more appropriate validation approach, whereas predictions of tidal height or scour velocity around a bridge abutment should be validated with Eulerian methods. Since Eulerian validation methods are common and well understood (Johnson et al, 1993; Umgiesser and Zampato, 2001; Hillmer and Imberger, 2005; Roulund et al, 2005; Caissie et al, 2005; Holt et al, 2005), they will not be further discussed in this research. Validation methods using particle tracking and field drifter data are less common in the literature, and are essentially qualitative (Toner et al, 2001; Thompson et al, 2003; Thorpe et al 2004). This dissertation presents the next steps toward the use of particle tracking for model validation purposes,

including the development of quantitative methods for assessing agreement between the field and modeled drifter paths.

Harcourt et al (2000) outlined the basic elements leading to separations between field and model drifter positions. Elements particularly relevant to the present work are 1) the numerical method for flow field determination, 2) the numerical method for drifter transport, 3) the model of the drifter physical response and 4) the uncertainty in the field data. As the purpose of model validation is to determine the adequacy of the model numerical methods, this research concentrates on: 1) the development of numerical methods for drifter transport in sections 2.2-2.3; 2) modeling drifter physical response in section 2.4; and 3) the inclusion of field data uncertainty in the validation methodology in sections 2.6-2.8.

Existing particle tracking methods treat drifters as mass-less water particles that passively advect with the surrounding flows (Yeung and Pope, 1989; Garrafo et al, 2001; Zhurbas and Oh, 2003); i.e., such model drifters are generally considered perfect Lagrangian particles. As a consequence, these methods ignore the drifter's mass, shape, and inertia when determining particle movement. Existing methods may therefore be limited in their ability to accurately reproduce observed drifter motion even if the calculated Eulerian velocity field were perfectly correct. For use in model validation and per Harcourt et al (2000)'s recommendations listed above, such simple particle tracking methods need to be tailored into "drifter models" that incorporate the physical features of the field drifters in the determination of the modeled drifter movement. Addressing this issue requires the development of a new drifter model because existing Lagrangian drifter models are limited in their representation of the physical forces contributing to field drifter movement. Thus, the development of the new drifter model is the first obstacle to overcome before particle tracking may be used for model validation.

A second obstacle to be overcome before using particle tracking for model validation involves improving the methods for comparing modeled and observed drifter paths. Existing methods are either visually based (Carey and Shen, 1995; Toner et al, 2001; Thorpe et al, 2004) or involve statistical analyses based on the displacement of and separation between modeled and observed drifters (Toner et al, 2001; Thompson et al, 2003). These methods qualitatively indicate model agreement over the duration of the drifter deployment, and are not used to assess the model's skill at reproducing the observed drifter velocities at multiple times during the simulation. They also typically involve comparisons of drifter paths over long time horizons (relative to model timestep) without regard to divergence between the modeled and observed flows. While these methods were effective for the purposes intended by their developers, they may not be extended for validating an hydrodynamic model. A better, more quantitative analysis methodology needs to be defined.

1.3. Objectives

This research has two principle objectives:

1. Incorporating physical forcing and inertia into particle tracking algorithms for comparison to field drifters.

2. Ddeveloping a methodology for quantify-ing a model's ability to reproduce field drifter paths with particle tracking.

These objectives address the two fundamental issues raised in section 1.2 that have previously limited the usefulness of field drifters for validating Eulerian hydrodynamic models. The secondary objectives of this research are to determine under what modeling conditions the hydrodynamic model and particle tracking may be considered skillful current-predictors, and to use particle tracking to describe the surface circulation patterns of within a subject waterbody.

1.4. Approach

This dissertation presents: 1) derivation of the "Generalized Acceleration-Based Inertia and Forcing

(GABI-F)" drifter modeling technique (section 2.4) for incorporating dynamic forces on drifter motion, 2) development of the Circle Assessment method (sections 2.6-2.8) for validating hydrodynamic models using drifter data, and 3) hydrodynamic modeling of field drifter experiments of near-shore currents in Marmion Marine Park (MMP), Western Australia, with the new innovations applied for model validation. For the hydrodynamic modeling, the Estuary and Lake Computer Model (ELCOM) was used (§3.3), as this model has been previously applied in predicting the MMP circulation patterns.

As shown in Chapter 4, modeled drifter velocities using the GABI-F drifter method are more comparable to the field drifter velocities than are velocities derived through applications of the existing Lagrangian and leeway drifter modeling techniques. The Circle Assessment method is also shown to improve upon the other assessment methods for use in model validation (Section 4.2). Using the GABI-F and Circle Assessment techniques, Marmion Marine Park model results under different setup conditions (winds, pressure gradients, grid resolution, and model timestep) were assessed to identify the model sensitivity to these parameters (Section 4.3). Model results were most sensitive to variability in the model timestep and in the wind forcing, and were relatively insensitive to model grid resolution and water surface slope. Based on the numerical approach in ELCOM, the larger influence of the model timestep and wind forcing on drifter paths suggests that the results were most sensitive to the prediction of the of the surface mixed layer depth, which directly influences the wind-driven surface layer current velocities.

This dissertation is organized as follows: Chapter 2 presents Lagrangian and GABI-F particle-tracking algorithm development, along with the new Circle Assessment method for model validation. Chapter 3 describes field drifter experiment conducted in the Marmion Marine Park and application of ELCOM for hydrodynamic modeling. Chapter 4 provides comparisons of field drifter data with modeled drifter data, demonstrating the value of the new GABI-F modeling technique and the Circle Assessment method. Conclusions derived from this work are presented in Chapter 5, along with recommendations for future projects relating to particle tracking and model validation.

1.5. Summary

The main goal of the presented research was to determine to what extent particle tracking may be used in conjunction with field drifter data for the purposes of hydrodynamic model validation. Traditional methods of model validation involve comparing Eulerian point measures (i.e., field samples) to output from the hydrodynamic model. While such methods are suitable for validating model-calculated Eulerian properties of the waterbody (e.g., water surface heights, temperatures, etc.), the methods may not be optimal for assessing the model calculated velocity fields or the contaminant transport pathways they imply. Particle tracking is uniquely suited for assessing modeled transport pathway as both involve assessing Eulerian data from a Lagrangian frame of reference.

As part of the effort to achieve the main goal stated above, two specific objectives for this dissertation research were defined:

#1. incorporate physical forcing and inertia into particle tracking algorithms for comparison to field drifters, and

#2. develop a methodology for quantifying a model's ability to reproduce field drifter paths with particle tracking.

Objective #1 addressed the inconsistency in particle tracking methods (which are designed to transport mass-less water particles) and their application to physical surface drifters. The resulting GABI-F drifter model is an improved particle-tracking technique which incorporates physical properties of the drifter and surrounding fluids in calculating drifter motion.

Objective #2 was necessitated due to the lack of suitable methodologies for meaningfully quantifying agreement between modeled and observed drifter paths

over short temporal and spatial scales. The developed methodology, namely the Circle Assessment method, relates separation between the field and modeled drifters to length and time scales relevant to the particular model simulation. Each of these innovations were tested by comparing model results with field drifter data from Marmion Marine Park, Western Australia as measured in March of 2003. Model results demonstrate the improvement in drifter modeling using the GABI-F technique as quantified through the Circle Assessment method.

1.6. Funding Acknowledgements

This work was conducted with generous financial support from the Centre for Water Research at the University of Western Australia, the Perth Water Corporation, the Australian-American Fulbright Association, the Texas Water Resources Institute, and The University of Texas at Austin.

2. Particle Tracking Methodology

2.1. Introduction

This chapter outlines methodologies for tracking particle movement through a waterbody, as well as techniques for validating a model's ability to reproduce observed particle trajectories. Existing particle-tracking and assessment methods are presented and compared to the new tracking and assessment methodologies developed herein. The new "Generalized Acceleration-Based Inertia and Forcing (GABI-F)" method advances prior Lagrangian particle tracking methods by incorporating the particle physical properties (size, mass, shape) along with the force balance that affects motion. The new Circle Assessment method improves upon existing assessment methods by 1) reducing the temporal integration of tracking error, and 2) quantifying model skill. Section 2.2 presents the theory behind Lagrangian particle tracking, with the associated use of empirical leeway factors described in section 2.3. Section 2.4 provides a derivation of the new GABI-F particle tracking method. Section 2.5 describes existing assessment methods for comparing observed and modeled particle paths. The new circle assessment methodology is developed in Section 2.6. This methodology, although specifically developed for the drifters used in the Marmion Marine Park experiment, is sufficiently general for application to any surface drifter.

2.2. Lagrangian Particle Tracking Theory

In this section, the methodology for Lagrangian particle tracking in Eulerian numerical models is described. Particle tracking is operationally defined as following the trajectory of a mass-less particle that passively advects with the flow field over time. A perfect Lagrangian particle will move identically to the surrounding water, with its position vector, $\vec{x}$, at time t, given as:

$$\vec{x}(t) = \vec{x}(t_0) + \int_{t_0}^{t} \vec{u}\, dt \tag{2.1}$$

where t_0 is the initial time for a known particle position, and $\vec{u}$ is the velocity vector of the water at the particle position. An exact solution of (2.1) requires a velocity field that is both spatially and temporally continuous. However, Eulerian hydrodynamic models provide velocities at discrete time intervals and locations, which will only serendipitously coincide with the Lagrangian particle position in a complex flow field. Therefore, a numerical particle tracking model coupled to an Eulerian hydrodynamic model must use a discrete form of eq. (2.1):

$$\vec{x}^{n+1} = \vec{x}^{n} + \vec{u}^{n+1/2}\Delta t \tag{2.2}$$

where Δt is the time interval from time step n to n+1; $\vec{x}^{n}$ and $\vec{x}^{n+1}$ are the particle positions at time step n and n+1, respectively; and $\vec{u}^{n+1/2}$ is a representative velocity for the particle over the discrete time step. For this discussion, the "representative velocity" is defined as the constant particle velocity over time interval Δt that results in the identical particle displacement to the continuously-varying velocity field (Figure 2.1). Using the common analogy of the drunken shuffle, the representative velocity is the velocity of the sober person who moves in a straight line between two points. In contrast, a drunk traveling between the same two points will follow a meandering path, similar to that of a particle moving within the continuously-varying velocity field.

The accuracy of the modeled representative velocity is a function of both the numerical model's ability to represent the physical system and the order of the spatial and temporal interpolation techniques used estimate the particle's movement (Bennett and Clites, 1987; Yeung and Pope, 1989; Ramsden and Holloway, 1991, Harcourt et al, 2000). Most existing particle tracking schemes use 1st-order accurate bilinear spatial interpolation with either 2nd or 4th order Runga-Kutta temporal interpolation (e.g., Bennett and Clites, 1987; Fuentes and Marinone, 1999; Garraffo et al, 2001; Chen et al, 2003). Another common (and simpler) approach is to neglect local spatial variability and model particle motion using the water velocity of the particle's grid cell without interpolation (i.e., a nearest neighbor scheme: Simpson and Gobat, 1994; Harcout et al, 2000; Thorpe et al, 2004;). The low-order spatial interpolations in these prior particle tracking schemes were not detrimental to the overall results because the underlying modeled velocity fields only represented the large-scale smooth velocity field, which was consistent with their research focus on large-scale motions. In contrast, when using particle tracking to calculate turbulent statistics in a finely-resolved DNS model, Yeung and Pope (1989) found spatial interpolation with 4th-order cubic splines was preferred to lower-order methods.

The present work develops a more skillful particle tracking method than the low-order spatially-smoothed methods of many prior researchers. The new method is arguably less skillful than the complicated high-order advection methods of Yeung and Pope (1989); however, the interpolation and time-stepping schemes are relatively standard and readily implemented – the principle new complexity is in moving the drifter consistently with local dynamic forcing. Focusing on an intermediate skill level is consistent with the present objective of using particle-tracking to assess the overall skill of a hydrodynamic model (See Section 1.3). For this purpose, particle tracking errors due to velocity interpolation need to be reduced, while recognizing that higher-order schemes may not be justified due to the underlying grid and time-scale limits of a RANS-based hydrodynamic model. Six spatial interpolation methods were analyzed and are described in Section 6.1. The 2-Dimensional Quadratic Lagrangian (2DQ) scheme was found to produce superior results for the present particle tracking purposes. The 2DQ approach is 3rd-order in space, and is similar to the method used for the discrete advective term in the ELCOM hydrodynamic model (Hodges, 2000). It may be hypothesized (but remains unproven) that a particle tracking scheme should have a spatial interpolation order equivalent to (or greater than) the order of the advective scheme in the hydrodynamic model. All particle tracking results presented herein were derived with the 2DQ interpolation scheme.

Appendices also present a brief discussion of temporal interpolation techniques, although only the Runga-Kutta 4th order technique was employed in this work. The Runga-Kutta 4th order technique has been demonstrated to have a high degree of accuracy in particle-tracking schemes (Ramsden and Halloway, 1991), and temporal interpolation is of secondary importance to spatial interpolation for particle tracking accuracy (Bennett and Clites, 1987; Yeung and Pope, 1988; Ramsden and Halloway, 1991). This 4th order scheme is also of higher accuracy than the combination of 1st and 2nd-order temporal schemes used for hydrodynamics in ELCOM.

2.3. Particle Tracking Using Leeway Factors

True Lagrangian particle tracking assumes the particle is mass-less and is perfectly responsive to accelerations in the surrounding fluid. Field drifters are imperfect Lagrangian particles as the drag and inertia are not identical to those of the displaced water parcels. These effects have previously been recognized in both drifter design (D'Asaro et al 1996; Johnson et al, 2003) and drifter models (Bennett and Clites, 1987; Harcourt et al, 2000, Thompson et al, 2003). As a modification to Lagrangian particle tracking, empirical leeway factors have been used to partially compensate for the

differences between water particles and field drifters (Bennett and Clites, 1987; Thompson et al, 2003). The leeway factor (α) approximates the wind acting on the above-surface portions of the field drifter such that (2.1) becomes:

$$\overrightarrow{x(t)} = \overrightarrow{x(t_0)} + \int_{t_0}^{t} \left(\vec{u} + \alpha \vec{u}_{Wind} \right) dt \qquad (2.3)$$

where $\vec{u}_{wind}$ is the surface wind vector at the drifter location. The leeway factor depends on the characteristics of the above-surface portions of the field drifter, and typical values are 0.036 for a life raft, 0.008 for a shallow-draft drifter with a short mast, and 0.0 for a completely submerged drogue (Thompson et al, 2003). This technique attempts to empirically compensate for wind drag, but neglects water drag and drifter inertia.

2.4. GABI-F Drifter Modeling Theory

Field drifters are not true "Lagrangian" particles because their movement is affected by drag and inertia so that they do not exactly match the water velocity. The Lagrangian particle tracking theory developed in section 2.1 does not consider either drag or inertia in determining representative particle velocities. This section develops a new theory for particle tracking/drifter modeling that models the physical properties of the field drifter. The goal of this new "Generalized Acceleration-Based Inertia and Forcing (GABI-F) model in this research is to improve the comparability of observed field and numerically-modeled drifter trajectories. From this point forward, the term "drifter modeling" is used in place of "particle tracking" to reflect the fact that the GABI-F model simulates drifter rather than particle movement.

2.4.1. Theoretical Derivation

For GABI-F drifter modeling, the drifter velocity is computed using an application of Newton's 2nd law. The calculation procedure incorporates drifter characteristics (mass, dimensions, shape), the water velocity near the drifter, and the local wind forcing on emergent drifter portions. The forcing equation describing drifter motion is:

$$\sum F_j = m \frac{du_{drifter,j}}{dt} \quad : \quad j = 1,2,3 \qquad (2.4)$$

where F_j represents the forces on the drifter acting in the "j" component direction, m is the mass of the drifter, and $u_{drifter,j}$ is the drifter component velocity. The net drag force is modeled with a drag coefficient c_d and the difference between the local fluid velocity and the drifter velocity. If each section of a drifter is individually modeled, then for the i'th drifter section we obtain

$$F_{j,i} = c_{d,i} A_i \rho_{f,i} \overline{\left(u_{f,j,i} - u_{drifter,j} \right)^2} \quad : \quad j = 1,2,3 \qquad (2.5)$$

where $\rho_{f,i}$, is the density of the fluid surrounding the i'th section of the drifter, $u_{f,j,i}$ is the representative velocity of the fluid in the 'j' direction around the 'i' section of the drifter, and A_i is the cross-sectional area normal to the flow field for the 'i'th section of the drifter. The overbar indicates property averaging over the area A_i, incorporating spatial variations in local fluid density and velocity to contribute to the drifter movement. The direction of the force vector depends upon the sign of the difference between the fluid and drifter velocity components. For example, if the fluid velocity is greater than the drifter velocity, then the fluid must exert a positive force on the drifter, pushing it to accelerate. However, if the fluid is moving in the direction contrary to the drifter, the force must be negative, causing the drifter to decelerate. The appropriate sign for drifter direction can be obtained from

$$\beta_{j,i} = \frac{u_{f,j,i} - u_{drifter,j}}{\left| u_{f,j,i} - u_{drifter,j} \right|} \qquad (2.6)$$

which can be applied with an expansion of the quadratic term in Eq. (2.5) to obtain

$$F_{j,i} = c_{d,i}A_i \times \overline{\beta_{j,i}\rho_{f,i}\left[\left(u_{f,j,i}\right)^2 - 2\left(u_{drifter,j}\right)\left(u_{f,j,i}\right) + \left(u_{drifter,j}\right)^2\right]} \quad : \quad j = 1,2,3 \tag{2.7}$$

Substituting eq. (2.7) into eq. (2.4) and rearranging produces the governing equation of the GABI-F technique for a drifter with 'N' sections:

$$\frac{du_{drifter,j}}{dt} = \frac{1}{m}\sum_{i=1}^{N}\left\{c_{d,i}A_i - \times \overline{\beta_{j,i}\rho_{f,i}\left[\left(u_{f,j,i}\right)^2 - 2\left(u_{f,j,i}\right)\left(u_{drifter,j}\right) + \left(u_{drifter,j}\right)^2\right]}\right\} \quad : j = 1,2,3 \tag{2.8}$$

Equation (2.8) presents a general formulation for developing a drifter motion model using forces. The method must be tailored to effectively represent the c_d for the specific characteristics of the field drifters. Furthermore, a discrete numerical method for estimating $u_{drifter}$ must be developed. Section 2.4.2 presents the application of eq. (2.8) for the field drifters used in this research (see section 3.2 for a description of the field drifters). An approximate numerical solution of eq. (2.8) for the drifters simulated in this work is presented in section 2.4.3.

2.4.2. Application to Cross-Sail Surface Drifters

The remainder of this section describes the application of the GABI-F formulation (2.8) as applied to calculating the movement of surface drifters. The motion of such drifters is limited to the horizontal (x,y) plane as they are unable to move vertically away from the water surface. Thus the following sections are tailored to a 2D version of the GABI-F method, and forces on each drifter section are vertically averaged.

Cross-sail surface drifters are a simple drifter type that has been used in assessing the surface currents of the Adriatic Sea (Poulain, 1999), coastal zones within the Indian Ocean (Johnson et al. 2003), and Lake Kinneret (Stocker and Imberger, 2003). Such drifters typically consist of two vertically-oriented rectangular sails, which are set perpendicular to each other to form an "X" when seen in plan view. These sails may be connected at their center by a rigid pole, which is supported by floats to ensure the negatively buoyant drifter remains at water surface. At the top of the pole, a transmitter may be installed for positional referencing and data transmission (Figure 2.2).

In applying the force calculations to the 2D cross-sail drifter, the drifter is divided into five sections (Figure 2.2b): the antenna (ant), the surface buoy (sb), the subsurface buoy (usb), the pole connecting the drogue to the subsurface buoy (pole), and the drifter sails (drogue). Each of these 5 drifter sections may have different cross sections, drag coefficients, and vertical extents, and each section may be surrounded by fluid moving at different velocities. For example, the antenna and surface buoy sections remain above the water surface and are acted upon by the surface winds. In contrast, the subsurface buoy, pole, and sails are constantly submerged and are acted upon by the water currents, which may exhibit vertical shear.

For a 5-section cross-sail drifter, eq. (2.8) may be rewritten as:

$$\frac{du_{drifter,j}}{dt} = \frac{\lambda_j}{m}\left(u_{drifter,j}\right)^2 + \frac{\xi_j}{m}\left(u_{drifter,j}\right) + \frac{\varepsilon_j}{m} \quad : \quad j = 1,2 \tag{2.9}$$

where

$$\lambda_j = Q_{j,ant} + Q_{j,sb} + Q_{j,usb} + Q_{j,pole} + Q_{j,drogue} \tag{2.10}$$

$$\xi_j = -2\left(\Psi_{j,ant} + \Psi_{j,sb} + \Psi_{j,usb} + \Psi_{j,pole} + \Psi_{j,drogue}\right) \tag{2.11}$$

$$\varepsilon_j = \gamma_{j,ant} + \gamma_{j,sb} + \gamma_{j,usb} + \gamma_{j,pole} + \gamma_{j,drogue} \tag{2.12}$$

and

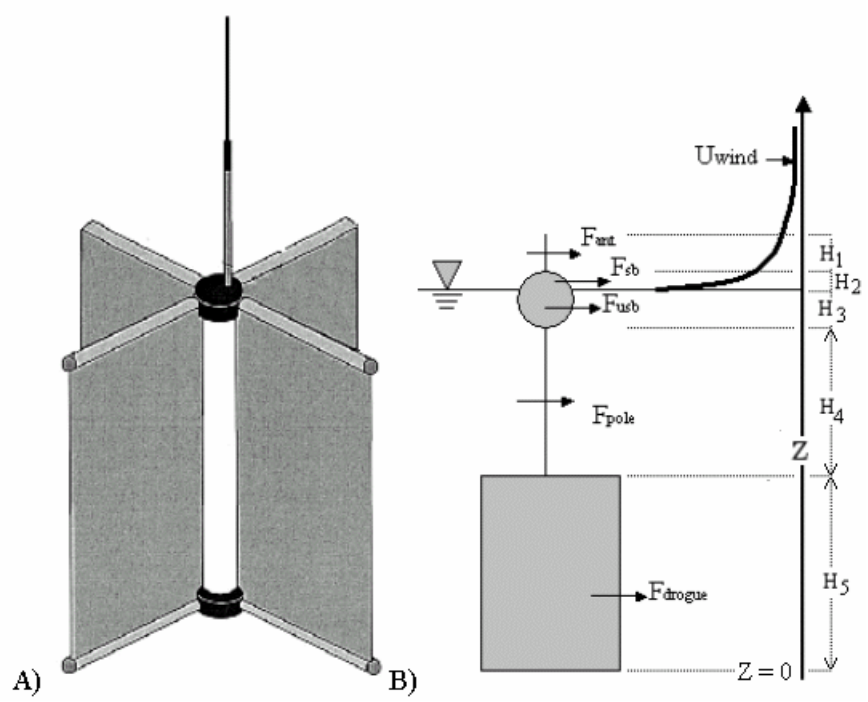

Figure 2.2 – Cross-Sail Surface Drifters, A) Perspective view similar to the Adriatic Sea Drifters from Poulain (1999), B) Drifter schematic for application of the GABI-F technique.

$$Q_{j,i} = \frac{c_{d,i}A_i}{H_i}\int_{H_{B,i}}^{H_{T,i}} \beta_{j,i}\rho_{f,i}dZ \tag{2.13}$$

$$\Psi_{j,i} = \frac{c_{d,i}A_i}{H_i}\int_{H_{B,i}}^{H_{T,i}} \beta_{j,i}\rho_{f,i}u_{f,j,i}dZ \tag{2.14}$$

$$\gamma_{j,i} = \frac{c_{d,i}A_i}{H_i}\int_{H_{B,i}}^{H_{T,i}} \beta_{j,i}\rho_{f,i}\left(u_{f,j,i}\right)^2 dZ \tag{2.15}$$

Thus, the coefficients λ_j, ξ_j, and ε_j of the quadratic RHS of eqs. (2.8) and (2.9) depend on the unknown binary variable $\beta_{j,i}$ from eq. (2.6) that represents the effect (i.e., acceleration/deceleration) of the force acting on the drifter. Therefore eq. (2.9) is nonlinear and cannot be directly solved. However the solution may be approximated numerically using the procedure described in section 2.4.3.

The mass term m in eq. (2.9) is:

$$m = m_{ant} + m_{sb} + m_{usb} + m_{pole} + m_{drifter} + \sum_{i=1}^{5} m_{added,i} \tag{2.16}$$

The m_{added} terms in eq. (2.16) account for the mass of the water in the immediate vicinity of the drifter sections that is dragged along with the drifter due to drifter geometry (e.g., for a cross-sail drifter, water between the sails tends to be moved with the drifter). Based on Wilson (1984), the added mass can be approximated as from the mass of the water filling the same volume as the drifter section as

$$m_{added,i} = c_{s,i}\rho_{f,i}V_i \tag{2.17}$$

where $c_{s,i}$ is an experimentally-defined coefficient and differs for sections of different shape, and V_i is the section's volume. Wilson (1984) and others (Lewis, 1988; Sahin et al, 1993) have investigated added mass coefficients, and argued that a $c_{s,i}$ of 1.0 is appropriate for cylindrical sections, 1.51 for spherical sections, and 0.76 for rectangular sections. For the drifters used in

this work, the antenna and pole sections were modeled using cylindrical sections coefficients, the buoys with spherical section coefficients and the drogue section with a rectangular coefficient. Unfortunately, researchers have not reported any coefficients for a cross-sail shape.

2.4.3. GABI-F Drifter Simulation – Solution Methods

The drifter acceleration term (i.e., LHS) of (2.9) is numerically approximated as a continuously smooth function by fitting a quadratic polynomial to the drifter velocities $u^{n}_{drifter,j}$, $u^{n-1}_{drifter,j}$, and $u^{n-2}_{drifter,j}$, where the superscript denotes the model timestep:

$$\frac{du^{n}_{drifter,j}}{dt} = \frac{3u^{n}_{drifter,j} - 4u^{n-1}_{drifter,j} + u^{n-2}_{drifter,j}}{2\Delta t} + O\left(\Delta t^{3}\right) \tag{2.18}$$

Equation (2.18) is a standard backward difference formula; however, the derivation is provided in Section 6.2 for completeness. First order Euler approximations of the drifter acceleration were also considered for use in this work, but were deemed less favorable as they limit the "Lagrangian memory" of the drifter to only a single previous timestep. Lagrangian memory, as defined by Addison (1997), is the numerical approximation of drifter inertia, causing a drifter to travel with velocities similar to the velocities it achieved previously in time. Substituting eq. (2.18) into eq. (2.9) produces:

$$\frac{2\Delta t\lambda_{j}}{Zm}\left(u^{n}_{drifter,j}\right)^{2} + \left(\frac{2\Delta t\xi_{j}}{Zm} - 3\right)\left(u^{n}_{drifter,j}\right) + \frac{2\Delta t\varepsilon_{j}}{Zm} - u^{n-2}_{drifter,j} + 4u^{n-1}_{drifter,j} = 0 \tag{2.19}$$

Equation (2.19) is a quadratic equation with one unknown ($u^{n}_{drifter,j}$) and unknown coefficients that are functions of $u^{n}_{drifter,j}$ through only the $\beta_{j,i}$ directional terms in eqs. (2.9)-(2.15). Each $\beta_{j,i}$ may take on only one of two values (±1) and, for a drifter modeled in N sections, there exists 2^{N} possible combinations of the $\beta_{j,i}$ terms. Each combination provides a solvable quadratic equation with 0, 1, or 2 numerically valid (i.e., non-complex) value(s) for the drifter velocity. Thus, the drifter model of eq. (2.19) has a maximum of $2(2^{N})$ possible solutions for the drifter velocity. For the present work with a drifter modeled in five sections, this provides 64 possible solutions. Proposing a numerical method with $2(2^{N})$ possible solutions is somewhat unusual, but is effective in the present work because many of the solutions will be inconsistent with the correct physics. Simple selection criteria (developed below) can be used to find the solution that best matches the forcing dynamics that are accelerating/decelerating the drifter. Furthermore, each solution is easily and directly calculable from a quadratic equation so, for 'M' drifters the maximum computational effort is $\sim 20M(2^{N})$ operations, which is fairly trivial for M < 100 and N < 5 for a hydrodynamic model with 10^{4} grid cells and O(100) operations per time step.

Selection criteria for the best drifter velocity out of the computed set are based on three concepts: 1) the resulting drifter velocity in eq. (2.6) must provide the same set of $\beta_{j,i}$ values used in the eq (2.19) solution; 2) the drifter acceleration must be less than the surrounding fluid, and 3) the "best" velocity should closest to the local fluid acceleration. These three tests are illustrated in Figure 2.3, and for descriptive purposes the computed set of candidate drifter velocities is denoted $u^{n}_{drifter,j}(ii)$ where ii = 1,….,2(2n) and $u^{n}_{drifter,j}(g)$ is the "g^{th}" entry in the set. The first concept is a simple question of consistency, as a velocity must be numerically consistent with the conditions from which it was obtained. This consistency is determined through a comparison (Test #1) between the $\beta_{j,i}$ values used in solving (2.19) and those produced when substituting $u^{n}_{drifter,j}(ii)$ for $u^{n}_{drifter,j}$ in eq. (2.6). If there is any inconsistency between the input and resulting $\beta_{j,i}$ values (as seen for candidate #2, section 3 in Figure 2.3) then the

			Test #1					Test #2			Test #3
Velocity			**β Values**					**Acceleration**		**Pass/Fail**	**Best**
candidate			**Section**					Ft/s²			**Velocity**
$u^{n}_{drifter,j}(ii)$			**1**	**2**	**3**	**4**	**5**				
1		Input	1	1	-1	-1	-1	Fluid	1.03	Pass	**Pass**
		Result	1	1	-1	-1	-1	Drifter	0.98		
		Match	✓	✓	✓	✓	✓	Drifter less?	✓		
2		Input	1	1	1	-1	-1	Fluid	1.03	**Fail**	**Fail**
		Result	1	1	-1	-1	-1	Drifter	N/A		
		Match	✓	✓	✖	✓	✓	Drifter less?	**N/A**		
3		Input	1	1	1	1	-1	Fluid	**1.03**	Pass	**Fail**
		Result	1	1	1	1	-1	Drifter	**0.54**		
		Match	✓	✓	✓	✓	✓	Drifter less?	✓		
.....											
64		Input	-1	-1	-1	-1	-1	Fluid	1.03	**Fail**	**Fail**
		Result	-1	-1	-1	-1	-1	Drifter	2.30		
		Match	✓	✓	✓	✓	✓	Drifter less?	✖		

Figure 2.3 – Selecting the best velocity candidate using the 3-test criteria. The best velocity will have consistent β values, will cause the drifter to accelerate less that the surrounding fluid, and will have the acceleration closest to that of the local fluid.

candidate velocity fails and is removed from consideration as the best estimate of $u^{n}_{drifter,j}$. Such an inconsistency indicates that the input $\beta_{j,i}$ values were not representative of the flows surrounding the drifter.

The second concept used in determining the selection criteria is that the acceleration of a GABI-F drifter must be driven by the fluid acceleration. Therefore the change in drifter velocity must mimic the change in the surrounding fluid velocities (Test #2). The accelerations will not be identical, however, and because of the drag and inertia of the GABI-F drifter, it will tend to accelerate less (Test #3). For example, consider a drifter moving at 10 cm/s within a flow moving at 11 cm/s. If the flow decelerates to 6 cm/s, fluids will act on the drifter to reduce its speed. With sufficient time, the drifter will also reach speeds close to 6 cm/s. However after the initial change in fluid velocity, the drifter will be slow to react (due to inertia) and it will temporarily travel faster than the surrounding fluids, although slowly decelerating to a speed of 6 cm/s. Based on this premise, the best drifter velocity is that which forces the drifter to accelerate at a rate close to but slightly less than the surrounding fluid.

In mathematical terms, the selected drifter velocity is the candidate velocity which satisfies:

Test #2:

$$\left|\frac{\partial u^{n}_{drifter,j}(ii)}{\partial t}\right| < \left|\frac{\partial u^{n}_{f,max}}{\partial t}\right| \qquad (2.20)$$

$$\text{and} \quad \left(\frac{\partial u^{n}_{drifter,j}(ii)}{\partial t}\right)\left(\frac{\partial u^{n}_{f,max}}{\partial t}\right) \geq 0$$

and best satisfies:

$$\text{Test \#3} \Rightarrow \frac{\partial u^{n}_{drifter,j}(ii)}{\partial t} \approx \frac{\partial u^{n}_{f,max}}{\partial t} \qquad (2.21)$$

where $\vec{u}^{n}_{f,max}$ is the fluid velocity at the drifter section over which the greatest force is applied as calculated with eq. (2.5). As shown in Figure 2.3, candidate velocities #1 and #3 both satisfy (2.20), whereas candidate #64 fails because it's velocity suggests a drifter acceleration exceeding fluid acceleration. Upon applying Test #3 (Figure 2.3), candidate velocity #1 is selected as the drifter velocity as the acceleration it implies is closest to the fluid acceleration.

The determination of $u^{n}_{f,max}$ is made independently at each model timestep for each modeled drifter, as $u^{n}_{f,max}$ is a function of currents and the properties of each drifter section in eq. (2.5). In a vertically homogeneous flow (e.g., a relatively steady-state wind-mixed layer), all sections of the drifter are surrounded by fluid with the same velocity u^{n}_{f}, which is therefore also $u^{n}_{f,max}$. With such a homogeneous flow it is not necessary to determine the forces acting on each individual section in order to apply equations (2.20) and (2.21). In contrast, when the wind speed or direction is changing, or if the drifter height (Z in Fig 2.2) is larger than the wind-mixed layer depth, then vertical heterogeneity in the horizontal velocity field may exist and different drifter sections may be influenced by different velocities and accelerations. Under such conditions, $u^{n}_{f,max}$ must be selected by comparing the forces on different drifter sections as calculated with eq. (2.5). For vertically stratified flows, the current that has the most influence on the drifter motion is the current which applies the greatest force to the drifter. For the drifters used herein, currents with velocity $u^{n}_{f,max}$ flow around the drogue section because of the drogue section's large cross-sectional area compared to that of the other drifter sections. Other drifter designs may have drifter sections with different properties that cause greater forces to be applied to sections other than the drogue section, thereby requiring that $u^{n}_{f,max}$ not be automatically set to the velocity around the drogue section. Examples include the life-raft drifters of Thompson et al. (2003) which had large above-surface elements acted upon by the winds, and the drifters of Poulain (1999) which lost their drogue sections halfway through the deployment (thereby eliminating the drogue section's influence on the drifter movement). Independently defining $u^{n}_{f,max}$ for each drifter at each timestep provides the flexibility of modeling various drifter scenarios, including scenarios where the drogue section or antenna section is lost midway through the experiment.

2.4.4. GABI-F Drifter Simulation – Summary

Modeling field drifters with the GABI-F method is a new approach in numerical particle tracking. The GABI-F method, described in sections 2.3.1-2.3.3, improves upon existing particle tracking schemes by including drifter properties and drag/inertia relationship between the drifter and the surrounding fluid. The method advances and extends the theoretical basis of Lagrangian particle tracking schemes developed and implemented by prior researchers (e.g., Bennet and Clites, 1988, Yeung and Pope, 1989, Toner et al, 2001). The method is a physically-based advance of the empirical leeway factors previously used for wind effects (Bennet and Clites, 1988, Thompson et al, 2003). The method presented for solving the force-based equations of drifter motion was preferred because it produced more stable results than other methods and included more of the "Lagrangian memory" deemed important by Addison (1997). The additional methods that were considered are described in Section 6.3.

2.5. Existing Modeled Drifter Assessment Methodologies

Comparing modeled and field-observed drifter paths provides a means of assessing hydrodynamic model skill. The most obvious approach for path comparison is by measuring the field/model drifter position separation after an *a priori* selected time interval: more skillful models should provide smaller separations. However, simple position separation comparisons are inherently integrative of model error (e.g., the error magnitude will always increase with time in a

diverging flow field). Thus, the error magnitude depends both on model skill and the relationship between the selected time interval and the flow velocities and divergence. It follows that model skill comparisons are problematic across different drifter types and different flow conditions using a position separation approach. It will be seen in this section that many existing assessment methods have similar shortcomings that limit their utility for quantitative comparisons and analysis. The subsequent section 2.5 describes the new Circle Assessment method for drifter path analysis, and illustrates advantages over existing methods for quantitative analysis. Example application through analyses of modeled and observed drifter paths within Marmion Marine Park using both existing methods and the Circle Assessment method are presented in Chapter 4.

2.5.1. "Spaghetti" Diagrams

The simplest way of displaying drifter data is by plotting the drifter paths on a chart. This method has been used by nearly all prior drifter experiments, including Bennett and Clites (1987), List et al (1990), Poulian (1999), Lacorata et al (2001), Chen et al (2003), and Paldor et al (2004). Such plots are often called "spaghetti" diagrams due to their likeness to a bowl of noodles (Toner et al, 2001). Analyses of model skill using spaghetti diagrams is typically a qualitative visual comparison of field and modeled paths, which emanate from a common origin and are traced over the entire drifter deployment. The assumption behind this approach is that a more skillful model will produce a modeled path more comparable to the observed drifter path. However, such analyses are qualitative and are only suitable for distinguishing between dramatic and obvious differences in model performance. Furthermore, such analyses are integrative of model error (as discussed for simple separation analysis in section 2.4 above).

In a recent paper describing the transport of Antarctic krill toward South Georgia Island, Thorpe et al (2004) described observed drifter data and particle tracking in the Parallel Ocean Climate Model (POCM). They applied spaghetti diagrams (Figure 2.4) to validate model skill in predicting drifter paths from the World Ocean Circulation Experiment (WOCE). The model was subsequently applied to estimate drifter paths when WOCE data was not available.

The spaghetti diagram plots shown in Figure 2.4 (reproduced from Thorpe et al, 2004) indicate that the observed general north-easterly currents are captured with the POCM model, but the model fails to capture the observed current eddies or the circulation around South Georgia Island. The modeled drifters also moved more slowly than the WOCE drifters, increasing the

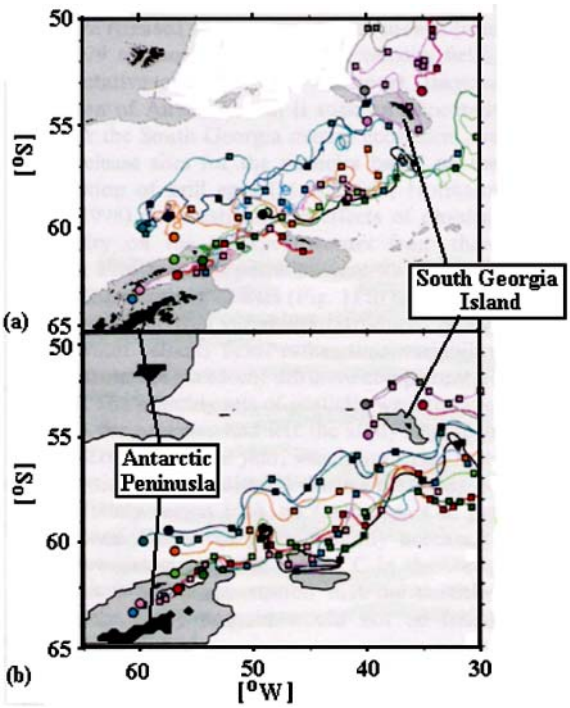

Figure 2.4 – POCM model validation using WOCE drifter data – A) paths of the WOCE drifters, B) modeled drifter paths. Circles indicate initial positions. Squares indicate 30-day intervals. Modified for clarity from Thorpe et al (2004) – Figure 2

predicted travel times between the Antarctic Peninsula and South Georgia from 4 to 7 months for some WOCE drifters. The authors blamed these differences on the coarse ¼° horizontal grid resolution of the

POCM.4C model. Despite such errors, their model was considered appropriate for predicting the likelihood of Antarctic krill transport to the South Georgia Island area.

The approach employed by Thorpe et al (2004) was unique in that they first used satellite and in-situ data to validate the modeled circulation, and gain confidence that they could use their model to predict drifter transport times and patterns. The precise particle paths and transport velocities were not a principle focus of Thorpe et al. (2004); instead they sought only to determine whether particles reached the target area within predefined time window. Therefore, their analysis methodology (i.e., comparisons of spaghetti diagrams and tracking arrival times) was not dependent upon their hydrodynamic model's ability to exactly reproduce the field drifter paths; the modeled drifter transport could be slower than the field drifter transport and still yield meaningful conclusions to satisfy the authors intentions. . Had the author's goals been to completely reproduce the WOCE drifter paths (and therefore fully predict the currents in their study area), their method would not have been successful because of their model's inability to pinpoint the drifter travel times and capture the observed current eddies.

Toner et al (2001) also assessed model skill by visual comparisons of spaghetti diagrams. They used the diagrams to determine their model's improvement in predicting drifter paths after "constraining" the modeled velocity field to reflect the velocities implied by the field drifter (Toner et al, 2001). Figure 2.5 (reproduced from Toner et al, 2001) depicts the original, unconstrained model path ('Model"), the "constrained" model path, and the field drifter path. The original modeled drifter did not move as fast as the field drifter, but the directions of travel were similar. The constrained model path is much improved over the modeled path, and is comparable to the field drifter path. The separation of the constrained and field drifter paths toward the end of the simulation suggests slow accumulation of error.

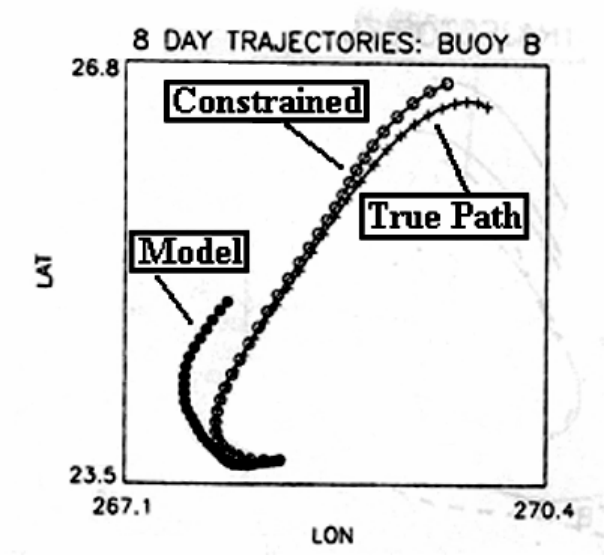

Figure 2.5 – Spaghetti diagram comparison method from Toner et al, 2001. Constrained path is more comparable to the True Path than the original Model path. Labels added for clarity.

Nairn and Kawase (2001) moved beyond the spaghetti diagram for a field deployment of drifters in Puget Sound. They generated spaghetti diagrams of the field drifters (Figure 2.6a), and plotted the model velocity vectors at the observed drifter location for individual model time steps (Figure 2.6b) to approximately replicate the spaghetti diagram. Their approach does not include a continuous model of drifter motion, but instead provides qualitative insight into the local velocities from the model and field data. By resetting the comparison point to the actual drifter location at each model time step, Nairn and Kawase (2001) eliminate the problem of long-time error integration in assessing model skill. However, their method does not completely remove an arbitrary time dependency in assessment; i.e., reducing the model time step may give a qualitative appearance of high skill simply due to the resetting of the comparison point to the actual drifter location. The Nairn and Kawase (2001) approach is similar to the original spaghetti diagram approach as a qualitative visual comparison.

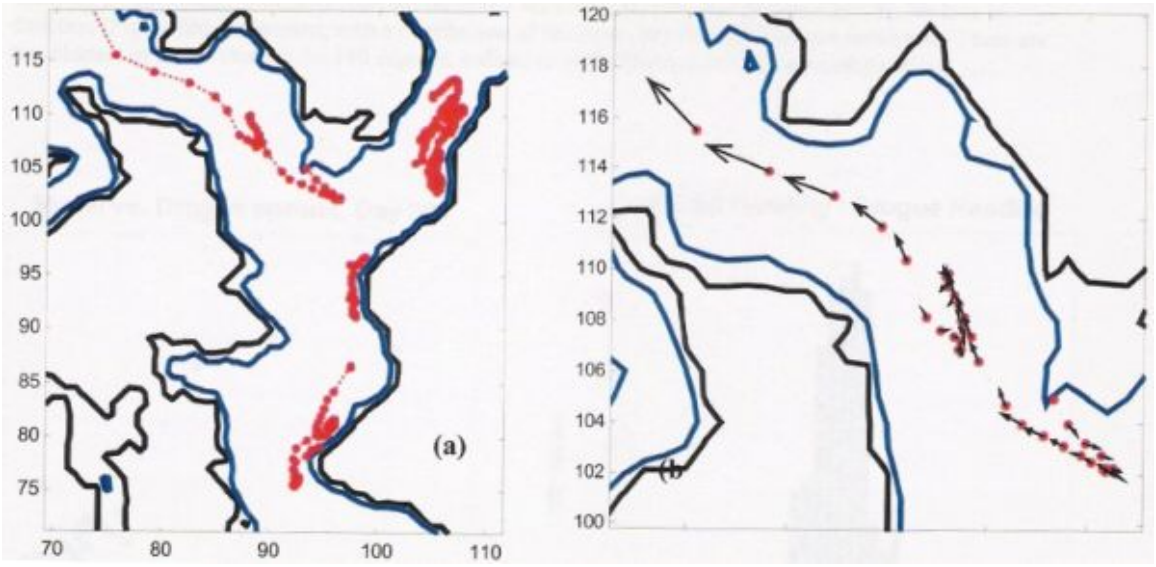

Figure 2.6 – Spaghetti diagrams of Puget Sound drifters A) Field drifter paths in red, B) modeled drifter vectors (black arrows) calculated at the field drifter positions (red dots) at each model timestep. Model skill is higher when the vector approaches the field drifter position at the next timestep (From Nairn and Kawase, 2001 - Figure 5)

2.5.2. The "Type I" Method

As noted by Toner et al (2001), drifter data from the world's oceans are abundant, but comparisons between observations and models are typically qualitative. The authors cited numerous "futile" attempts at comparing model-derived paths with observations. and used the observed Lagrangian trajectories to modify the local Eulerian velocity field to reduce model and observed path differences. In essence, they extracted Eulerian velocity data from Lagrangian drifter tracks, and reworked their hydrodynamic model solution to produce modeled drifter paths more comparable to the field drifter paths.

In assessing model skill, they defined a quantitative "type I" Lagrangian error metric (Toner et al, 2001):

$$L(t) = \frac{\left\|\gamma(t)\right\|}{\int_{t_o}^{t} \left\|\frac{d\eta}{ds}\right\| ds} \tag{2.22}$$

where

$$\gamma(t) = x(t) - \eta(t) \tag{2.23}$$

and x(t) is the computed drifter path and η(t) is the observed drifter path. The || || operator is defined as the square root of the dot product of its contents. The Type I metric (2.22) is therefore the displacement between the modeled and observed field drifter normalized by the field drifter displacement from the t_0 position. This metric is computed for each of the field and modeled drifter pairs in their experiment.. By analyzing time-histories of L(t) from multiple model runs (Figure 2.7), Toner et al (2001) concluded smaller values of L(t) corresponded with greater model skill.

The improvement of the constrained model in Figure 2.7 compared to the original model is also evident in the spaghetti diagram plot of the modeled and observed paths (Figure 2.5). The spaghetti diagram is arguably more valuable, however, because it indicated that the original model under-predicted the observed drifter velocities; this under-prediction is not discernible from the Type 1 error metric.

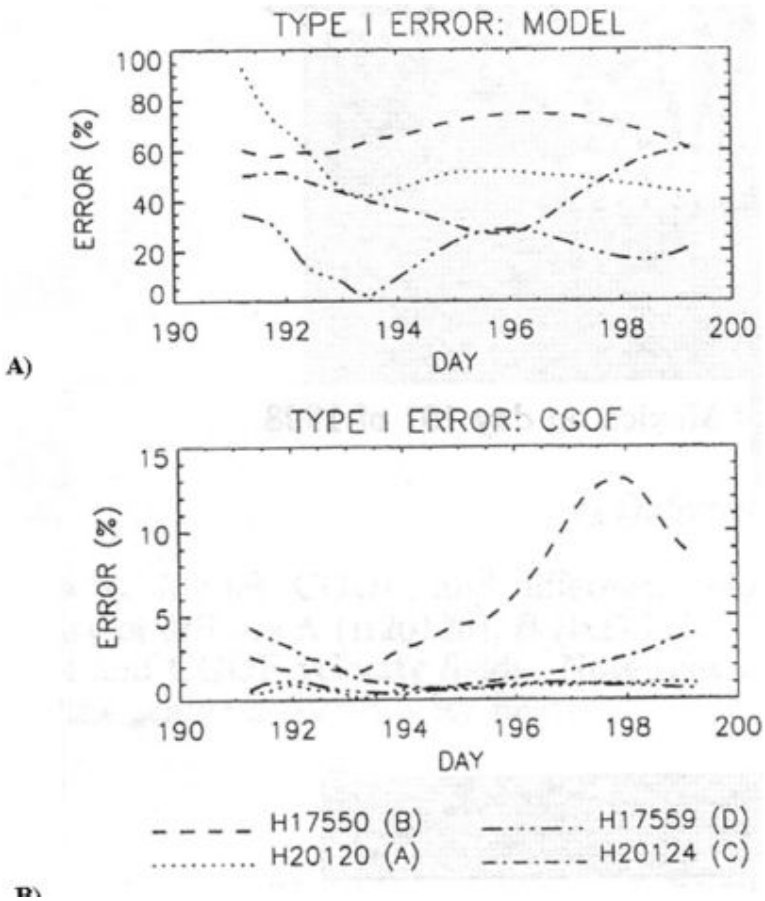

Figure 2.7 – Type 1 error metrics plotted as percentage error, from Toner et al (2001), A) Original model, B) Constrained model showing greater agreement with field data because the percentage errors are smaller for each modeled drifter. H17550, H20120, H17559, and H20124 are separate model simulations. Results from the H17550 simulation are shown in the spaghetti diagram plot in Figure 2.5.

For the present purposes, the main contribution from Toner et al (2001) is the quantitative methodology for comparing model and observed drifter positions using the Type I metric. The quantitative nature of the Toner et al (2001) approach should provide for more subtle comparisons across different modeling methods than achievable with spaghetti diagrams alone. However, like the spaghetti diagrams, the normalized displacement metric applied to the continuous path of a model drifter is inherently integrative of model error. Furthermore, the metric loses the directional information on model error that is available from spaghetti diagrams. Thus, the combination of methods appears necessary for assessing hydrodynamic model skill using the approach of Toner et al (2001).

2.5.3. The "Statistical Separation" Method

Thompson et al (2003) used model particle tracking and observed drifter positions to determine an expected search radii in coastal search-and-rescue operations near the Scotian Shelf. To assess confidence in their search radii, they developed a set of metrics for assessing the predictive skill of their prototype hydrodynamic model based on the separation between modeled and observed drifter locations. The drifter model used leeway factors (section 2.2) to approximate the effects of direct wind forcing on drifter motion. Two quantitative metrics were developed based on

drifter displacement statistics using sets of multiple drifters (in contrast to Toner, et al, 2001, whose metric applies to a individual drifters). Thompson et al (2003) defined $\vec{x}_1^{\,o}(t),\ldots \vec{x}_n^{\,o}(t)$ and $\vec{x}_1^{\,p}(t),\ldots \vec{x}_n^{\,p}(t)$ as the observed and predicted positions of n drifters at time t, where all n drifters were initially deployed a small distance apart.. Their metrics were: 1) the median of the observed separation over the time interval [t0,t] for a set of drifters

$$S^o(t) = \text{median}\left\{\left|\vec{x}_1^{\,o}(t) - \vec{x}_1^{\,o}(t_0)\right|,\ldots. \left|\vec{x}_n^{\,o}(t) - \vec{x}_n^{\,o}(t_0)\right|\right\} \quad (2.24)$$

and 2) the median of the separation between the time t position of the observed and modeled drifters

$$S^p(t) = \text{median}\left\{\left|\vec{x}_1^{\,o}(t) - \vec{x}_1^{\,p}(t)\right|,\ldots. \left|\vec{x}_n^{\,o}(t) - \vec{x}_n^{\,p}(t)\right|\right\} \quad (2.25)$$

Thompson et al (2003) did not name their method, but for convenience in discussion, and are herein referred to as the "Statistical Separation" method. The metric S^o is the radius of a circle centered on $\vec{x}^{\,o}(t_0)$ that encompasses 50% of the field drifters at time $t > t_0$. Similarly, the metric S^p is interpreted as the radius of a circle which, when centered on the predicted position of each drifter, will encompass 50% of the field drifters at time t. Thompson et al (2003) assessed model skill by comparing time histories of S^o and S^p as shown in Figure 2.8. concluding that the model performs well when $S^o(t) >> S^p(t)$.

In describing Figure 2.8, Thompson et al (2003) wrote:

> *"Comparing the solid and dotted lines it is clear that the model has significant predictive skill of the two most energetic deployments, i.e., trial 1 and trial 3. For trials 2 and 4 the model prediction is not much better than the initial position."*

The plots show that in trials 1 and 3, the median

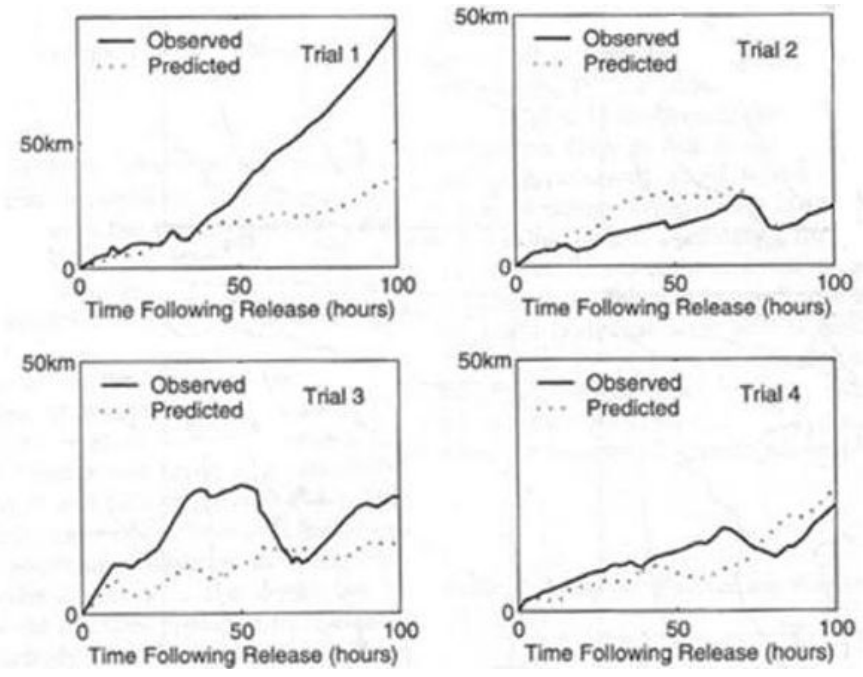

Figure 2.8 – Statistical Separation metrics S^o (solid line) and S^p (dotted line).. (Reproduced from Figure 7 of Thompson et al, 2003)

separation between field and modeled drifter is less than the median displacement of the field drifter. In Trials 2 and 4, the separation is nearly equivalent to or exceeds the field drifter displacement. The authors did not numerically quantify their comparisons of S^o and S^p in some form of ratio, and only presented Figure 2.8 to demonstrate qualitative agreement between their model and their field data.

The Thompson et al (2003) analysis method was suitable for the purposes of the authors, who were interested in determining an expected search radius in coastal search-and-rescue operations. However, their method does not qualitatively or quantitatively measure model skill in reproducing observed drifter velocities; similar to Toner et al (2001), their approach only provides a general sense of model skill from model/field drifter separation. The separation is a function of time-integrated speed and directional differences between the field and modeled drifter. As the S^o vs. S^p comparison cannot discriminate between speed and direction errors, the method cannot provide insight into the sources of model error or help intuit model improvements to reduce error. For example, consider the results in Figure 2.8 for Thompson et al (2003)'s trial 1 at time = 100 hrs, where the median field drifter displacement is 100 km and the modeled separation from the field drifter is 30 km (Figure 2.9). The modeled drifter has a 50% probability of being located anywhere within the "uncertainty circle" centered on the field drifter position, where the circle has a radius equal to the stated displacement S^p. The black squares represent possible drifter locations where the modeled drifter speed is exactly equal to that of the field drifter. In contrast, the open circles indicate potential drifter locations where the modeled drifter direction is exactly equal to that of the field drifter, but the speed is incorrect. When the model correctly reproduces the field drifter speed, the model drifter's trajectory may be off by 17.3 degrees and still be within the uncertainty circle. However, when the direction is correct, the model drifter speed may be in error by ±30% of the field drifter speed.

Although S^o and S^p metrics cannot quantify the hydrodynamic model skill in representing drifter paths, they do provide a method for quantitatively comparing model results using different forcing conditions or numerical techniques. Thus, analysis of S^p sensitivity to adjustments in wind forcing or leeway factors might be useful for trial-and-error model calibration to improve model skill for drifter position prediction.

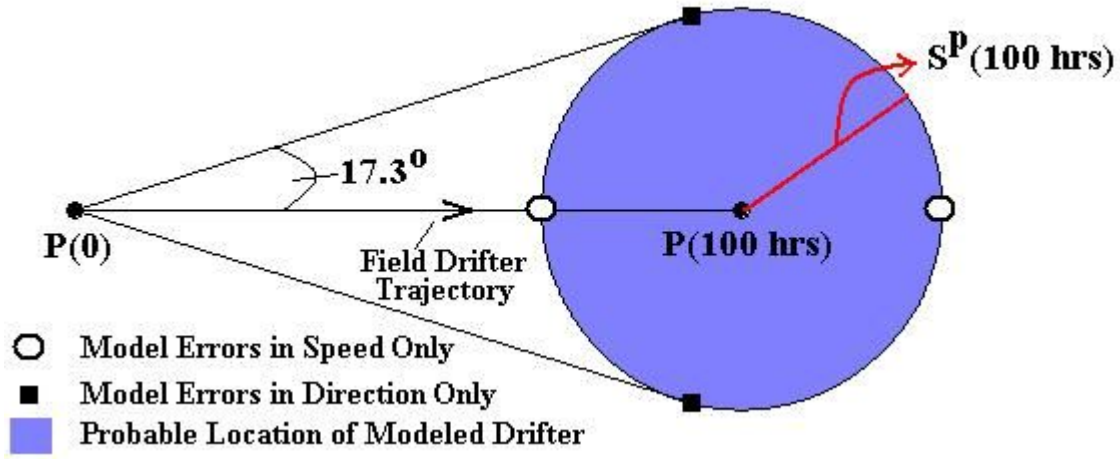

Figure 2.9 – Spatial Relationships suggested by S^p(100 hrs) for Trial 1 of Thompson et al (2003). Modeled drifter has a 50% probability of being within 30 km of the field drifter, equivalent to a search area of 2,826 km^2.

However, there are many possible paths to the correct drifter location, so simply reducing S^p cannot be taken as proof that the underlying hydrodynamics are correctly modeled. This observation motivates the new "Circle Assessment" method discussed in the following section, which is designed to quantitatively evaluate model skill in representing the drifter path rather than simply the drifter position.

2.6. The "Circle Assessment" Method

2.6.1. Introduction

This work presents a new method of comparing observed drifter trajectories and modeled drifter trajectories. The method, herein named the "Circle Assessment" method, is designed to evaluate how well a numerical model reproduces the local velocity field implied by statistical evaluation along the path(s) of one or multiple individual drifters (rather than combined statistics of a drifter set as in Thompson et al, 2003 described in section 2.4.3 above). The Circle Assessment method is motivated by the observation that the modeled drifter paths will integrate the hydrodynamic and drifter model errors, thus eventually leading to separation of model and field results. It follows that any absolute method of quantifying error over a continuous drifter path will have results that depend on the time interval over which the path is considered. To bypass this problem, this research proposes evaluating the paths over times during which the modeled drifter results are considered "perfect" and merely "acceptable." In a general sense, modeled drifter results may be considered "perfect" when they are continuously within some target radius (δ) of the field drifter position, which herein will be called the "target circle." Similarly, modeled drifter results may be considered "acceptable" if they are outside of the chosen target radius (δ) but remain within a larger error circle (with error radius ξ). Rather than using the traditional approach of evaluating a single model drifter released at the initial time (t0) and initial location (x0), the Circle Assessment method applies to model drifters released at each known field drifter position and time. The path length and time before each modeled drifter moves out of the error circle (i.e., diverges) provides quantitative measures of the agreement between the velocity field experienced by the field drifter and the velocity field experienced by the modeled drifter (section 2.3) at each position along the drifter track. Statistical analysis of the path lengths/times prior to separation (section 2.5.3) allows the Circle Assessment method to be used to evaluate model performance under different forcing/velocity conditions (section 4.3).

The basic theory of the Circle Assessment method leads to numerous approaches for determining model skill. For clarity, the theoretical basis for each approach is developed in sections 2.6.2-2.6.4. The individual approaches for skill determination are presented in section 2.7 and 2.8, as each approach is based upon one of two methods for determining the time over which the field drifter and model drifter paths are compared.

2.6.2. Theoretical Development

The Circle Assessment method applies a tertiary "perfect/acceptable/flawed" evaluation of model skill, wherein a modeled portion of the drifter transport path is considered "perfect" when a model drifter is located within the field drifter position's target circle (with radius δ) both at the start and finish of time period τ (Figure 2.10). Likewise, the drifter transport path is considered "acceptable" when the model drifter is located within the field drifter position's error circle (with radius $\xi > \delta$) but outside of the target circle after time period τ . These definitions are based on the premise that any position with the observed drifter's target or error circles is equally valid.

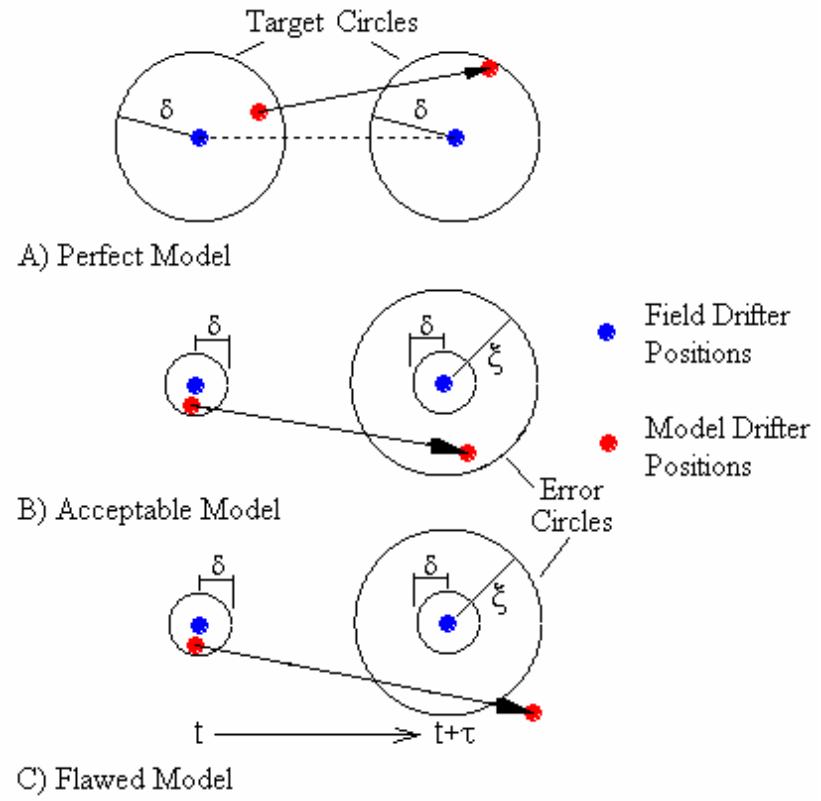

Figure 2.10 – "Perfect/Acceptable/Flawed" analysis from the Circle Assessment method. A) Perfect models are those for which the model drifter is within the field drifter target circle at times t and t+τ, B) Acceptable models predict the model drifter to be within the t+τ error circle but outside of the target circle, C) Flawed models predict the model drifter to be outside the t+τ error circle

Due to errors in the modeled velocity field and the drifter model, modeled drifters will eventually travel outside of the field drifter's target and error circles. As time progresses from drifter deployment, separation between the modeled and field drifter paths will suggest the model is initially perfect, progressing to acceptable, and finally flawed. Greater model skill is implied when the model transports drifters within the target circles rather than only within error circles, and for periods τ over which the displacement of the field drifter is greater. Additionally, the time and field drifter displacement necessary for model/field drifter path separation may be used to impose limits on the acceptable errors to the calculated drifter velocity. This concept, although equally valid for separation quantified by δ or ξ, is described below and applied in this work for target circles only. Subsection 2.5.4 describes the relative utility of the error circle as presented in this work.

2.6.3. "Perfect Classification" Using Target Circles

The Circle Assessment method uses the displacement of the field drifter and the target circle radius to quantify the acceptable ranges of modeled drifter speeds and directions within which the model is still to be considered "perfect." Smaller ranges in speed and direction indicate that the perfect model must be more accurate in its calculation of the observed velocity field. Over time τ, the field drifter will travel some sinuous path between points P(t) and P(t+τ); to represent this motion with particle tracking, a modeled

drifter would move with the speed U_{field}, where the separation between P(t) and P(t+τ) is $U_{field}\tau$ (Figure 2.11).

For a modeled drifter located in the field drifter's target circle at time t to arrive within the uncertainty circle at time t + τ, it must be displaced a distance L_d in the range:

$$U_{field}\tau - 2\delta \le L_d \le U_{field}\tau + 2\delta \tag{2.26}$$

depending on its initial and final positions within the target circles (Figure 2.11). The displacement range translates into a range of required drifter speed ($U_{drifter}$) as a function of U_{field} and δ:

$$U_{field} - \frac{2\delta}{\tau} \le U_{drifter} \le U_{field} + \frac{2\delta}{\tau} \tag{2.27}$$

Similarly, the range in drifter direction is given as:

$$\hat{u}_{field} - \theta \le \hat{u}_{drifter} \le \hat{u}_{field} + \theta \tag{2.28}$$

where direction is denoted with the $\hat{u}$ symbol and θ is the maximum difference in direction between the field and modeled drifter permissible for the modeled drifter to be transported to the field drifter's target circle at time t + τ (Figure 2.11), given as:

$$\theta = \tan^{-1}\left(\frac{2\delta}{U_{field}\tau}\right) \tag{2.29}$$

In defining the "drifter target ratio" (κ) as the ratio of field drifter displacement and twice the target circle radius:

$$\kappa \equiv \frac{U_{field}\tau}{2\delta} \tag{2.30}$$

the bounds (denoted with { } brackets) on acceptable modeled drifter speed and direction, respectively, are obtained by substituting (2.30) into (2.27) and (2.29):

$$\left\{U_{drifter}\right\} = \left(1 \pm \frac{1}{\kappa}\right) U_{field} \tag{2.31}$$

and

$$\{\theta\} = \pm \tan^{-1}\left(\frac{1}{\kappa}\right) \tag{2.32}$$

Therefore through (2.31) and (2.32) the drifter target ratio (κ) quantifies the allowable discrepancy in modeled drifter speed and direction (with respect to the speed and direction of the field drifter) that will still indicate the model successfully predicts drifter transport. For example, with a field drifter initially located at point P(t) when κ = 2, the bounds on the modeled drifter's acceptable speeds and directions are

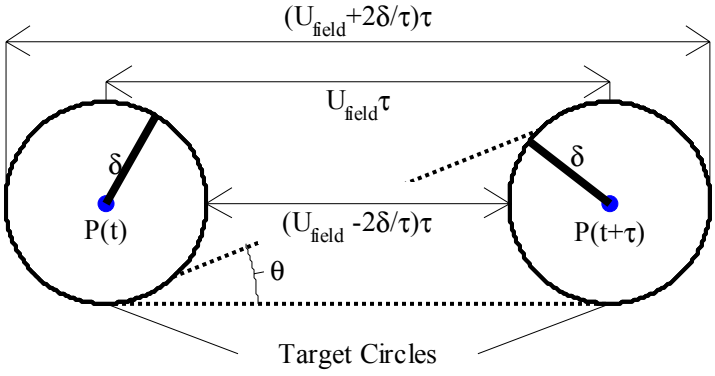

Figure 2.11 –Target circles around points P(t) and P(t+τ), demonstrating the parameters of the Circle Assessment technique. Arrows indicate displacement dimensions between target circles.

$U_{field} \pm 50\%$ and $\hat{u}_{field} \pm 26.5°$. When $\kappa = 3$, these ranges are decreased to $U_{field} \pm 33\%$ and $\hat{u}_{field} \pm 18.4°$. Therefore as κ increases, the ranges of acceptable error in the modeled speed and direction decrease (Figure 2.12), and model must be more successful in reproducing the observed velocity field to be considered "perfect."

The bounds of modeled speed and direction calculated with Eqs. (2.31) and (2.32) represent the absolute extremes of their variables, and a "perfectly" modeled drifter may not have both its speed and direction equal to these bounds. Considering a situation where $\kappa = 2$, the modeled drifter speed may equal 150% of U_{field} only if the modeled drifter direction was parallel to the field drifter direction. The modeled drifter would also have to be initially located on the field drifter's target circle at time t at the point farthest from the $t+\tau$ target circle. For modeled drifters initially located at any other location within the t target circle, the allowable modeled speed would be less than 150% of U_{field}. Similarly, for the modeled drifter's directional difference to equal the bounds predicted from Eq. (2.32), the drifter must travel at a speed equal to approximately 111% of U_{field} and be located on the field drifter's target circle at time t at one of the points perpendicular to the field drifter's direction of travel. Given that drifter motion is a result of the interplay between its speed and direction, the ranges of each velocity component implied by κ must be used cautiously in describing model skill. The ranges serve only as indicators of the model's margin for error, and must not be misconstrued as implying actual

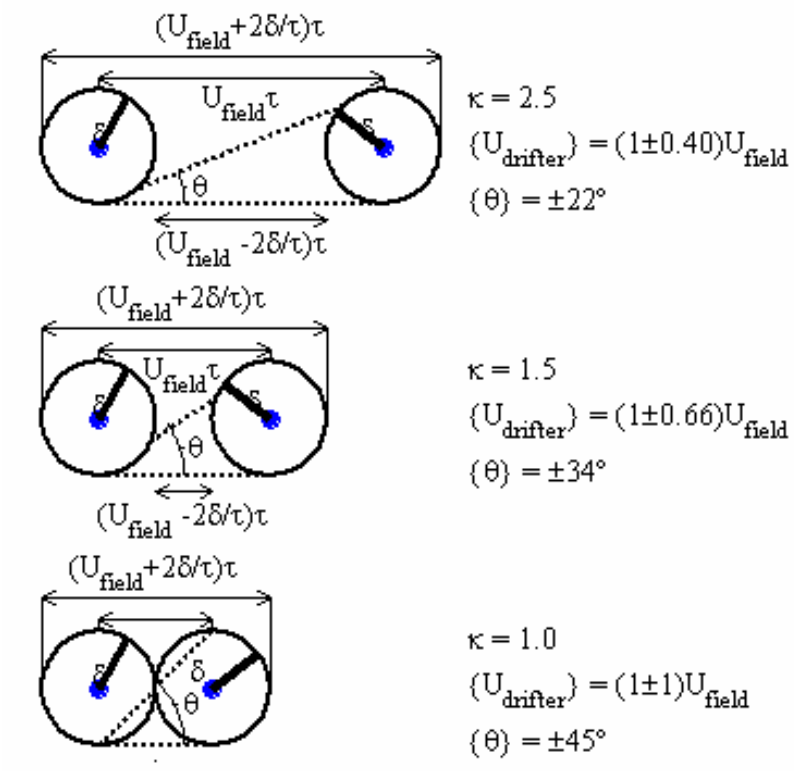

Figure 2.12 – Decreasing error ranges with increasing drifter target ratio (κ) due to increased field drifter displacement.

discrepancies between modeled and observed drifter velocities. (This point is developed further in Section 4.3).

As implied in Figure 2.12c, when κ decreases below one the field drifter's target circles overlap and ranges of error calculated from Eqs. (2.31) and (2.32) no longer apply (Figure 2.13). In this situation, modeled drifters in the overlap region may potentially travel in any direction (at certain speeds) and still remain in the $t+\tau$ target circle. As shown with drifters #4-#6 (Figure 2.13), the model could predict drifter movement in directions completely opposite to that of the field drifter and still be considered "perfect." Such situations are completely unacceptable for assessing model skill, making $\kappa = 1$ a threshold value for implementation of the Circle Assessment technique. Values of τ used in Eq. (2.30) should be selected so that $\kappa \geq 1$.

In many situations, field drifter displacement (and therefore κ) will increase with time. As such, to implement the circle assessment technique it is necessary to define a time at which κ is to be evaluated when assessing model skill. Two appropriate times were considered herein:

> $\tau = \tau_d$: *the "separation time", defined as the first time at which the modeled drifter path separates from the field drifter path by a pre-defined distance (either the radius of the target circle or the error circle)*
>
> $\tau = \Delta t$: *the timestep of the hydrodynamic model over which the model drifters move on a straight path.*

The first time choice is variable, and its value will depend on the model's ability to successfully predict the observed drifter paths. As such, analyses using the separation time will indicate the skill of the model. In contrast, the second time choice is fixed, and is more useful at indicating trends in the modeled velocity field with respect to the velocity field implied from the field drifter motion. Descriptions of analyses using divergence time are given in the following section; Model timestep analyses are discussed in section 2..8.

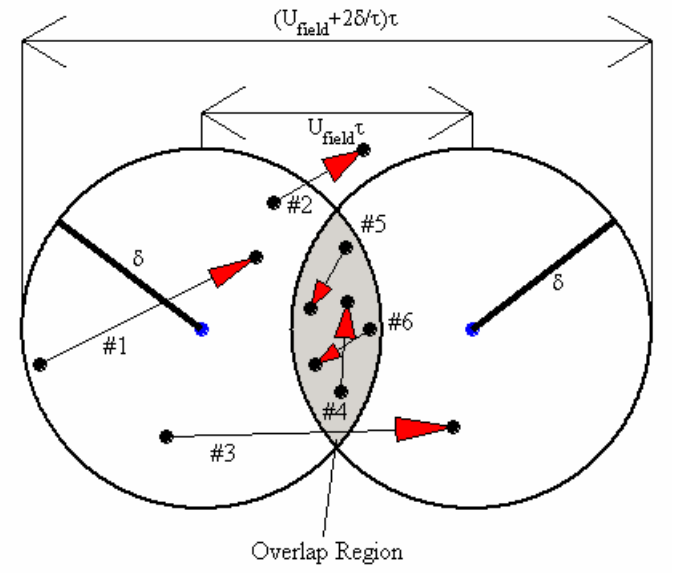

Figure 2.13 – Overlapping target circles when $\kappa < 1$. Drifter movement (arrows) in the overlap region (grey) can be contrary to the field drifter movement making Eq. (2.31) and Eq. (2.32) inapplicable.

2.7. Circle Assessment Method #1 - Separation Time Analysis

2.7.1. Definition

It can be argued that any hydrodynamic model combined with any drifter model will eventually produce divergent predictions of drifter position in a sufficiently complex flow field. The separation time (τ_d) of the modeled drifter path is defined as the time at which the modeled drifter first separates from the field drifter by a pre-determined distance. Within this research, two separation times are considered: 1) the "perfection time" (τ_p) defined as the time when the modeled drifter first departs the target circle of the field drifter, and 2) the "acceptable time" (τ_a) defined as the time when the modeled drifter first departs the error circle of the field drifter. Analyses based on the model perfection times and acceptable times provide different insights into model behavior because they are based on different time and length scaleS.

2.7.2. "Perfection" Analyses using Target Circles

As discussed in Section 2.6.3, a model is considered to "perfectly" reproduce the field drifter motion if the model drifter is separated from the field drifter by a distance less than the target circle radius (δ). At all times prior to the perfection time (τ_d), the modeled drifter is located at a position in space that is within one target circle radius from the field drifter position, suggesting that the model accurately predicts the drifter position within the target circle bounds for that position. The perfection time is therefore the limit after which the model was unable to reproduce the observed drifter motion to the degree of certainty conveyed with the target circle.

Evaluating the drifter target ratio (2.30) when $\tau = \tau_d$ produces the largest κ value for which the hydrodynamic model skillfully (or "perfectly") predicts drifter movement. This value, referred to as κ_{max}, is given as:

$$\kappa_{max} \equiv \frac{U_{field}\tau_d}{2\delta} \tag{2.33}$$

and larger κ_{max} values imply greater model skill in predicting drifter movement. As τ_d may be greater than, equal to, or less than the model timestep (Δt), modeled and field-observed drifters speeds from multiple model timesteps may be used in computing κ_{max}. Figure 2.14 demonstrates determinations of κ_{max} in situations when 1 and 3 timesteps (and therefore 1 and 3 drifter velocities) are included. For instances when $\tau_d \leq \Delta t$ (Figure 2.14A) κ_{max} is calculated directly from Eq.

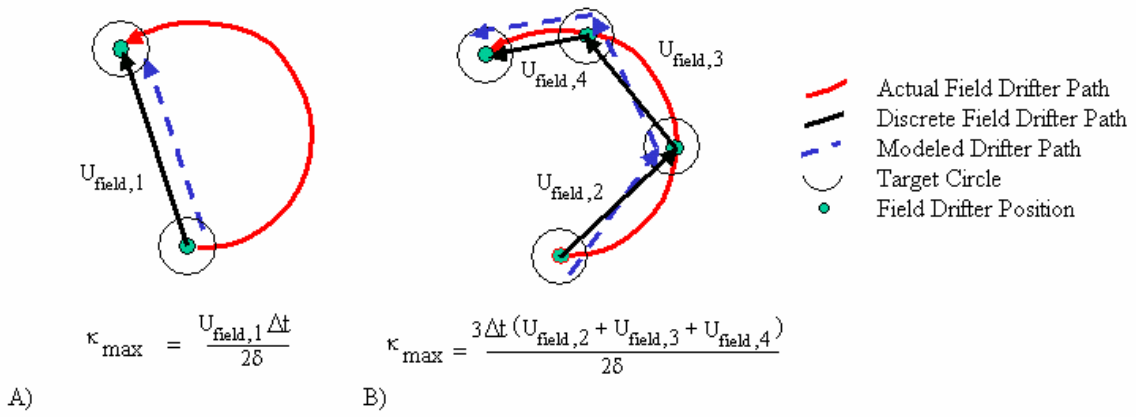

Figure 2-14 Calculating κ_{max} over 1 & 3 model time steps – A) over a single time step κ_{max} is calculated from Eq. (2.33), B) over multiple time steps, κ_{max} is calculated using the sum of the field drifter displacements over each time step.

(2.33). In situations where $\tau_d > \Delta t$, the U_{field} term in Eq. (2.33) becomes the sum of the U_{field} values over each timestep included in τ_d (Figure 2.14B). Equations (2.31) and (2.32) are only applicable for situations when $\tau_d \leq \Delta t$, therefore κ_{max} may not be useful for determining the smallest error ranges for acceptable modeled drifter speeds and directions.

Figure 2.15 illustrates the concept of κ_{max} using field drifter data from the March 25, 2003 Marmion Marine Park drifter deployment (See Chapter 3). In this example, the modeled drifter path (blue arrow) over a 1200 second timestep separates from the field drifter path (black line) by a distance equal to the target circle radius (δ = 10m) only after 1161 seconds. Over this time, the field drifter was displaced by 151m, which results in κ_{max} = 7.57 from (2.30). Using (2.31) and (2.32), this κ_{max} value implies that the modeled drifter speed must have been within ±13% of the field drifter speed, and its directional deviation was less than 7.5°. It is also illustrative to note how the position of the modeled drifter with respect to the field drifter changes over the shown period. Initially the modeled drifter was located to the right of the field drifter path, whereas for τ > 540s, the drifter was on the left. This change in orientation reflects the equivalency of all positions within the field drifter's target circle as the change does not affect the validity of the modeled drifter path.

The perfection time analysis, equation (2.33), may be applied at any time throughout the drifter experiment. To simplify the analysis, however, it is suggested that κ_{max} be calculated for each P(t) corresponding to the field drifter position at the

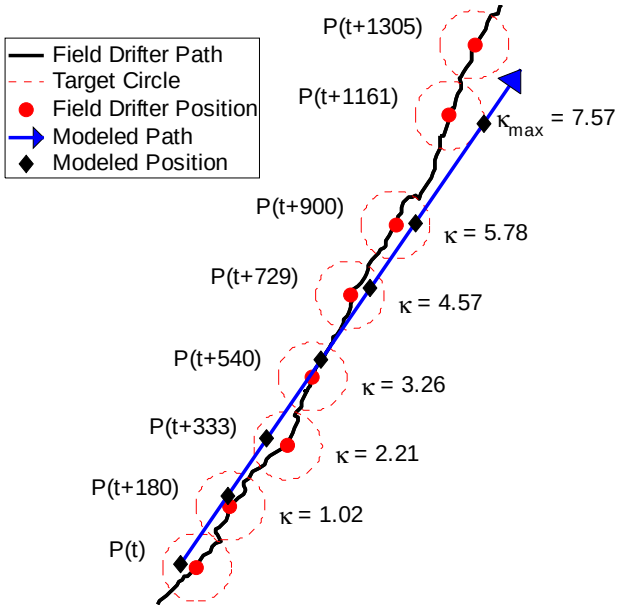

Figure 2.15 - κ_{max} defined as the largest κ value at which the modeled drifter remains within the field drifter's target circle. In this figure, κ_{max} = 7.57 as the modeled drifter is no longer in the field drifter's target circle when τ > 1161. Data from the March 25, 2003 drifter experiment (See Chapter 3).

beginning of each model timestep. Depending on the duration of the field experiment, calculating κ_{max} at each timestep should provide a sufficient sample set for statistical analysis of the implied error ranges in speed and direction. Standard statistics of the κ_{max} values (mean, standard deviations, percentiles) from all drifters and times during the all experiments are used to quantify the model's success.

2.7.3. "Acceptable Classification" Using Error Circles

By limiting model and field path comparisons to times preceding the perfection time (Section 2.7.2), the behavior of the modeled drifters after "perfection" is not included in model analysis. This presents a possible situation in which two modeled drifters may have similar κ_{max} values, with one model better reproducing the field drifter path after the perfection times (Figure 2.16). To ameliorate this problem, error circles are used in making model assessments after the separation time.

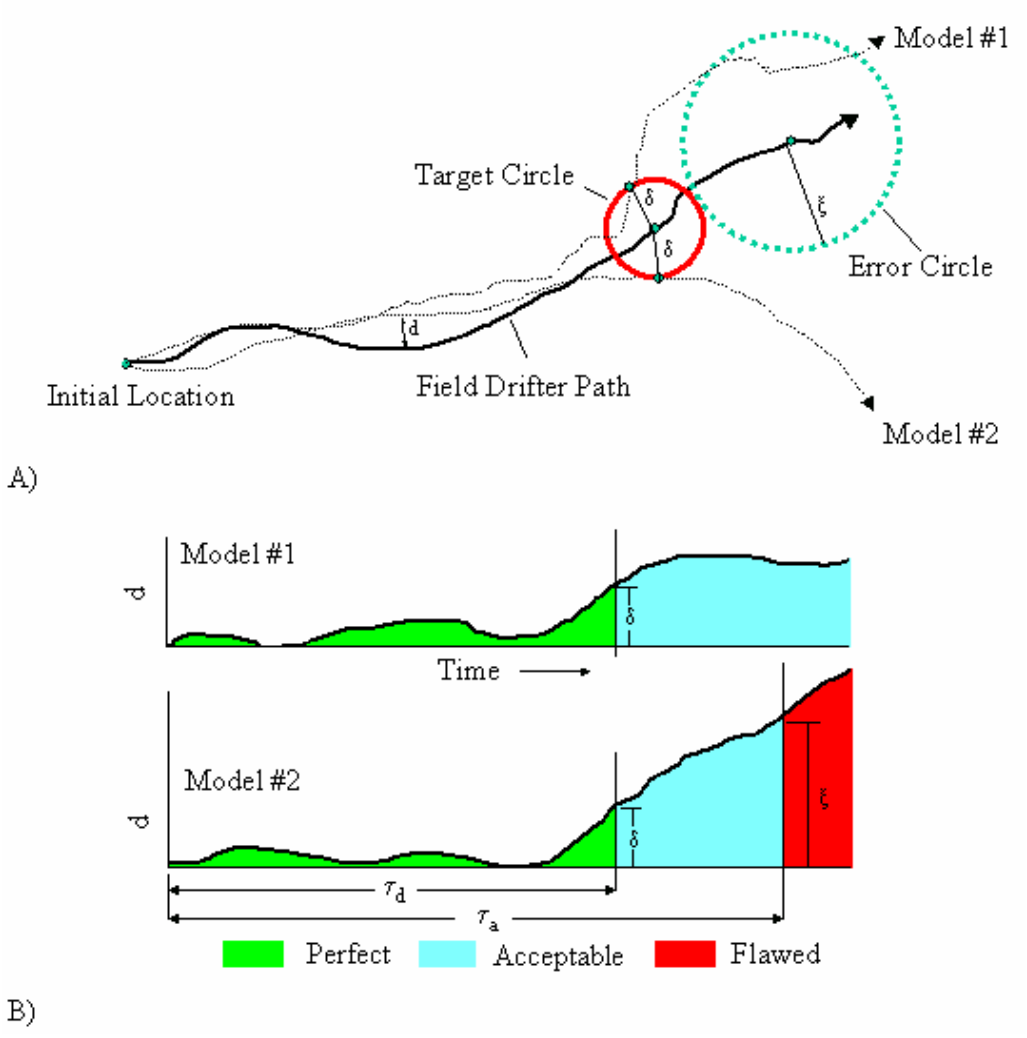

Figure 2.16 – Acceptable/Flawed Classification using Error Circles – A) drifter paths showing separation with field drifter relative to δ and ξ, B) separation (d) with time. Model #1 is a better representation of the field drifter path although Model #1 and Model #2 have identical κ_{max} values.

Whereas target circles mark the threshold between perfect and acceptable model results, error circles mark the threshold between acceptable and flawed models. The error circle always encompasses the target circle, and the time required for a modeled drifter to travel outside of an error circle is greater than the model perfection time. As shown in Figure 2.16, modeled drifters #1 and #2 have identical perfection times (and therefore identical κ_{max} values), however the model #1 drifter path lies within the shown error circle when the model #2 drifter path does not. This indicates that model #1 better represents the field drifter path after the perfection time. By the end of the shown simulation, model #2 is considered a "flawed" model in that it predicts drifter motion outside of the error circle and therefore does not well represent the motion of the field drifter. Model #1 and Model #2 may be compared using the acceptable time (τ_a) as this is the time required for each model to become flawed. Using the example in Figure 2.16, Model #2 is less skillful than Model #1 in representing the field drifter motion because Model #2 has a shorter acceptable time

2.8. Circle Assessment Method #2 - Model Timestep Analyses

2.8.1. Success Probability and κ-scores

Upon setting $\tau = \Delta t$ in (2.30), κ reflects the model skill required to successfully transport drifters over each model timestep. This tests the model's ability to accurately represent the field drifter's path using a single representative velocity (See Figure 2.1). If the model predicts drifter transport into the $t+\Delta t$ target circle, then it is "perfect," and by determining the percentage of drifter-timesteps (defined as the number of drifters multiplied by the number of timesteps the drifters were deployed) over which the model is "perfect" it is possible to determine the model's likelihood of successful drifter transport. This "success probability" may then be compared to those obtained from different model setups (i.e., changes in model timestep, grid resolution, forcing, or drifter model), thus providing a means for assessing model improvement with setup alterations.

One problem with assessing model skill solely based on it's success probability is that the degree of difficulty in correctly modeling drifter movement at each timestep is not included in the skill assessment. Along with calculating the success probability, the model timestep analysis incorporates an alternative assessment method, the κ-score, in its determination of model skill. The model κ-score is defined as:

$$\kappa\text{-score} = \frac{\sum_{j=1}^{N} \kappa_{A,j}}{\sum_{j=1}^{N} \kappa_{P,j}} \times 100\% \qquad (2.34)$$

where $\kappa_{A,j}$ is the κ value achieved for drifter-timestep "j", $\kappa_{P,j}$ is the maximum possible κ value for the drifter-timestep as calculated from (2.30) (with $\tau = \Delta t$), and N is the total number of drifter-timesteps in the model simulation. For drifter-timesteps when the model predicts drifter transport into the $t + \Delta t$ target circle, $\kappa_{A,j} = \kappa_{P,j}$ and the κ-score is unchanged. For instances at which the model fails to predict drifter transport into the $t + \Delta t$ target circle, $\kappa_{A,j}$ is the maximum κ value over drifter-timestep j for which the model "perfectly" predicted drifter transport. In such cases, $\kappa_{A,j}$ is similar to κ_{max} except that the τ_d term in Eq. (2.33) is limited to values less than Δt.

The κ-score is therefore a weighted mean descriptor of model success, with the weighting equivalent to the achieved κ value. The weighting is necessary given that larger separations between target circles require a more precise model to correctly predict drifter transport and that the model assessment method must not penalize the model too strongly for any incorrectly modeled drifter movement under such conditions. For example, consider a drifter-timestep where $\kappa = 5$ and the model drifter diverges from the field drifter path after 95% of the model timestep. Had the timestep been shorter by 5%, the model would have

correctly predicted drifter transport and the κ value for the shorter timestep would have been 4.75. With Eq. (2.34), the successfully modeled 95% of the drifter timestep would be included in the model assessment as $\kappa_{A,j}$ = 4.75, and the model's failure to completely model drifter movement over the timestep would be reflected as $\kappa_{P,j}$ = 5. The contribution to the overall κ-score from this drifter-timestep would be 95%. Without weighting, the "near-miss" by the model at successfully predicting drifter transport at this drifter-timestep would not be distinguishable from complete model failures at predicting correct drifter transport.

2.8.2. Comparative Failure Analysis

While using κ-scores and success probabilities to quantify model skill (§2.8.1), the model timestep analysis focuses on instances of model success. Instances of model failure (when the modeled drifter fails to enter the field drifter's target circle) may prove equally insightful as to the relative merits of one simulation over another. As an example, consider three simulations, each incorporating a different drifter model (Figure 2.17). Comparisons of the model results (at a selected instance within the simulations) indicate that the GABI-F drifter model successfully transports the drifter into the field drifter's target circle when the Lagrangian and Leeway drifter models both fail. For this instance, results from the simulation using the GABI-F drifter model are clearly favorable. Tallying the number of instances for which similarly favorable results were achieved, and comparing this tally with that of when an alternative simulation produced favorable results provides a relative measure of the ability of each simulation to reproduce the observed drifter motion. This type of failure analysis, as it is used only to compare one set of drifter results to another, is heretofore referred to as "comparative failure analysis."

2.8.3. Causative Failure Analysis

Failure analyses may also serve diagnostic purposes to suggest how a model or model setup might be

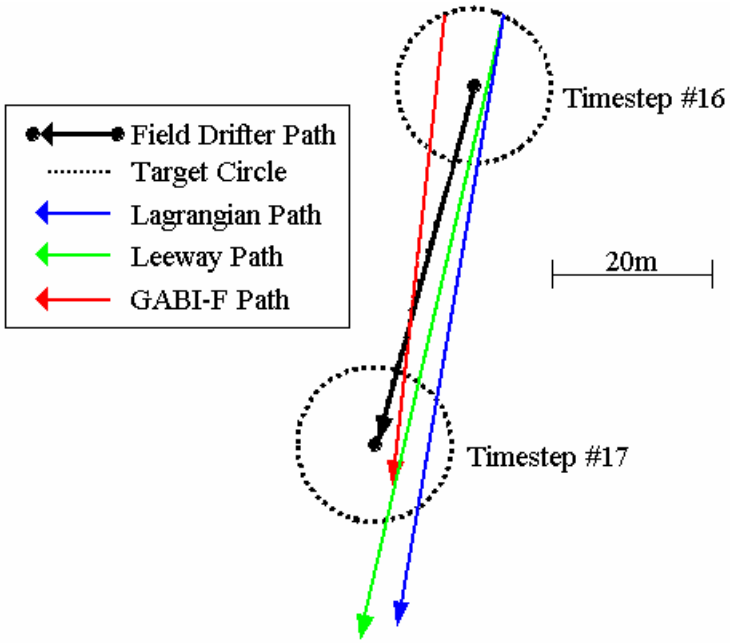

Figure 2.17 – Comparative failure analysis for comparing drifter model's relative merit. Over the same timestep, the GABI-F drifter model predicts successful drifter transport when the Lagrangian and Leeway models predict the drifter will travel past the target circle. Data shown from the D2 (March 21) simulation of field drifter #3 (See §3.6, §4.2).

improved. For example, in Figure 2.17 drifters transported according to the Leeway and Lagrangian model each traveled through field drifter's target circle. In these instances, the simulations were unsuccessful because the model drifter speeds were too high despite that their headings were within the acceptable range required for success (See §2.6.2). If a large percentage of drifter-timestep failures were caused by excessive modeled drifter speed, the conclusion could be made that the model tends to over-predict drifter velocities. Model enhancements to correct this identified problem could then be implemented, hopefully yielding improved drifter path solutions in future simulations. As this type of failure analysis strives to identify causes of model failure, it is heretofore referred to as "Causative Failure Analysis."

While conducting a Causative Failure Analysis, instances of failed drifter movement over each timestep are classified based on the reason(s) the model failed to adequately predict drifter movement. Modeled drifters that fail to enter the $t + \Delta t$ target circle must meet one of the following 4 conditions (Figure 2.18):

Condition #1 – "Direction Error" – Modeled drifter's speed is within the acceptable range for its initial position, but its direction is not suitable for its speed.

Condition #2 – "Speed Error" – Modeled drifter's direction is within the acceptable range for its initial position, but its speed not suitable for its direction of travel.

Condition #3 – "Combination Error" – Both the modeled drifter's speed and direction are within the acceptable ranges for its initial position, but the combination makes the transport unacceptable

Condition #4 – "Total Error" – Both the modeled drifter's direction and speed are outside of the allowable ranges for the drifter's initial position.

Analyzing the condition under which a modeled drifter failed to enter the target circle may suggest factors in a model that led to the failure. For example, consistent under-predictions of the current speeds may indicate insufficient energy input into the model, suggesting (perhaps) the model's predicted mixed layer is too deep, the wind speeds are underestimated, or the model is excessively energy-dissipative. Similarly, consistent errors in the drifter direction may indicate bias within the model wind forcing or transport algorithms, or perhaps patterns of wind variability that are not captured by the available field sensors. The κ values for instances of model failure are also important, as lower κ values imply greater inaccuracy of the predicted velocity field. Failures for instances of higher

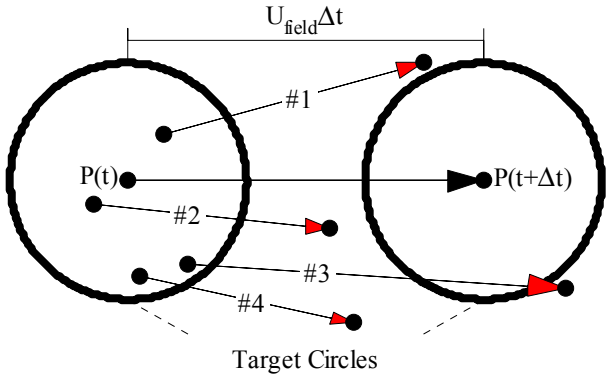

Figure 2.18 – Conditions for model inadequacy identifiable with the Circle Assessment method using the model timestep to define κ. Black arrow indicates field drifter transport pathway, red arrows indicate failed model drifter transport pathways. Numbers refer to the failure conditions described in text.

κ values may not be as illustrative of problems in the model setup. As such, causative failure analyses using the model timestep are likely to be subjective with the results open to multiple interpretations.

Figure 2.19 contains a set of sample results from a fictitious analysis using the model timestep. In this sample, 53 out of 100 simulated drifters arrived in their $\tau+\Delta t$ target circles. Of the 47 drifters that were modeled unsuccessfully, 67% failed because of their predicted speed, and 97% of those drifters failed because they traveled too fast. Most drifters that failed due to their modeled direction traveled on courses that deviated from the field drifter course in a counter-clockwise direction, and the majority of failures were due to predicted speeds rather than predicted directions of travel.

Number of Drifters		4					
Number of timesteps		25					
Total Evaluations		100					
Percentage Success		53%					
Percentage Failure		47%					
k-values for Successes			Speed Error Range		Direction Error Range		
mean		1.5	66.67%		33.65357		
Std. Deviation		1.3					
min		0.4	250.00%		<>		
max		3.7	27.03%		15.10762		
25th Percentile		1.1	90.91%		42.22789		
Median		1.4	71.43%		35.49918		
75th Percentile		2.3	43.48%		23.47311		
Failure Summary							
k-values for Failures			Speed Error Range		Direction Error Range		
mean		3.4	29.41%		16.38		
Std. Deviation		1.2					
min		1.2	83.33%		39.79		
max		9.4	10.64%		6.07		
25th Percentile		2.8	35.71%		19.65		
Median		3.8	26.32%		14.74		
75th Percentile		4.5	22.22%		12.53		
Failure Conditions				too slow	too Fast	CW	CCW
#1 - Direction Only			11%			20%	80%
#2 - Speed Only			67%	3%	97%		
#3 - Combination			0%				
#4 - Both Speed & Direction			22%	45%	55%	34%	66%
Individual Failure Descriptions							
Failure #	k value	Condition	Description				
1	3.5	2	Fast				
2	3.7	2	Fast				
3	1.2	4					

Figure 2.19 – Sample results from the Causative Failure Analysis. Important points are highlighted in gray.

One possible interpretation of the results in Figure 2.19 is that the model over-predicted the drifter's speed, on average. This is evident in those model drifters which failed to reach their $\tau+\Delta t$ target circles, but also might be evident in the successfully modeled drifters because those instances tended to have lower κ values (and therefore higher ranges of error in their allowable modeled drifter speeds). It is possible that the modeled drifters had speeds near the higher end of their error ranges thereby supporting the possibility the model is over-predicting drifter speed. To check this possibility, the model setup could be adjusted to include more energy dissipation and thereby reduce the predicted drifter velocities.

Another interpretation of the results in Figure 2.19 is that the model is more suitable to reproducing low-speed currents. The model was more successful for instances when κ values were low, and given that all analyses are based on the identical model timestep, lower κ values indicate lower field drifter velocities. The range in κ values in the results also suggests that the field drifters underwent an acceleration during the field experiment, and that this acceleration may not have been resolved in the model. This suggests (among other possibilities) that perhaps the model input forcing (wind data, tidal information) may not be accurate or may not be representative of the forcing during the experiment in the vicinity of the drifters. This possibility could be tested by using alternative input data (if available) or by modifying the input data and re-running the model in order to assess any changes to the predicted drifter movement.

The causative failure analysis, while necessarily not providing conclusive evidence of model behavior, does provide the user with the ability to make informed inferences as to how the model results might be improved through various model adjustments. In the process of developing a validated numerical model of drifter movement, it is envisioned that the causative failure analysis be used in conjunction with the separation analyses (§2.7) and other model timestep analyses (§2.8.1-2.8.2) to both assess and improve model skill. After various iterations and improvements based on the model timestep analyses, the separation time analyses may be used to assess and define the achieved skill of the refined hydrodynamic model.

2.9. Methodology Summary

Existing particle tracking models simulate the movement of field drifters as mass-less, Lagrangian water particles. Prior researchers' (section 2.2) used empirical leeway factors to adjust for direct wind effects on field drifter paths, but have not quantitatively modeled forces acting on the drifter beneath the water surface. The new GABI-F drifter model (section 2.3) incorporates the drifter and fluid physical properties to model drag and inertia effects on drifter motion.

Researchers who have developed comparative techniques for assessing model skill using drifters each tailored their method to suit the intended purpose of their work (Section 2.4). For example, because Thompson et al (2003) were only interested in developing search radii for rescue operations, they developed a statistical analysis method based solely on drifter displacement rather than on drifter speeds and directions. Toner et al (2001) developed a similar method to assess model improvements, using the ratio of model/field drifter separation to field drifter displacement as an indicator of model skill. Each of these published methods, while applicable for the intended purpose of the developers, is unsuitable for quantifying the skill of a hydrodynamic model in reproducing the observed directions and speeds of drifter transport. The principle limitations of each method are their dependence on drifter displacement (while losing information on the direction of drifter transport) and the long time-horizons of their comparisons, without considerations of error integration due to model and field drifter divergence.

The circle assessment method (section 2.6-2.8) was developed to assess hydrodynamic model skill through comparisons between modeled and observed

drifter paths over numerous short time-horizons (relative to the length of the drifter experiment). The method is based on the drifter target ratio (Eq. (2.30)), which relates the displacement of the field drifter to user defined length scales for model assessing model performance.. An hydrodynamic model is considered "perfect" if it predicts the transport of modeled drifters to locations within a distance δ of the field drifter. An acceptable model is similarly defined, where the predicted drifter position is within a distance ξ of the field drifter and $\xi > \delta$. The skill of the hydrodynamic model is determined through statistical analysis of the drifter target ratio defined at each drifter-timestep based on either the model timestep or the model divergence time. The drifter target ratio also provides a method for quantifying the allowable errors in modeled drifter speeds and directions which allow the model to still be considered "perfect" in it's ability to reproduce drifter motion. Implicit in this approach is that more skillful models will have lower ranges of error in their predicted drifter speeds and directions.

In assessing the model's success in reproducing the observed field drifter paths (and therefore the observed waterbody currents) at multiple times throughout a simulation, the circle assessment method allows for the comparison of model results from periods with different forcing conditions. Two time periods (the separation times or fixed time intervals) may be used in the circle assessment method, with each period providing different yet valuable information concerning model performance. The circle assessment method results may also provide model diagnostic information leading to model improvements.

Analysis using perfection times, defined as the times after which modeled and field drifters are separated by a distance greater than a user-defined length scale for model perfection, are used to quantify the model's ability to reproduce observed drifter speeds and transport directions. For times greater than the perfection times, comparisons between modeled and observed paths are less meaningful because the model and field drifters may then be transported by different forcings. This key insight allows for evaluation of the local velocity field in the hydrodynamic model without the conclusions being distorted once the modeled and observed drifter paths have separated. Such comparisons after separation are, however, indicative of model behavior on scales larger than required for model perfection. Periods of model acceptability (but not model perfection) may prove insightful for describing the ability of a model to reproduce drifter paths.

Alternatively, when the circle assessment method is applied over a pre-defined time period (such as the model timestep) the method provides both model skill and diagnostic information which may indicate trends in model performance. For example, the circle analysis results may indicate that the model perfectly predicts drifter transport over 33% of all drifter-timesteps, and is (on average) under-predicting the drifter velocity. Such a result may then direct the modeler to make adjustments to the model setup in order to achieve greater agreement with the field data. Assessments with this method are more subjective than those made using the separation time, and are intended for use in making model-setup improvements so that subsequent analyses using non-diagnostic metrics (κ-scores, success probabilities, and κ_{max} values) indicate greater agreement between the model and field drifter paths.

3. Model & Field Experiment Setup

3.1. Introduction

This chapter provides background information on the hydrodynamic model used in this work and on the Marmion Marine Park (MMP) study area in Western Australia. Section 3.2 contains a description of the numerical methods incorporated within the ELCOM hydrodynamic model, and the numerical model setup specific for MMP is detailed in section 3.3. The final sections (§3.4-3.6) include a discussion of the MMP field experiment setup and results. Sections 3.2 and 3.3 include a brief literature review concerning the ELCOM hydrodynamic model and previous studies conducted at Marmion Marine Park, respectively. Results from the MMP numerical modeling are presented in Chapter 4.

3.2. The ELCOM Hydrodynamic Model

Hydrodynamic modeling of MMP was conducted using the Estuary and Lake Computer Model (ELCOM) from the Centre for Water Research at the University of Western Australia. ELCOM is a three-dimensional hydrodynamic model that solves the unsteady 3D-Reynolds-averaged Navier-Stokes equations using a semi-implicit free surface method with quadratic Euler-Lagrange momentum discretization (Hodges, 2000). The free-surface evolution is governed by vertical integration of the continuity equation for incompressible flow in the water column applied to the kinematic boundary condition (e.g., Kowalik and Murty 1993). The fundamental numerical scheme is adapted from the TRIM approach of Casulli and Cheng (1992) with modifications for scalar conservation, numerical diffusion, and implementation of a mixed-layer turbulence closure (Hodges et al, 2000; Simanjuntak et al 2006). The physical domain may be discretized according to either a rectangular Cartesian or a perturbation curvilinear coordinate system (Hodges and Imberger, 2001), and grid cell vertical dimensions may vary across grid layers but are uniform within each horizontal layer. The grid stencil conforms to the Arakawa-C format (Arakawa and Lamb, 1977), with velocities defined on the cell faces and scalar values calculated at the cell centers.

A previous version of the model, using the vertical mixing model of Laval et al, (2003) instead of that from Simanjuntak et al (2006), has been successfully applied to study internal wave dynamics (Laval et al, 2003) and surface circulation patterns (Marti and Imberger, 2004) in Lake Kinneret, Israel. This dissertation presents one of the first applications of the ELCOM model including the mixed-layer turbulence closure of Simanjuntak et al (2006), and is one of two concurrent applications of ELCOM to MMP. The other ELCOM application to MMP (Hillmer and Imberger, 2006) has validated ELCOM use in predicting MMP circulation by comparing the modeled circulation to the Eulerian velocity data gathered and presented by Zaker et al (2001, 2002). This is the first use of field drifter data in estimating the ability of the ELCOM model to predict surface layer circulation.

3.3. Marmion Marine Park Description

3.3.1. Site Description

Marmion Marine Park (MMP) is a shallow ecological reserve off the coast of Western Australia (Figure 3.1), approximately centered at latitude 31º45' S and longitude 115º 45' E. It is bounded on the east by a

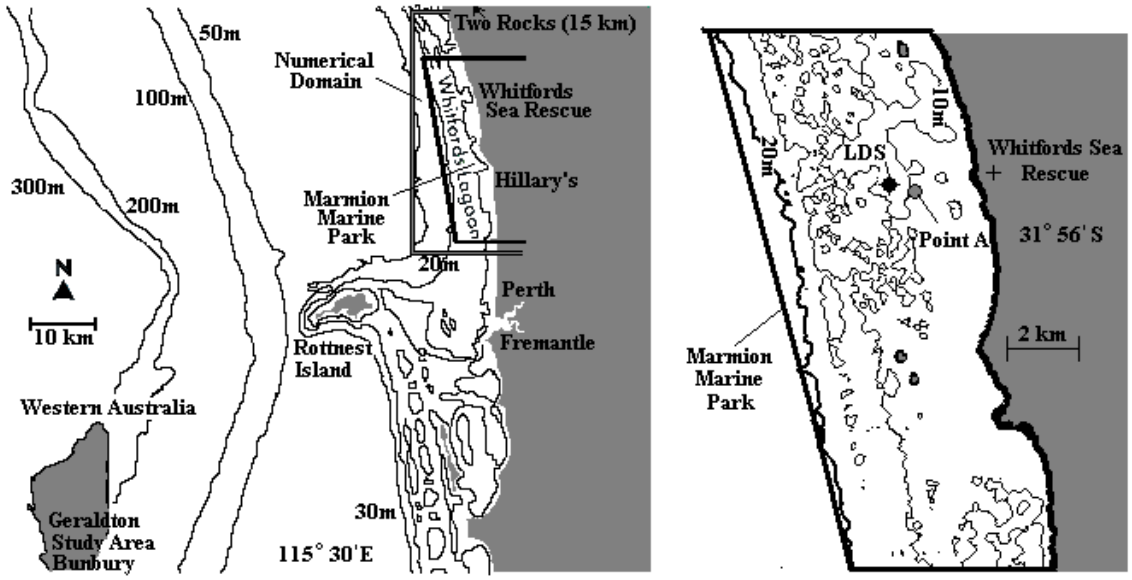

Figure 3.1 – Map of Marmion Marine Park, Western Australia.

north-northwest tending shoreline and on the west by submerged coral reefs approximately 10 km from shore. The reserve encompasses 27 km in the N-S direction, from Hillary's Boat Harbor in the south to Burns Beach in the north. The field experiment was conducted in March 2003 with support from the Perth Water Corporation, the Centre for Water Research at the University of Western Australia, and the Australian-American Fulbright Association. Field sampling was conducted in Whitford's Lagoon, a shallow (< 14m deep) lagoon shoreward of submerged reefs. These reefs separate the lagoon from the influence of the southward Leeuwin Current further offshore (Zaker et al, 2001). The lagoon is characterized by low tides, strong southerly summer breezes, and low vertical stratification (Hodgkin and Di Lollo, 1958; Zaker et al. 2001). Based on a 1993 field study at this site, the surface circulation and mixing processes in this region are dominated by surface wind stress forcing being balanced by bottom drag with the predominant current being aligned alongshore (Zaker et al., 2001) .

Within Whitford's Lagoon is the Beenyup outfall, which discharges treated effluent from the Beenyup Waste Water Treatment plant. This plant treats much of the waste generated by the city of Perth, Australia, and is predicted to increase its discharge due to the steady increase in population living around the area (Lord and Hillman, 1995; Zaker et al, 2002). Based on extensive studies of effluent plumes in other areas (e.g., Fisher et al, 1979; Lee and Neville-Jones, 1987; Roberts et al., 1989), it is expected that dilution and dispersion of the effluent plume in MMP plays a role in maintaining the health of the marine park ecosystem. Understanding these plume processes was the impetus for the previous and present research conducted within the area.

3.3.2. Field Experimental Setup

As part of a 5-day experiment designed to estimate advection and dispersion within MMP, four surface drifters were deployed and tracked for a period ranging from 3-10 hours per day on March 20-21 and March 25-27, 2003 (Table 3.1). For reference purposes, each drifter deployment is forthwith referred to as "DX" where X is an integer from 1 to 5 corresponding to the day out of the 5 experiment-days upon which the drifter deployment occurred. The drifters were designed and fabricated by staff at the Centre for Water Research at the University of Western Australia with

Table 3.1 – Field Drifter Deployment Schedule for 2003 MMP Sampling

		Experiment Times		
Date	Deployment Name	Deployment	Retrieval	Duration
March 20	D1	11:47	16:27	4 Hrs. 40 Min.
March 21	D2	06:29	15:25	8 Hrs. 56 Min.
March 25	D3	06:37	15:33	8 Hrs. 56 Min.
March 26	D4	06:25	14:30	8 Hrs. 05 Min.
March 27	D5	06:22	16:18	9 Hrs. 56 Min.

funding and deployment partially supported by the Perth Water Corporation. Drifters were deployed early in the morning except for the first day of the experiment, when the Lake Diagnostic System (LDS) weather station was being deployed. The LDS is a buoy-mounted weather station (CWR#1, 2003), and was located approximately 2.3 km offshore (Figure 3.1), and measured wind speed, wind direction, solar radiation, air temperature, and humidity at 9-10 second intervals over most of the experiments (See Section 3.5).

On each day, the drifters were deployed in a triangular cluster over point A (Figure 3.1). Drifter #1 was located at point A, while the three other drifters were located at the corners of a roughly equilateral triangle centered over point A with the apex 150 m north of A. The drifters deployed at the triangle corners were given identification numbers 2, 3 and 4 starting from the north apex and proceeding clockwise.

The GPS-equipped drifters (Figure 3.2) consisted of a set of two vertically oriented metal frames, across each of which a tarpaulin sail was fastened to provide a large drag area. The frames were held mutually perpendicular, giving the drifter a cross shape in plan view. The center of each drifter's sail was located at 2 m depth, with the sail portion of the drifter extending from a depth of 1.5 m to 2.5 m. To reduce wave-induced vertical motion, a horizontal triangular tarpaulin was attached to the bottom of each drifter. A rigid pole running through the center of the frames connected the frames to the floats and transmitting antenna. At the base of this pole, the GPS data logger and power supply were fastened to the frames in a water-tight container. Near neutral buoyancy was achieved by adding weights to the bottom of the frames. The weight of each drifter was approximately 26 kg.

Each drifter recorded its position (latitude and longitude) at 9.5±1 second intervals. Single positions were also reported via SMS mobile phones once every 30 minutes so that the drifters could be easily retrieved, and these positions served as a backup for when an internal logger malfunctioned. Drifters differing in

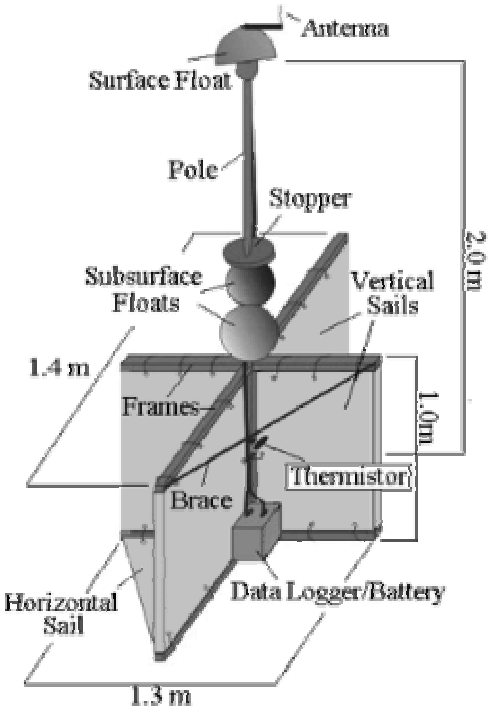

Figure 3.2 – Field Drifter Schematic with dimensions. Each drifter weighted 26 kg, and recorded its position from GPS satellites at 9-10 second intervals.

cross-section but utilizing the same differential GPS technology have been shown to have root-mean-square (RMS) error in the horizontal position of ±10 m (Stocker and Imberger, 2003). The error in the relative position of two drifters has been estimated (95% confidence) to be less than 5 m (Stocker and Imberger, 2003) based on separate tests.

3.4. ELCOM Model Setup & Boundary Conditions

3.4.1. Introduction

While developing the MMP hydrodynamic model, numerous model setups were implemented to assess model sensitivities and obtain greater agreement between observed and predicted drifter velocities. Disagreement between observed and predicted drifter velocities may arise from any combination of error sources, including:

limitations of the ELCOM hydrodynamic model's numerical algorithms

limitations of the MMP model setup and available boundary condition data

inaccuracies in the drifter model used to calculate drifter transport

As the purpose of this research is to assess inaccuracies in the drifter model, the effect of limitations in the ELCOM algorithms, model setup and boundary conditions must be minimized. ELCOM's algorithms have been well validated through many previous projects (See Section 3.2), however the model has been used only once to predict surface water velocities in a coastal system (Hillmer and Imberger, 2006). As such, its capabilities in this realm have not yet been rigorously tested and its limitations for coastal simulation are heretofore unknown. However, the TRIM model that is a predecessor of ELCOM and uses similar methods has been applied, with some success, in numerous coastal simulations, including MMP (Zaker et al., 2001). In the present work, numerous MMP model setups were considered and used in simulations in order to ascertain model sensitivity to setup parameters (grid resolution, time step). Alternative boundary condition (i.e., wind data and pressure gradient assumptions) data were also incorporated when available. The result of using multiple model setups in assessing model skill is that, strictly speaking, the skill of the ELCOM hydrodynamic model is not being directly assessed. Instead, the skill of the ELCOM model *and* setup for simulating MMP currents is being assessed. . That is, error conditions 1 and 2 above are not individually distinguished, as this would require another level of testing that is beyond the scope of the present work. To reflect this fact, the model and setup combinations discussed in the remainder of this work are denoted as the "ELCOM-MMP" model. The following subsections describe the numerous variations in setup parameters used in developing the ELCOM-MMP model.

3.4.2. Computational Grids & Numerical Setup

The extent of the computational domain used in ELCOM-MMP simulations is similar to Zaker et al (2001) and Domain 2 from Hillmer and Imberger (2006), spanning 27.5 km in the N-S direction and 15 km in the E-W direction. The north, west, and south offshore boundaries of MMP were modeled as open boundaries, with a Dirichlet condition for the free surface height and a Neumann condition imposed for momentum transport. Open boundary sea level heights were imposed based on the large-scale coastal sea level gradient and the small diurnal tides were neglected (ff. 3.4.6).

Three computational grids were used in simulating the MMP system, each consisting of rectilinear cells with 1 m vertical grid spacing. The "base case" computational grid consisted of 250m x 250m grid cells aligned with the y-axis parallel to the north. This setup was similar to that used by Zaker et al (2001) and Hillmer and Imberger (2006), and was used as the basis for comparing results from setups with other grid resolutions. Simulations were also conducted

using computational grids with 500m x 500m cells and 100m x 100m cells (*ff.* 4.3.4).

For nearly all ELCOM-MMP setups, models were integrated forward in time at a 10 minute timestep, which is larger than the 120s timestep from Zaker et al (2001) and the 200s timestep from Hillmer and Imberger (2006). The smaller time step is not required for numerical stability with ELCOM, and the larger time step reflects the scales typically used in coastal modeling (Mariano et al, 2002), which are of interest in the present work. Furthermore, as demonstrated by Hillmer and Imberger (2006), the ELCOM model at a smaller time step with open boundaries requires additional damping layers at the boundaries to prevent barotropic waves from being internally-reflected. Undamped reflection of such waves leads to spurious high-frequency oscillations in the solution. Such damping was not needed by Zaker et al (2001) as the TRIM method is numerically more dissipative (due to linear advection in TRIM compared to quadratic advection in ELCOM) and therefore barotropic waves are naturally damped (in TRIM) before significantly developing. At a larger model timestep, numerical dissipation in ELCOM is increased on par with TRIM and effectively damps the higher-frequency oscillations associated with barotropic reflections. In effect, the Hillmer and Imberger (2006) approach damps barotropic waves at the boundaries, whereas the Zaker et al. (2001) and the present approach damps the barotropic waves throughout the domain. A comparative study of how such different approaches affect the modeled drifter paths remains a subject for future work (see Chapter 5). To assess the effects of model timestep on the predicted drifter paths, simulations were conducted using 5, 10, and 20 minute timesteps for the ELCOM-MMP 250m x 250m grid setup (*ff.* 4.3.5).

Since the initial velocity field across MMP cannot be specified, the model requires a "spin-up" period to remove the influence of the initial conditions. Zaker et al (2002) used a two-day spin-up with a constant wind forcing for their MMP simulations. In the present work, spin-up times of 0.5-5.0 days (at 0.5 day increments) were tested using measured wind conditions. The 3.5 day spin-up was selected as sufficient to damp the initial barotropic oscillations that occur due to initial adjustment. For spin-up times greater than 3.5 days, there was a 2.8% RMS difference in surface water speed and a 1.3° RMS difference in surface water direction, which is considered negligible for the present work.

3.4.3. Bathymetry

The bathymetry data used in ELCOM was developed from the nautical charts produced by the Australian Department of Planning and Infrastructure. The charts were manually digitized using ArcView GIS from ESRI, inc., and bathymetric grids were extracted from TIN models of the coastal area. The reference datum for the bathymetry is the NMV/F/6A datum for the Fremantle tide gauging station located approximately 64 km south of point A in Figure 3.1. Depths were measured from mean sea level (MSL), and the mean tidal range for MMP is 0.70 meters (Lord and Hillman, 1995).

As shown in Figure 3.3, the area around point A (the sewage outfall) is 8 to 10 m deep. Southwest and southeast from the outfall lay shallow, isolated reefs and shoals where depths range from 4 to 6 m. The deepest waters in the vicinity of point A are located 500 m to the west in an alongshore channel , where the maximum depth reaches 14 m. The corresponding bathymetry values at the grid cell centers define the discrete bathymetry for the ELCOM model grid.

3.4.4. Wind Forcing

The model was forced with wind data based on measurements from the Whitfords Sea Rescue Station at Ocean Reef (Figure 3.1) and those measured by the LDS (Figure 3.5). The Whitfords Sea Rescue Station anemometer was mounted on top of the building to a height of 10 m above the mean water surface, and was

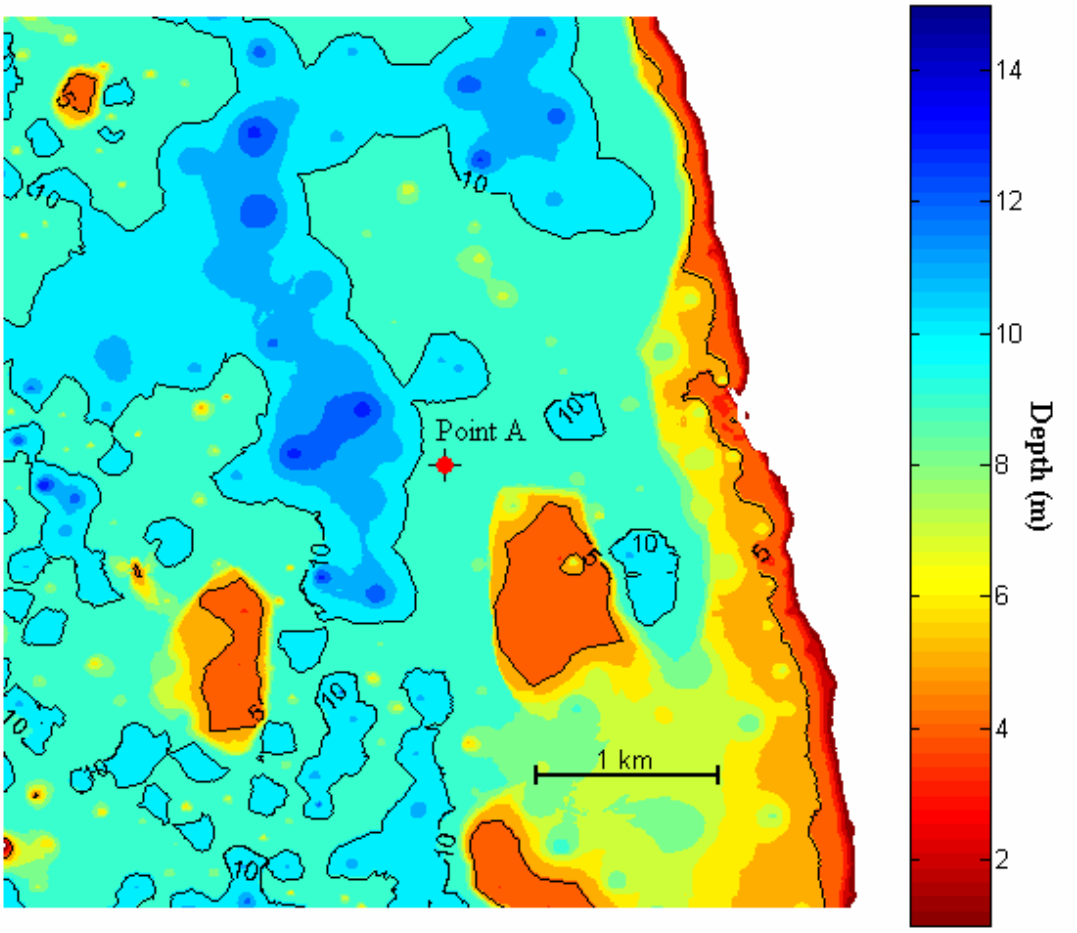

Figure 3.3 – Bathymetry about Point A of the Marmion Marine Park Study Area

approximately 20 m onshore from the water. Based on my personal observation of the Whitfords station, branches from a large tree impeded the winds blowing from the south and south east, although to my knowledge, independent testing of the Whitfords data has not been made to determine the magnitude of the interference. The LDS anemometer (See section 3.2) was mounted 2m above the ocean surface, 2.3 km west from the Whitfords station. For use in the ELCOM model (and in comparisons with the Whitford's data) the LDS data were used to estimate the winds 10m above the water surface following the procedures of Amorocho and Devries (1980). Wind data from the LDS unit were only available from March 22-27 due to a lightning strike on the morning of March 21, which required repairs to the unit on March 22.

As show in Figure 3.4, MMP winds varied over the 8-day period from March 20 to March 27, 2003. Wind speeds peaked predominantly in the afternoon, and were lowest in the early morning. Relatively steady winds from the NE and S were observed throughout March 21 and March 26, respectively, whereas wind shifts approaching 180° occurred during March 20, March 25, and March 27. The lightest winds were recorded on March 27, when winds were undetectable

at the Whitfords Sea Rescue Station (not shown) for a 3-hr period (3:00AM-6:00AM) before the drifter deployment and for 1 ½ hrs after the deployment (7:00AM-8:30AM). The winds recorded by the LDS unit on March 27 (Figure 3.4) were also light and variable.

As the winds at the two stations are in relatively good agreement for most of the experiment (ff. 4.3.2), MMP winds were assumed uniform over the study area for all but one set simulations. This assumption was all that could be justified based on analyses of the two available wind datasets. The slight differences between datasets suggested periods of wind shear and curl over the domain, but such wind features (if they actually existed) could not be resolved with confidence from the available data and were therefore not incorporated into the model forcing. To assess ELCOM-MMP

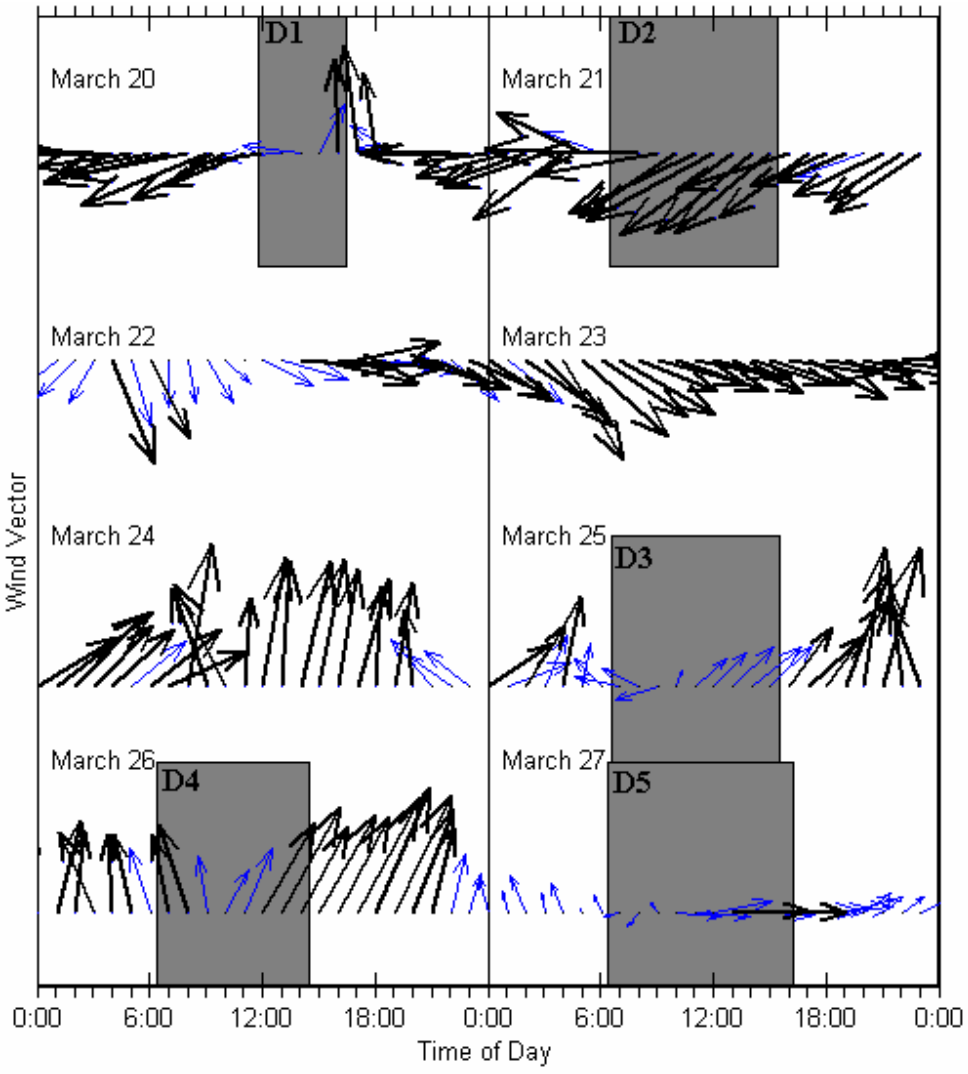

Figure 3.4 – Wind Data For MMP from March 20-27, 2003. – wind vectors presented in oceanographic convention, indicating magnitude and direction towards which the wind is blowing. Grey boxes indicate periods of field drifter deployment. Black arrows indicate wind speeds greater than 5 m/s. Data from the Whitfords Sea & Rescue Station is shown on March 20-21. LDS data is shown on March 22-27.

sensitivity to slight variations in wind forcing, separate simulations were conducted using Whitfords Sea & Rescue station data and LDS data (when the LDS data was available). The one set of simulations in which the wind was not uniform across the domain was conducted with winds spatially and temporally linearly interpolated (in space and time) from the LDS and Whitfords Sea and Rescue Station Data (ff 4.3.2). The effect of the various wind datasets on the ELCOM-MMP model results is discussed in Section 4.3.2.

3.4.5. Atmospheric/Water Heat Transfer

ELCOM includes standard models for heat transfer between the atmosphere and water (Hodges, 1998). The air temperature, net radiation, relative humidity, and incoming short-wave radiation data (Figure 3.5) collected by the LDS between March 22 and March 27 were used as ELCOM input. When modeling March 18-21, LDS data from March 25 were used. This approximation was necessary due to the lightning strike on the LDS on March 21 which rendered the unit inoperable until repairs were made on March 22. Approximating March 18-21 conditions with March 25 data was the best option given the available data, although the effects of the March 20-21 cold front (which generated the lightning) are not included within the model. This approximation is unlikely to contribute significant error into drifter paths calculated by the ELCOM-MMP models as the surface thermodynamics have marginal impact on the modeled drifter paths (§6.4).

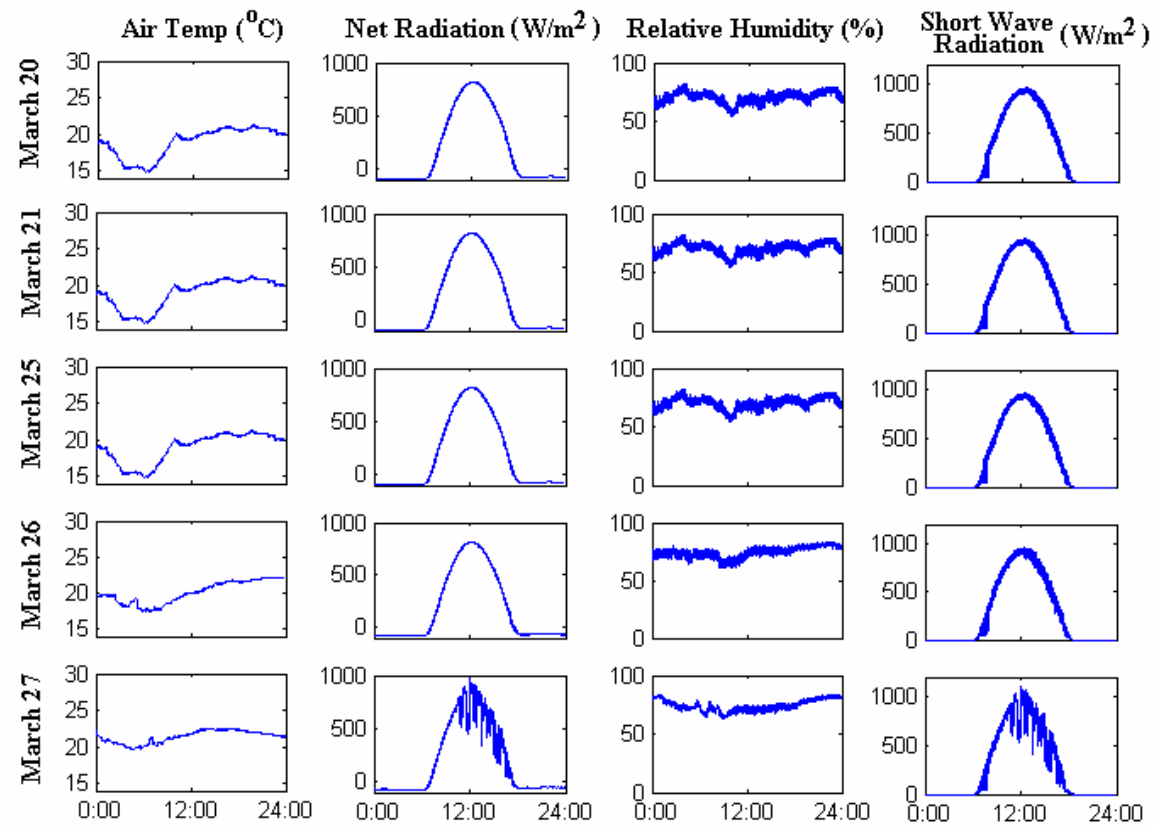

Figure 3.5 – Meteorological Data measured with the LDS. Data was used as boundary condition input for the ELCOM surface thermodynamics computations. Data from March 25 is used when modeling all time periods before March 22.

On the days of drifter deployment, diurnal fluctuations in air temperature and solar radiation were observed (Figure 3.5), with the temperatures reaching a minimum of 14-18 °C by 6:00am and peaking at 22-25 °C in the afternoon. Temperatures above 25 °C were recorded during the afternoon on March 20, after which a cold storm front passed through the area, reducing the temperatures and causing the lightning. Net and short-wave solar radiation peaked at approximately 950 W/m^2 and 1050 W/m^2, respectively, slightly after noon on each day. The average duration of daylight was 10.3 hrs for the days of the experiment.

3.4.6. Water Surface Slope & Tidal Forcing Data

Following Zaker et al (2002), the model was forced with a constant steric gradient (i.e., sea level slope) of 1.75×10^{-7} m/m, equivalent to the gradient of the Leeuwin Current offshore from MMP (Thompson, 1984; Godfrey and Ridgway, 1985; Smith et al, 1991) that is the principal large-scale coastal barotropic forcing. This gradient was imposed by fixing the water surface elevation at the northern model boundary at 0.0 m MSL, and then fixing the southern boundary at 4.8 mm below MSL. Elevations for cells along the western boundary were determined by linear interpolation based on the cell's distance from the southern boundary.

In following Zaker et al (2002), MMP water surface oscillations due to tidal forcing were not included in the ELCOM modeling. Accurate tidal forcing data for Marmion Marine Park is difficult to obtain because the tide gauges along the Australian coast are not referenced to a common vertical datum (personal comm.. – Tony Lamberto, Aust. Dept. of Planning and Infastructure, 2003), so coastal tidal gradients cannot be properly quantified for model boundary conditions. Similar problems have been reported by researchers working along the Texas coast (Ward et al, 1990), underscoring the need for improvements to the world-wide network of tidal gauging stations. Exclusion of tidal forcing, while unavoidable, is not considered detrimental to the present work because it has been established that the MMP circulations are predominantly wind-driven (Zaker et al, 2002). This conclusion from Zaker et al (2002) was confirmed by comparing results from the present model using both southward and northward water surface slopes as well as a perfectly flat water surface slope: differences in modeled drifter behavior were insignificant when the wind speeds were high (See Chapter 4.3.3).

3.5. Circle Assessment Methods & Drifter Model Setup

3.5.1. Implementing the Circle Assessment Method

The Circle Assessment method, as presented in sections 2.5.2 – 2.5.5, may be tailored by the model user to suite the user's purposes. The values of δ and ξ (the target and error circle radii) need to be specified before applying the circle assessment method. Potential values for these radii may scale as the mean eddy diameters of the flow, or may take on values reflective of other physical features of the observed currents. Such possibilities were not considered in this research. For the work presented herein, the target circle radius (δ) was taken to be ten meters, as this is the known RMS positional accuracy of the GPS coordinates recorded by each drifter (See Section 3.3). Values of ξ were set to the gridsize used in the ELCOM model simulations, either 500 m, 250 m or 100 m (see Section 3.4). These radii values were selected because they provide information relating model performance to limitations in the model setup and input data.

Through using the drifter's GPS positional accuracy as the target circle radii, the uncertainty in the drifter position is incorporated into the analysis method. The 10 m RMS accuracy of the GPS position indicates that the actual position of the drifter is, on average, within 10 m from the reported drifter position; it is impossible to pinpoint the field drifters position to any location within the 10 m circle surrounding the drifter position. As a result, when a model is

considered "perfect" based on the 10 m target circle radius, the model has successfully transported the modeled drifter into the area within which the field drifter is likely to reside. The model cannot perform better in that the actual position of the field drifter is not known with any greater precision than the 10 m target circle radius.

The model gridsize was used to assess model performance between perfect and flawed (i.e., using error circle ξ) because the gridsize reflects the distance over which the model-calculated Eulerian velocity field is unknown. Subgrid-scale variations in the modeled Eulerian velocity field are non-existent within the ELCOM hydrodynamic model used in this work (see Section 3.2) and drifters located within the same grid cell are likely to move with similar velocities due to their small separation relative to the scales of velocity variation over multiple grid cells. Separation between model and field drifters by a distance greater than the gridsize, therefore, indicates when the modeled and field-observed velocities are sufficiently different to prevent the model from capturing the observed drifter motion. In such instances, the modeled drifter velocity is influenced to a greater extent by the velocity in a grid cell adjacent to the cell containing the field drifter. As the Eulerian velocities calculated for each grid cell may be different, modeled drifter divergence of distances greater than the grid cell size suggest that the modeled drifter may travel at an incorrect velocity even if the field drifter velocity in the adjacent grid cell were exactly correct.

Time intervals when the model performance is acceptable were defined in this work as periods when the modeled drifters have separated between 10 m and either 100 m, 250 m, or 500 m (depending on the model gridsize). Such periods were quantified by identifying the mean number of model timesteps ($\bar{N}$) that pass between when the model is "perfect" (i.e., model/observed separation within the target radius δ) and when the model becomes "flawed" (i.e., model/observed separation greater than error radius, ξ). As shown in Figure 3.6a, $\bar{N}$ is calculated by plotting model/field drifter separation (d) against time (for each drifter-timestep – see section 3.5.2), using the model gridsize and timestep as normalization factors, respectively. The "Acceptable Time," or the time at which the average modeled drifter separated from the field drifter by the length of a grid cell, is the determined as the intersection of the mean separation line and a horizontal line intersecting 1 on the ordinate (Figure 3.6b).

The "acceptable time" is a measure of how far forward in time a model drifter can be integrated before the accumulation of position error is greater than the error circle. This might be used to predict the uncertainty in a drifter position by successively seeding new drifters in a radius of ξ every $\bar{N}$ time steps.

3.5.2. Model Drifter Deployment

Deploying a set of model drifters only at the deployment positions of the field drifters is an approach suitable for analysis methods that integrate model error (e.g., spaghetti diagrams). However, to provide a better understanding of the model error all along the observed drifter track, it is necessary to deploy model drifters along the observed track, similar to the approach of Nairn and Kawase (2002) as shown in Figure 2.6b; i.e., one model drifter should be deployed at the observed drifter position for each time step, so that after 'n' time steps there are 'n·b' drifters being tracked where "b" is the number of field drifters simulated in the model. While deployment of a new model drifter at each time step allows the evolution of drifter model error to be studied, the approach assumes that the observed drifter position is absolutely correct. Unfortunately the present field drifter positions are only known to within 10m (i.e., the target circle), so placing a single drifter at each time step may lead to diagnosis of model error that is affected by the uncertainty in the observed position. To account for the observed drifter uncertainty, multiple model drifters can be initiated at around each observed drifter position. In the present work 33 new model drifters

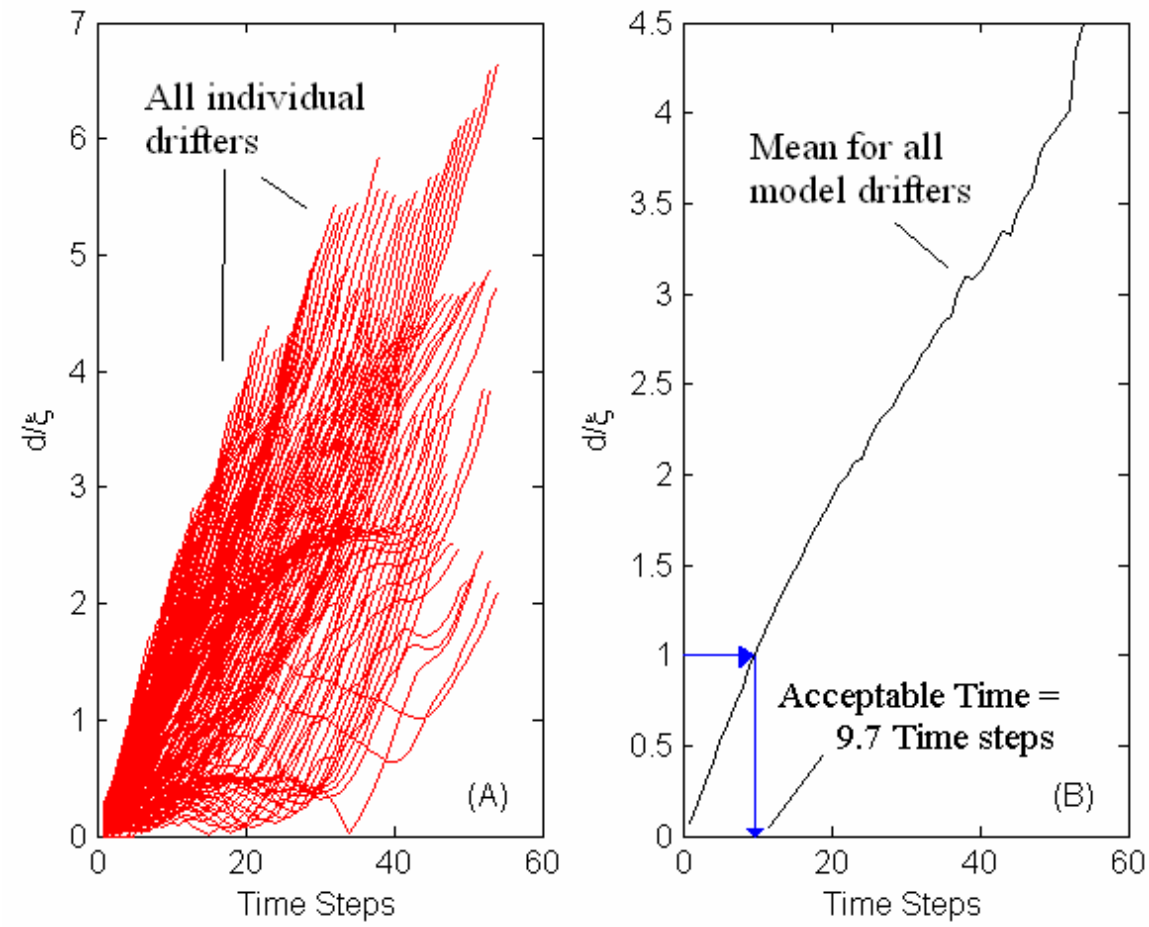

Figure 3.6 – Calculating" Acceptable Time" – A) evolution of d/ξ for each modeled drifter-time step (§2.5.5, ff 3.5.2), B) averaging d/ξ at each timestep. Acceptable time is defined as the time when the mean d/ξ = 1. Data shown is from the D3 base-case simulation (ff 4.3).

were initiated throughout the field drifter target circle (Figure 3.7) at each time step. The modeled drifters were located on two concentric rings about the field drifter position, with 16 evenly-spaced drifters per ring at radial distances of δ and δ/2. The remaining modeled drifter was located at the center position of the field drifter. This distribution of modeled drifters throughout the field drifter target circle provides sufficient coverage of the target circle, including its extremes.

3.5.3. Drifter Model Setups

To properly apply the GABI-F drifter model to cross-sail drifters, the properties (mass, length, area, etc) of each drifter section must be provided to the drifter model (Section 2.3.2). All of the GABI-F drifters modeled in this research had the characteristics presented in Table 3.2. With the exception of the drag coefficient, all entries in Table 3.2 were taken drifter design plans and from measurements made on March 19, 2003 before the MMP D1 experiment began. Drag coefficients for the drifter sections were not measured, and were assumed unity. This assumption was based on

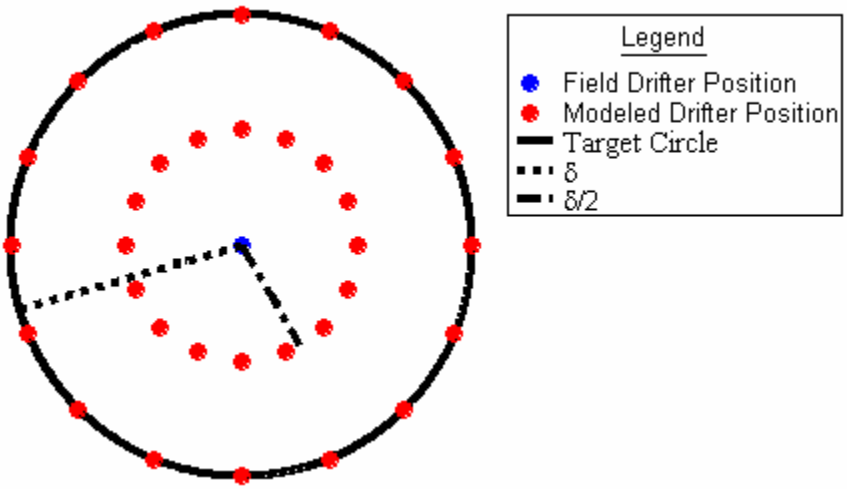

Figure 3.7 – Modeled drifter deployment within the field drifter target circle. 33 modeled drifters are simulated for each field drifter location at each model timestep. Modeled drifters are located at the field drifter position and in 2 16-drifter rings about the field drifter position.

scales of published drag coefficients for smooth cylinders in flows between Re = 100 and Re = 10,000 (Kundu and Cohen, 2002). Model sensitivity to the drag coefficient and the potential impact of the assumed drag coefficients on modeled drifter paths are discussed in Section 6.6.

Table 3.2 – GABI-F Drifter Properties in ELCOM-MMP

	Drifter Section Properties			
Drifter Section	Mass (kg)	Area (m^2)	Length (m)	Drag Coefficient
Antenna	1	0.01	0.3	1
Above Surface Buoy	0.1	0.01	0,1	1
Under-Surface Buoy	0.2	0.2	0.2	1
Pole	3	0.001	1.3	1
Drogue	26	1.5	1	1

For simulations using leeway factors (Section 2.2) to modify drifter Lagrangian velocities, each leeway factor (α) was set to 0.001. This low value reflects the small above-surface features on the cross-sail drifters used in this work, and is consistent with the leeway factors reported by Thompson et al (2003) for objects ranging from life rafts to completely submerged floats. A sensitivity analysis relating model results to the variations in the leeway factor (Section 6.7) also indicted greatest agreement between modeled and observed drifter paths when $\alpha = 0.001$.

3.6. Field Drifter Paths & Results

3.6.1. Introduction

This section contains a description of the observed field drifter paths, and a detailed discussion of the MMP currents implied by these paths. The purpose of the section is to highlight features of the observed drifter motions that may prove difficult to capture with the model setup, and to identify trends in the field drifter patterns which might provide insight into MMP current response under varying forcing conditions. This section describes the field drifter paths when considered as a group, as well as the individual drifter paths on each of the 5 experiment days. The ability of the ELCOM model to reproduce the observed field drifter paths is discussed in Chapter 4.

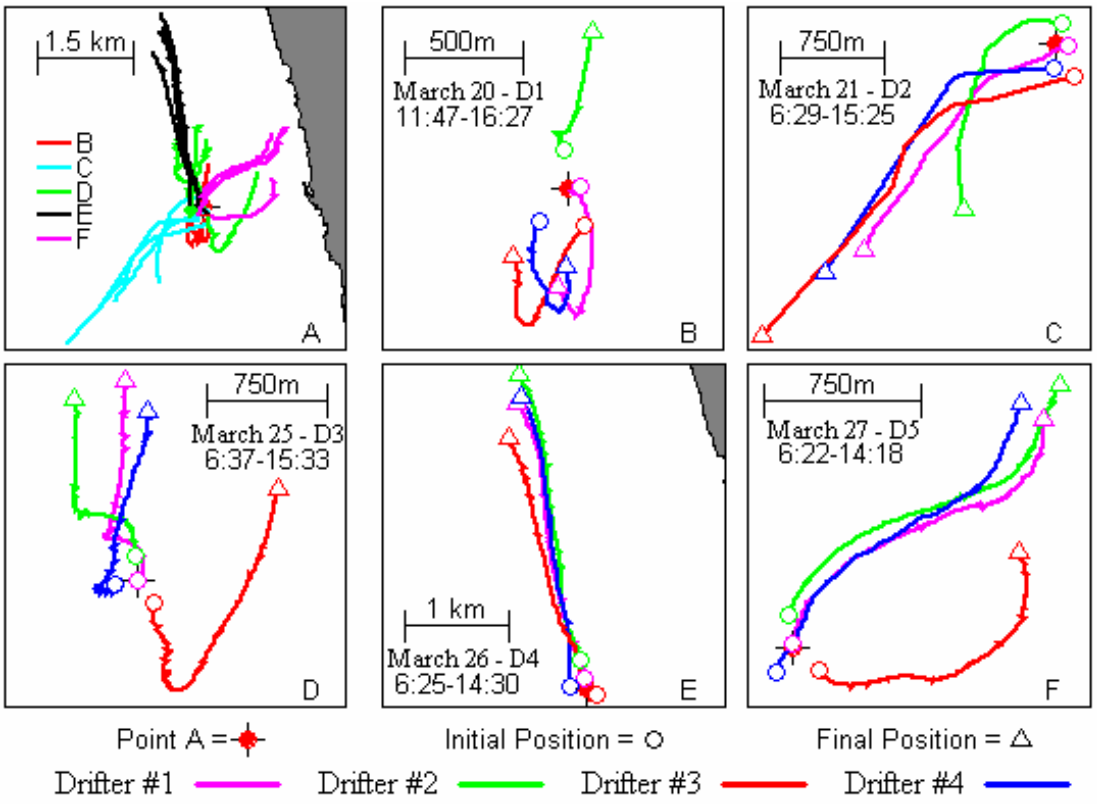

Figure 3.8 – Observed Field Drifter Paths, A) 5-day composite, B) March 20, 2003, C) March 21, 2003, D) March 25, 2003, E) March 26, 2003, F) March 27, 2003. Circles indicate path starting-points. Triangles indicate path end-points.

3.6.2. 5-Day Composite Results

For the five days of drifter deployment, the drifter paths did not follow repeating daily patterns (Figure 3.8a). During D1, D3 and D4 the drifters traveled predominantly in the alongshore direction (Figure 3.8b, 3.8d, 3.8e), whereas during D2 and D5 they traveled along a NE-SW line (Figure 3.8c, 3.8f). Over D2 and D4 (Figure 3.8c, 3.8e), all four drifters moved in a coherent fashion that arguably indicates their deployment in a single flow feature with a length scale greater than 150 m (the drifter initial separation at deployment). However, for each of the other deployments (Figure 3.8b, 3.8d, 3.8f), a single drifter initially moved in a substantially different direction from the others, indicating the initial deployment was within a locally-diverging flow. The periods suggestive of a diverging flow were also the days on which the wind speeds were generally less than 5 m/s and reversals in wind direction were observed (Figure 3.4).

3.6.3. March 20, 2003 Results

On March 20, strong winds out of the northeast in the morning were replaced by weaker winds out of the south in mid-afternoon. This transition took place in the first two hours after drifter deployment (Figure 3.4), during which time the wind speeds decreased from over 10 m/s to below 1 m/s. By late afternoon and into the evening on March 20, the wind speed returned to the higher morning magnitude, although the direction was slightly more from the east.

The drifter motion on this day (D1) implies the drifters were deployed into a diverging current (Figure

3.9A). Upon deployment, drifter #1 and drifter #2 were separated by only 171 m, but their initial travel directions differed by 165°. Drifters #3 and #4 initially traveled southward like drifter #1, indicating a flow divergence existed near the drifter deployment (point A). By 3:30pm, nearly 4 hours after deployment, drifters #1 and #4 were separated by only 86 m and were traveling in nearly opposing directions (Figure 3.9B). At this time, drifter #3 had begun the directional reversal that occurred later for drifter #1indicating that the current reversal did not occur at identical times across the study area. Drifter speeds during the initial flow divergence were all less than 5 cm/s. Shortly after 3:30 pm, all drifters were traveling northward at speeds greater than 5 cm/s (maximum speeds approached 10 cm/s).

The course reversal for drifters #1 and #3 was in the CW direction, while that for drifter #4 was in the CCW direction, implying the existence of eddy structures with length scales on the order of 100 m (i.e., the drifter separation) during the reversal. These eddy structures are considerably smaller than the 250 m grid resolution used in the base ELCOM-MMP model (See Section 3.2), so it is not expected that the model could resolve such effects.

With the stronger, more constant late afternoon winds (Figure 3.4) on March 20, the four drifters moved steadily northward. This northward acceleration occurs approximately one hour after the wind shift recorded at the Whitfords station, suggesting a time lag between water current reversal and wind shift. Similar time lags in the ELCOM model (*ff.* section 4.2) suggest the model is successfully reproducing the dynamics of the currents responding to significant wind changes.

3.6.4. March 21, 2003 Results

Winds on March 21 were consistently strong, exceeding speeds of 5 m/s for 90% of the day and

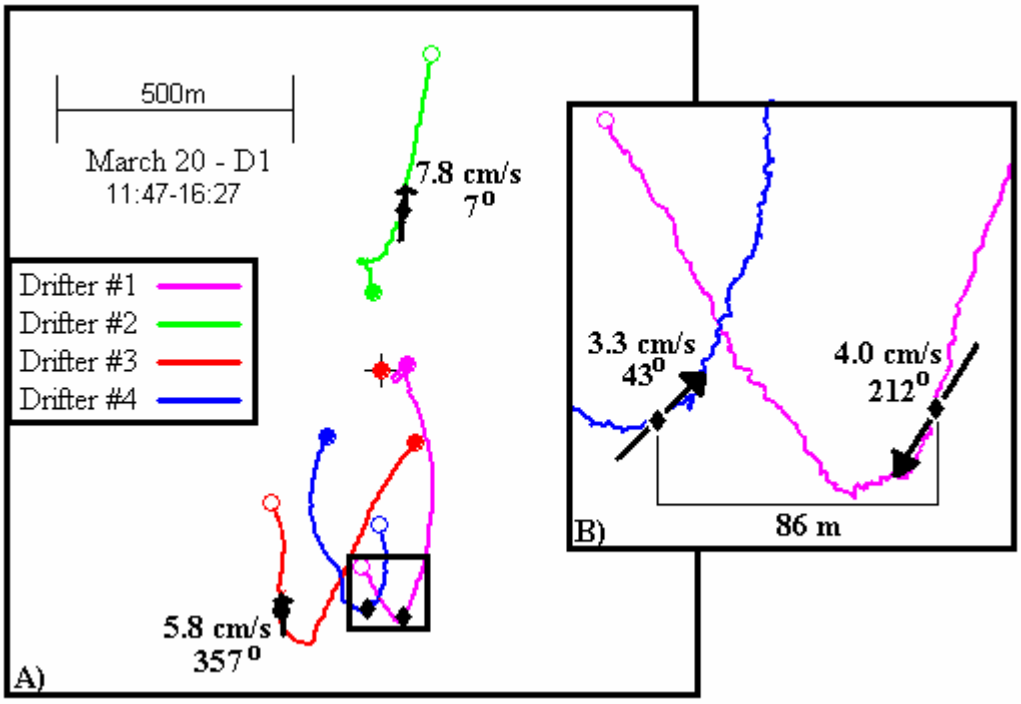

Figure 3.9 – Divergent Field Drifter Paths on March 20. Arrows indicate drifter velocities at 3:30 pm, before the drifters accelerate to the north. Closed circles indicate initial positions, open circles indicate retrieval locations.

exceeding 7.5 m/s for 48% of the day. The winds were initially out of the east during drifter deployment, and then shifted to blow out of the northeast for the remainder of the day (Figure 3.4). During the wind shift, the wind speeds continuously hovered between 4.3 m/s and 6.2 m/s and did not significantly diminish as observed during the March 20th wind shift. D2 drifter motion mimicked the winds, with the initial winds out of the east causing westward drifter motion and the subsequent winds from the northeast giving the drifters a more southwesterly course. However, unlike within the D1 deployment, the D2 drifter trajectories switched from westerly to south-westerly without any time-lag with respect to the wind shift. The lack of a time-lag in the drifter's response to the relatively small wind shift suggests MMP currents adjust to changing wind forcing differently depending on the directional characteristics and the behavior of the wind during the shift.

All four GPS position data loggers failed on March 21. Backup positions were obtained through SMS mobile phones (at 30 minute intervals) and by a handheld GPS unit monitored in the boat while following drifter #1. The positional accuracy of the hand-held GPS unit is equivalent to that of the drifters, however the position fixes for each drifter incorporated greater error due to the unknown distance between the boat and the drifter. The target circles for positions resulting from hand-held GPS measurements were expanded to 16 m to approximate the separation between the drifter and the boat. A malfunction with the SMS phone on drifter #4 prevented position data from being recorded after 9:00 a.m., and the last position recorded for this drifter was from the hand-held GPS unit taken when the drifter was retrieved. Upon discovery of the SMS phone malfunction on drifter #4, the SMS phones on drifters #1 and #2 were remotely re-programmed to transmit position data

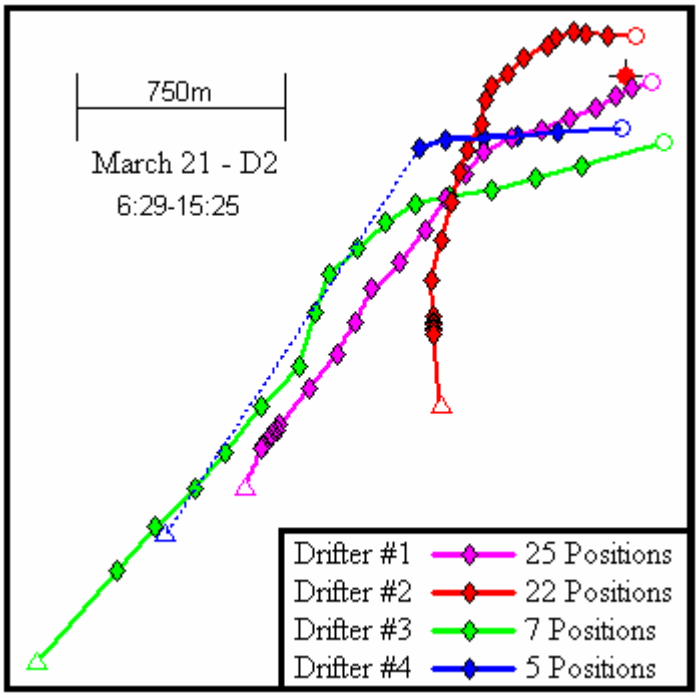

Figure 3.10 – Field Drifter Trajectories & Positions observed on March 21, 2003. Circles indicate initial positions, triangles indicate retrieval locations. Diamonds indicate recorded drifter positions. Dashed line indicates uncertain path for Drifter #4.

every 2 minutes. The re-programming was not successful on drifter #3.

As a result of the various equipment malfunctions, the positions of each drifter were recorded between 7 and 25 times over the 8-hr experiment (Figure 3.10). The median time interval between measurements was 30 minutes, with the intervals ranging from 2 minutes to 6.5 hours.

3.6.5. March 25, 2003 (D3) Results

In the early morning of March 25, prior to drifter deployment, the LDS measured winds principally varying from out of the SW to S with fluctuating speeds both above and below 5 m/s. Just before the D3 deployment, the winds at the LDS dropped consistently below 5 m/s and shifted to be out of the east. As with the March 20 drifter paths (section 3.5.3), the initial drifter motion on March 25 implies a divergence of the currents near the drifter deployment (Figure 3.11): drifter #3 initially travels southward; drifter #4 starts eastward then reverses to the west; drifter #1 starts eastward then moves north; and drifter #2 moves consistently northward. The drifter velocities at deployment were less than 2 cm/s, with the exception of drifter #3, which traveled in a less sinuous path than the other four drifters at a speed of 4 cm/s. By 11:30am, all drifters increased speed on a northward track, with speeds further increasing throughout the afternoon (Figure 3.11).

The change in D3 drifter headings that occurred by late morning occurred approximately one and a half hours after the winds diminished and shifted to a NNE heading. This response to changing winds is consistent with the current shifts observed on March 20 (Section 3.5.3). On both days, wind speeds decreased to near 0 m/s before the wind shift, temporarily eliminating the principal force driving MMP current motion. The large time lag between the wind shift and the current response (relative to the short lag observed on March

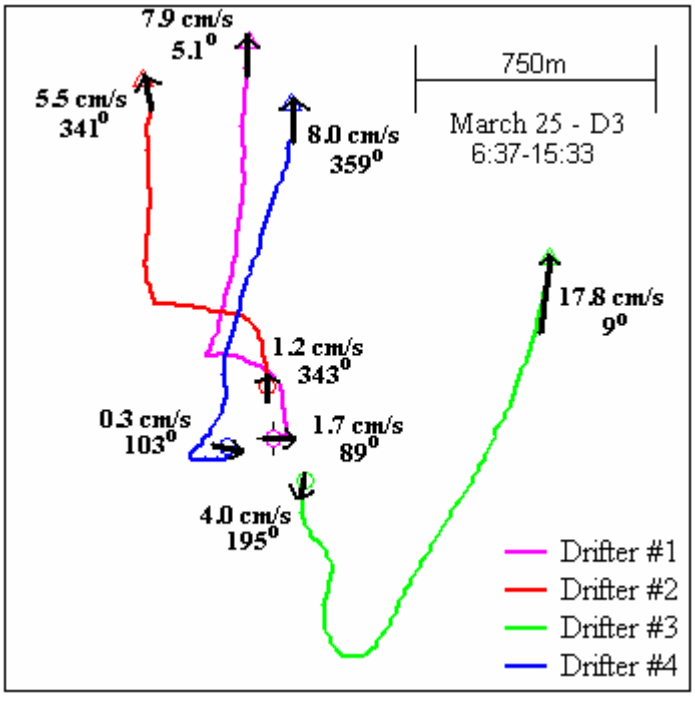

Figure 3.11 – Field Drifter Paths from D3 - March 25, 2003 – Circles indicate initial positions, triangles indicate final positions. Black arrows indicate path direction.

21 – Section 3.5.4) may be due to the loss of forcing energy during the wind shift, which would have slowed or even eliminated currents existing before the shift. The time-lag may be due to the time it takes for wind-induced shear to penetrate to depth and create a substantial current. It can be argued that a hydrodynamic model may be considered skillful if it predicts the timing of current responses compared to wind shifts, regardless of whether the model adequately reproduces the field drifter paths during the low velocity conditions surrounding reversals. The ability of the ELCOM-MMP models to reproduce such current reversals and time lags is discussed in Section 4.4.

3.6.6. March 26, 2003 (D4) Results

Out of the five drifter experiment days, the winds on March 26 were the steadiest. The LDS-measured wind speeds were lower than on March 25, with winds blowing out of the SSE at speeds from 5-7 m/s (Figure 3.4). After 11:00 am, the winds shifted slightly to blow out of the SSW and speeds increased to 7-10 m/s. It was only after 8:00PM that the wind speeds decreased below 5 m/s, well after the end of the D4 experiment.

The four field drifters followed steady NNW headings (Figure 3.12) for the entire deployment, consistent with a wind out of the south. The median drifter speed (9.9 cm/s) was larger than on any of the other experiment days, and the drifters moved a greater distance than on any other day. Dispersion among the drifters was small, causing drifters #1, #2, and #4 to separate only 85m over the 3.25 km distance they traveled from deployment. Drifter #3 did not travel as far north as the other drifters, and was retrieved 360 m to the southwest of drifter #1. Position data for drifter #4 was only recorded from the SMS phone transmissions (See section 3.5.4) and hand-held GPS measurements, providing 18 total position fixes during the deployment period. The data loggers for the other field drifters functioned properly.

3.6.7. March 27, 2003 (D5) Results

On March 27, the winds were light and variable

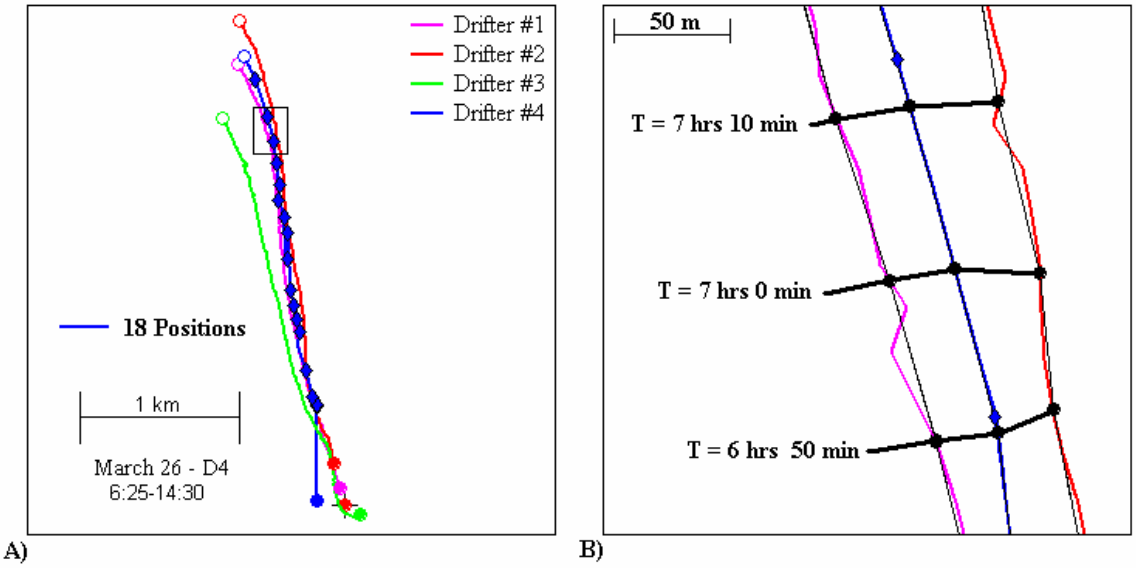

Figure 3.12– Field Drifter Paths from March 26, 2003 – A) Full Experiment paths with SMS & Hand-Held GPS positions for Drifter #4, B) Path similarity between drifters #1, #2, and #4 during the afternoon. Black lines connect the drifter positions at the time specified.

compared to the strong, consistent winds of March 26. The wind speeds measured by the LDS rarely exceeded 5 m/s, and the direction of the wind shifted from initially out of the SE to out of the west by noon (Figure 3.4). These onshore breezes had speeds up to (but rarely exceeding) 5 m/s.

Drifters #1, #2, and #4 initially traveled to the NE (Figure 3.13), with drifter #3 diverging from the others and traveling ESE until traveling N toward the end of the deployment. As on March 20 and March 25, the period of divergence occurred when the wind speeds were less than 5 m/s and when the drifters moved at speeds below 3.6 cm/s. Similar to March 26, drifter #4 on March 27 malfunctioned and did not record the GPS positional data. The drifter #4 data in Figure 3.13 were measured using the hand-held GPS and SMS mobile phones, resulting in 29 known positions.

3.6.8. Field Drifter Paths & Analysis – Summary

The analyses of field drifter paths in sections 3.6.2 – 3.6.7 illustrate trends within the relationships between wind speeds, wind shifts, flow divergence, and drifter transport. Flow divergence (i.e., diverging field drifters) was observed when wind speeds were consistently less than 5 m/s, which was typically followed by a directional shift, as on March 20, March 25, and March 27. The flow divergence disappeared as the wind speeds increased (generally in the afternoon). When wind speeds increased above 5 m/s, all drifters traveled in the same general direction. These drifter results suggest that current uniformity is prevalent under high wind conditions, defined as periods when the wind speeds increase above 5 m/s. This observation is consistent with the findings from Zaker et al (2002).

Periods of flow divergence also coincided with wind directional shifts of 90° to 180°. Wind speeds tended to be low (< 4 m/s) before wind shifts, with the

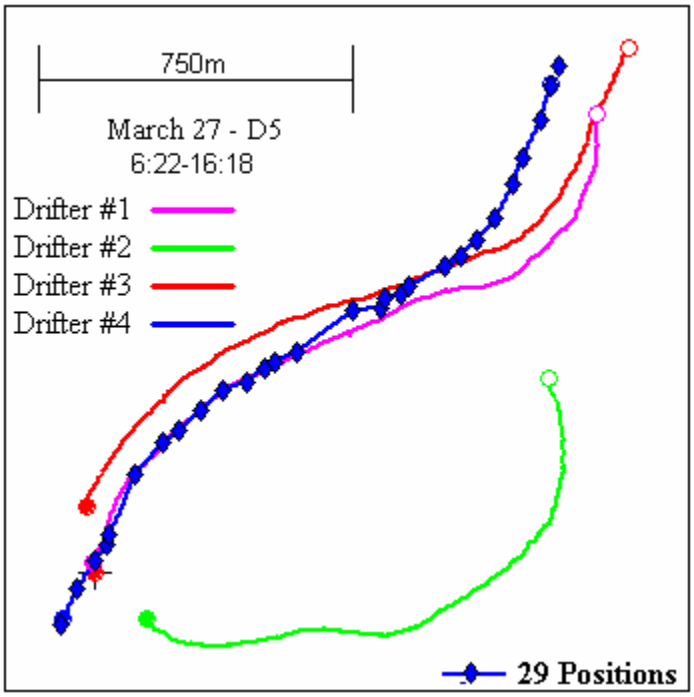

Figure 3.13– Field Drifter Trajectories from D5 - March 27, 2003. Closed circles indicate initial positions, open circles indicate retrieval locations.

wind speed increasing after the shift. On occasions when the wind speeds before and after shifts are less than 5 m/s (March 20, March 25), the field drifter paths changed direction approximately 1.2 – 1.5 hours after the wind shift. When the wind speeds before and after the wind shifts exceed 5 m/s, the field drifters changed course at approximately the same time as the wind shift. These trends suggest that the temporal response of the MMP currents to shifts in the wind depend on the wind speed before the shift.

As shown in Chapter 4, modeling the MMP currents with the ELCOM model described in this chapter is difficult when the wind speeds are below 5 m/s. The 250m horizontal grid cell size is greater than the observed length scales (< 150 m) of flow divergence at low wind speeds; it is unlikely that any of the observed divergent flows are present in the model results. In contrast, ELCOM can successfully model periods of non-diverging flow when the wind speeds exceed 5 m/s. The MMP currents most suitable for ELCOM modeling are on March 21 and March 26 as well as on the afternoon of March 25 after the wind shift. Simulations conducted at the 500m grid resolution are too coarse to resolve small velocity differences among the drifters in all simulations. The 100m grid ELCOM-MMP setup produces modeled drifter results most comparable to the field drifter data. However, even the 100m grid resolution is too coarse to resolve most of the divergence-causing eddy features common when winds are low.

3.7. Summary

This chapter described the study area within Marmion Marine Park, the field experimental design, drifter design, and previous studies conducted in the area. Winds near MMP were found to be variable from one-day to the next, and during the course of each day. The drifter trajectories also varied on similar timescales, with periods of slow, sinuous movement interspersed among periods of rapid, steady drifter movement. The range of time and space scales associated with the drifter movement (especially at low wind speeds) provides a challenge for modeling MMP. The results of the ELCOM modeling of MMP and the field drifters is presented and discussed in the next chapter

4. Model Results & Discussion

4.1. Introduction

This chapter provides a detailed analysis of the ELCOM model results for Marmion Marine Park (MMP) with emphasis on the use of the GABI-F technique and the Circle Assessment methodology. Section 4.2 compares results from simulations using the GABI-F, Lagrangian, and Leeway drifter modeling techniques (§2.2-2.4). Results are analyzed using spaghetti diagrams (§ 2.5.2), the Type I method (§ 2.5.3), the statistical separation method (§ 2.5.4), and the Circle Assessment method (§2.5-2.8). In section 4.3, the Circle Assessment results from GABI-F modeling under differing forcing conditions and model setups are discussed. Chapter 5 contains conclusions and a discussion of the remaining work to be undertaken in the area of GABI-F drifter modeling as a potential model validation technique.

4.2. Comparing Drifter Modeling Techniques

4.2.1. Introduction

This section contains comparative evaluations of ELCOM-MMP model results from the "base case" model setup (See Section 3.4). Properties of the base case model setup are given in Table 4.1. Wind data from the Whitfords Sea and Rescue Station were used when simulating time periods during which the wind data from the LDS unit were unavailable. Simulations were conducted using each of the three drifter modeling methods (Lagrangian, Leeway, and GABI-F modeling – See sections 2.2-2.4), and discussions of model result analyses by each assessment method (Spaghetti Diagrams, Type I metrics, Statistical Separation metrics, and the Circle Assessment method – See Sections 2.5-2.8) are presented in individual subsections.

With each assessment method, analyses of model results were tailored to assess both the hydrodynamic model setup and the drifter model. Specifically, assessment methods were evaluated based on their ability to:

1. depict the extent to which the ELCOM-MMP model reproduced the observed field drifter motion, and

2. compare/contrast the three drifter modeling techniques in terms of their relative ability to reproduce the observed field drifter motion.

The following discussions demonstrate that drifter results obtained with the GABI-F drifter model compare more favorably to the observed field drifter motion than do results obtained with the Lagrangian and Leeway drifter models. Improvements due to GABI-F modeling were most evident at the relatively short assessment time-scales (timesteps and κ_{max} times) within the Circle Assessment method. Differences between the drifter model results were less evident when results were analyzed over longer timescales (acceptable times and simulation durations) using either the Circle Assessment, Type I, or Statistical Separation analysis method. Differences between drifter models were often difficult to discern based on Spaghetti diagrams.

Table 4.1 – Base Case ELCOM-MMP Setup Properties

Property	Value
Grid Cell Size	250 x 250 x 1 meter cells
Timestep	10 minutes
Wind Forcing	LDS data (when available)
Water Surface Slope	South - 1.75×10^{-7} m/m

The following discussions also demonstrate that analysis methods based solely on the model drifter's initial deployment position and subsequent track may only provide insight as to the model's ability to predict larger-scale motions of the field drifters. Such methods, namely the Spaghetti Diagram, Type I, and Statistical Separation methods, provide limited insight as to a model's ability to reproduce the field drifter's local speed and direction at any time or location because the methods temporally integrate positional error. Once the model drifter has moved substantially away from the field drifter, further analysis of position error is essentially meaningless as the flow fields around the model and field drifters may not be significantly related. Analysis of the drifter motion after the positional error becomes meaningless, however, does provide information relating to the model's ability to reproduce the general, larger scale patterns of the field drifter motion. The Type I and Statistical Separation analysis methods are well suited to such larger-scale analyses.

The Circle Assessment is the only method (investigated herein) suitable for model/field comparisons at small timescales. The method limits the temporal integration of model error by limiting the duration of individual modeled-observed path comparisons to time intervals over which the field and model drifter are sufficiently close together. Thus, the interval over which the field and model drifters are sufficiently close (when the model is "perfect") provides an interval over which the model flow field and the flow field implied by the field drifter may be compared. By using the target circle radius as a length scale over which to identify modeled-field drifter path separation, the Circle Assessment method also allows for quantification of the model's ability to reproduce the best possible representation of the observed drifter's speed and direction. Additionally, the Circle Assessment method also provides some insight into the model's ability to reproduce larger-scale patterns of drifter motion through the "acceptable time" analysis (Section 2.7.3). The "perfect" and "acceptable" model classifications within the Circle Assessment therefore provide model skill assessments at local and larger scales, making analyses using the Type I and Statistical Separation methods unnecessary. Analyses using spaghetti diagrams should always be conducted because this method is the only method suitable for describing the drifter paths and making maps. Interpretations of model results, however, should not solely depend on spaghetti diagram analyses.

4.2.2. Results Analysis with Spaghetti Diagrams

Although the Spaghetti Diagram method (Section 2.5.1) cannot quantitatively assess model-field agreement, it can graphically indicate the predicted transport path. This path description is lost in the statistical quantification of model behavior using the Circle Assessment, Type I, or Statistical Separation assessment methods. While such paths are easy to understand, they may not reflect overall model skill because they are integrative of model error over time. Errors in modeled drifter velocity at earlier times will contribute to the difference in positions of model and field drifters at all later times. As a consequence, agreement between the model and field drifter positions at later times requires the model to have been accurate at all preceding times. Such a "perfect" result would indicate a high level of model skill and is extremely unlikely given the uncertainty in the model boundary conditions. A corollary to this "perfect" scenario is that differences in drifter position at any given time do not imply any relationship between the model and field drifter motion at that time. As such, interpretations of spaghetti diagram plots should be made with caution.

Figure 4.1 presents spaghetti diagrams of the modeled drifter paths from each base-case simulation (D1-D5) with each of the 3 drifter models (Lagrangian, Leeway, and GABI-F). With the exception of the D5 simulations (Figure 4.1 D5A-C), the spaghetti diagrams indicate that modeled drifters traveled at speeds greater than the field drifters, resulting in larger modeled drifter displacements over the duration of

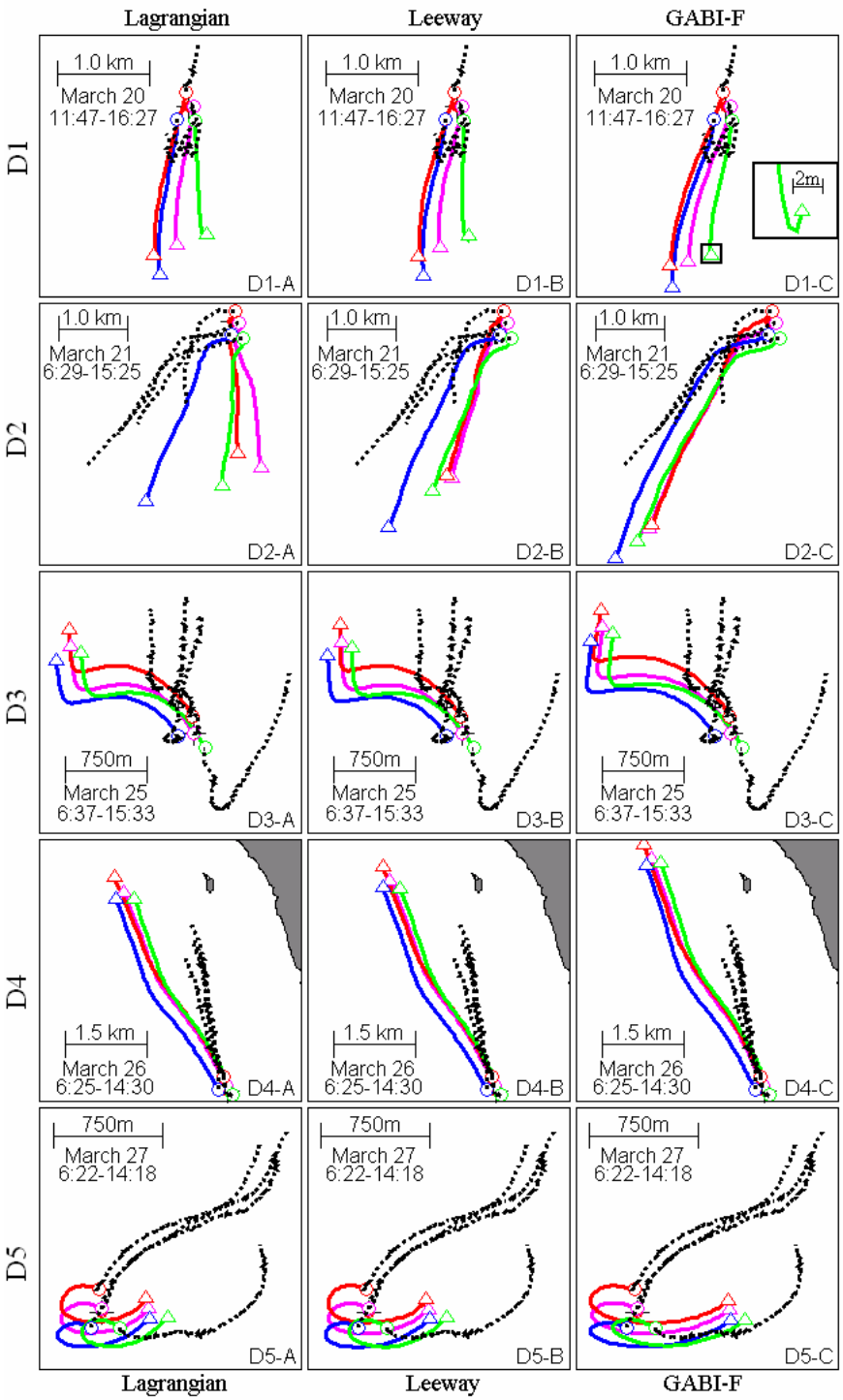

Figure 4.1 – Spaghetti Diagram Plots of Model Results by drifter method. Lagrangian drifters shown in Column A, Leeway Factor results in Column B, GABI-F Results in Column C. Drifter days shown by row. Field drifter paths shown as dotted lines. Symbols as in Figure 3.7

each deployment. The ELCOM-MMP model was entirely unable to capture the initial flow divergences observed during D1, D3, and D5. This result was not unexpected as model grid scales on the order of ¼ of the typical length scale of the flow divergence are required to minimally resolve a divergence (Hodges, personal comm., 2005). Using the initial drifter separation (approximately 150 m) as the divergence length scale, the ELCOM-MMP model would need grid cells of approximately 30-40 m in length, which is well below the grid cell dimensions practical for this work. Even with such fine grid resolution, it is likely that capturing the divergence occurring at low wind speeds would require more complete knowledge of the spatial structure of wind than was available based on the LDS and Whitfords station data. This possibility is explored in §4.3.2. In a qualitative sense, the modeled drifter paths suggest reasonable agreement with the observed drifter paths when the observed flow divergence is ignored. For example, D1 field drifters #1, #3, and #4 all initially traveled southward until they reversed direction in the mid afternoon (Figure 4.1 D1A-C). The modeled drifters on that day also traveled southward, and began to reverse their heading by the end of the drifter experiment (See Inset on Figure 4.1 D1C). This demonstrates that the model correctly reproduced the larger-scale dynamic motions of the field drifters, although the timing of the modeled drifter direction reversal is somewhat delayed. Similar results are seen in the D3 simulation (Figure D3a-c) when all of the field drifters shifted to a northward heading by early afternoon after an 11:00AM wind shift. The modeled drifters also experienced this northward shift, which occurred over a 1.2 hr period nearly 1.2 hrs after the wind shift (Figure 4.2).

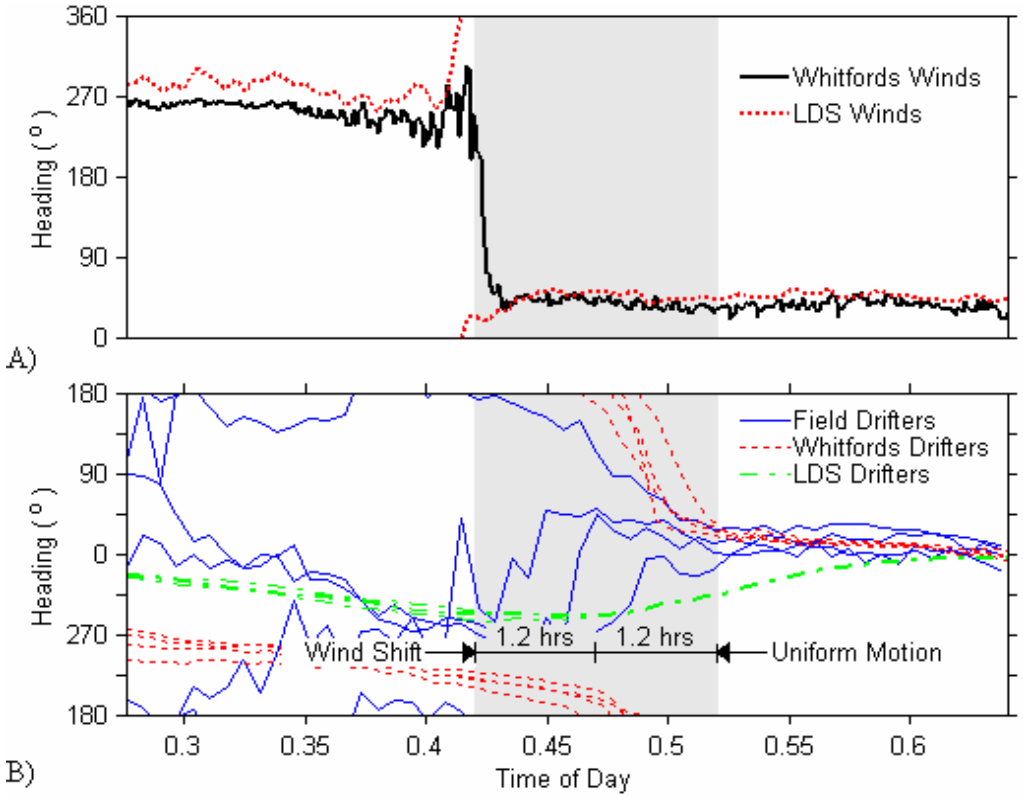

Figure 4.2 – Modeled & Observed Drifter Responses to the March 25 wind shift – A) LDS and Whitfords winds shifted just after 10:00am, B) modeled and field drifters shifted direction approximately 1.2 hours after the wind shift, and drifters all followed a northerly heading 2.4 hours after the wind shift. Modeled drifter results are from simulations using the LDS and Whitfords wind forcing datasets (f.f. 4.3.2)

The relative agreement in the timing of the field drifter and modeled drifter direction shifts (Figure 4.2) indicates that the model is reasonably reproducing the larger-scale directional behavior of the surface currents during the D3 simulation (March 25). This conclusion can be reached from an analysis of trends within the drifter paths, even though the model drifter paths are clearly displaced further to the west than those of the field drifters (Figure 4.1 D3a-c). Although such analysis is necessarily qualitative, it provides a zeroth-order indication of the model's capabilities. However, because the spaghetti plots are started from the field drifter deployment positions, the method necessarily integrates model error. A key observation from results with diverging drifters is that drifter deployment during periods of weak forcing may lead to initial errors that distort the spaghetti plots and could suggest inappropriate conclusions regarding model skill. For example, wind speeds at the time of D3 drifter deployment were relatively low compared to those recorded at the time of the drifter retrieval (See Figure 3.4). Spaghetti diagram plots for model drifters deployed at the time of D3 drifter deployment (Figure 4.2 D3a-c) demonstrate large separations between model and field drifter paths. These path discrepancies (and the rates of separation between the modeled and field drifter paths) are diminished by comparing paths originating from field drifter positions at later times when the wind speeds were higher and all drifters had begun traveling northward (Figure 4.3). Assessments of model skill using spaghetti diagrams may therefore vary depending upon the timeframe used for model-field comparisons.

While the ELCOM-MMP spaghetti diagrams were useful in assessing model skill at reproducing large scale behaviors of the surface currents, they were less useful in comparing results using different drifter models. As shown in Figure 4.1 above, only slight differences in modeled drifter paths for D1, D3, D4, and D5 were obtained when using different drifter models. Only for the D2 simulations (Figure 4.1 D2a-c) were the differences in modeled drifter paths generated with different drifter models greater than the

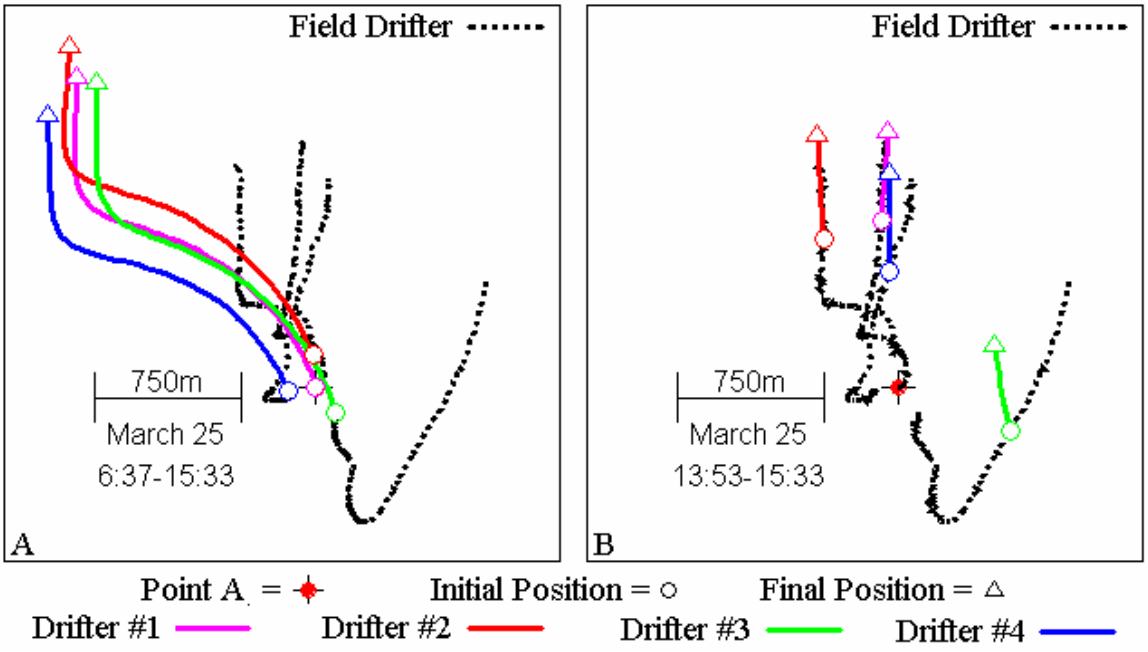

Figure 4.3 – D3 (March 25) Spaghetti Diagrams – A) Full Deployment Simulation, B) Late Deployment Simulation. Drifter paths from late deployment simulation are more comparable to field drifter paths than are paths from the full deployment simulation.

separation between the modeled drifter and field drifter paths. This suggests that the choice of drifter model was only significant for the D2 simulations, where the spaghetti diagrams indicate (perhaps arguably) the GABI-F drifter model produces the results most comparable to the field drifter paths. The modeled Lagrangian drifters (Figure 4.1 D2a) followed a more southward heading rather than the south west heading of the field drifters. In contrast, the GABI-F paths (Figure 4.1 D2c) followed nearly identical headings as the field drifters. The Leeway paths (Figure 4.1 D2b) are somewhat intermediate between the Lagrangian and GABI-F paths in that they followed a generally south-southwest heading. All D2 modeled drifters had path lengths larger than the field drifter paths, indicating that the model was over-predicting the drifter speeds.

For clarity in the following discussion, the D2 spaghetti diagrams from Figure 4.1 are reproduced in Figure 4.4 at a larger scale. In general, the D2 field drifters initially traveled to the west, and then shifted to a south-westerly course. This initial westward drifter movement was captured in the GABI-F results, and less so in the Leeway results. In contrast, only Lagrangian modeled drifter #4 exhibited any initial movement to the west, as this drifter diverged from the other Lagrangian modeled drifters which traveled predominantly to the south (Figure 4.4A). Such divergence was not evident within the modeled drifter paths obtained with either the Leeway or GABI-F modeling techniques. The differences in modeled drifter paths demonstrated in Figure 4.4 all stem from the degree to which the drifter models each include influences of the surface wind when determining drifter motion. The influences of the surface winds on modeled drifter motion are best elucidated through analyses of the modeled Eulerian water velocity fields produced by the ELCOM-MMP base-case model.

Figures 4.5-4.7 show the model-calculated Eulerian velocity field in the vicinity of point A at times of 30 minutes, 2 hours, and 4 hours and 10 minutes after the deployment of the field drifters. Each figure shows the speed contours at 2-m depth, as well as the modeled water velocity-vectors at the center of the ELCOM-MMP grid cells. The field drifter paths are shown in dashed lines with the field drifter positions indicated by the squares. Green lines and triangles show the drifter paths calculated with the GABI-F technique, and the blue lines and circles show the drifter paths calculated from the Lagrangian technique.

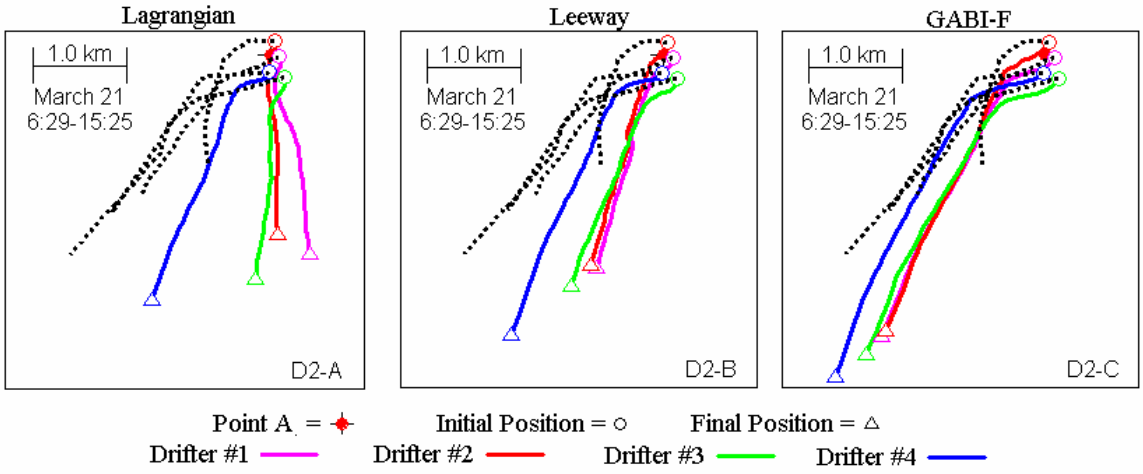

Figure 4.4 – Spaghetti Diagram plots of drifter paths from the D2 (March 21) simulations. A) Lagrangian drifter paths, B) Leeway drifter paths, C) GABI-F drifter paths. Field drifter paths are shown with black dashed lines.

For clarity, the paths derived with the leeway technique were not included; these paths lie between the Lagrangian and GABI-F paths as shown in Figure 4.4. The wind speed and direction toward which the wind was blowing are shown in the upper right corner of each figure.

Thirty minutes from deployment, the modeled drifters were located at the center of a low-velocity (less than 4.0 cm/s) patch of water (Figure 4.5). North of the drifters, the modeled velocities exhibited divergence, suggesting water was flowing around the patch containing the drifters. Water to the north-west of the drifters traveled toward the south-west, whereas the

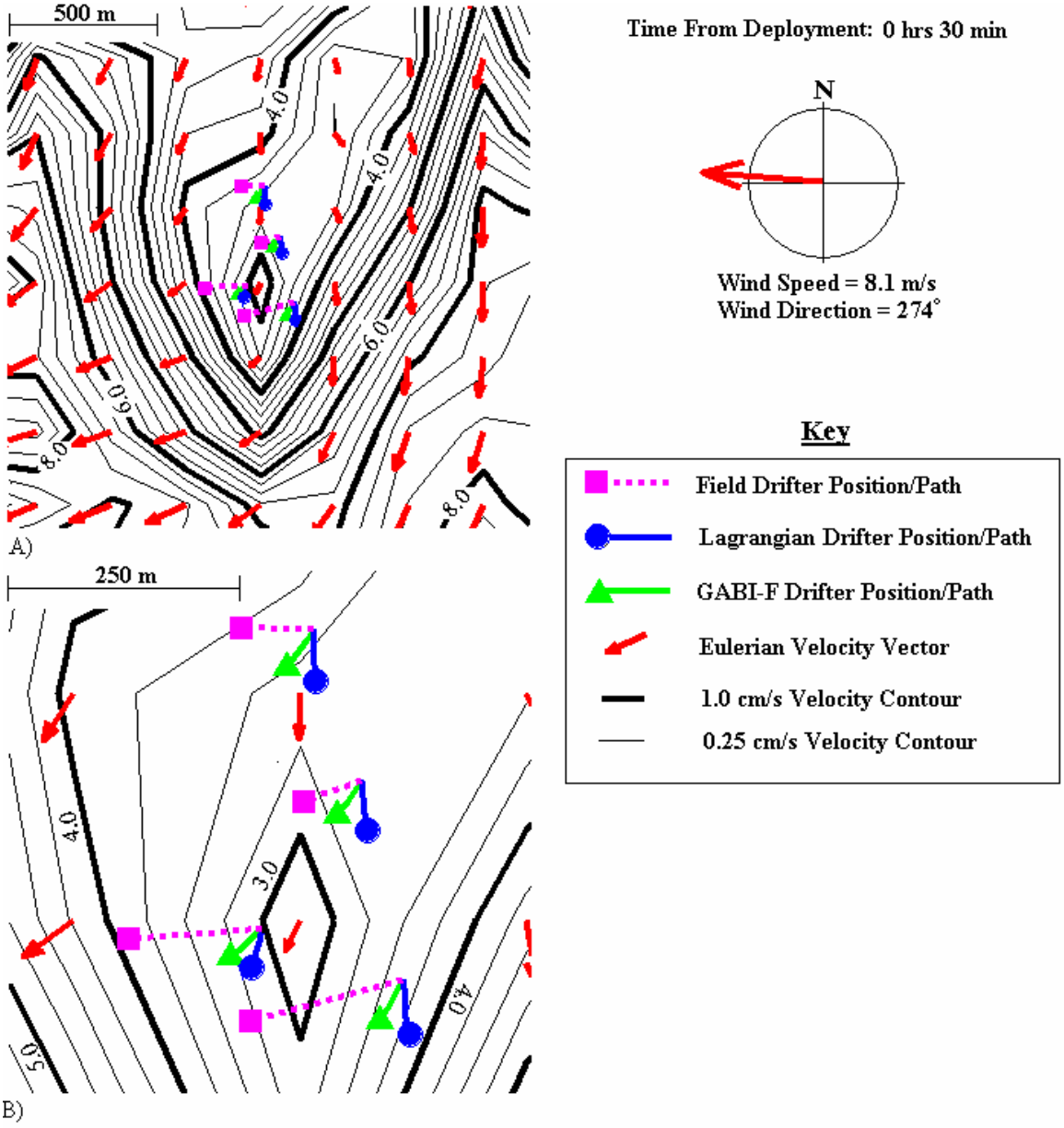

Figure 4.5 – Model Velocity Field for D2 Simulation, 30 minutes after drifter deployment. Contours indicate water speed (cm/s), arrows indicate model-calculated Eulerian velocity field.

north-eastern waters traveled toward the south-east. South of the drifter patch, water speeds increased (up to 8.0 cm/s), with directions ranging from the south-south-west at points 750 m east of the drifters to west-south-west at points 500 m to the west of the drifters. Each of the field drifters had by this time traveled to the west, with drifters #3 and #4 (the southern-most drifters) located within faster currents and having traveled 150m more than drifters #1 and #2. In contrast, the modeled Lagrangian drifters each traveled slowly to the south. Lagrangian drifter #4, which was (initially) the western-most drifter, began diverging from the others as it traveled slightly west of south.

The GABI-F paths (green lines/triangles on Figure 4.5) are in-between the field and Lagrangian paths. The GABI-F drifters traveled more to the west than the Lagrangian drifters due to the influence of the strong westward-blowing wind on the modeled drifter's antenna and surface float. As a result of this western movement, the GABI-F drifters entered regions of faster-moving water sooner than did the Lagrangian drifters, hastening the separation between the two groups. After 2 hours from deployment (Figure 4.6), the mean separation between pairs of Lagrangian and GABI-F drifters was approximately 200 m. The GABI-F drifters moved up to 3.0 cm/s faster than the Lagrangian drifters, and only Lagrangian drifter #4 traveled in the generally west-south-west direction as did the field and GABI-F drifters.

The modeled drifter positions 2 hours after deployment (Figure 4.6) suggest that separation between the Lagrangian and GABI-F drifters will continue over subsequent model time steps. Each of the GABI-F drifters is located within areas of faster moving waters, whereas the Lagrangian drifters (with the exception of #4) are still located within a patch of slow-moving water around their deployment positions. The GABI-F drifters are also approaching areas of even faster water movement which indicates they will soon accelerate away from the Lagrangian drifters, which are located within currents with small speeds and speed gradients in the direction of drifter motion.

The improved results from the GABI-F technique are most evident after 4 hours and 10 minutes since the deployment (Figure 4.7). At this time, the winds have shifted to a more south-westerly course, as have the field and GABI-F drifters. The Lagrangian drifters, with the exception of drifter #4, are still moving to the south at relatively slow speeds, as they are mired in a diminishing patch of slow moving water. Field drifters #1 and #4 are within 100m of their GABI-F counterparts, and the mean divergence between the Lagrangian and GABI-F drifters is now larger than the mean separation between the GABI-F and field drifters. These results suggest that the base-case ELCOM-MMP model skillfully calculated the MMP water velocities and that the model skill would not be apparent if only Lagrangian drifter modeling were used in comparing modeled and observed drifter motion. In this example, GABI-F drifter modeling is needed to more accurately reproduce the field drifter motion.

Although Figures 4.5-4.7 are useful at indicating the superiority of the modeled GABI-F paths, they are also indicative of potential problems in using spaghetti diagrams to make comparisons. Based on the field drifter paths upon deployment, the water velocity in the vicinity of Point A should have been 0.08-0.11 m/s, and no patch of slow-moving water was suggested by their movement. With such a patch existing in the model results, the field and modeled drifters initially diverged, and only two of the GABI-F drifters followed paths that eventually caused them to approach within 200 m of the field drifter locations after four hours from the drifter deployment (Figure 4.7). Thus the errors in the initial modeled drifter velocities contributed to subsequent drifter velocities being incorrect, and this error integration lead to the observed separation in modeled and field drifter paths. Although GABI-F drifters #1 and #4 were relatively close to the field drifters in Figure 4.7, their speeds at the time of the figure were 35% greater (on average) than the field

drifter speeds. This over-prediction of observed field drifter speed contributed to the eventual south westward separation between the field and GABI-F drifters (Figure 4.4C), as the net speed of the modeled drifters exceeded the net speed of the field drifters. This demonstrates how spaghetti diagrams, alone, may not be the sufficient for assessing model skill, because they may show modeled and observed drifters in close proximity but they do not provide any insight into the drifter movement after the time at which the diagrams were made. Therefore spaghetti diagram analyses using Figure 4.7 and Figure 4.4 might yield different conclusions regarding model skill.

4.2.3. Lagrangian Results using the Type I Analysis Method

Results from analyses using the Type I error metric from Toner et al (2001 -See Section 2.4.2) are presented for individual drifters (Figure 4.8) and as a composite average over all drifter experiments (Figure

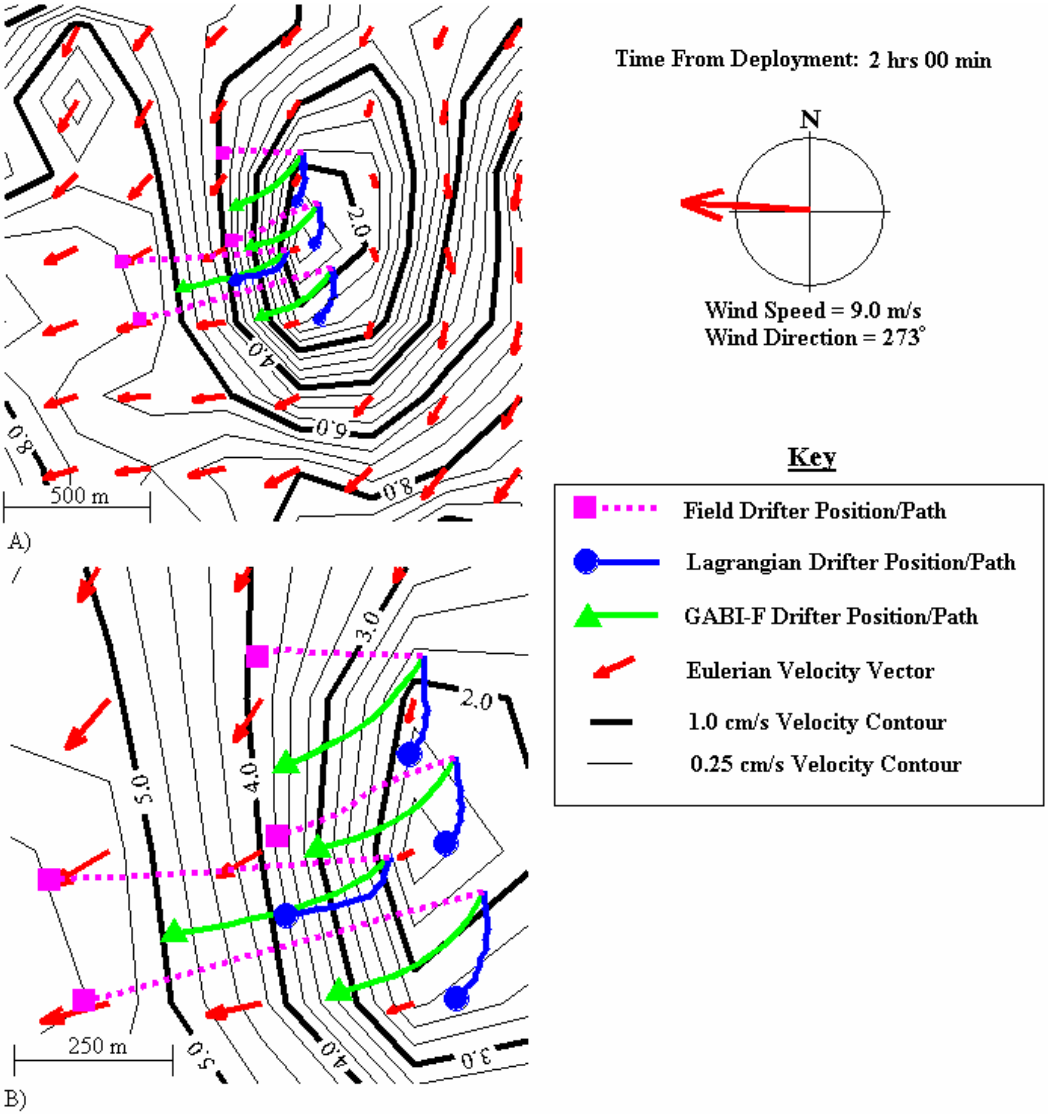

Figure 4.6 – Model Velocity Field for D2 Simulation, 2 hours after drifter deployment. Contours indicate water speed (cm/s), arrows indicate model-calculated Eulerian velocity field.

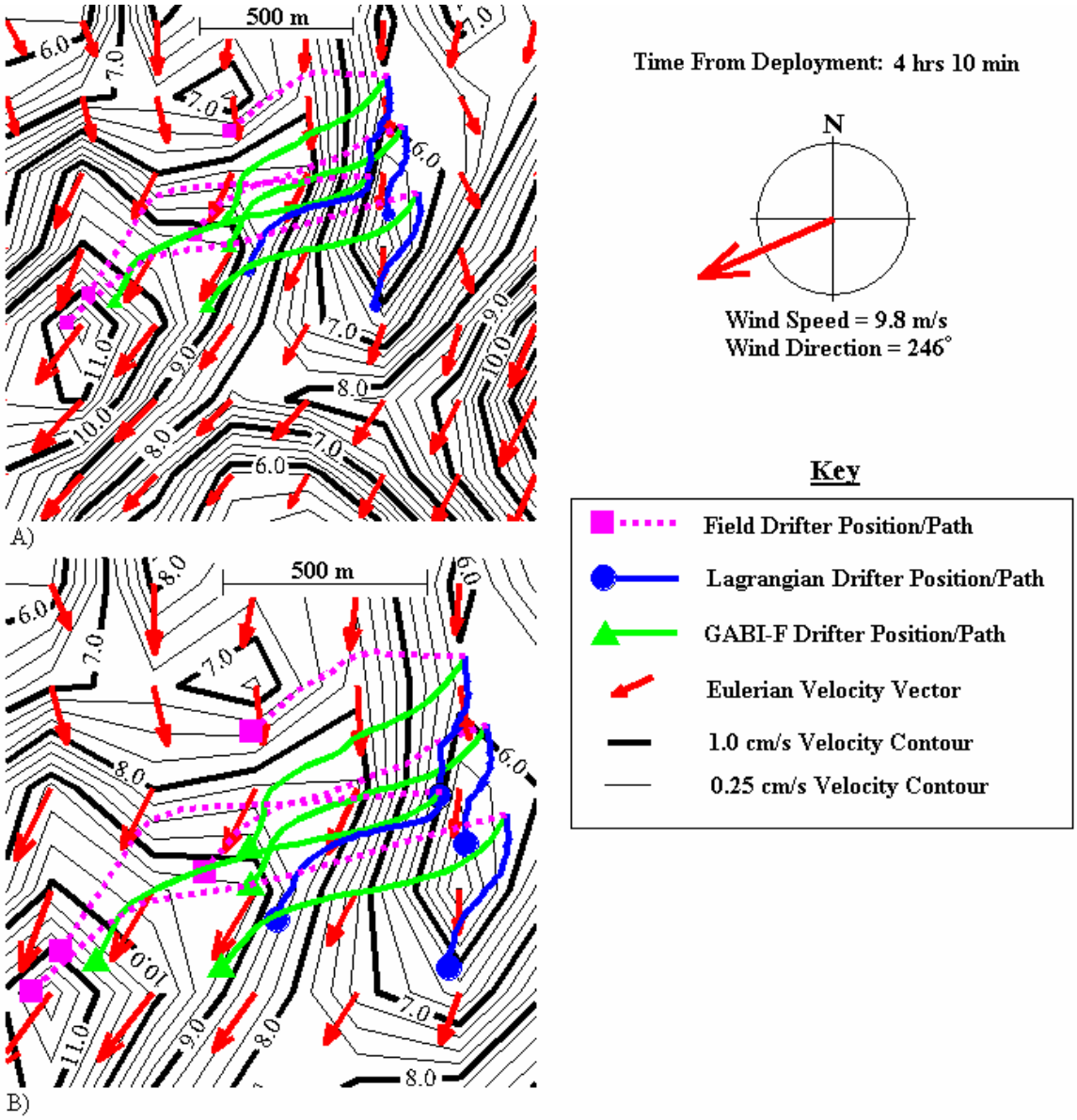

Figure 4.7 – Model Velocity Field for D2 Simulation, 4 hours and 10 minutes after drifter deployment. Contours indicate water speed (cm/s), arrows indicate model-calculated Eulerian velocity field.

4.9). Toner et al (2001) used four Type I error metrics to compare their model under various setup conditions and conducted limited analysis as to what their metrics implied about their model's skill overtime. For the work presented herein, twenty different drifter experiments (4 drifters per day over 5 days) were conducted. The twenty resulting Type I metrics provide consistent indications of model skill over the duration of the simulations but also indicate that the model tended to perform less skillfully immediately upon drifter deployment. The four sets of metrics plotted in Figure 4.8 were selected because they demonstrate the range in Type I metrics derived from the model. It is useful to remember that the Type I metric is defined as the ratio of the separation between the modeled and field drifter divided by the displacement of the field drifter, as quantified in Eq. (2.22).

The Type I metrics for drifter #2 from the D1 simulation (Figure 4.8A) are much greater than 100%, suggesting poor model skill and over-prediction of drifter speed and displacement. As shown in Figure 4.1 D1a-c, field drifter #2 traveled northward whereas the modeled drifters #2 traveled in the opposite direction. The nearly 180° directional difference in motion caused the separation between the modeled and field drifters to be large compared to the field drifter displacement, leading to the high Type I metrics. The metrics begin to decline after 3 hours, corresponding to the period when the modeled drifter begins to slow down and reverse its heading to a more northward direction. It is likely that the metrics would have continued to decline had the field drifters been deployed for a longer time period, as it is likely that the consistent model over-prediction of drifter speeds would allow the modeled drifter to lessen it's separation with the field drifter.

The Type I metrics from drifter #2 in the D2 simulation (Figure 4.8B) imply higher model skill than the D1 analyses (Figure 4.8A), which is consistent with the spaghetti diagram (Figure 4.1). The slight decline of the plot of the drifter #2 metrics from the D4 simulation (Figure 4.8C) after 3 hours from

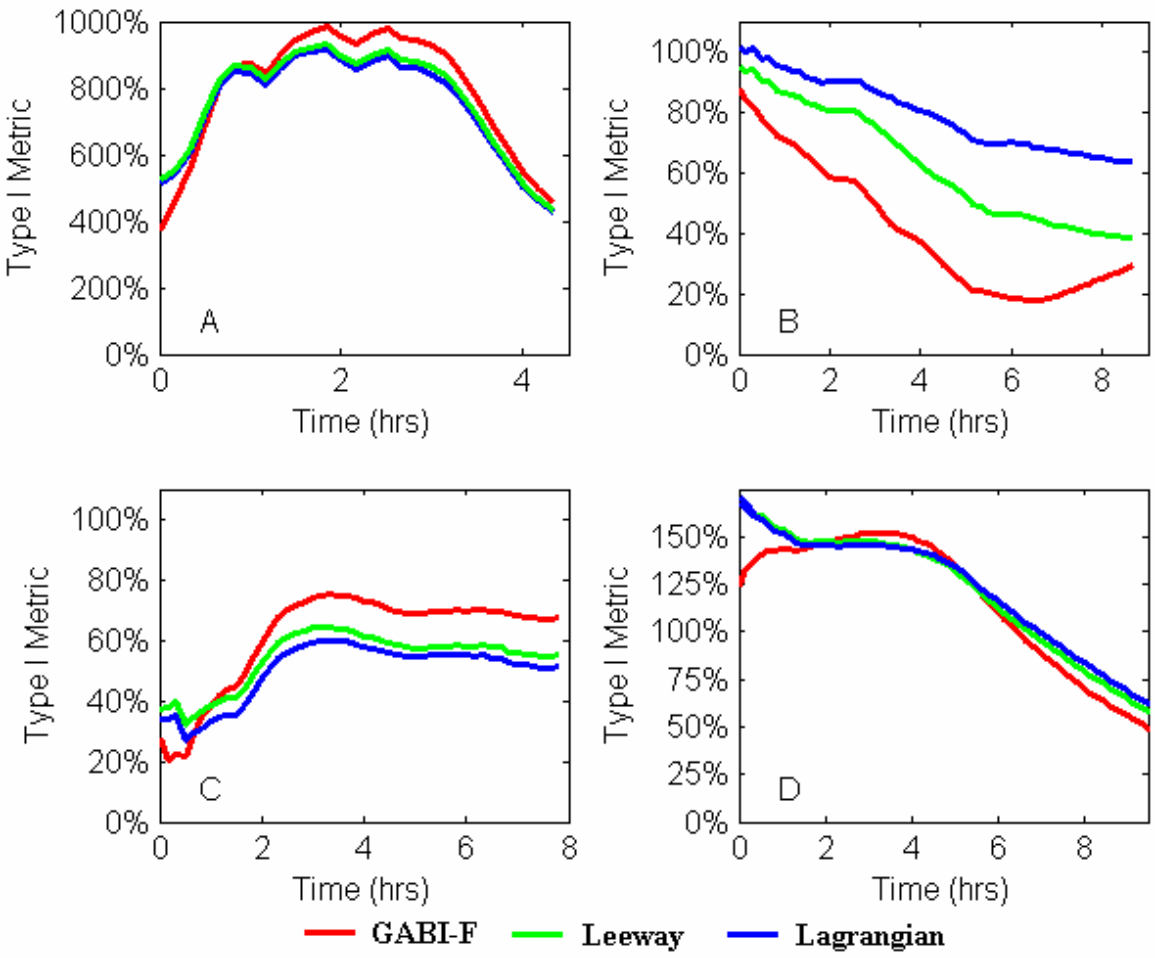

Figure 4.8 –Type I error metrics for MMP drifter simulations – A) D1 Drifter #2, B) D2 Drifter #2, C) D4 Drifter #2, D) D5 Drifter #4.

deployment suggests that divergence between the modeled and field drifters was approximately proportional to field drifter displacement for the remainder of the D4 simulations. These results suggest that the model is transporting drifters in the direction of the field drifter motion, thereby providing confidence that the model is accurately reproducing the surface velocities within MMP.

The results from the D5 simulation (Figure 4.8D) show how the Type I metrics can suggest a model is skillful when the spaghetti diagrams suggest the opposite. As shown with the spaghetti diagrams (Figures 4.1 D5a-c), modeled drifter #2 failed to follow the field drifter path. The modeled drifter initially traveled at speeds less than half of the corresponding field drifter (and in the wrong direction), producing large separations relative to the field drifter displacement. While the observed and modeled final speeds were comparable, the incorrect early behavior shown in the spaghetti diagrams suggests poor model skill. In contrast, the Type I metrics (Figure 4.8D) substantially decrease four hours after deployment, indicating improvement in model skill that is not discernible from the spaghetti diagram. The decreasing metric occurs because the separation between the model and field drifters remains relatively constant while the field drifter's displacement is increasing. As the model and field drifter were in substantially different places in the flow field, the correlation of their motion is arguably indicative of a larger-scale coherent motion that is well-represented by the model.

Both spaghetti diagrams and Type I metrics are integrative of model error because they are devised from a drifter's displacement from its deployment position. Conflicting interpretations of model skill from the two analysis methods, however, are possible because temporal trends in Type I metrics imply modeled drifter behavior with respect to the field drifters at any time within the simulation. This temporal behavior is not discernible from spaghetti diagrams unless the spaghetti plots also include temporal references for the displayed drifter paths. For example, the decrease in Type I metrics in Figure 4.8D after 4 hours from deployment implies that the model is improving. Through inspection of the spaghetti diagrams (Figure 4.1 D5a-c), it is obvious that both the modeled and field drifter paths tend toward the north-east at some point within the simulation. However, without temporal markers in the spaghetti diagram plot, it is impossible to discern that both modeled and field drifters headed to the north-east after 4 hours from the deployment (which caused the reduction in the Type I metric and the implied improvement in model skill). In this example, analyses of the spaghetti diagram plots are likely to suggest low model skill rather than improvements in model skill simply because the large separation in model and field drifter paths is the most obvious feature of the plots.

In comparing the drifter paths derived from simulations using each of the three drifter models, the Type I metrics shown in Figure 4.8 demonstrate 2 key features:

Modeled drifter paths from each of the three drifter models are more similar to each other than to the field drifter paths, and

Immediately upon deployment, GABI-F paths are often more comparable to field drifter paths than are Leeway or Lagrangian paths

These features were also apparent within the Spaghetti Diagram analyses presented in §4.2.2, and analyses with the Type I metric did not provide any new insight regarding the benefits of one drifter model over another.

As with the Spaghetti Diagram analyses, only for the D2 simulation do the Type I metrics suggest any benefit for using one drifter model over another. Within Figure 4.8B, the Type I metric from the GABI-F drifter model is always less than the metrics derived from the leeway and Lagrangian drifter modeling, indicating greater ELCOM-MMP model skill with the GABI-F model. Along with their lower relative magnitude, the GABI-F metrics were decreasing faster

than the other metrics until approximately 5 hours from deployment. This faster decrease also suggests greater model skill in that the GABI-F drifter was separating from its corresponding field drifter at a slower rate than calculated with the other drifter models. The increase in the GABI-F metric after 5 hours from deployment is due to the increased speed of the modeled drifters at this time. Increasing the modeled drifter speed caused increasing separation with the field drifter, and resulted in the large final separation observed in the spaghetti diagram plots (Figure 4.1 D2c). Speed increases were not suggested by the leeway or Lagrangian Type 1 metrics (Figure 4.8B), which is consistent with the smaller final separation between modeled and field drifters demonstrated in the D2 spaghetti diagram plots (Figure 4.1 D2a-b).

Composite Type-I metrics for all drifters deployments (D1-D5) support the conclusions that model skill generally improves overtime (Figure 4.9) as the longer-time drifter motion is dominated by larger-scale currents that can be readily captured by the model. The mean Type I metrics derived with each drifter model decrease with increasing time from deployment, indicating that the average separation between modeled and field drifters is increasing less than the increase in field drifter displacement. This suggests that the modeled drifter is traveling in a direction similar to that of the field drifter, and provides confidence that, over the duration of the simulation, the model is predicting drifter motion in a way that reasonably reflects the observed drifter

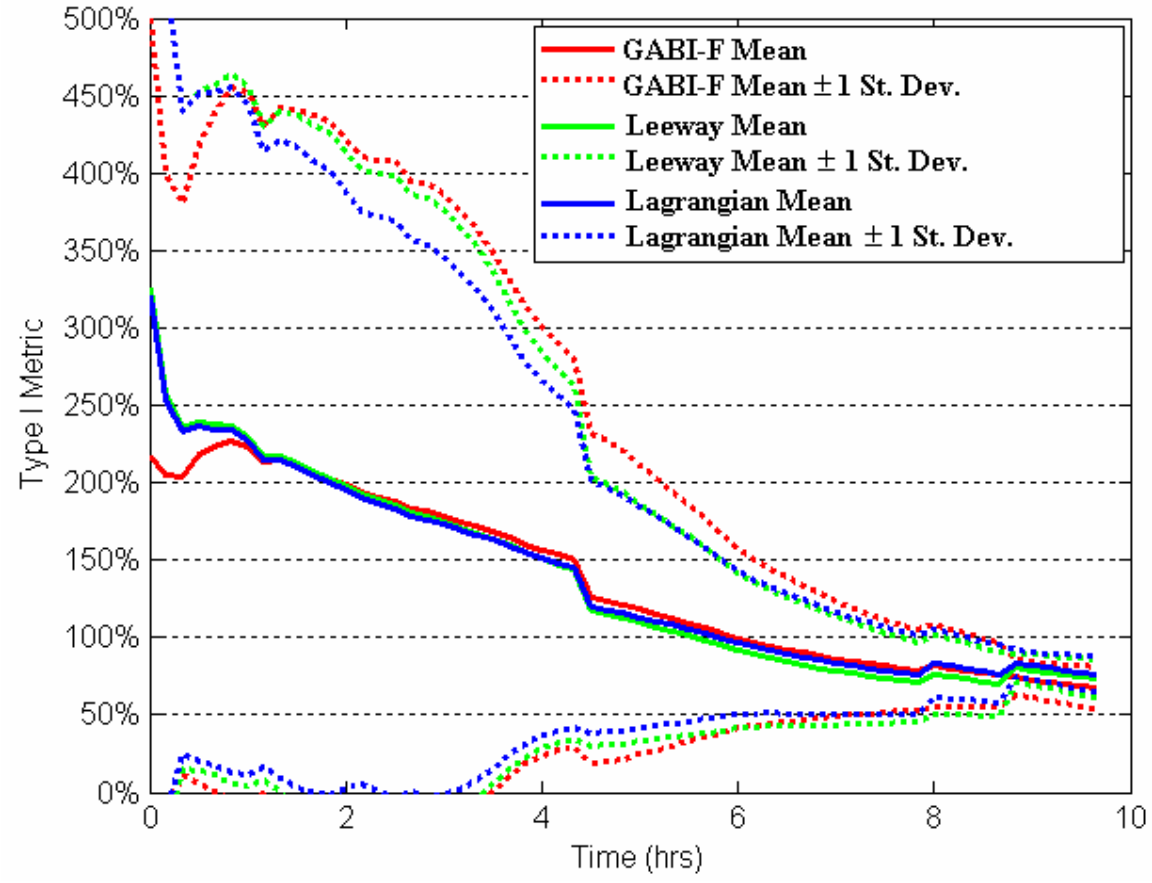

Figure 4.9 –Composite type I metrics vs. deployment time for all drifter simulations. Solid lines indicate mean values, dashed lines indicate mean values ± 1 standard deviation.

motion. The composite Type-I metrics also demonstrate the statistically insignificant differences in drifter paths derived from the different drifter models, especially as time from deployment increases. As shown in Figure 4.9, the mean metrics from each set of drifter model results are practically indistinguishable after 1 hour and the ranges of metric values at each time are nearly coincident. The minute differences in Type I metrics due to use of alternate drifter models supports the theory presented in Chapter 1 that a more precise drifter model (i.e., the GABI-F model) is necessary for model assessment over short time and length scales, but unnecessary as these scales increase and the integration of drifter paths is dominated by the large-scale currents.

4.2.4. Statistical Separation Results

The statistical separation method of drifter path analysis (Thompson et al. 2003, Section 2.4.3) compares the time-histories of the displacement of a cluster of field drifters to the time-histories of the median separation between modeled and field drifters. Using this analysis method, a model is considered valid if the median separation distance between the field drifter and its corresponding modeled drifter is less than the displacement distance of the centroid of the smallest polygon containing all members of a defined cluster of field drifters at the time of analysis. In addition, better models are those that predict smaller separation distances between the model and corresponding field drifter relative to the field drifter displacement.

The results of the statistical separation analyses on drifter paths derived from the base case ELCOM-MMP setup are shown in Figure 4.10. In applying this analysis methodology, the averaged displacements and separations from all 20 (5 days with 4 drifters per day) field and model drifters were used to obtain a general understanding of the model performance (Figure 4.10A). For assessing model skill during each simulation, the four drifters from each deployment day were used when calculating field drifter displacement and median model-field separation (Figure 4.10B-F). For clarity, field drifter displacement is plotted with solid lines in Figure 4.10, whereas the median drifter separations obtained when using each of the three drifter models are shown with broken lines. Model skill is high when the median model-field drifter separation is less than the median field drifter displacement, and greater skill is implied as the difference in the these median distances increases.

The statistical separation results depicted in Figure 4.10 show the same trend as seen in the Type I analysis results: the model performance tends to improve with increasing time from deployment. Statistical separation analysis results from the D2, D4, and D5 (Figure 4.10C, E, F), as well as the composite results from all drifter simulations (Figure 4.10A) indicate the ELCOM-MMP model provides a statistically reasonable representation of the field drifter motion. In contrast, the results from the D1 and D3 simulations show separation between the field and modeled drifters is greater than the median field drifter displacement throughout both simulations (Figures 4.10B, D). Flow divergence during these drifter deployments, combined with the statistical separation method's reliance on sets of field drifters, both contribute to the unskillful model assessments for the D1 and D3 deployments.

Unskillful model assessments with the statistical separation method are likely when the field drifters indicate flow divergence because the divergence tends to keep the centroid of the drifter cluster from displacing steadily increasing distances from its original location. The D1 deployment is a perfect example in that field drifters #1, #3, and #4 initially traveled south with drifter #2 diverging from the others and following a northward heading (See Figure 3.7). The result of this divergence is that the displacement of the centroid of the polygon bounding all field drifters was small compared to instances when flow divergence was not present. The small displacement compared with mean separations comparable to those achieved on

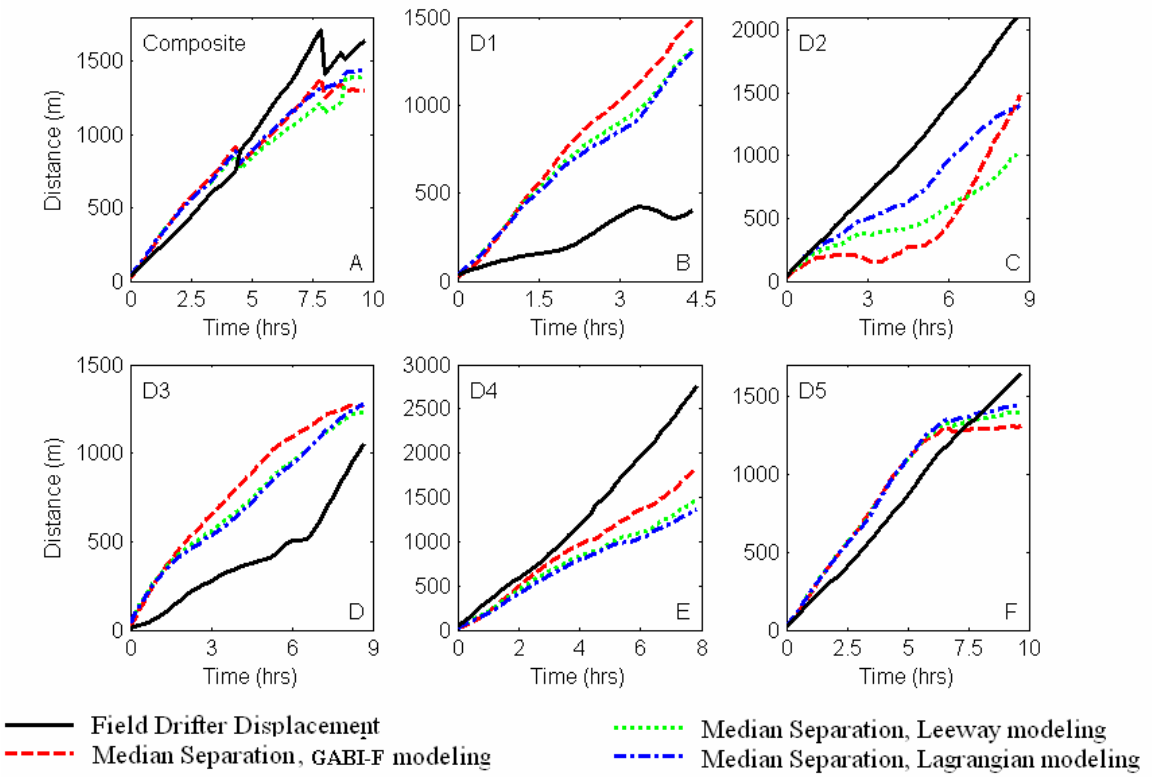

Figure 4.10–Statistical Separation Results from ELCOM-MMP Base Case Simulations: A) Composite of median values for simulations D1-D5, B) D1 simulation results, C) D2 simulation results, D) D3 simulation results, E) D4 simulation results, F) D5 simulation results. Solid lines indicate field drifter displacement; broken lines indicate separation between model and field drifters for each drifter model.

the other deployment days resulted in the unskillful model assessment for the D1 deployment. The divergence in field drifter paths from the D3 experiment also caused the small field drifter displacement indicated in Figure 4.10. Unlike the D1 experiment, however, the field drifters were deployed over a sufficient period of time such that the initial flow divergence disappeared and all four field drifters began moving as a group to the north. At this time (approximately 6 hours after deployment), the displacement of the field drifter set began to increase rapidly (Figure 4.10D), and it is likely that displacement would exceed the median model-field drifter separation had the drifters been retrieved 1-2 hours later. The D5 simulation results (Figure 4.10E) follow the same trends indicated for the D3 results, with the exception that the flow divergence was sufficiently short-lived to allow the drifter displacement to increase sufficiently to exceed the modeled drifter separation before the drifter deployment ended.

A second noticeable trend in the statistical separation results presented in Figure 4.10 is that the choice of drifter model does not significantly affect the skill assessment.. With the exception of the D2 simulations, the differences in mean separation derived from different drifter models were always less than the differences between the mean separation and field drifter displacement. As such, it is difficult to conclude that one drifter model produces improved results when compared to another drifter model based on the

statistical separation methodology: all that can realistically be said is that each model performs similarly over the duration of the analysis. The D2 simulation, however, does suggest that the GABI-F method at least initially improves upon the leeway and Lagrangian drifter methods (Figure 4.10C). The improvement is evident up until approximately 6 hours from the drifter deployment, corresponding to the time at which the model begins to over-predict drifter speed causing the separation to increase. Similar decreases in model skill at this time were suggested with the Type I metric (See Section 4.2.3) and to a lesser extent with the Spaghetti diagrams (Section 4.2.2).

In summary, the statistical separation analyses presented in Figure 4.10 and discussed above suggests the following:

1. The ELCOM-MMP model becomes more skillful as drifter deployment time increases and integration of the larger-scale currents dominates the assessment metric.

2. Different drifter models perform statistically similarly over longer times.

3. The statistical separation technique is unsuitable for diverging flow.

As the conclusions #1 and #2 correspond well to those from the Type I analysis (See Section 4.2.3), the statistical separation analyses does not provide any new insight into model skill in representing drifter movement. As the Type I analysis is not influenced by flow divergence, it appears superior to the statistical separation method.

4.2.5. Circle Assessment Results – Overview

As described in section 2.6, the Circle Assessment method is designed to be applied at multiple times during each simulation, with comparisons between field drifter and modeled drift paths originating from the position of the field drifter at the time of the comparison. Within this research, the Circle Assessment method was applied for each field drifter at the beginning of each modeled timestep. Over the course of the 5-day experiment, this resulted in 960 drifter-timesteps (See Section 3.5.2) over which comparisons between the observed and modeled drifter paths were made. The following sections (§4.2.6-§4.2.9) contain interpretations and explanations of the Circle Assessment results, focusing on how the analysis method is more illustrative of model skill than the Spaghetti Diagram, Type I, or Statistical Separation methods (sections 4.2.2-4.2.4). The Circle Assessment results also indicate that the GABI-F drifter model produces improved predictions of the field drifter motion when compared to the Lagrangian and Leeway drifter models. The improved results, however, are only distinguishable for comparisons made over time scales that are limited to a small number of model timesteps. Comparisons made over longer time periods become influenced by the integration of error in the drifter positions, and this error source dominates the decrease in error gained with use of the GABI-F drifter model instead of the leeway or Lagrangian drifter models.

The Circle Assessment method compares modeled drifter paths to field drifter paths using two types of analyses: 1) the model timestep analysis, and 2) the separation analysis (see Section 2.7, 2.8). Because of the different timescales involved, each analysis type provides different information regarding model skill at reproducing drifter movement. As implied by its name, the model timestep analysis provides statistical information on the likelihood of correctly modeling drifter movement (i.e., within the positional accuracy/target circle of the field drifter) over a single model timestep. In contrast, the separation analyses provide measures of the lengths and times over which the model correctly predicts drifter movement, and these times may be greater than, less than, or equal to the model timestep. This dual approach toward quantifying model skill provides a degree of robustness to the results analysis that is not available with any of the other analysis techniques (i.e., spaghetti diagrams, Type I metrics, and statistical separation) discussed in this work.

4.2.6. Model Timestep Analysis - κ-scores and Success Probability

The model timestep analysis is ideally suited to a binary "good/bad" assessment of model skill as the method compares drifter paths over fixed intervals. For a model to be considered good, it must predict drifter transport into the field drifter's target circle at the end of the timestep (See Section 2.8.1). The model success probabilities and κ-scores, Eq. (2.34), describe the likelihood that such perfect drifter transport will be achieved. As shown in Table 4.2, κ-score values from simulations using the Lagrangian and Leeway drifter models were identical at 66%. Simulations with the GABI-F drifter model produced a higher κ-score (74%) indicating that the GABI-F drifters were more likely to follow the paths implied by the field drifter data. The model success probabilities from simulations using the GABI-F drifter model were also nearly 75% higher than those achieved when using the Leeway or Lagrangian drifter models (Table 4.2).

As model success probabilities reflect the frequency at which the drifters were successfully transported over individual model timesteps, the higher GABI-F success probability corroborate the conclusions drawn from the κ-score analysis. The model success rates, however, are also relatively low, suggesting that the base case ELCOM-MMP model only perfectly reproduces drifter motion once out of ever 3-5 opportunities, regardless of the drifter model used for calculating drifter motion. The two conclusions drawn from these results are:

1) the GABI-F model is more successful at reproducing the field drifter motion, and

2) The base-case ELCOM-MMP model is largely unsuccessful at calculating drifter transport within the positional accuracy of the field drifter.

Together, these conclusions imply that discrepancies between the model and field drifter paths are influenced to a greater extent by aspects of the ELCOM-MMP model setup other than the choice of drifter model. This concept is explored further in Section 4.3 where simulations using the GABI-F drifter model and various alternative ELCOM-MMP model setups are compared. Essentially, section 4.3 describes how drifter modeling may be used to diagnose problems within the hydrodynamic model setup.

In developing the analysis above, numerous properties of the model timestep analysis method were elucidated, and these properties must be understood to properly interpret model κ-score and success-probability results. Both success probabilities and κ-scores range from 0-100%, with 100% indicating that all modeled drifters were correctly transported into their respective field drifter's target circle at the end of the model timestep. The difference between the two measures is that model success probabilities have direct interpretations regarding model skill, whereas κ-scores are more of an abstract measure. For example, a model with 50% success probability has perfectly transported one out of every two model drifters into the field drifter's target circle. A 50% κ-score, however, does not suggest the model will correctly transport one out of two drifters, nor does it suggest the model will correctly transport all drifters for ½ the model timestep. A 50% κ-score, however, is clearly better than a 25% κ-score, and comparisons of κ-score values calculated

Table 4.2 – Model Timestep Analysis Results for base-case ELCOM-MMP simulations

	Model Timestep Analysis	
Drifter Model	κ-score	Success Probability
Lagrangian	66%	21%
Leeway	66%	20%
GABI-F	74%	34%

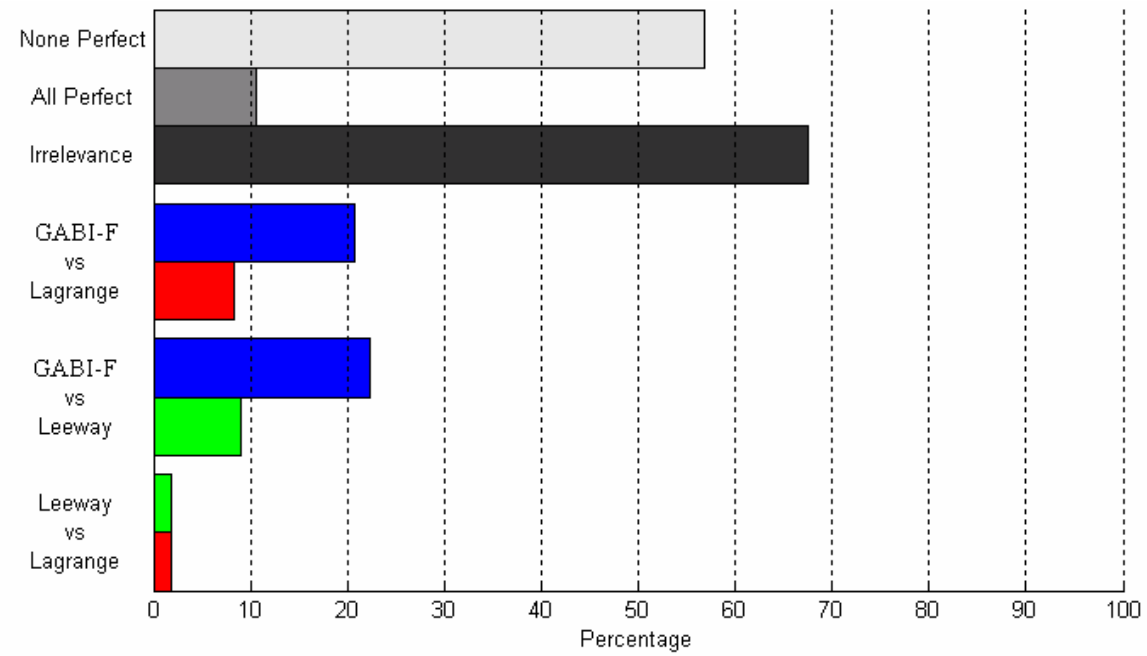

Figure 4.11 – Comparative Failure Analysis Results – base case ELCOM-MMP simulations. Results from the GABI-F simulations are shown in blue, Leeway results are in green, and Lagrangian simulation results are shown in red.

for multiple simulations provides insight into the relative efficacy of each of the simulation setups.

Proper selection of the model timestep is critical for obtaining meaningful results with the model timestep analyses, as the timestep and field drifter speed dictate the distances over which model timestep analyses are made. If the timestep and drifter speed are small, they are more likely to produce a small field drifter displacement relative to the field drifter's target circle radius. In such a situation, the field drifter's target circles may overlap (see Figure 2.13) thereby increasing the range of drifter velocities the model could calculate that would correctly transport the drifters. For any given model application, κ-scores and success probabilities will increase if the model timestep is sufficiently decreased (See Section 4.3.5 for an example). Indeed, in the limit as timesteps decrease to 0, κ-score and success probabilities will approach 100%. Such a situation is not conclusively indicative of any increases in model skill; the increases may be caused by increased model skill or may be simply attributed to the overlap in target circles as the timestep duration decreases. As such, κ-score and success probability values from simulations with different timesteps should not be compared. Model timestep analyses are not suitable for assessing the impact of alternative model timesteps on model skill. This property of the model timestep analysis method is further discussed in Section 4.3.5.

4.2.7. Comparative Failure Analysis

Figure 4.11 presents results from the comparative failure analysis (§2.8.2) of the base-case ELCOM-MMP simulations, with the results from each drifter-timestep categorized into comparative scenarios. Each scenario indicates the percentage of drifter timesteps which were perfectly modeled with one drifter model but were imperfectly modeled an alternative drifter model. Additionally, the "None Perfect" and "All Perfect" scenarios, respectively, indicate the percentages of drifter-timesteps which were imperfectly and perfectly modeled with all of drifter models. The "irrelevance," defined herein as the

percentage of drifter-timesteps over which the choice of drifter model did not influence the simulation results, is given as the sum of the percentages for the "None Perfect" and "All Perfect" scenarios.

As shown in Figure 4.11, 68% of all instances of drifter transport did not demonstrate improved results from simulations with any of the three drifter models, and in 57% of all drifter-timesteps the drifter motion was not perfectly reproduced with any of the drifter models. Assuming discrepancies between the field and model drifter paths are not due to inaccuracies in the drifter model calculations, these results support the conclusion derived from the success-probability analysis (§4.2.6) that the drifter model is not the greatest source of error in predicting drifter transport. The logic behind this conclusion is intuitive, for if the greatest source of error in the drifter motion were due to the choice of drifter model, then the "Irrelevance" and "None Perfect" values shown in Figure 4.3 would be less than 50%. For example, with a "None Perfect" value of 57%, more than half of the model drifters were modeled imperfectly irrespective of the drifter model used in the simulation. Therefore switching from one drifter model to another did not improve the model results for over 50% of all drifter time-steps, and some other aspect of the ELCOM-MMP model setup must be contributing more error to predicted drifter paths.

Of the 33% of instances of drifter transport comparisons for which the choice of drifter model was important (i.e., importance = 100% - irrelevance), simulations using the GABI-F model produced successful results more often than those using the Lagrangian or Leeway models (Figure 4.11). As shown, the GABI-F drifter model produced improved results over the Lagrangian drifter model in 21% of all comparisons. In contrast, the Lagrangian model results showed improvements over the GABI-F model results) for only 8% of all comparisons, thus suggesting a net GABI-F improvement for 13% of all drifter timesteps. In comparison with the Leeway drifter model, the GABI-F method produced a similar net improvement of 13%. Comparisons between the Leeway and Lagrangian drifter models (Scenarios #7 and #8) indicate no relative net-benefit from incorporating either method into the ELCOM-MMP simulations. Conclusions drawn from the comparative failure analysis are:

1. ELCOM-MMP base case simulations are less than 50% likely to perfectly predict drifter transport over the model timestep,

2. Simulations using the GABI-F drifter method are more likely to successfully predict drifter transport than are simulations using the Lagrangian or Leeway drifter models, and

3. Simulations using the Lagrangian or Leeway drifter models are equally likely to perfectly predict drifter transport.

These conclusions are in accord with those derived from the κ-score and success-rate analyses discussed in section 4.2.6.

4.2.8. Causative Failure Analysis

Within causative failure analysis, model results are analyzed only to identify why drifter transport was imperfect rather than to describe the degree of "imperfection." As presented in Section 2.8.3, failure to correctly model drifter transport at any given drifter-timestep may be due to one of the following conditions:

"Direction Error" – Modeled drifter's speed is within the acceptable range for its initial position, but its direction is not suitable for its speed.

"Speed Error" – Modeled drifter's direction is within the acceptable range for its initial position, but its speed is incorrect for its direction of travel.

"Combination Error" – Both the modeled drifter's speed and direction are within the acceptable ranges for its initial position, but the combination makes the transport unacceptable

"Total Error" – Both the modeled drifter's direction and speed are outside of the

acceptable ranges for the drifter's initial position.

The relative proportion of failures due to each of these four error types may indicate trends in the model drifter's predicted velocity. These trends may, in turn, lead to methods for improving the hydrodynamic model results. For example, if a majority of model failures were due to the model drifter's predicted direction of travel (i.e., Direction Error), then it is possible that the hydrodynamic model has a directional bias within its solution procedure. Alternatively, if the model failures are mostly attributed to speed errors, results may be improved by adjusting the mixed-layer depth within the model solution algorithms (§4.3.5). Modeling problems leading to Total Errors are more problematic to diagnose as they incorporate both speed and direction errors. As such, total errors are "worse" errors, and simulations with a lower percentage of total errors may be considered more skillful. Model skill assessments are also possible through relative analyses of combination error failures. Drifter movement that fails due to combination error must be very close to being considered "perfect" as both the drifter's speed and direction are within the acceptable ranges. Therefore the proportion of failures due to combination error and due to the other error conditions provides an indication of how often the model was nearly-perfect and therefore more skillful. Figure 4.12 presents the causative failure analysis results from the base-case ELCOM-MMP simulations.

Numerous trends are evident in the base-case ELCOM-MMP causative analysis results (Figure 4.12). Irrespective of the drifter model, total errors dominate the error results. This indicates that where the model imperfectly represents drifter transport, the imperfection is most likely due to errors in both the model drifter's speed and direction. Speed errors were also consistently the second most prevalent error type and were much more common than direction errors regardless of the drifter model used. These trends jointly suggest that the base-case ELCOM-MMP model fails mostly due to its inability to consistently reproduce the observed drifter speeds. Based on this analysis, improving the ELCOM-MMP model setup to better reproduce the field drifter speed seems the most promising avenue toward improving the agreement between the model and field drifter paths.

As indicated in the discussion of success-probabilities (§4.2.6), the GABI-F drifter model was the most successful approach for calculating drifter

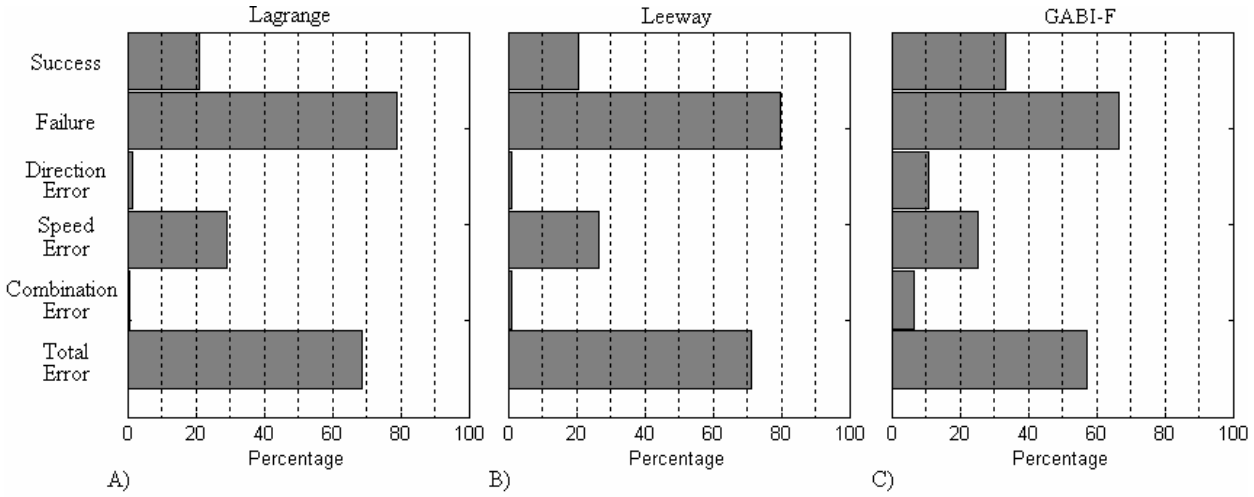

Figure 4.12 – Causative Analysis Results by Drifter Model – A) Lagrangian modeling results, B) Leeway modeling results, C) GABI-F results.

transport. This assertion is also evident in Figure 4.12. For example, the greatest percentage of combination error failures were obtained with the GABI-F drifter model, indicating that the model produced drifter paths closer to perfection more often that did the Lagrangian or Leeway drifter models. The GABI-F drifter model also produced proportionally less total error failures, indicating it is more likely to at least correctly predict the drifter's speed or direction (if not both). For the Lagrangian and Leeway drifter models, speed errors occurred in 98% of drifter-timestep failures (Total speed errors are determined as the sum of speed errors and total errors). Speed errors were proportionally less of a problem within the GABI-F model results (83%). Although the improvement in speed errors when using the GABI-F model is slight relative to their size (ie 98% error reduced to 83% error), the improvements are directly discernible from the Causative analyses. In fact, the relatively uniform high percentage of speed errors suggests that the errors are caused by other aspect of the ELCOM-MMP setup rather than the drifter model.

By definition, achieving speed failure requires that the model drifter travels either too fast or too slow. The relative percentage of fast : slow drifters provides and indication of the tendency of the ELCOM-MMP model to either under-predict of over-predict drifter speed. As shown in Table 4.3, simulations with the Lagrangian and Leeway drifter models tended to over-predict drifter speed. In contrast, the speed failures from the GABI-F simulations (Table 4.3) are more evenly caused by model over- and under-prediction. This even distribution, in comparison to the fast-favoring distributions for the Leeway and Lagrangian models, suggests that the GABI-F drifter model tends to decrease the modeled drifter speed, bringing it closer to the speed of the field drifter and yielding greater agreement between the field and model drifter paths.

Table 4.3 – Quantification of Speed Failures for the base case ELCOM-MMP results

Drifter Model	Speed Failures[1]	Fast Failures[2]	Slow Failures[2]
Lagrangian	70%	78%	22%
Leeway	72%	80%	20%
GABI-F	68%	49%	51%

[1] Speed Failure percentages shown relative to the total number of drifter-timesteps simulated.

[2] Fast and Slow Failure percentages are relative to the total number of speed failures for each drifter model

4.2.9. Separation Analyses using κmax

The second type of Circle Assessment analysis uses the separation between the field and modeled drifter in order to assess model skill (§2.7.1-§2.7.3). Whereas the model timestep analyses (§2.8) compared drifter paths over fixed time intervals, the separation analyses compare drifter paths over time periods defined by the separation between the modeled and field drifters. For relating modeled drifter separation to field drifter displacement, κ_{max} values (Eq. (2.33)) are used. Higher κ_{max} values indicate that the modeled drifter results were considered "perfect" (i.e., separation less than the target circle radius) over a longer drifter pathlength, reducing the allowable range in modeled drifter speeds and directions according to Eqs. (2.31) and (2.32). Higher κ_{max} values also tend to indicate that the model drifter path was considered "perfect" for longer periods of time. This general relationship, although observed in the MMP simulations, will not always be true because the κ_{max} values are functions of both the field drifter velocity and the perfection time. Therefore higher κ_{max} values may be obtained when the field drifter velocity is higher or when the model calculates perfect drifter motion for longer periods of time. This concept is discussed further below, after the base-case ELCOM-MMP κ_{max} results are presented and analyzed. In the following discussion, "perfection times" (§2.6.3) are always presented to lessen any potential misinterpretation of model skill implied by the κ_{max} results.

Examples of comparisons of data from the D2 ELCOM-MMP simulation (Figure 4.13) indicate the typical occurrence of

higher κ_{max} values for drifters modeled using the GABI-F technique. All modeled drifter paths indicated in Figure 4.13 represent the best modeled drifter paths out of the 33 modeled drifters used to simulate each field drifter (See Figure 3.6 in Section 3.5.2). As each of the 33 modeled drifters simulated at each drifter-timestep is initially located at a different point within the field drifter's target circle, the "best" modeled paths using each of the drifter models may be derived from different locations within the initial target circle. Such a situation occurs in Figure 4.13A where the best paths from the Leeway and Lagrangian models originate from the same point, but the best GABI-F path has a different origin. While comparing paths originated at different locations is counter-intuitive, it follows from the assumption introduced in section 2.6.1 and carried throughout this research. The Circle Assessment method assumes that a field drifter is equally likely to occupy any point within its target circle, thus making any such point a valid starting point for drifter modeling.

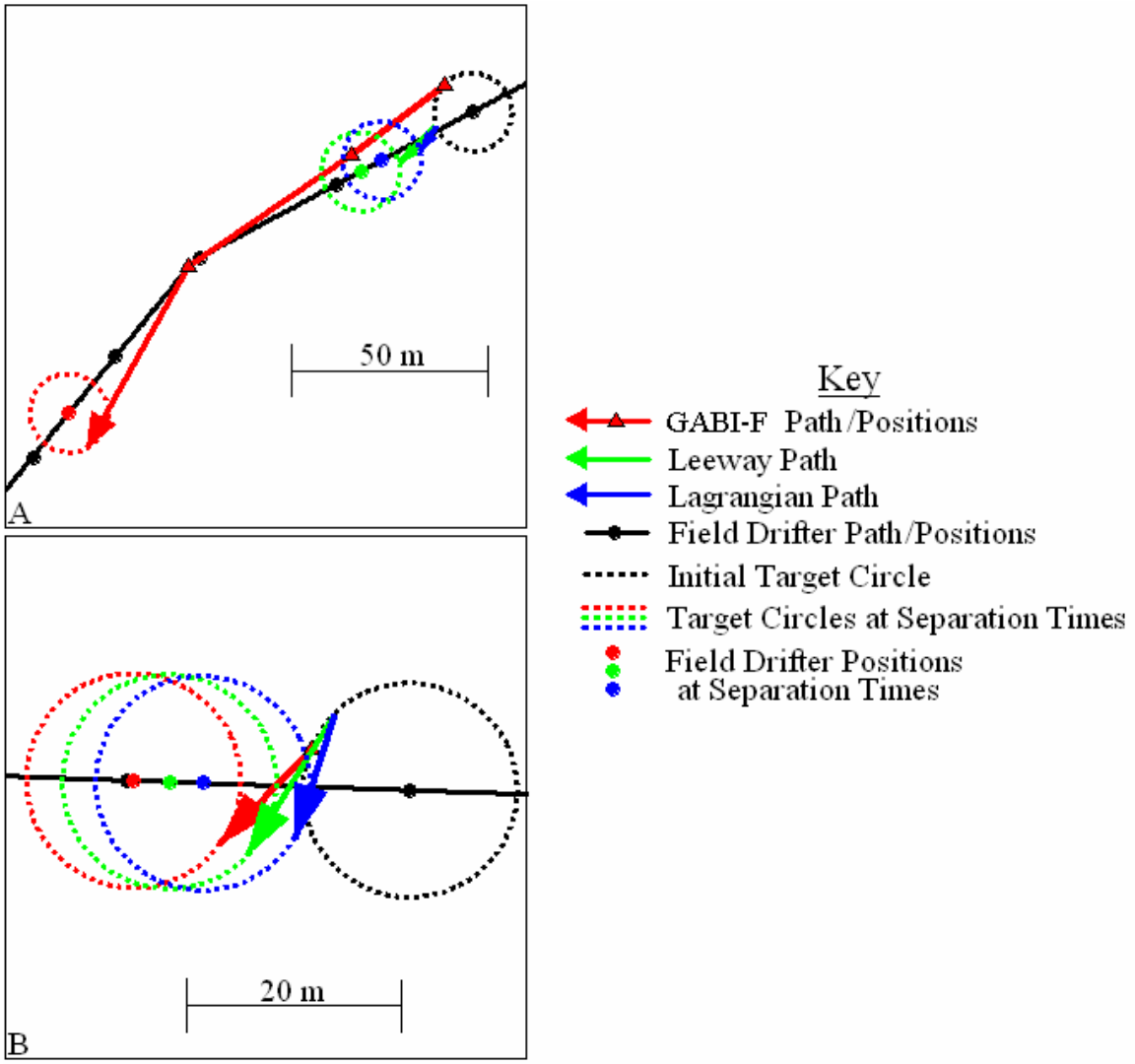

Figure 4.13 – Drifter Model Comparisons using Separation Analyses – A) Separation time much greater than the model timestep, B) Separation time less than the model timestep. In each scenario, the GABI-F drifter path (red) more closely approximates the field drifter path (black). Data from the D2 base-case ELCOM-MMP simulation

In Figure 4.13A, both the Leeway and Lagrangian modeled drifters traveled in suitable directions but at speeds much slower than the field drifter. The slower drifter speeds resulted in relatively rapid separation between the field and modeled drifters, and limited the κ_{max} values to 1.6 and 1.3 for the Leeway and Lagrangian drifter models, respectively. At the drifter-timestep shown in Figure 4.13A, the Leeway and Lagrangian separation times were on the order of 400s, or 2/3 of a model timestep. In contrast, the GABI-F drifter traveled at a speed comparable to that of the field drifter, achieved a κ_{max} value of 6.5, and remained "perfect" for nearly 3.5 timesteps. The improvement due to the use of the GABI-F drifter model is evident from the κ_{max} and separation time values, as well as the spaghetti diagram plot in Figure 4.13A.

A similar conclusion on the relative merits of the three drifter models may be drawn based on Figure 4.13B, although the improvement among model results is not as dramatic as in Figure 4.13A. In Figure 4.13B, each modeled drifter had separation times less than the model timestep, and their directions of travel were more to the south than was that of the field drifter. None of the drifter models would have been deemed successful through the model timestep analyses, as the modeled drifter positions at the end of the timestep were all separated from the field drifter by distances exceeding one target circle radius. As such, in this instance the model timestep analysis is unable to distinguish any improvement due to the use of the GABI-F model. In contrast, the simulations shown in Figure 4.13B indicate improvement amongst the drifter model results, with κ_{max} values ranging from 1.3 for the GABI-F model to just under 1.0 for the Lagrangian method. This example demonstrates how κ_{max} analyses may provide insights into model behavior that are too subtle for the model timestep analysis methods. The κ_{max} analyses, however, do not provide insight into the causes of separation between the modeled and field drifters, which is available through failure analysis using the model timestep analysis methods (§2.8.3 and discussed above). Therefore both the model timestep and separation time analyses provide complementary techniques to characterize and compare the results from different simulations.

Over the 960 drifter-timesteps from all of the drifter modeling (D1-D5), comparisons of κ_{max} results achieved with each drifter model consistently indicated improvement with the GABI-F technique. Figure 4.14 shows percentage improvement in κ_{max} values achieved when modeling individual drifter-timesteps with one drifter model over another. As shown, the GABI-F drifter model produced superior results over 72% of the drifter timesteps when compared with the Leeway drifter model, and 71.0% of the drifter timesteps when compared with the Lagrangian drifter model. The Lagrangian drifter model also improved upon the Leeway drifter model as it produced superior results for 58% of the drifter-timesteps. Mean κ_{max} values obtained over all of the 5 drifter-deployment simulations were 1.8, 1.5 and 1.5, respectively for the GABI-F, Leeway, and Lagrangian methods. These κ_{max} results indicate that the GABI-F model produces improved representations of the MMP field drifter paths (with respect to the Lagrangian and Leeway modeled paths). This same conclusion was also reached from the model timestep analyses.

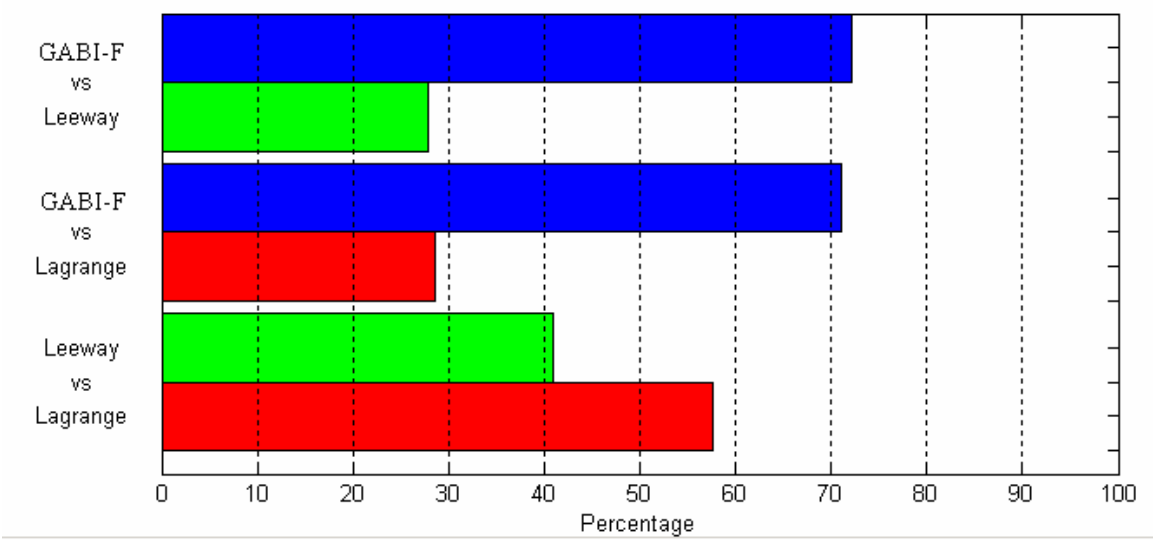

Figure 4.14 – Comparing κ_{max} results by drifter model – ELCOM-MMP base case simulations. For 71% and 72% of the drifter-timesteps, the GABI-F drifter model produced higher κ_{max} values than did the Lagrangian or Leeway models, respectively.

The κ_{max} analyses provide tools for comparing drifter paths derived under different model setups. As shown above, κ_{max} values from drifters modeled with the GABI-F technique were often higher than those from drifters modeled at the same time and location using the Leeway or Lagrangian techniques. Analyses using κ_{max}, however, are not very illustrative of the hydrodynamic model's absolute ability to reproduce the field drifter motion. For example, consider the implications of having a mean κ_{max} value of 1.8 as achieved for the MMP simulations with the GABI-F technique. At κ_{max} = 1.8, the average modeled drifter separated from its corresponding field drifter by a distance equal to the target circle radius after the field drifter traveled a distance equal to 3.6 times the target circle radius (See Eq. (2.33)). This information does not imply any definitive relationship between the field drifter path and the modeled drifter behavior. If the field drifter moves very slowly, then the model drifter might be perfect for an extraordinarily long time, and yet have a small κ_{max} simply because the field drifter path-length is short. The same small κ_{max} might result from rapid field drifter motion that is poorly captured by the model so that the separation occurs in less than a model time step. Thus with two plausible explanatory scenarios and only one single comparative metric, it is difficult to draw conclusions on model skill. Comparing κ_{max} values from drifters modeled under different setups but at the same place and time within the model domain, however, eliminates the ambiguity in the κ_{max} interpretations because the field drifter's motion is identical in each simulation. Thus, rather than an absolute scale of model skill, κ_{max} is a diagnostic tool for comparing the effectiveness of different modeling approaches.

To further clarify how the separation analyses using κ_{max} are biased by drifter speeds, consider two scenarios (Table 4.4): A)"fast" drifters moving at 10 cm/s in the field and at 11 cm/s in the model, B) "slow" drifters moving at 1 cm/s in the field and 1.1 cm/s in the model Given a target circle radius of 10 m and a 1 cm/s absolute speed difference between the model and field, scenario A drifters will remain perfect for 1000 seconds while the field drifter displaces 100 m. In this situation, κ_{max} = 5 and the modeled drifter speed is 110% of that of the field drifter. In comparison, although scenario B drifters have the same relative

Table 4.4 - κ_{max} calculations for fast and slow field & modeled drifter speeds

Scenario	Field Speed	Model Speed	Speed Differences		τ_d (s)	Field Displacement	κ_{max}
			Absolute	Ratio			
A	10 cm/s	11 cm/s	1 cm/s	110%	1000 s	100 m	5
B	1 cm/s	1.1 cm/s	0.1 cm/s	110%	10000 s	100 m	5

speed difference as the scenario A drifters, their lower speeds cause equal separation while the field drifter displaces a smaller distance. As such a larger perfection time (τ_d) is required for $\kappa_{max} = 5$ for scenario B. The increased perfection time for scenario B reflects that a model must be perfect for a longer duration of time when the drifter speed is slow to obtain equal κ_{max} results as for when the drifter speed is large.

The example presented in Table 4.4 and discussed above demonstrates how separation time and field drifter speed combine in κ_{max} to describe model skill. Using the κ_{max} analysis as presented in Section 2.5, models will be considered more skillful if they correctly model fast drifter movement over a short period of time than if they correctly model slow drifter movement for the same period of time. This trait finds its cause in the size of the target circle, which (for this research) remained constant and uniform for all drifters, irrespective of relative field drifter speeds. Alternative approaches for defining κ_{max} in ways that reduce the drifter speed bias on model results are presented in Section 5.3.

4.2.10. Perfection Time & Acceptable Time Analysis

As discussed in Sections 2.7.2 and 2.7.3, model perfection times and acceptable times provide quantitative measures of the model's ability to perfectly and acceptably predict drifter transport. Perfection times are the times before which the model drifter is separated from the field drifter by a distance equal to the target circle radius. Acceptable times are the times (from model drifter deployment) at which the model and field drifters separate by a distance equal to the error circle radius, indicating that the model changes from producing "acceptable" to "flawed" results. In this research, the positional accuracy of the field drifter GPS readings (~10m) was used to define the target circle radius (§3.5.1). Therefore the model is considered "perfect" when it successfully predicts drifter transport within the positional uncertainty of the field drifters. Error circle radii equal to the model grid size (250m for the base case ELCOM-MMP simulations) were used in determining model acceptable times. Model acceptable times are always greater than model perfection times, and model perfection is more difficult to achieve than model acceptability. The relative importance of each time metric ultimately depends upon the intended purpose of the model user. If the model is to be used to reproduce the exact paths and velocities observed with the field drifters, then validation using perfection times is more relevant. If, however, the model is to be used to determine the general circulation patterns present within a subject waterbody, acceptable times become more suitable validation tools than perfection times.

Longer perfection and acceptable times indicate that the model reproduced the field drifter motion for longer periods of time, thereby implying greater agreement between the model and field drifter paths. Just as the κ_{max} analyses are biased by the field drifter speeds, perfection and acceptable times will be larger for instances where the field drifter speeds are less (assuming the model reproduces the motion of both faster and slower moving field drifters equally well). Therefore perfection time and acceptable time analyses should be used only to compare results from different model setups.. As shown in Table 4.5, analyses of perfection and acceptable times suggest different

Table 4.5 – Mean Perfection & Acceptable Times for the ELCOM-MMP results

	Perfection			Acceptable		
Drifter Model	Time	σ^1	Separation Rate	Time	σ^1	Separation Rate
Lagrangian	471 s	<>	2.13 cm/s	97.2 min	<>	4.29 cm/s
Leeway	467 s	1%	2.14 cm/s	96.4 min	1%	4.32 cm/s
GABI-F	580 s	23%	1.72 cm/s	92.5 min	5%	4.50 cm/s

[1] σ is the percent deviation of the time entry with respect to the time entry from the Lagrangian simulations (See Eq. (4.1))

conclusions as to the relative merit of one drifter model over another.

Based on perfection times (Table 4.5), the GABI-F drifter model produces improved results with respect to the Leeway and Lagrangian drifter models, and model perfection occurred for nearly a complete timestep. Based on the acceptable times, however, the Lagrangian method produces superior results as its acceptable time is largest (approximately 9.7 timesteps). The importance of this inherent shift in superiority amongst drifter models, however, is lessoned by considering the deviation of acceptable and perfection times from each of the three drifter models. The percent deviation (σ_I) in perfection/acceptable times from each drifter model is calculated as:

$$\sigma_i = \frac{\left|\tau_i - \hat{\tau}\right|}{\hat{\tau}} \cdot 100\% \qquad (4.1)$$

where τ is the perfection or acceptable time for each drifter model "i" and $\hat{\tau}$ is the perfection or acceptable time from the Lagrangian drifter model. As shown in Table 4.5, the GABI-F perfection time represents a 23% increase over the Lagrangian perfection time. In contrast, the Lagrangian acceptable time is only 5% greater than the GABI-F acceptable time. This small relative difference in acceptable times suggests that the results from each of the three drifter models are nearly identical over the larger temporal and spatial scales incorporated in the acceptable time analyses. Indeed, this uniformity in drifter model results over larger scales is consistent with the conclusions drawn from the Type I metrics and Statistical Separation analyses (Section 4.2.3-4.2.4). Analyses using the Type I and Statistical Separation metrics suggested the differences in drifter paths from each model became insignificant as the duration of the drifter deployment increased.

A second notable feature shown in Table 4.5 is that the rates of separation between the field and modeled drifters increase by more than 100% during the period in which the modeled drifter motion is considered acceptable but not perfect. The separation rates are given as:

$$\frac{\partial d}{\partial t} = \frac{\delta}{\tau_d} \quad \text{for perfection} \qquad (4.2)$$

$$\frac{\partial d}{\partial t} = \frac{\xi}{\tau_a} \quad \text{for acceptability} \qquad (4.3)$$

where d is the separation between the field and modeled drifter, δ is the target circle radius, ξ is the error circle radius, and τ_d and τ_a are the perfection and acceptable times, respectively. The increase in separation rate after the model is no longer "perfect" is consistent with the notion of error integration in a spatially heterogeneous velocity field. In such a field, previous model errors in drifter velocity become compounded in time as the modeled drifter is continuously transported at velocities differing from the velocity of the field drifter. This effect is especially relevant when the model and field drifters have separated a sufficient distance so that the model drifter is located within flows that differ from the flows transporting the field drifter. In such a situation, the model and field drifters would continue to separate even if the model correctly determined the water

velocity at the location of the modeled drifter. The observed increase in separation rates at larger times (Table 4.5) provides further proof that error integration is significant in the modeled drifter path calculations, and corroborates the error-integration discussion with respect to spaghetti diagram analyses (Section 4.2.2).

4.2.11. Method Assessment Summary

In the preceding sections 4.2.2-4.2.10, results from the base case ELCOM-MMP simulations were presented and discussed. The objectives of the analyses were to:

Determine the relative merit of GABI-F, Lagrangian, and Leeway drifter models,

Assess the capacity of each analysis method for model validation using drifter data, and

Assess the skill of the ELCOM-MMP model in reproducing the observed field drifter paths.

The results were analyzed using the established spaghetti diagram, Type I metric, and Statistical Separation methods, as well as the new Circle Assessment method developed in this research. Through analyses using each drifter model and assessment method, the ELCOM-MMP model was found to be more capable of reproducing the larger-scale behavior of the field drifters than the smaller-scale variations in movement observed in the field data. The model was reasonably successful at determining the general speeds and directions of drifter motion, as well as the timing of changes in drifter velocity due to changes in the winds driving the MMP circulation.

Differences in drifter results obtained with the three drifter models were often difficult to distinguish when using the established analysis methods. These methods each compare modeled and field drifter paths from the point of drifter deployment, and the comparisons spanned the entire time of the deployment. These methods integrate model error by continuing to compare drifter paths after the model drifter has separated from the field drifter. As such, the spaghetti diagram, Type I metric, and Statistical Separation analysis methods continue drifter path comparisons even after the modeled and field drifters have separated to the point where they may have entered areas of diverging flow. The Circle Assessment method is advantageous as it is not as error-integrative as the established assessment methods. The method involves numerous comparisons of modeled and field drifter paths initiating from the field positions at numerous times through the deployment, and limits the comparisons to times before which the modeled and field drifters separate by pre-defined distances. Also, by comparing the modeled and field drifter paths at numerous instances over the entire simulation, the Circle Assessment method provides statistical information indicative of hydrodynamic model skill. While each analysis method proved useful in elucidating properties of the modeled and observed MMP flows, information gleaned from the Circle Assessment method was most insightful for assessing ELCOM-MMP skill over both short and long time scales.

Through analysis using spaghetti diagrams (Figure 4.1, Section 4.2.2), results show that the hydrodynamic model was unable to predict the exact paths of the field drifters regardless of the drifter model used in the simulations. The spaghetti diagram results did indicate, however, that the ELCOM-MMP model was able to reproduce the general characteristics of motion, including general directions and speeds of drifter travel. The method shows agreement between the observed and modeled larger-scale current dynamics, i.e., the direction reversals during the D2 and D4 deployments. The spaghetti diagram results also indicate that the GABI-F drifter model more accurately reproduced the field drifter paths during the D2 simulation than did the Leeway or Lagrangian drifter model; for all other deployments (D1, D3-D5) the differences in drifter paths from each drifter model were small compared with the differences between the model and field drifter paths.

The main drawbacks of the spaghetti diagram method are that the method is inherently both

qualitative and integrative of model error. The main benefit of the spaghetti diagram method is that the results are easily understood when presented on maps of the subject area. This ease of comprehension, however, is perhaps tempered by the potential misinterpretation of the predicted drifter paths. As modeled drifter paths predicted after the model and field drifters have sufficiently separated may no longer be indicative of the actual physical flows transporting the field drifter, assessments of the drifter transport over longer time periods may be incorrect. While this may be a problem for using modeled drifters in the hydrodynamic model validation process, it is not likely to drastically affect drifter modeling usage for other purposes such as search and rescue (Thompson et al, 2003) where modeled drifter paths may be used to define areas in which the missing object is likely to reside.

Results of analyses using the Type I and Statistical Separation techniques (Sections 4.2.3-4.2.4) corroborated those derived from the spaghetti diagram analysis, namely that the benefits of one drifter model over another are often difficult to ascertain. Results from both analyses methods suggested that the ELCOM-MMP model tended to improve as the duration of each simulation increased, indicating that the model was better at reproducing the larger-scale motion of the field drifters than the smaller-scale local variations indicated by the detailed motion in the field drifter paths. The statistical-separation method proved to be especially sensitive to divergence in the set of field drifter paths, as such divergence made the displacement of the median field drifter position small relative to the separation between modeled and field drifters. Neither the Type I or Statistical Separation methods indicated whether the modeled drifter paths differed from the field drifter paths due to differences in modeled speed and/or direction, and neither method could quantify model skill based on parameters relating to numerical or forcing conditions of the hydrodynamic model. Similar conclusions were reached through both the Type I and Statistical Separation methods. As only the latter of these two methods was negatively affected by flow divergence, it follows that only the former of the two methods (i.e., the Type I metric analysis) is suitable for use in assessing model skill with drifters.

The numerous and varied analysis techniques available within the Circle Assessment method (Section 4.2.5-4.2.10) provided consistent measures of the comparative skill of the ELCOM-MMP model in reproducing the field drifter motion over short time and length scales. Each method of analysis indicated that, relative to the Leeway and Lagrangian models, the GABI-F drifter model produced drifter paths more akin to the field drifter paths. For example, the model timestep analysis results indicated that ELCOM successfully reproduced drifter motion for nearly 34% of all drifter-timesteps with the GABI-F drifter model, compared with approximately 20% of all drifter-timesteps for the Lagrangian and Leeway models (§4.2.6). Analyses of the κ_{max} values indicated that the GABI-F model produced improved results with respect to the Lagrangian and Leeway models for nearly 70% of the simulated drifter-timesteps (§4.2.9). Improvement in the mean perfection time using the GABI-F model were also determined (§4.2.10).

The only analysis that did not indicate the superiority of the GABI-F model was the acceptable time analysis (§4.2.10). Based on the mean acceptable times, the ELCOM-MMP model acceptable transports the drifters over 9-10 model timesteps (90-100 minutes) irrespective of the drifter model used in calculating the transport. The slight differences in acceptable times from each drifter model were insignificant relative to the magnitude of the acceptable time, leading to the conclusion that as the time-horizon of model/field comparisons increase, the fraction of path-error due to the drifter model decreases. Specifically, when the model drifter is close to the field drifter, then the differences in the mechanics of the drifter motion (in each drifter model) is important and dominates the results. However, once sufficient separation occurs that the model is considered

"acceptable" rather than "perfect", the principle driver of error is the difference between the velocity at the field drifter position and the velocity at the model drifter position. This difference in velocity with position within the waterbody is principally determined by the model's representation of the velocity field. Thus, the mechanics of drifter motion become small parts of the model error at longer times.

The irrelevance of the drifter model at longer timescales of analysis was consistent with the results and conclusions derived from the Type I metrics, Statistical Separation analyses, and spaghetti diagrams. In this way, the conclusions drawn from these more established analysis methods were also discernible from the Circle Assessment analyses. The Circle Assessment method is therefore a more informative method in that it provides information on the model's ability to reproduce the field drifter motion over both short and long time horizons, unlike the other assessment methods which were deemed useful only over long time horizons (§4.2.2-4.2.4).

The main drawback to the Circle Assessment method was illustrated in the discussion of the κ_{max} parameter and how it must be used for comparative purposes only; the κ_{max} parameter does not definitively illustrate model skill in reproducing the field drifter motion. However, κ_{max} remains a successful parameter for comparing results from different model setups. The principle drawback of the method is its dependence on both the field drifter speed and the separation time, which provides multiple possible explanations for high or low κ_{max} values. Thus, only the model timestep analysis method is suitable for assessing the model skill with respect to the field drifter data, but this capability is also limited for reasons discussed in Sections 4.2.6-4.2.8. As such, the techniques included in the Circle Assessment method need to further development before the method can be used to meaningfully quantify a model's ability to reproduce observed field drifter data. Improvements are suggested and preliminary analyses are provided in Section 5.3.

For the remainder of this Chapter, the Circle Assessment method is applied to ELCOM-MMP simulations using the GABI-F model for the purpose of identifying the relative importance of model setup parameters. As the Circle Assessment results indicate that the GABI-F drifter model produces better agreement with field drifters than the other drifter models at short timescales the remaining effort principally applies the Circle Assessment and GABI-F approaches. Spaghetti diagrams, however, are still used to provide qualitative insight into drifter/current behavior under various modeling conditions.

4.3. Comparing Model Results From Various Model Setups

4.3.1. Introduction

This section presents and discusses ELCOM-MMP results obtained through various model setups and forcing conditions. Model error may be attributed to many factors, including inaccuracies in the model forcing and inaccuracies in the model's numerical approximation of the observed physical phenomena. The intent of this analysis is to identify conditions under which the model is more skillful and therefore more likely to produce accurate velocity fields. Based on the conclusions from the previous section, only drifters modeled with the GABI-F technique were used in this analysis, and only the Circle Assessment method was used to quantify differences between model results. Spaghetti Diagrams were used in a qualitative manner to determine when/where greater agreement between the modeled and observed drifter paths occurred.

The modeling effects due to changes in the following environmental forcing variables were considered:

Wind data sources

Water surface slope

Table 4.6 – Model Setup Descriptions for ELCOM-MMP Simulations

	Setup Variable			
Setup Name	Wind Data	Water Surface Slope	Grid Resolution	Timestep
Base-Case	LDS	South - 1.75×10^{-7} m/m	250m x 250m	10 minutes
Setup #1	Whitfords	South - 1.75×10^{-7} m/m	250m x 250m	10 minutes
Setup #2	MIX[1]	South - 1.75×10^{-7} m/m	250m x 250m	10 minutes
Setup #3	LDS	North - 1.75×10^{-7} m/m	250m x 250m	10 minutes
Setup #4	LDS	Zero - 0 m/m	250m x 250m	10 minutes
Setup #5	LDS	South - 1.75×10^{-7} m/m	500m x 500m	10 minutes
Setup #6	LDS	South - 1.75×10^{-7} m/m	100m x 100m	10 minutes
Setup #7	LDS	South - 1.75×10^{-7} m/m	250m x 250m	5 minutes
Setup #8	LDS	South - 1.75×10^{-7} m/m	250m x 250m	20 minutes

[1] The MIX wind dataset is a spatially variable dataset interpolated linearly in space and time from the LDS and Whitfords wind datasets – See Section 4.3.2.

Additionally, the modeling effect due to changes in the following numerical model parameters were considered:

Model timestep

Model grid resolution

Alternative algorithms for computing the hydrodynamic solution were not considered a focus of this research; however, some effects of different parameterizations for vertical mixing models is examined in Section 6.8. As described in the "Future Work" section (§5.3), such analyses should be conducted to determine factors that contribute the most error in the predicted drifter paths. For this comparative analysis of model results, each modeling scenario altered only one parameter of the base-case conditions, as illustrated in Table 4.6. Simulations testing each of the four setup variables are discussed and analyzed in the following subsections (4.3.2-4.3.6). For the following discussions, all references to model setups are made using either the setup name shown in Table 4.6 or by referring to the setup variable value being tested in the simulation being discussed. For example, in discussing the effects of wind datasets, the base-case setup could also be referred to as the "LDS" setup.

4.3.2. Wind Forcing Analysis – Base Case, Setup #1 and Setup #2

To determine the effect of alternative wind data on the modeled drifter paths, 3 sets of simulations were conducted: 1) the base-case setup using data from the LDS, 2) Setup #1 using data measured at the Whitford's Sea and Rescue Station, and 3) Setup #2 using the MIX dataset of winds interpolated from the LDS and Whitfords data (See below). Each simulation models the D3-D5 drifter deployments (data from the LDS unit was not available during the D1 and D2 experiments – see Section 3.4.4).

The wind data from LDS and Whitfords are in good agreement during portions of the experiment (e.g., 10:00 to 20:00 on March 26 – Figures 4.15, 4.16), and in poor agreement at other times (e.g 00:00 to 10:00 on March 25). Thus, it may be argued that there are times when a uniform wind field is a reasonable approximation of the forcing conditions, and there are times when it is perhaps a poor approximation. During the time periods in which windfield non-uniformities occur the ELCOM-MMP model forced with a uniform wind is less likely to produce modeled drifter paths comparable to the observed field drifter paths.

Wind data from the LDS are similar to data from the Whitfords station although identifiable differences in both speed and direction imply the existence of wind

shear during portions of the experiment. As measured by the LDS and at the Whitfords station, the winds were nearly identical on March 23 and until late evening of March 24 (Figure 4.15). By 20:00 hrs that evening, both stations measured lower wind speeds than earlier in the afternoon, but by midnight the LDS recorded faster winds blowing to the NE when the Whitfords station recorded slower winds blowing toward the northwest. Similar differences continued throughout March 25, with stronger winds recorded earlier in the afternoon at the Whitfords station. Greater wind speeds were also measured by the LDS during the morning on March 26, with the winds blowing more toward the east than those measured by the Whitfords station. The trend of higher speeds at the LDS station continued on March 27, although the directional agreement between the two wind datasets was good during the afternoon on this day.

On March 25, the winds measured by the LDS and at the Whitfords station showed large differences in speed and to a lesser extent direction (Figure 4.16).

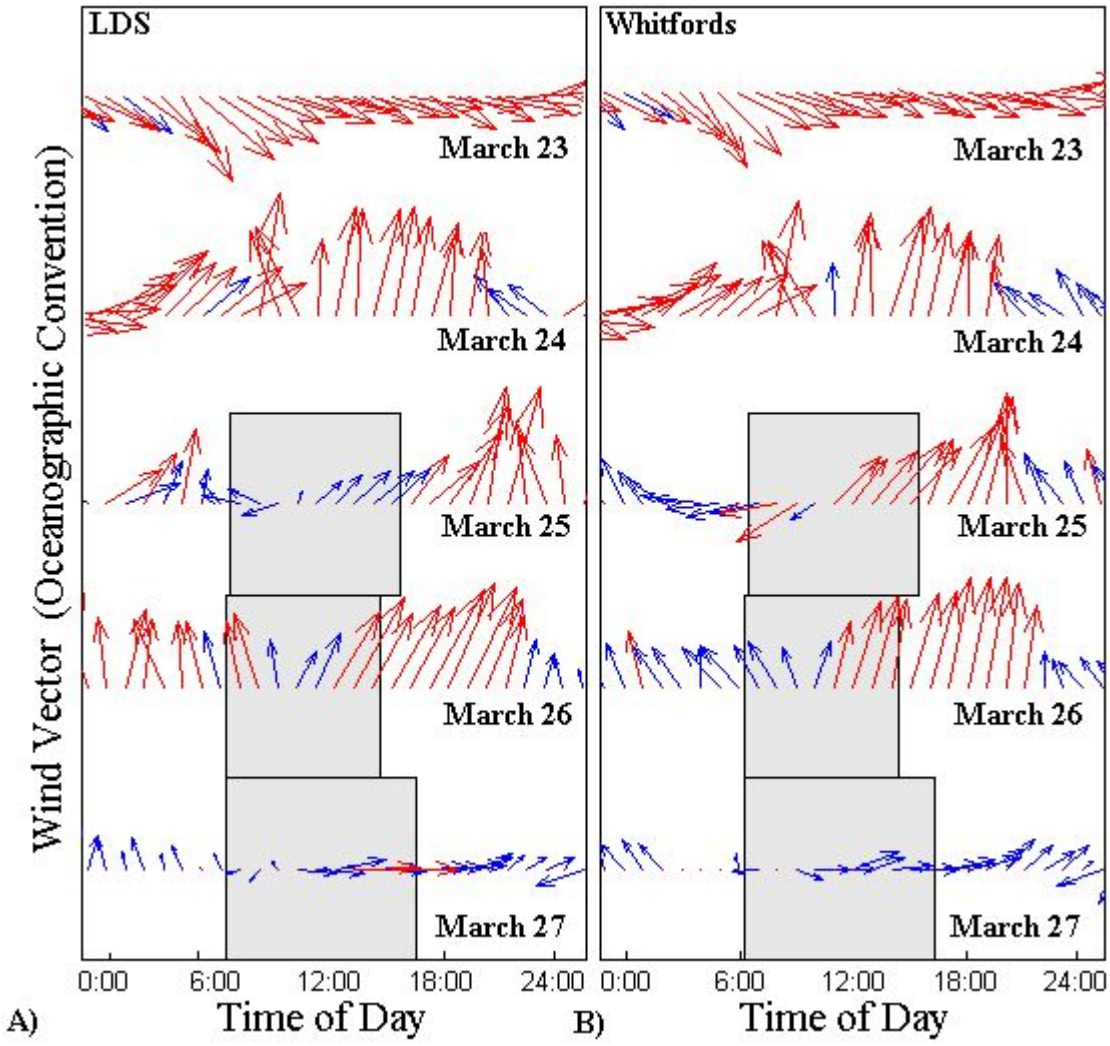

Figure 4.15 – Wind Data from the A) LDS, and B) Whitfords Sea Rescue Station – wind vectors presented in oceanographic convention, indicating magnitude and direction to which wind is blowing. Grey boxes indicate periods of field drifter deployment. Red arrows indicate wind speeds greater than 5 m/s.

In the early morning (prior to drifter deployment), the LDS measured-winds principally varied from out of the SW to S with fluctuating speeds both above and below 5 m/s. Just before deployment, the winds at the LDS dropped consistently below 5 m/s and shifted to be out of the east. In contrast, the winds at Whitfords station were more consistent, being out of the SE and smoothly shifting to be out of the east just prior to deployment. The Whitfords winds were also more consistent with speeds below 5 m/s through the early morning and increasing above 5 m/s just after deployment. Thus, the differences in wind direction and speed in the early morning became principally differences of speed (LDS lower) at the time of the drifter deployment (Figure 4.16). Throughout the drifter deployment on March 25, winds measured at the LDS were consistently nearly 2 m/s slower than the Whitfords winds, except during the 10:00 am wind shift when the wind speed was small at both stations.

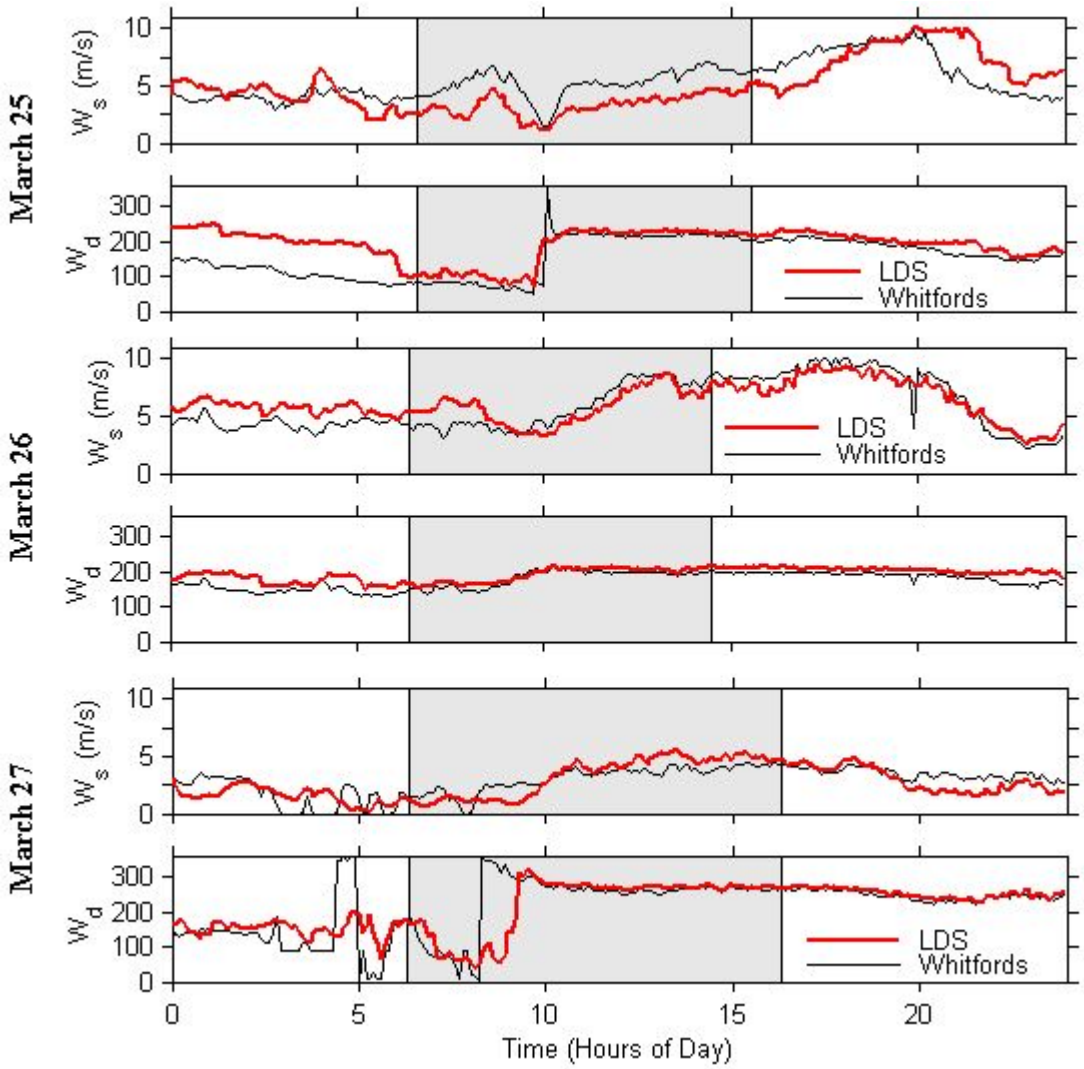

Figure 4.16 – Wind Speeds (W_s) and Wind Direction (W_d) Data from the LDS, and Whitfords Sea Rescue Station – March 25, 26, and 27, 2003. Wind vectors presented in oceanographic convention, indicating magnitude and direction to which wind is blowing. Grey boxes indicate periods of field drifter deployment.

Compared with the March 25 data, LDS and Whitfords data on March 26 and March 27 agreed very well (Figure 4.16). On March 26, the wind speeds and directions measured at the two wind stations were comparable after the initial deployment of the drifter, with the greatest differences occurring in the morning hours before drifter deployment. Wind differences were also greatest in the pre-deployment hours on March 27, when the measured speeds differed by 1-2 m/s and directional differences fluctuated between 10° and 90°. Wind speeds on March 27 were the lowest measured on all of the experiment days, and did not exceed 5 m/s for more than 1 hr on this day.

Using simple linear interpolation techniques on the LDS and Whitfords data, the MIX wind dataset was created as an approximation of the unknown wind forcing across the domain. Because data is available at only two stations that are separated in the E-W direction but not N-S, the MIX dataset is spatially and temporally varying in the E-W direction, and only temporally varying in the N-S direction (Figure 4.17).

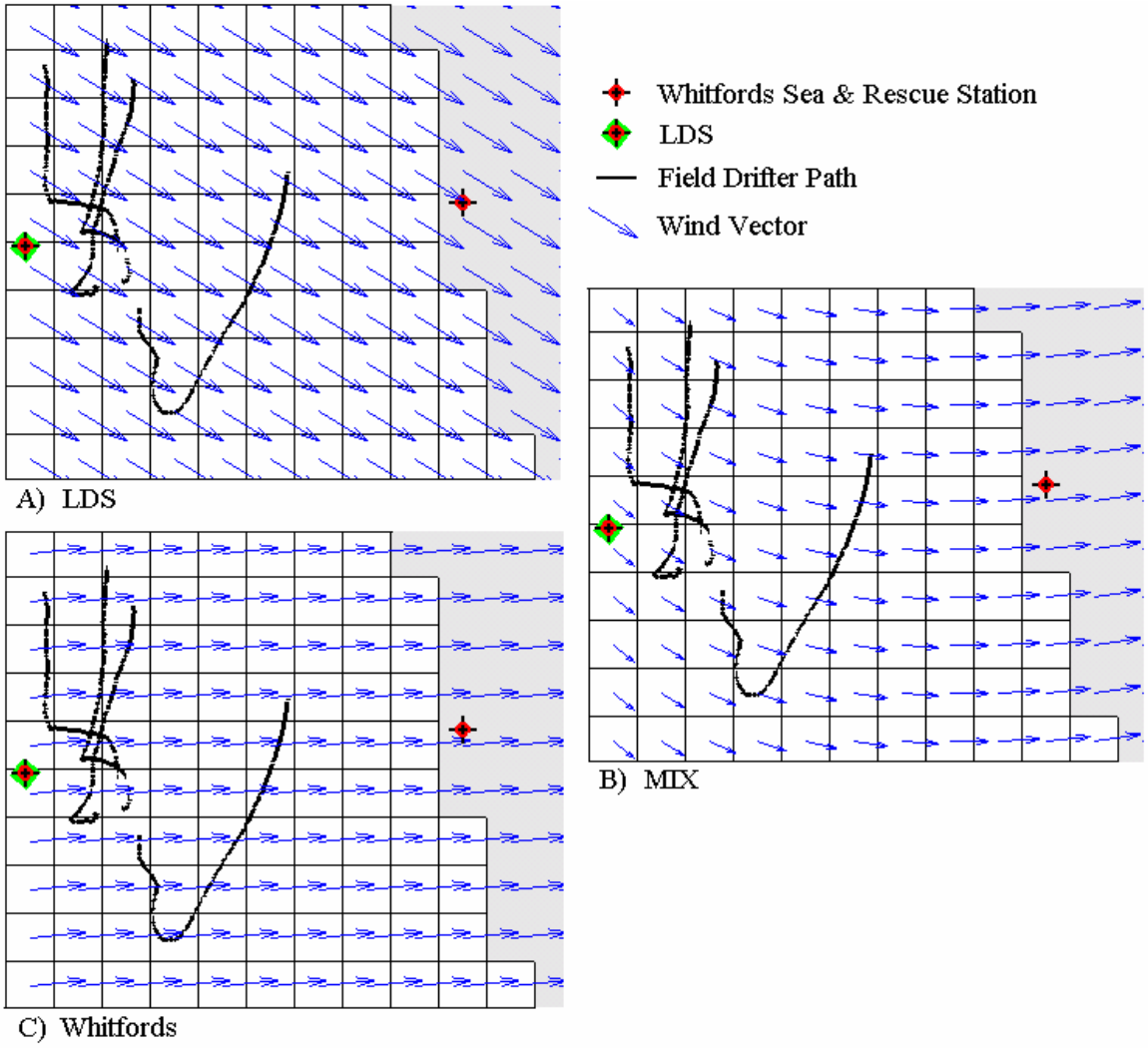

Figure 4.17 – Interpolated Winds from the LDS and Whitfords Datasets. A) LDS winds, B) MIX winds, C) Whitfords winds. Data shown is from March 25, 2003 at 7:20AM. Squares indicate model grid cells, and D3 field drifter data are shown for reference.

While it is unlikely that the actual winds driving MMP circulation were uniform in the N-S direction, this assumption within the MIX dataset was necessary as the two stations cannot adequately identify shear, rotation, convergence or divergence in the wind field over the entire region.

Forcing the model with different wind boundary conditions caused substantially different model drifter paths as seen on spaghetti diagram plots (Figure 4.18). The differences are greatest for the D3 and D5 simulations, where the model drifters initially traveled in contrasting directions when forced with the LDS and Whitfords wind datasets (Figure 4.18 D3A, D3C, D5A,

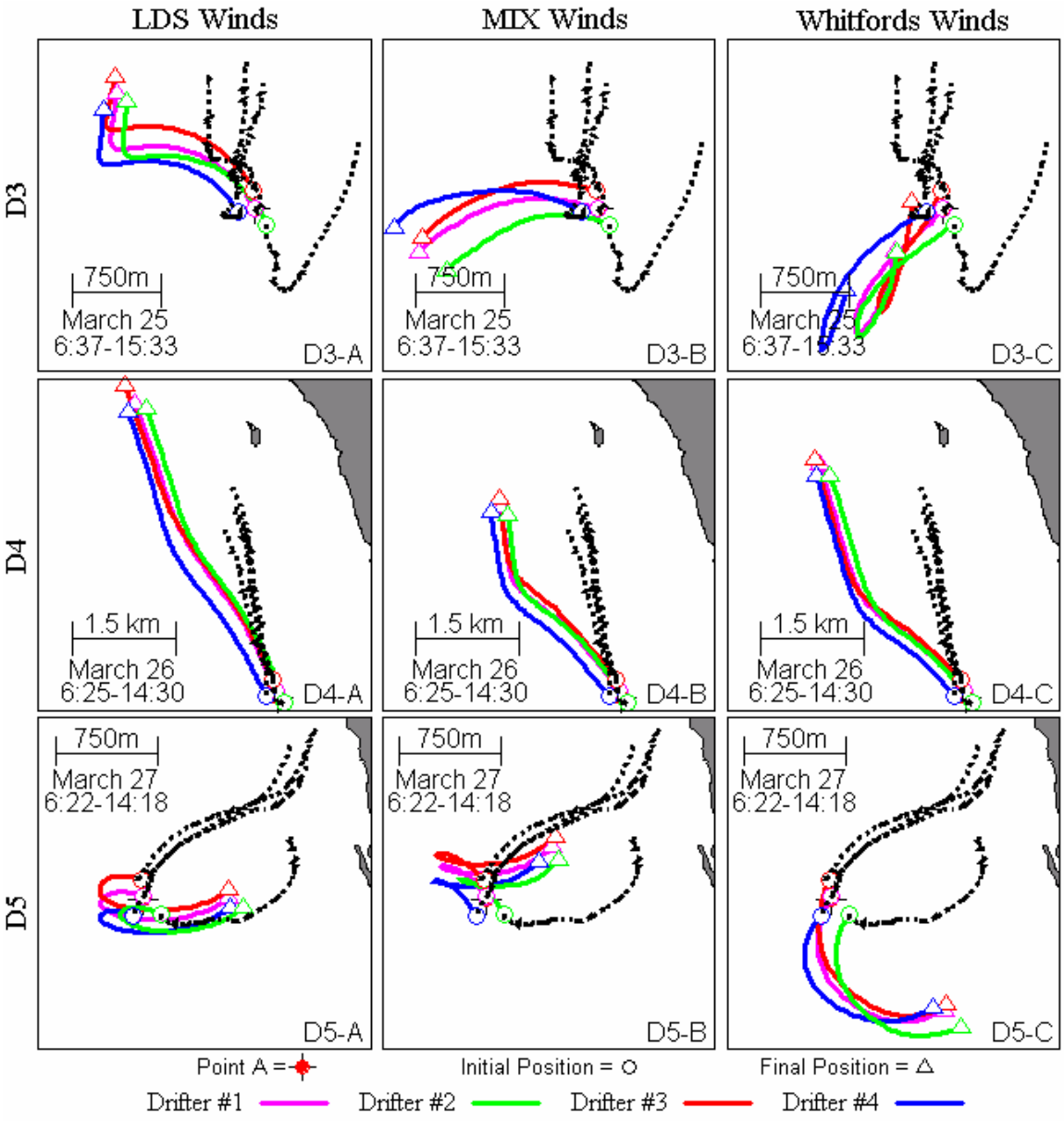

Figure 4.18 – Spaghetti diagram plots of model results by wind data. LDS-forced simulations shown in Column A, MIX-forced simulations in Column B, Whitfords-forced simulations shown in Column C. Drifter days shown by row. Field drifter paths shown as dotted lines.

D5C). The simulations using the MIX dataset produced drifter paths somewhat between the other two sets. By the end of the simulations, however, the model drifters all followed similar headings (although the direction reversal is not apparent for D3 MIX in Figure 4.18, it does occur just before the end of the simulation). At the end of the simulations, the differences in winds measured at the Whitfords and LDS stations were small (Figure 4.16) and the wind speeds were generally high. At the times of drifter deployment on each of these days, the wind speeds were low (less than 5 m/s), which might contribute to the model's inability to reproduce the observed field drifter trajectories at those times.

As the differences between the LDS and Whitfords winds were small on March 26, the D4 drifter paths derived from the three model setups were more similar (Figure 4.18 D4A-C). The "Whitfords" paths indicated a generally slower, more westward current than implied by the "LDS" paths or field drifter paths. In contrast, the LDS drifter paths imply that the modeled drifters traveled faster than the field drifters, but still on a more westward course. Setup #2 with the MIX wind dataset produced model drifter displacements closest to that of the field drifters (Figure 4.18 D4B), suggesting that the model drifter speeds were comparable to the field drifter speeds. Regardless of wind forcing, however, the D4 model drifters always tended more to the north-west than the field drifters. This common trait from the base case, #1 and #2 model setups results suggests that either the applied wind fields are shifted from the actual winds across the region, or that the ELCOM-MMP model poorly predicts the water velocities around the time of the D4 drifter deployment. The latter may result in the initial drifter movement into a different region of the flow field, driving the separation between the model and field drifters.

Based on the above analyses of spaghetti diagrams, model setups using different wind forcing (within the bounds of the two wind data sets) produces different drifter paths. For the D4 simulations, the MIX wind forcing best reproduces the field drifter motion. However, for the D3 and D5 simulations, the LDS wind forcing produces superior results. Circle Assessment results for the same setups are presented in Table 4.7. These results indicate that, when averaged over the three deployment simulations, the results obtained from LDS wind forcing were consistently superior to those obtained using either the MIX or Whitfords wind forcing. Higher κ-score values were obtained from the LDS-forced simulations, and the success probability for perfectly predicting drifter transport over the model timestep was nearly double that achieved with the MIX and Whitfords forced simulations. Furthermore, the higher mean κ_{max} and perfection times from the LDS simulation also suggest that the LDS forced base-case model setup is more appropriate. Only the acceptable times suggest the LDS is not perhaps the most suitable wind forcing, as the acceptable time is greatest for the Whitfords forced simulations. Acceptable times from all the simulations, however, suggest that the ELCOM-MMP models acceptably reproduce the drifter motion for 8-10

Table 4.7 – Circle Assessment Results for ELCOM-MMP wind forcing simulations

	Model Timestep Analysis		Separation Analysis		
Wind Forcing	κ-score	Success Probability	Mean κ_{max}	Perfection Time	Acceptable time
LDS[1]	73%	33%	1.7	573 s	93 min
Mix	63%	18%	1.3	455 s	84 min
Whitfords	55%	16%	1.1	415 s	100 min

[1] LDS results presented are different the base-case results presented in§4.2.6, §4.2.10 and §4.3.4-§4.3.6 because Table 4.7 only considers data from the D3-D5 deployments.

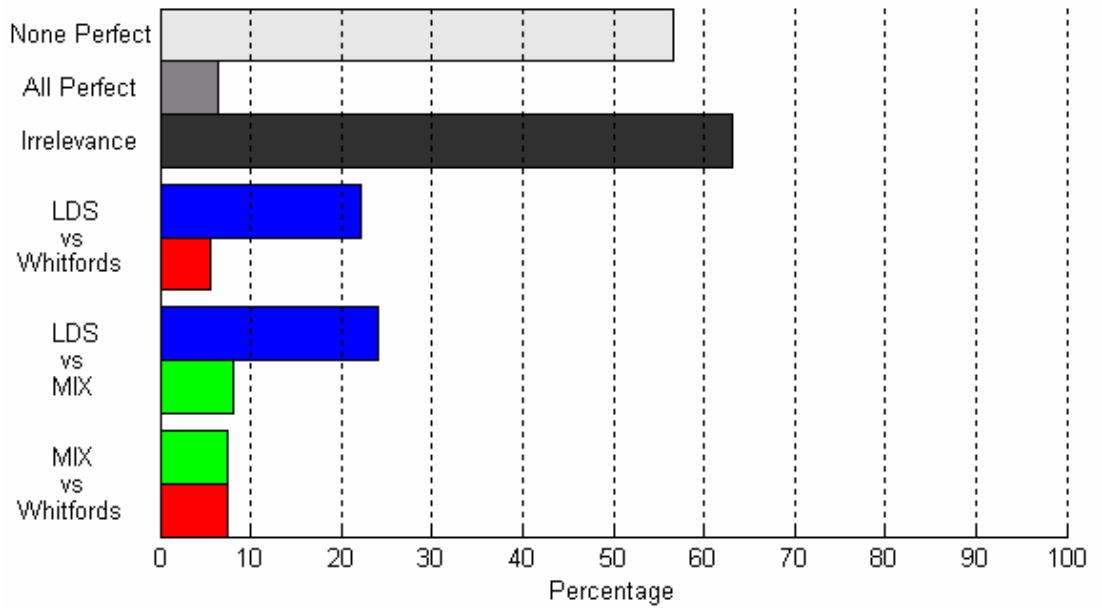

Figure 4.19 – Comparative Failure Analysis Results –ELCOM-MMP wind forcing simulations. Results from the LDS simulations are shown in blue, MIX results are in green, and Whitfords simulation results are shown in red.

timesteps and therefore adequately predicts the larger-scale behavior of the MMP surface currents.

Model results from the comparative failure analysis (§2.8.2) for the LDS-, MIX-, and Whitfords-forced simulations support the conclusion that the LDS wind forcing produces the best agreement between the model and field drifter paths (Figure 4.19). Results from the LDS-forced simulations improved upon those from the MIX-forced and Whitfords-forced simulations for 24% and 22% of all drifter-timesteps, respectively. No net improvement in model results was achieved when using the MIX wind dataset in place of the Whitfords wind dataset, as both situations yielded 8% improvements when compared to each other. The greatest net improvement was achieved when using the LDS dataset instead of the Whitfords dataset, resulting in a 17% net gain in instances of model perfection.

Although the results in Figure 4.19 indicate that the LDS-forced dataset is more likely to produce perfect model reproductions of the field drifter transport, the key insight from the results is that alterations to the wind forcing did not affect results for 63% of the simulated drifter-timesteps. This result is indicated by the "Irrelevance" entry in Figure 4.19, which is defined as the sum of the "All Perfect" and "None Perfect entries" (See section 4.2.7). This percentage is similar to that shown in Figure 4.11 detailing comparisons of base-case ELCOM-MMP simulations using each of the three drifter models. Conclusions drawn from this comparative failure analysis are:

> *#1 Drifter model selection is as equally important as the wind forcing dataset in obtaining more accurate calculations of ELCOM-MMP drifter motion.*
>
> *#2 Errors in the wind forcing are not likely to be the largest contributor of error to the modeled drifter paths.*

Conclusion #2 above is tentative given the lack of spatial resolution in the MMP winds recorded during the drifter deployments, and is stronger with respect to simulations during which the recorded LDS and Whitfords winds were in greater agreement. Potentially, model results could be improved if the

winds at the locations of the drifters were known, perhaps through windfield modeling. However, based on the analysis presented herein, greater agreement between the model and field drifter paths is likely to be achieved through improvements to other aspects of the ELCOM-MMP model rather than to improved knowledge of the wind forcing during the drifter deployments.

4.3.3. Water Surface Slope Analysis - Base Case, Setup #3 and Setup #4

Zaker et al (2002) modeled MMP with a constant surface slope equivalent to the steric height gradient which drives the southward Leeuwin current offshore from MMP. For both Zaker et al (2002) and the present research, the steric height approximation was necessary as the actual water surface slopes could not be measured as a part of the field experiment. Furthermore, tidal records along the Western Australian coast cannot be used for model forcing because the tide-gauges are not referenced to a common vertical datum (Tony Lamberto, Aust. Dept. of Planning and Infastructure – Pers. Comm.) nor are they referenced to the MMP bathymetry datum. These deficiencies make it impossible to determine the horizontal surface gradient implied by the tidal excursions at two tidal stations along the coast. Approximating the MMP water surface slope by the gradient that generally drives the Leeuwin Current (Thompson, 1984; Godfrey and Ridgway, 1985; Smith et al, 1991; Zaker et al, 2002) seems reasonable, but necessarily neglects the more localized tidal effects of topography and weather systems. To test the sensitivity of the modeled circulation within the MMP to the imposed free surface gradient, 3 sets of simulations were conducted: 1) the base-case setup using a southward steric gradient of 1.75×10^{-7} m/m as in Zaker et al, 2002, 2) Setup #3 using the same steric gradient (1.75×10^{-7} m/m) oriented northward, and 3) Setup #4 using a horizontal water surface (referred to herein as a "ZERO" slope). Each set of simulations consisted of modeling all of the drifter deployments (D1-D5).

As shown in Figure 4.20, spaghetti diagrams from each setup and drifter deployment indicate that the surface slope had a small but detectable influence on the model drifter paths. In comparison with the ZERO slope simulations, simulations using a southward water surface slope predicted drifter movement more to the south, and those using a northward slope predicted movement more to the north. For the D1 drifter deployments, the northward water surface slope tended to impede the model drifter's movement to the south, resulting in a lower net south-ward displacement than in the ZERO slope or South slope simulations (Figure 4.20 D1, D2). This lower net-southward movement yielded less separation between the model and field drifter paths for the D2 deployment (Figure 4.20 D2-B,C). The northward and ZERO slope simulations for the D1 deployment also suggest greater model drifter path agreement with field data, for in each case the model drifters clearly shifted direction to a northward course as did the field drifters. The direction reversal also occurred within the southward-sloping D1 simulation (Figure 4.20 D1-A), but to a lesser extent and at a later time than in the northward sloping or ZERO slope simulations.

Although discernible with spaghetti diagrams, the drifter path changes due to water surface slopes are substantially smaller than the differences between the model and field drifter paths. With the exception of the D5 simulation, reversals of the water surface slope (i.e., from south to north) did not cause the overall pattern of the drifter paths to significantly change. Recognizing that differing wind forcing did cause changes to the overall pattern of model drifter paths (See Figure 4.18), the water surface slope seems to be, at best, a secondary contributor to MMP circulation.

The conclusion that water surface slope is of secondary importance in driving MMP circulation is consistent with the conclusions from previous studies conducted in the area. Specifically, Zaker et al (2002) concluded that MMP circulation is predominantly wind-driven with only minimal dependence on local

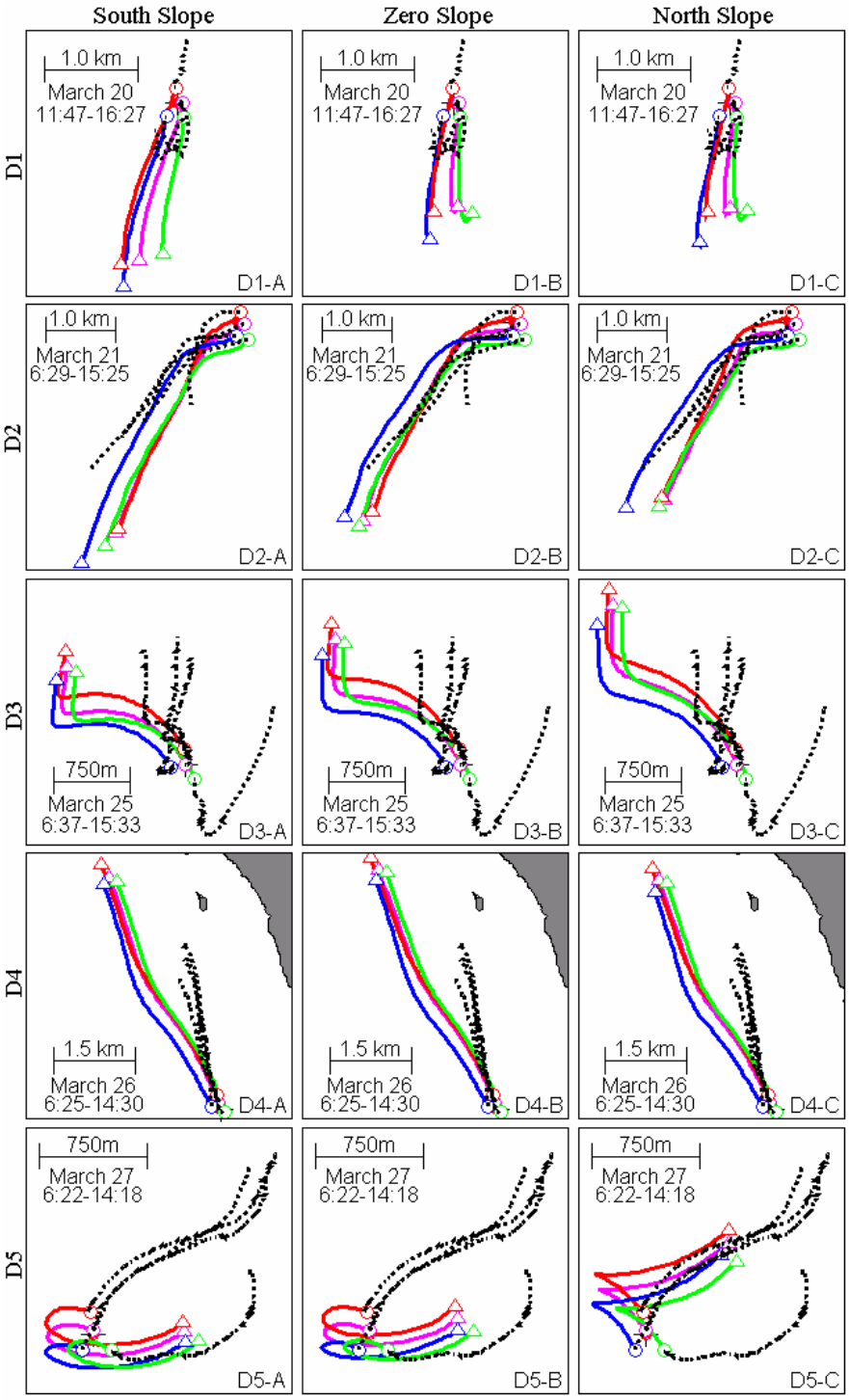

Figure 4.20– Spaghetti Diagram Plots of Model Results by water surface slope. Southern slope results shown in Column A, Zero slope results in Column B, North slope results in Column C. Drifter days shown by row. Field drifter paths shown as dotted lines. Symbols as in Figure 4.18

pressure gradients when the wind speeds dip below 5 m/s. As shown in Figure 4.16, wind speeds during the D4 deployment rarely dipped below 5 m/s, and differences in modeled drifter paths derived with each of the three water surface slopes were negligible compared with the displacement of the drifters from their deployment position (Figure 4.20 D4A-C). In contrast, wind speeds during the D5 deployment rarely exceeded 5 m/s (Figure 4.16), and drifter paths modeled with the northward slope differed greatly from those modeled with the southward slope (Figure 4.20 D5A-C). This result indicates that the ELCOM-MMP model was sufficiently sensitive to slope changes at low wind speeds, further supporting the conclusion from section 4.2 that the model reasonably reproduces the large-scale dynamics of the MMP currents.

Results from the Circle Assessment analyses (Table 4.8) also suggest that water surface slope is a secondary contributor to MMP circulation. For each of the parameters listed in Table 4.8, little differences in results were obtained from the 3 sets of slope simulations. The κ-score, success rate, mean κ_{max} and separation time for the ZERO slope simulations were all higher than achieved with the other slope simulations, suggesting that approximating MMP with a uniform flat-surface rather than a uniform sloping surface would produce more accurate results. The gain in accuracy, however, is small considering the near equality of the Circle Assessment results amongst the 3 sets of surface slope simulations. As with the wind forcing analysis (Section 4.3.2), the key insights from the circle assessment results are that the ELCOM-MMP model is unable to perfectly predict drifter transport nearly 65% of the time but that it is able to acceptably transport the model drifters for 93-96 minutes (nearly 10 model timesteps). Based on this analysis, improved agreement between the model and field drifter paths is likely to be achieved through improvements to other aspects of the ELCOM-MMP model rather than to improved knowledge of the water surface slope during the drifter deployments.

4.3.4. Grid Resolution Analysis - Base Case, Setup #5 and Setup #6

To determine the effect of variations in grid cell size on the modeled drifter paths, 3 sets of simulations were conducted: 1) the base-case setup using a 250m x 250m horizontal grid, 2) Setup #5 using a 100m x 100m grid, and 3) Setup #6 using a 500m x 500m computational grid. Each set of simulations consisted of modeling the D1-D5 drifter deployments, and used a constant 10-minute timestep. The bathymetry for each model setup was interpolated from nautical charts using GIS methods (See Section 3.4.3). As such, the bathymetry used on the 100m x 100m grid has more detail than that used on the 250m x 250m or 500m x 500m grids (i.e., the 250m x 250m grid bathymetry was not simply re-sampled in creating the bathymetries for the other model setups).

Table 4.8 – Circle Assessment Results for ELCOM-MMP surface slope simulations

	Model Timestep Analysis			Separation Analysis		
Surface Slope	κ-score	Success Probability	Speed[1] Failures	Mean κ_{max}	Perfection Time	Acceptable time
South	74%	34%	22%:23%	1.8	579 s	93 min
Zero	77%	39%	19%:20%	1.9	610 s	94 min
North	77%	37%	21%:18%	1.8	602 s	96 min

[1] Speed Failures shown as the percentage of drifter-timesteps that failed due to model over-predictions and under-predictions of drifter speed, respectively.

Analysis of the spaghetti diagrams of the model drifter paths from each of the 3 simulation sets (Figure 4.21) leads to two main observations:

1. a consistent relationship between grid resolution and model skill is not readily discernible from the spaghetti diagram analyses, and

2. drifter paths derived from simulations with different grid resolutions are more comparable to each other than to the field drifter paths.

For example, consider the results from the D2 and D4 simulations. For the D2 simulations at both the 100m and 250m grid resolution, the ELCOM-MMP model over- predicts the drifter's speed and displacement toward the end of the simulation, despite that the direction of motion is approximately correct for each drifter. Using the more coarse 500m grid (Figure 4.21 D2-C), the modeled drifters traveled distances only slightly greater than the field drifters, and followed similar headings. In contrast, the D4 500m grid simulation produced a large over-prediction in drifter displacement due to a consistently large over-prediction of drifter speed. This over-prediction of speed decreased within the base-case 250m simulation, and is largely diminished at the 100m grid scale. Similar trends of decreasing separation with increasing grid resolution were evident in the D1, D3, and D5 simulations, although the differences in model drifter paths were small compared with the path separations from the field drifters.

With the exception of the D2 simulations, the spaghetti diagram plots in Figure 4.21 suggest that the 100m grid resolution provides the most comparable drifter paths with respect to the field data. The improvement with larger grid resolution, however, is only significant for the D4 simulation, as the drifter paths for the other deployment days remain separated from the field drifter paths regardless of the model grid resolution. The similarity in drifter paths within each D1-D5 simulation set indicates that the ELCOM model has reached a convergent solution for the Eulerian velocity field and that large changes to this velocity field are not likely if the ELCOM-MMP models were to be run on even higher-resolution grids.

While higher-resolution grids may produce better representations of the observed flow divergence, the capacity of the ELCOM-MMP model to reproduce such currents may also be limited by the lack of spatial resolution within the various wind-forcing datasets (See Section 4.3.2). As discussed in section 3.6, the flow divergence suggested by the field drifters often occurred over length scales less than 100m, and that the model grids used in this research would be too coarse to reproduce the observed spatial variability in drifter motion. As expected, even the simulations at the 100m grid resolution were unable to resolve the flow divergences during the D1, D3, and D5 deployments. Simulations at grid resolutions finer than 100m were computationally impractical and were not attempted. Based on the spaghetti diagram analyses, however, it is

Table 4.9 – Circle Assessment Results for ELCOM-MMP grid resolution simulations

	Model Timestep Analysis			Separation Analysis		
Grid Resolution	κ-score	Success	Speed[1] Failures	Mean κ_{max}	Perfection Time	Acceptable Time[2]
100 m	62%	26%	10%:31%	1.4	540 s	107 min
250 m	74%	34%	22%:23%	1.8	580 s	93 min
500 m	69%	26%	25%:25%	1.6	536 s	77 min

[1] Speed Failures shown as the percentage of drifter-timesteps that failed due to model over-predictions and under-predictions of drifter speed, respectively.
[2] Acceptable times calculated using 250m as the error circle radius

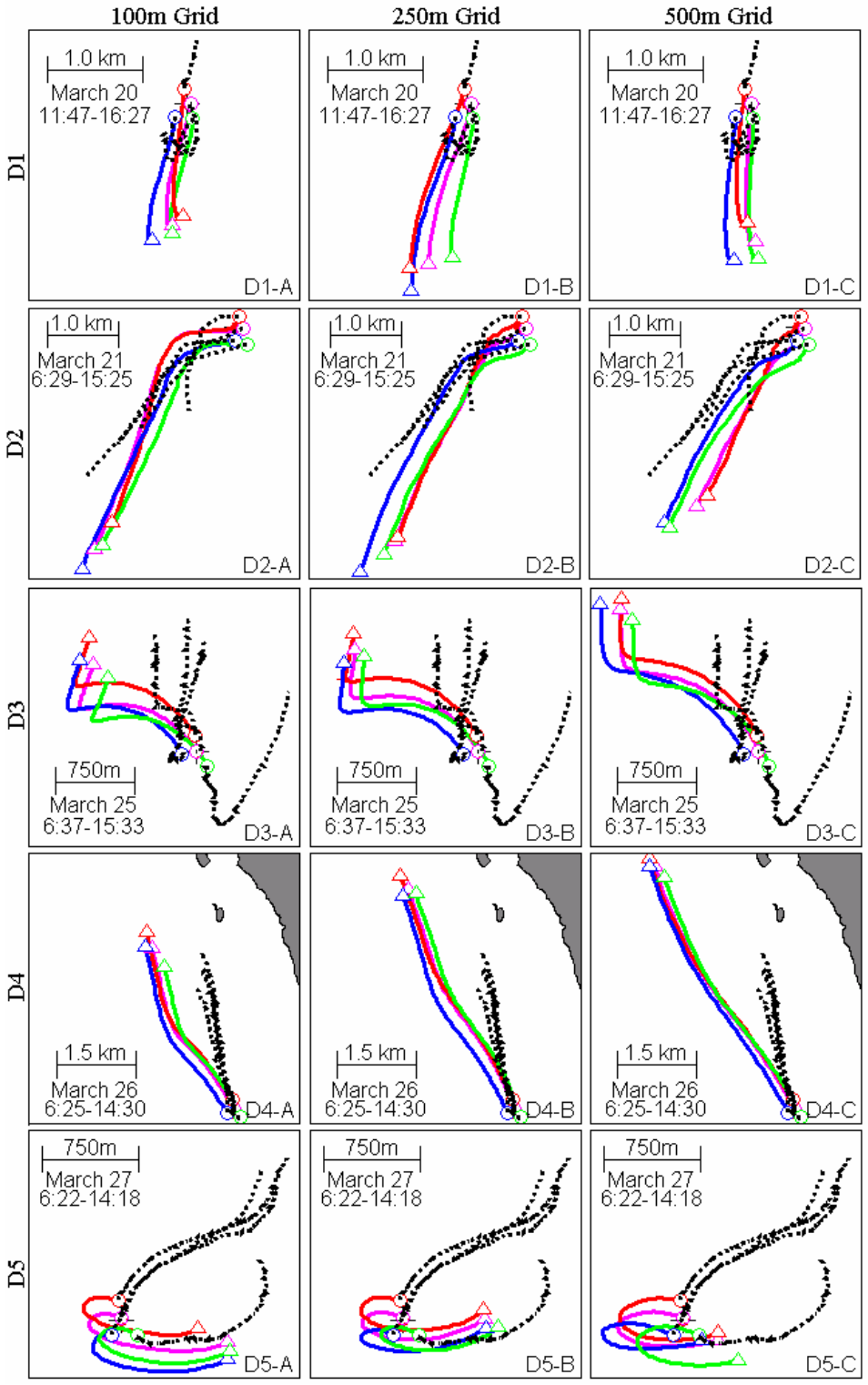

Figure 4.21 – Spaghetti Diagram Plots of Model Results by model grid resolution. Results from the 100m grid shown in Column A, 250m grid results in Column B, 500m grid results in Column C. Drifter days shown by row. Field drifter paths shown as dotted lines. Symbols as in Figure 4.18

unlikely that the modeled drifter paths from such higher-resolution simulations would be significantly more representative of the field drifter data.

Results from the Circle Assessment analyses (Table 4.9) suggest that the simulations on the 100m grid actually are slightly less accurate than those using the 250m grid, and are of equivalent accuracy with those using the 500m grid. The comparatively low κ-score, success rate, and κ_{max} values calculated for the 100m grid resolution are due to the tendency to under-predict the drifter velocities at that grid scale. For 31% of all drifter timesteps modeled with the 100m grid resolution, the modeled drifters failed to enter the target circle one timestep after their deployment because they traveled too slowly. For such simulations the ELCOM-MMP model was three times more likely to fail due to speed under-prediction than over-prediction. In contrast, the simulations using the 250m and 500m grids were nearly equally likely to fail the model timestep analysis due to over-prediction and under-prediction of field drifter speed. The conclusion that the drifters modeled on the 100m grid generally travel more slowly is also supported by the relative displacements of drifters as shown in the spaghetti diagram plots from the D1, D3, and D4 simulations (Figure 4.21).

Through the comparative failure analysis of all the drifter-timesteps, model grid resolution is found to play an insignificant role in reproducing the MMP field drifter paths (Figure 4.22). For 71% of all drifter timesteps, model results were unaffected by the grid resolution, as all modeled drifters either entered next drifter-timestep's target circle or all modeled drifters failed to enter the next drifter-timestep's target circle. Compared with results shown in Figure 4.19, ELCOM-MMP model results were affected more by alterations in the wind forcing than in the grid resolution. Also from Figure 4.22 it is evident that no net-improvement in model results is obtained when modeling with the 250m grid instead of the 500m grid (or vice versa). A net improvement of 8%, however, was achieved when modeling with the 250m grid instead of the 100m grid, and only a 1% net improvement was achieved when modeling with the 100m grid rather than the 500m

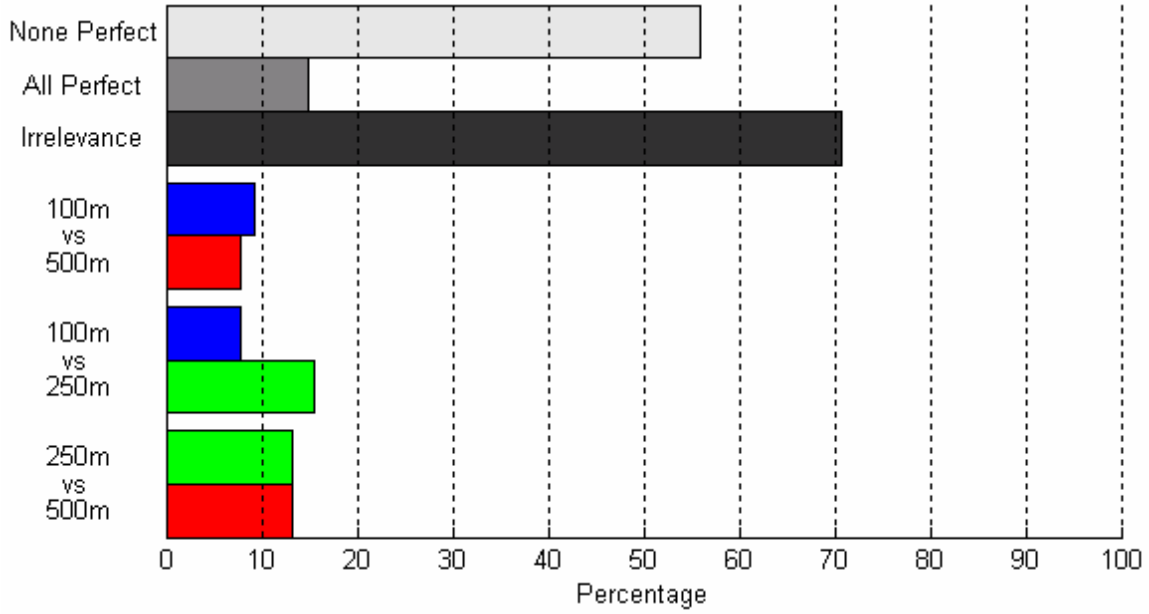

Figure 4.22 – Comparative Failure Analysis Results –ELCOM-MMP grid resolution simulations. Results from the 100m simulations are shown in blue, 250m results are in green, and 500m simulation results are shown in red.

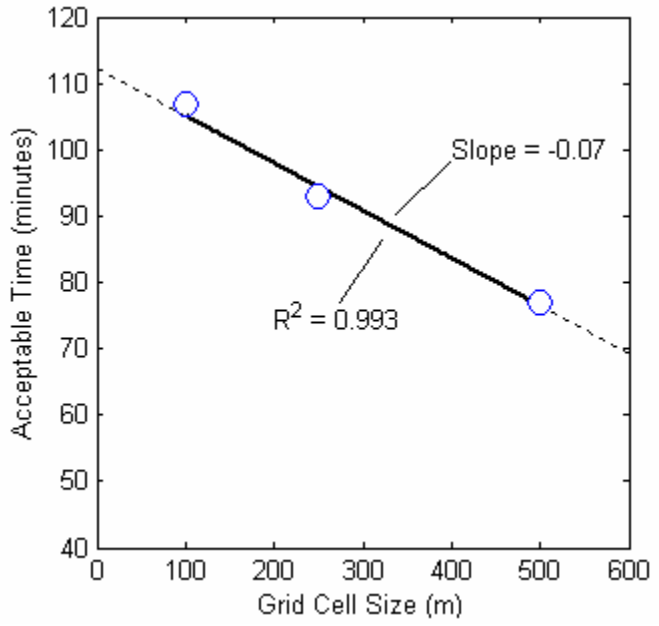

Figure 4.23 – Model Acceptable times vs. grid cell size from the ELCOM-MMP simulations

grid. These results combine to suggest that the modeled drifter paths (at scales of the perfection analyses) are statistically unaffected by the grid resolution, at least for the range of resolutions included in this analysis.

In contrast to the circle assessment results detailing model perfection at the small (10m) local scales, the model acceptable time results clearly suggest model skill improves with finer grid resolutions. As shown in Figure 4.23, there is a nearly perfect linear (1st-order) relationship between grid resolution and model acceptable time. Conclusions as to the validity of this linear relationship would require that simulations be conducted at other grid resolutions to provide more data points for the regression analysis. However, the general trend of increasing acceptable time with decreasing grid cell size is evident from the data presented. As no similar trends were observed in the perfection time data (Table 4.9), it is reasonable to conclude that while larger-scale properties of the MMP currents will be continuously improved with decreases in model grid cell size, model skill at reproducing local drifter motion may not be affected.

The main conclusion drawn from the analyses presented in this section is that ELCOM's numerical grid resolution is only a significant factor in the model's ability to reproduce the larger-scale features of the MMP circulation. The skill of the ELCOM-MMP model for perfectly predicting drifter motion over shorter time and space scales is not clearly dependent upon the numerical grid resolution.. Alterations to the water surface slope (§4.3.3) and wind forcing (§4.3.2) produced greater affects on the relative accuracy of the modeled drifter paths than did changes to the grid resolution. Further attempts to increase the smaller-scale agreement between the model and field drifter paths should not focus on improving the grid resolution.

4.3.5. Timestep Analysis - Base Case, Setup #7 and Setup #8

To determine the effect of variations in model timestep on the modeled drifter paths, 3 sets of simulations were conducted: 1) the base-case setup using a 600s timestep, 2) Setup #7 using a 300s timestep, and 3) Setup #8 using a 1200s timestep. Each set of simulations consisted of modeling the D1-D5 drifter deployments on a 250m x 250m uniform grid with LDS wind forcing and a southward water surface slope. The circle Assessment results from each of the simulation sets are presented in Table 4.10.

As discussed in Section 4.2.5, κ-scores and success probabilities are highly dependent upon the length of model timestep over which they are calculated. As the timestep decreases (and assuming the field drifter's velocity is constant), the separation between the field drifter at the beginning and end of the timestep decreases, eventually reaching a point where the field drifter's target circles intersect (see Figure 2.13). In the limit of an infinitesimally small timestep,

Table 4.10 – Circle Assessment Results for ELCOM-MMP timestep simulations

	Model Timestep Analysis			Separation Analysis		
Timestep	κ-score	Success Probability	Speed[1] Failures	Mean κ_{max}	Perfection Time	Acceptable Time
300 s	95%	81%	1%:5%	1.5	528 s	31 min
600 s	74%	35%	21%:23%	1.8	580 s	93 min
1200 s	35%	6%	20%:54%	1.4	543 s	115 min

[1] Speed Failures shown as the percentage of drifter-timesteps that failed due to model over-predictions and under-predictions of drifter speed, respectively.

the two target circles practically coincide, guaranteeing the model would adequately predict drifter transport; i.e., the drifter transport in a sufficiently small time step is always smaller than the uncertainty in the drifter position. This trend toward higher κ-scores and success probabilities with shorter timesteps is evident in Table 4.10. The success probabilities jumped from 6% at 1200s to 35% at 600s and 81% at 300s, and similar increases in κ-scores were also obtained. Interpreting these trends in the model results is difficult because it is impossible to discern (using only the data in Table 4.10) their true cause. It is possible that the model actually did improve with the shorter timestep, and that the displacement of each field drifter over the model timestep is still sufficiently large to prevent the target circles from overlapping. It is also possible, however, that the model's ability to reproduce the observed drifter motion actually decreased but that the decrease is masked by the overlap in the field drifter's target circles. These two contrasting yet plausible explanations make the use of κ-scores and success probabilities inappropriate for assessing model skill for these simulations.

Although the trends in κ-scores and success probabilities may be interpreted in multiple ways, the trends in the failure analyses in Table 4.10 remain unambiguous. As indicated by the speed failures for simulations with the 600s timestep, the model was nearly as likely to over predict drifter speed as it was to under-predict drifter speed (21% compared with 23% of all drifter-timesteps). For simulations using the 1200s timestep, the model was more likely to under predict drifter speed as it failed due to slow speeds in 54% of all drifter timesteps and failed due to high speeds in only 20% of all drifter timesteps. This increase in model under-prediction of drifter speeds may be indicative of a relationship between model timestep and water current speeds in the modeled surface layer. This topic is revisited below.

Separation Analysis results shown in Table 4.10 are consistent with those obtained in assessing model response to wind variation, water surface slope, and model grid resolution (Sections 4.3.2-4.3.4). The base-case ELCOM-MMP model setup (shown as 600s in Table 4.10) tends to produce average higher κ_{max} and perfection time values than the other model setups, although the differences in mean values (0.3-0.4 for κ_{max} and 37-52s for perfection time) are not significant. The small differences in κ_{max} and perfection times from the different simulation sets suggest that at the small time and space scales used within the circle assessment methods, the model performs similarly regardless of timestep.

Despite being similar at smaller scales, the model's ability to reproduce drifter movement over larger time and space scales is dependent upon the model timestep. As indicated in Table 4.10 and Table 4.11, model acceptable times increased from 31 minutes to 83 and 115 minutes as model timesteps increased from 300s to 600s and 1200s. This increase in acceptable time with increasing timestep indicates that the separation between the field and modeled drifter occurs at a faster rate when the model is run

Table 4.11 – Acceptable Time Data from the ELCOM-MMP Timestep simulations

	Acceptibility[1]			Perfection[2]	
timestep	Number of timesteps	Acceptable time	Rate of separation	Perfection time	Rate of separation
300s	6.2	31 min	13.4 cm/s	528 s	1.9 cm/s
600s	9.3	93 min	4.5 cm/s	580 s	1.7 cm/s
1200s	5.8	115 min	3.6 cm/s	543 s	1.8 cm/s

[1] Rate of separation over model acceptable time is based on a final separation of 250m
[2] Rate of separation over model perfection time is based on a final separation of 10m

with a shorter timestep. It is notable that the increase in separation rates with decreasing timestep is only evident during the period when the model is considered "acceptable" rather than "perfect" in regard to its ability to reproduce drifter motion (Table 4.11). As such, causative failure analysis (Section 2.8) is not useful in identifying the cause of the increased separation rates observed when the model is acceptable and run with smaller timesteps. To assist in identifying the causes of the increased separation rates, spaghetti diagrams are analyzed below.

Separation between the model and field drifters is caused by the model's inability to correctly determine the drifter's speed and/or direction. Increasing rates of separation with decreasing model timestep therefore requires decreases in the model's ability to reproduce the field drifter motion. For example, if the model over predicts drifter speed by 20% with a 600s timestep, at a 300s timestep the amount of speed over-prediction should increase to cause an increase in the separation rate. While the magnitudes of such increases may not be quantified through spaghetti diagram analysis, the effects of the increases on drifter displacement may be noticeable. As shown in Figure 4.24, drifter displacement over the duration of each simulation is greatest when modeled with the 300s timestep. This is especially evident in the D2 and D4 simulations, where the drifters modeled with the 300s timestep displaced by distances 3 and 4 km (respectively) greater than those drifters modeled with the 1200s timestep. From the acceptable times and spaghetti diagram analyses, it is concluded that the ELCOM-MMP models tend to over-predict drifter speed at lower timesteps.

A second conclusion drawn from the spaghetti diagrams is that drifter paths modeled with the 1200s timestep tended to be more comparable to the field drifter paths than were those modeled with the 600s or 300s timesteps (when considered over the entire drifter deployment). At the larger timestep, the modeled drifters tended to travel shorter distances of the deployment duration, and tended to follow the headings of the field drifters. The agreement between the field and modeled drifters in the D4 deployment (Figure 4.24 D4-C) is nearly complete, as the modeled and field drifter paths rarely separated by more than 100 m. Similar results were obtained for the D3 simulation (Figure 4.24 D3-C), although the model was unable to correctly predict the motion of field drifter #3 which was caught in an un-resolvable diverging current. Only for the D5 simulation were modeled drifter results arguably more accurate when using the smaller timesteps. It is also notable that the D5 modeled drifter paths for the 300s simulation were similar to those derived with the MIX wind dataset (Setup #2 - Figure 4.18 D5-B) and those derived when modeling with a northward water surface slope (Setup #3 – Figure 4.20 D5-C).

From the spaghetti diagram and circle assessment analyses presented above, the following observations were made:

1. The ELCOM-MMP model tends to over-predict drifter speeds when using a 300s timestep,

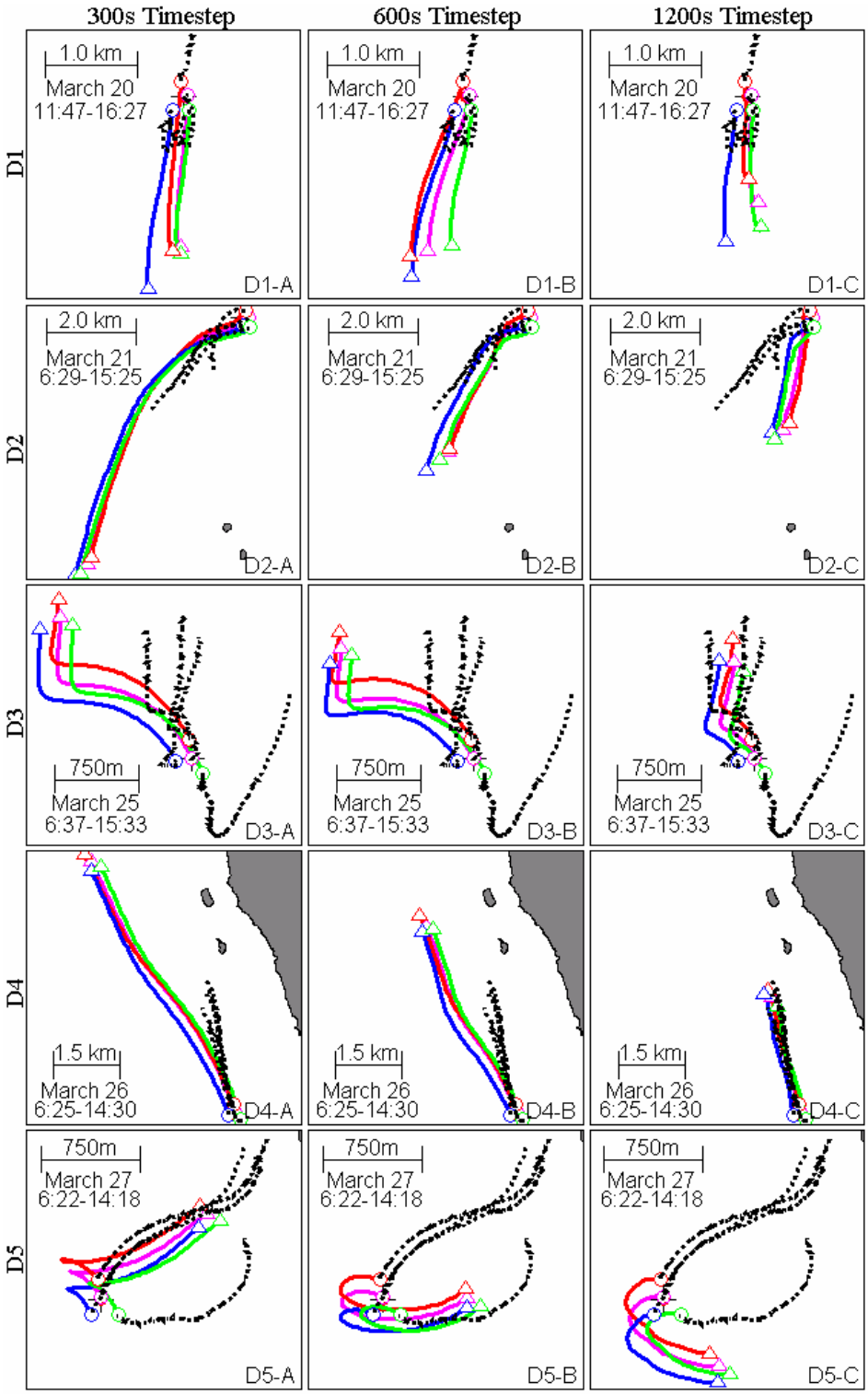

Figure 4.24 – Spaghetti Diagram Plots of Model Results by model timestep. Results with the 300s timestep grid shown in Column A, 600s timestep results in Column B, 1200s timestep in Column C. Drifter days shown by row. Field drifter paths shown as dotted lines. Symbols as in Figure 4.18.

2. The ELCOM-MMP model is more likely to under-predict drifter speeds when modeling with a 1200s timestep, and

3. Results from the D5 simulation with the 300s timestep were more comparable to field drifter data and similar to those derived when using the MIX (rather than LDS) dataset or the northward water surface slope.

As discussed in both Zaker et al. (2002) and section 4.32 above, MMP currents are principally wind driven, so the sensitivity of the model results to the time step suggests that the modeled transfer of momentum from the wind to the currents is not invariant with the time step. Within ELCOM, a vertical mixed-layer model is used for distributing wind momentum (Hodges et al, 2000). Within the mixed layer model, wind momentum is evenly distributed throughout a surface-mixed layer, the depth of which is dependent upon numerous factors including wind speed, available mixing energy, existing density stratification, vertical grid resolution, and time allowed for mixing. If the mixed-layer depth is under-predicted, then the wind-introduced momentum is concentrated over smaller depths and the surface water velocities are over-predicted (Figure 4.25). In contrast, if the mixed-layer depth is over-predicted, then wind-introduced momentum is distributed over a larger volume and the surface water velocities are under-predicted. Based on the drifter results discussed above, it is hypothesized that the ELCOM-MMP model retains a time-sensitivity in the mixed layer depth prediction; i.e., an increase in the mixed layer depth predicted over a single 1200s time step is not the same as the net increase predicted over four 300s time steps with the same wind. Thus, the mixed layer is too thin when ELCOM is run with a 300s timestep and is, at least occasionally, too thick when ELCOM is run with a 1200s timestep. Such conditions would explain observations #1 and #2 above.

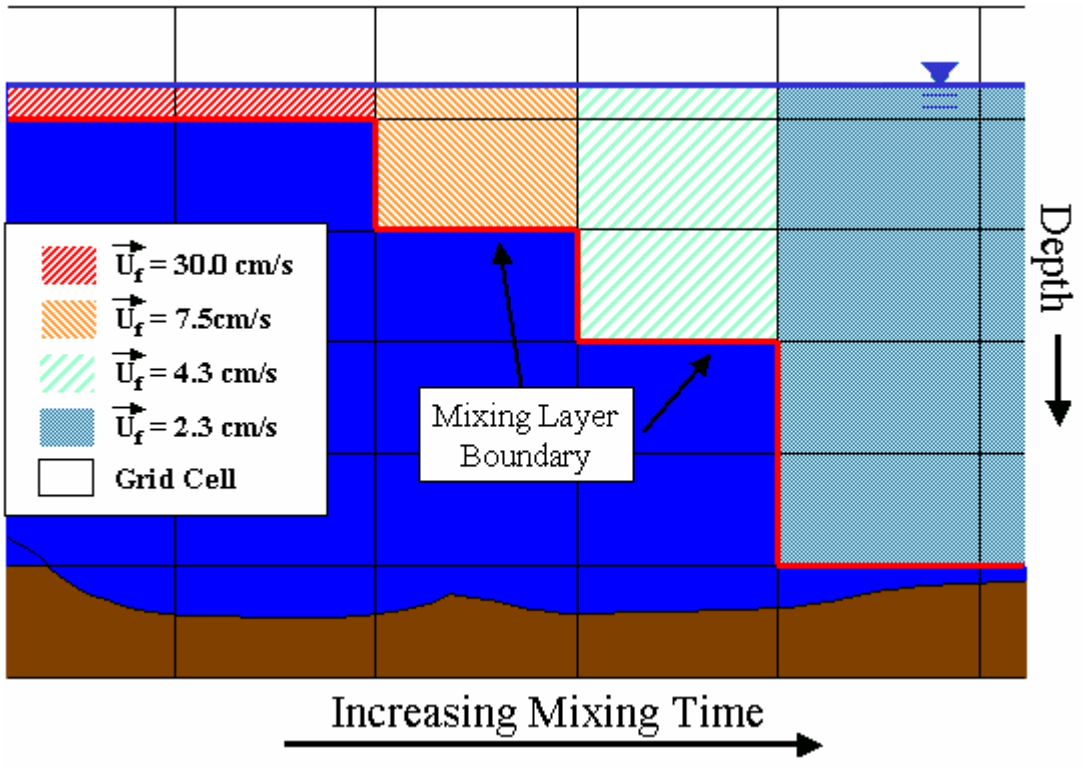

Figure 4.25– Mixing Layer Depths in relation to mixing time. As the mixing time increases, more momentum is distributed over a greater depth and the mixed layer velocities decrease.

The mixed-layer depths calculated at drifter #1 for the D4 simulations (Figure 4.26) support the hypothesis presented above. As shown, the mixed layer depth for simulation using the 300s timestep is relatively constant over the entire deployment, and is shallow (Approximately 0.9 m). This depth corresponds to the depth of water in the surface layer of the computational grid. Similar mixed layer depths were calculated within the 600s simulation, although the mixed layer extended to the top two layers of grid cells for approximately 1-hour near the end of the deployment. These relatively shallow mixed-layer depths are consistent with the high-velocities/large displacements calculated for the modeled drifters from these simulations (Figure 4.24 D4-A,B). In contrast, the mixed-layer depth for portions of the 1200s-timestep simulation exceeded 9 meters, suggesting the water column was well-mixed almost to the bottom. Within the 1200s timestep simulation, the drifter speeds calculated during the times when the mixed layer was thick were approximately 1 cm/s. When the mixed layer was thin, the same drifters traveled at speeds greater than 4 cm/s. The agreement in timing of the drifter acceleration and the changes in mixed layer depth is good but not perfect. The lag between mixing depth changes and model drifter accelerations is due in part to the slowed response of the GABI-F drifter as it reacts to the changing forces applied by the surrounding fluids (See Section 2.5).

The explanation for the behavior of the modeled drifters during the D5 simulation is also linked to the

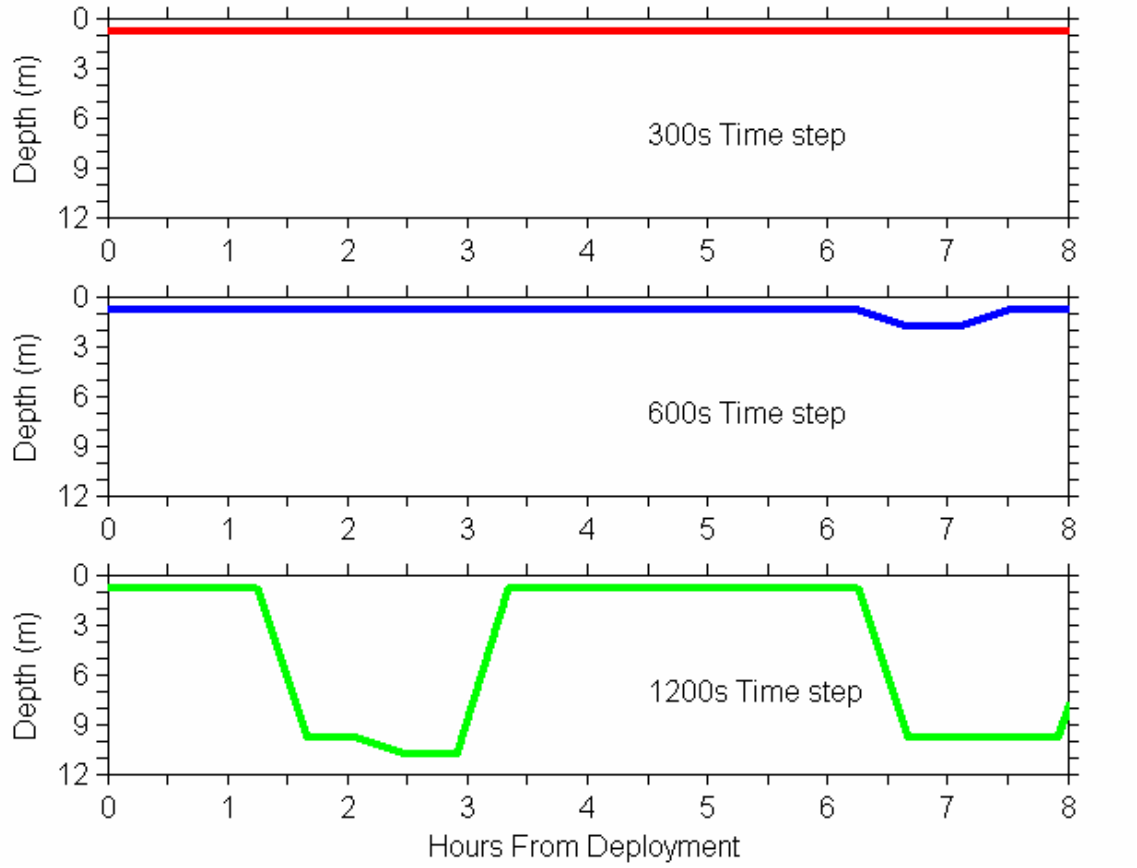

Figure 4.26 – Mixing Layer Depths with model timestep. Depths determined along the field drifter #1 path during the D4 deployment (March 26). Substantial vertical mixing of momentum due to wind forcing only occurs at the larger timesteps.

mixing depth, although the timestep is not the controlling factor. During the D5 deployment, the wind stress from the Whitford's station is very low (winds often were not measurable – See Figure 4.16), which likely lead to difficulty in properly determining the mixed layer depth. Increasing the wind stress (with the MIX or LDS dataset) likely changed the modeled mixing depth to cause the observed changes in drifter paths. The above idea is presented to illustrate how quantitative analysis of field/model drifter tracks can lead to a better understanding of model sensitivity and errors. The in-depth analysis of the time-sensitivity of the ELCOM mixing-model behavior (as warranted by the above results) is outside the scope of the present research. The topic is discussed briefly, however in Section 5.3 and in Section 6.8 where drifter results from simulations using alternative mixing models are discussed. Based on the analysis presented in this section, a detailed investigation of the ELCOM mixed-layer model seems the most likely avenue toward improving the degree to which the model reproduces the field drifter motion over short time and length scales.

4.3.6. Modeling with variable ELCOM-MMP Setups - Summary

Using the GABI-F drifter modeling technique, spaghetti diagrams, and the Circle Assessment method, results of various ELCOM-MMP simulations were analyzed to determine model sensitivity to changes in model setup. As outlined in Table 4.9, nine model setups were simulated to assess the effects of alternative wind forcing, water surface slopes, grid resolutions, and model timesteps on the predicted drifter paths. Conclusions drawn from this analysis are that:

1. The greatest discrepancies between modeled drifter paths were from simulations using alternative timesteps.

2. Modeled small-scale drifter motions are influenced more by the model wind forcing than by the water surface slopes or model grid resolution,

3. Model skill at reproducing the large-scale behavior of the MMP surface currents increases with increasing numerical grid resolution.

The sensitivity of the modeled drifter paths to model timestep is linked to the vertical mixing model in ELCOM. This model evenly distributes momentum due to wind forcing through the water column from the surface to a certain mixed-layer depth. In situations where the mixed layer depth is too shallow, predicted surface currents will be too high as the momentum due to the wind forcing is concentrated within the upper portion of the water column. In contrast, if the mixed layer is too deep, wind momentum will be diluted as it is evenly distributed over a larger volume of water, thereby causing the predicted drifter speeds to be too slow. The model timestep is one factor that contributes in determining the mixed layer depth, as it limits the amount of time over which vertical mixing could occur. Circle Assessment analyses linked periods of excessive model drifter speeds to periods within which the calculated mixed layer depths were shallow. Such periods were longer and more frequent within the 300s and 600s timestep simulations, and occurred infrequently in the 1200s simulations. These results suggest that a larger (600s) model timestep is needed to properly reproduce vertical mixing and the resulting surface currents within the ELCOM-MMP simulations.

Based on all of the results presented in this section, improvements in model skill are most likely to arise with improvements in the vertical mixing model used in ELCOM. Further refinements to the model grid or improved knowledge of the MMP wind forcing and water surface slopes are likely (in theory) to produce improved model drifter paths, removing the timestep sensitivity of the vertical mixing model. The analyses included in this section demonstrate how drifter modeling can be used to diagnose potential problems in the model numerics and model setup. As such, drifter modeling represents a new, functional approach for model validation and assessing improvement.

5. Conclusions and Recommendations

The two main objectives of this research are:

> *developing a drifter modeling technique that determines drifter movement based on the forces applied to the drifter by its surrounding fluids, and*
>
> *developing a model assessment technique that quantifies the model's ability to reproduce the observed velocities of field drifters*

Both of these objectives have been accomplished, and their application provided insight into the ability of the Estuary and Lake Computer Model (ELCOM) to represent currents within Marmion Marine Park (MMP), Western Australia. This chapter: 1) summarizes the work and conclusions of this research, 2) discusses the implications of this research in modeling circulation within MMP, and 3) provides recommendations for future work in drifter modeling and modeling MMP currents.

5.1. Summary Discussion

5.1.1. Research Goal

Drifter modeling involves using a hydrodynamic model to calculate the fate and transport of a substance immersed within the water body. In this research and in and increasing number of projects around the world (See §2.5 and §6.9), drifter modeling is also being used to assess model skill at reproducing observed drifter paths within a subject waterbody. A long term goal is to use drifter modeling in conjunction with field drifter data to validate the hydrodynamic model in terms of its capacity for reproducing water body circulation patterns. This research represents the first steps toward achieving this goal. Specifically, through this research an improved drifter modeling technique was developed and a method for quantifying and assessing model skill using drifter data was created.

5.1.2. The GABI-F Drifter Model

When modeling drifter motion in wind-driven surface currents, the drifter modeling technique must incorporate the effects of the winds on drifter transport. Existing Lagrangian drifter models (§2.2) assume the drifter moves in perfect accord with the water surrounding the drifter's submerged drogue section, effectively neglecting the direct influence of wind on drifter motion. As such, Lagrangian models represent the less-realistic side of the spectrum of drifter modeling (Figure 5.1). Leeway models, which are simple Lagrangian models enhanced with leeway factors (§2.3), incorporate more of the wind's influence on drifter motion by adding a fraction of the wind speed to the speed of the drifter. The appropriate fractional value is best determined experimentally, is usually constant for any given drifter design, and is not proportional to the wind speeds. The leeway model therefore incorporates a rather inflexible approximation of how wind might affect drifter motion and is not based on established physical principles of fluid flow. The "Generalized Acceleration-Based Inertia and Forcing (GABI-F)" drifter model developed in this research (§2.4) incorporates both wind and water current forcing in determining drifter motion, and better reflects the physics driving such motion than either of the other drifter models.

With respect to the Lagrangian and Leeway drifter models, the GABI-F model is "more realistic" in its representation of what causes field drifters to move. The GABI-F model involves the calculation of drifter velocities based on accounting for all of the forces

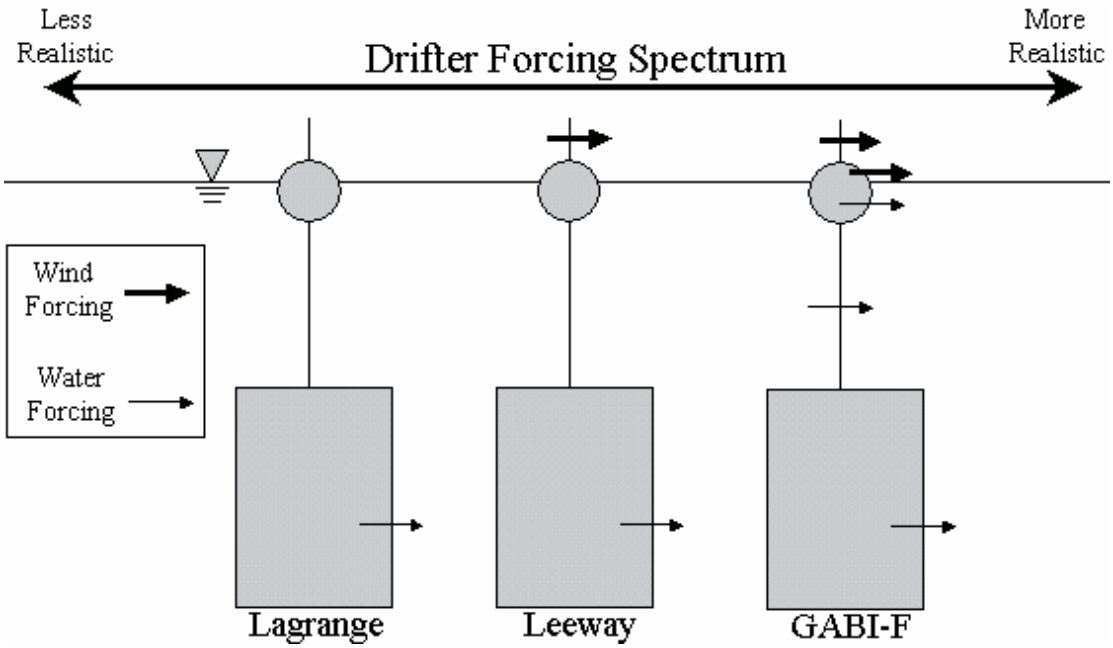

Figure 5.1 – Drifter Forcing Spectrum – forcing included in the Lagrange, Leeway, and GABI-F drifter modes. More forcing is included in each model progressing from left to right.

acting on sections of the drifter. For the drifters in this work, five sections were used: two wind-forced sections and three water-forced sections (§2.4.2). Each section may be acted upon by fluids with different velocities (i.e., allowing a sheared water column), and the forces on each section depend on the difference in the fluid and drifter velocities over the model timestep. Drifter velocities are determined by dividing the sum of the forces on the drifter by the drifter mass and approximating the drifter acceleration using a standard 2^{nd} order numerical approximation (§2.4.3). As such, the drifter velocity at any given time step is partially dependent upon its velocity at the previous two time steps. This simulated drifter inertia slows the modeled drifter's response to changes in the surrounding fluid velocity, making it behave more like the physical drifter the method strives to simulate.

Differences in predicted drifter motion may be considerable when modeling is conducted using the GABI-F rather than Lagrangian or Leeway drifter models (§4.2.2). By moving the drifter in exact accord with the surrounding water, the Lagrangian method ignores wind and drag effects on drifter motion. In instances of low water velocity but relatively high wind speeds, Lagrangian and GABI-F drifters may travel divergent paths as the winds cause the GABI-F drifters to accelerate to and travel at greater velocities (§4.2.2). This path separation poses a problem when assessing the improvement between Lagrangian and GABI-F modeling because comparisons between the two modeled drifters (using accepted existing analysis techniques - §2.5) are essentially meaningless: as the drifters are located at different positions within the waterbody at any given time after the separation, their local velocities are different and their future paths are uncorrelated. Similar problems arise when using existing analysis techniques to compare drifter modeling results against field-observed drifter data. This problem, referred to in this research as "error integration," (§2.5) had to be addressed before drifter

modeling could be used to assess hydrodynamic model skill.

5.1.3. The Circle Assessment Method

Existing methods for comparing modeled drifter data, specifically the spaghetti diagram method (§2.5.1), the Type I method (§2.5.2) from Toner et al (2001) and the Statistical Separation method (§2.5.3) of Thompson et al (2004), are all based on comparing drifter paths from the moment of drifter deployment. The methods provide qualitative information concerning the adequacy of one drifter dataset compared to another (§4.2) but are not useful in quantifying model skill as they are all integrative of model error. The Circle Assessment method of drifter analysis developed in this research (§2.6-§2.8) reduces error integration and quantifies the error in modeled drifter velocities through comparisons of two or more sets of drifter data.

Central to the Circle Assessment method are the concepts of the target and error circles (§2.6.1). Target circles demark the area around the field drifter position within which the modeled drifter may reside for the model to be considered "perfect" in its ability to reproduce field drifter motion. Similarly, error circles demark the area about the field drifter position within which the model drifter may reside for the model-predicted velocity field to be considered "acceptable" but not perfect. Error circles are always larger than target circles, requiring the model to more accurately predict drifter motion to be considered "perfect." Using this concept, the dimensionless parameter κ, defined as the separation between target circles normalized by the target circle radius (§2.6.3), may be used to assess model skill in reproducing field drifter motion. Larger values of κ imply larger relative separations between target circles, and for the hydrodynamic model to be skillful (or "perfect") in such instances it must predict drifter velocities closer to those implied by the field drifter data.

Two groups of analyses are incorporated within the Circle Assessment, and each group differs in the time value used to define κ. The Model Timestep analyses (§2.8) use the model timestep in defining κ, and statistically evaluate the model's ability to perfectly predict drifter transport over each model timestep. Aside from quantifying the likelihood of perfect drifter transport, instances of imperfect drifter modeling are scrutinized to provide both diagnostic and relative insight into model behavior under differing modeling setups (§2.8.2-2.8.3). In contrast, the Separation analyses (§2.7) define κ with the model perfection time, defined as the time required for the model and field drifters to separated by a distance equal to the target circle radius. The resulting value , κ_{max}, becomes the maximum κ value at which the model is considered perfect (§2.7.2), and is then indicative of ranges of allowable modeled drifter error in both speed and direction for maintaining model perfection. Through comparing κ_{max} values for each modeled drifter at each model timestep from different model setups, statistics of the model setup's accuracy in calculating drifter velocity may be obtained and the model skill may be quantified.

While κ_{max} values are used to define model skill at scales comparable to the smaller target circle radius, model acceptable times are used for quantifying model skill at the larger scales defined by the error circle radius (§2.7.3). Comparisons of model acceptable times derived from differing model setups indicate the extent to which the hydrodynamic model predicts the larger-scale circulation patterns of the subject waterbody. By using κ_{max} and model acceptable times to quantify model skill, the duration of comparisons between drifter datasets is limited to time periods before when the drifters in question diverge by a distance equal to the target or error circle radii (§2.6.3). In this way, error integration is limited in that the separation of the field and model results reduces the time over which the two datasets are compared. Unlike the previously existing drifter analysis methods which ignored separation, the Circle Assessment method uses

separation as a parameter to indicate the limit until which drifter results may be compared.

5.1.4. Hydrodynamic Modeling – Marmion Marine Park

To assess improvements in drifter modeling with the GABI-F technique and results assessment with the Circle Analysis method, the Estuary and Lake Computer model (ELCOM) was used to predict the circulation of drifters within Marmion Marine Park (MMP), Western Australia. Marmion Marine Park is a shallow (< 14 m) coastal preserve (§3.3) within which surface currents are principally driven by the local winds (Zaker et al, 2002). Drifter and meteorological data (§3.4,§3.6) were collected (with assistance from this researcher) within MMP over a 5-day period in March, 2003 as part of a larger water-quality project between the Centre for Water Research at The University of Western Australia and the Perth Water Corporation.

ELCOM simulations of Marmion Marine Park were conducted to assess the model's ability to predict the observed drifter motion as well as to determine the changes in the predicted drifter paths caused by alterations in model setup. The Circle Assessment results indicated that the GABI-F drifter model, when applied over short temporal and spatial scales, consistently produced drifter paths more comparable to the observed drifter data than did the Lagrangian or Leeway drifter models (§4.2). For example, the Model Timestep analysis of GABI-F drifter paths suggested that the ELCOM model has a 35% chance of perfectly predicting drifter motion over the model timestep (Table 4.2). Using the Lagrangian and Leeway drifter models, the Model Timestep analysis the predicted drifter motion was "perfect" for only 21% and 20% of the simulations, respectively. In contrast, model acceptable times were similar from simulations using each of the three drifter models, indicating that over larger time and space scales the choice of drifter model has less impact on the accuracy of the modeled drifter paths.

Using the GABI-F drifter model and the Circle Assessment method, ELCOM's sensitivity to wind forcing, water surface slope, grid resolution, and timestep were assessed (§4.3). Wind data were recorded at two locations within MMP during three of the five experiment days (§3.4.4), and the wind speeds and directions recorded at each location were not always in good agreement (§4.3.2). The discrepancies (often only slight) in the wind fields caused differences in the modeled drifter paths of the same approximate magnitude as those observed in comparing paths generated from ELCOM simulations using one wind data set and varying the drifter model (§4.2). These results suggested that, for obtaining accurate model drifter paths within the MMP simulations presented herein, the choice of drifter model is as significant as the choice of wind forcing. In contrast, model results were not significantly affected by altering the water surface slope imposed within each simulation (§4.3.3). Results from simulations using alternative numerical grid resolutions (§4.3.4) also indicated that reducing the grid cell size does not improve the model's ability to "perfectly" predict drifter movement over short time and length scales. Changing the grid resolution does, however, affect the model's skill over the larger time and space scales defined by the model acceptable time and error circle radius. Although the number of grid resolutions simulated was not sufficient for quantifying the relationship, model acceptable time clearly increases with finer grid resolution (Figure 4.22).

Model simulations with varying timestep (§4.3.5) suggested model skill at reproducing small-scale characteristics of the field drifter motion is unaffected by changes in timestep. However, comparative failure analyses indicated that while models run with different timesteps were equally likely to fail in predicting perfect drifter transport, the cause of the failures differed. Specifically, models run with larger timesteps tended under-predict drifter speeds whereas models run with shorter timesteps tended to over-predict drifter speeds. Thus modeled drifter speed is related to the model timestep, which suggests that the solution

procedure within the ELCOM model is non-time invariant. This time-invariance and the lack of model sensitivity to grid resolution, wind forcing, and water surface slope (§4.3.2-§4.3.4) combine to suggest that that aspects of the numerical solution procedure within ELCOM are the largest contributors of error in the modeled drifter paths. Fully testing this assertion was outside of the scope of this project (see the "Future Work" discussion in §5.3), however, the model acceptable times from the variable timestep simulations support the notion. Over the times when the model is considered "acceptable" rather than "perfect," drifters modeled with the 300s timestep separated from the field drifters at rates nearly three-times those calculated for drifters modeled with 600s or 1200s timesteps (Table 4.11). The faster drifter speeds (indicated by the greater separation rates) were due to the model's concentrating wind-induced momentum into a surface mixed layer that was too shallow. As the model timestep increased the average mixed-layer depth also increased (Figure 4.25), causing wind momentum to be spread over a greater fraction of the water column volume resulting in decreased drifter speeds. Therefore it was the time-dependence of the vertical mixing model within ELCOM that principally contributed to the errors in drifter modeling, suggesting the possibility that improving the mixing model might lead to more accurately predicted drifter paths.

5.2. Conclusions

The conclusions that may be drawn from the present work are:

1. The new GABI-F drifter model produces drifter paths more comparable to field drifter data collected from wind driven surface currents than do previously existing Lagrangian and Leeway drifter models.

2. The Circle Assessment methodology for analyzing model skill in reproducing observed drifter paths is superior to previously existing techniques due to its ability for quantifying model skill over both short and long temporal and spatial scales, and its reduction of error integration in time,

3. The Estuary and Lake Computer Model (ELCOM) acceptably predicts drifter motion within Marmion Marine Park, Australia over large time and space scales {O(250 m) and O(90 minutes)}

4. ELCOM perfectly models approximately 35% of MMP drifters over short time and space scales {O(10 m) and O(10 minutes)}

5. The vertical mixing model within the Estuary and Lake Computer Model (ELCOM) is likely the greatest contributor to the observed discrepancies between modeled and field drifter paths within Marmion Marine Park, Australia

6. Incomplete knowledge of the environmental forcing conditions (i.e., winds, tides, water surface slopes) is not likely the greatest contributor to the observed discrepancies between modeled and field drifter paths within Marmion Marine Park, Australia.

5.3. Recommendations for Future Work

The research presented herein investigates the use of field drifters and drifter modeling to validate water velocities calculated by numerical models. As demonstrated (§2.4, §2.6-§2.8), the first steps toward this goal involved 1) deriving the GABI-F drifter model for calculating drifter motion based on force calculations, 2) developing the Circle Assessment method for quantifying the hydrodynamic model's ability to reproduce observed field drifter velocities, and 3) applying both the GABI-F method and Circle Assessment method to assess an existing hydrodynamic model. Many possible nuances and subtleties in implementing each of these three steps were left unaddressed as the present work focused on answering the fundamental research question: "Can particle tracking be used to improve model validation?" The answer is affirmative, but further improvements to both the GABI-F and Circle Assessment methods are both possible and desirable. The analysis of the ELCOM model results (§4.2-§4.3) also yielded insight

into possible approaches toward improving model performance, both in application to determining MMP circulation and in applications to other subject water bodies.

The GABI-F method for calculating drifter movement (§2.5) includes numerous assumptions in both the derivation and solution procedure. For example, the drag coefficients for each drifter section were assumed to be unity, whereas in reality they should be functions of both the drifter shape/materials and the Reynold's number of the surrounding fluids (Kundu and Cohen, 2002). The drag coefficient determines how quickly the GABI-F drifter reaches equilibrium with the surrounding fluids (see §6.6), and therefore controls how fast the drifter responds to changes in the forcing to which the drifter is subjected. Modeled drifters with larger drag coefficients respond faster to forcing changes, which may be important when model currents are driven by unsteady winds (as with the D3 simulations, for example – see §4.3.2). Therefore the results from GABI-F drifter modeling may be unfounded if improper coefficient values are used so that the modeled drifter does not respond to current changes as quickly or slowly as the field drifter. To alleviate potential problems that might arise when assuming drag coefficients are constant and set to unity (as in this work), a method needs to be developed to assign coefficients based on the properties of the drifter and the flow conditions surrounding the drifter.

A second aspect of the GABI-F method that requires further scrutiny is the solution procedure (§2.5.3), which involves the selection of the "most appropriate" potential drifter velocity based upon the acceleration of the surrounding fluid. This approach is somewhat synthetic and, although effective, may not be optimal. Other approaches toward deriving and solving the force-balance equations presented in §2.5 may lead to cleaner solution procedures based to a greater extent on the calculated physics of the fluid flow. One possibility is to modify the solution procedures so that they are time-invariant and not directly linked to the model timestep (See Eq. (2.18)). Such a solution procedure could yield even greater accuracy in the predicted drifter motion than what is presented in this research. Based on the research presented here, the solution procedure for the GABI-F drifter model must still be considered as a source of potential error when comparing observed and modeled drifter motion.

To improve the Circle Assessment method, one approach might be to determine appropriate target circle radii based on length-scales of the flow field rather than on the positional error of the drifter. In theory, GPS technology will continue to improve until the errors in drifter position are either negligible or miniscule in comparison to the scales of the flow field. The Circle Assessment method, as presented in this work, fails as the drifter's positional uncertainty approaches zero. At such negligible error scales, κ values approach infinity irregardless of the displacement of the field drifter (§2.6) thereby negating any relationship between model skill in predicting velocity fields and drifter positions. Linking the Circle Assessment method to definable scales of the modeled or observed flow field (for example the median eddy width as discernible from field drifter paths) allows the Circle Assessment method to be applied to all systems even as GPS technology improves.

Another improvement to the Circle Assessment method would be revising the perfection analyses to eliminate speed bias. As demonstrated in sections 4.2.9 and 4.3, both the κ_{max} and perfection time indices are limited by their dependence upon the field drifter speed. Ideally, a model could be considered "improved" (in comparison to another model or model setup) if it perfectly predicts drifter motions for longer times over longer path lengths. The κ_{max} parameter, however, is only indicative of the path lengths whereas the perfection time is only indicative of the time period over which the model performs perfectly. Some combination of these (or similar) parameters may be more indicative of model skill than just separate κ_{max} and perfection time values. For example, the

"perfection index" (Φ) could be the product of κ_{max} and perfection time normalized by the model timestep:

$$\Phi = \frac{U_{field}\tau_d^2}{2\delta\Delta t} = \kappa_{max}\frac{\tau_d}{\Delta t} \quad (5.1)$$

Defined in this way, the perfection index is larger with increasing field drifter path-length and increasing perfection time. Use of this metric, and possibly others, may provide more unequivocal measures of model skill through drifter modeling.

While the GABI-F and Circle Assessment techniques may be improved, there is no guarantee that the improvements will lead to greater agreement between the modeled and observed field drifter paths. Discrepancies between modeled and observed drifter paths may arise due to:1) numerical approximations used in the hydrodynamic model algorithms, 2) initially unknown deficiencies of the model setup, 3) inaccuracies in the model boundary conditions/forcing data, and 4) inaccuracies in the drifter modeling technique . Error sources #2, #3 and #4 were addressed in §4.3 and throughout this research. Future efforts in drifter modeling need to address error source #1.

Every hydrodynamic model makes numerical approximations of the physical processes that drive fluid flow, and many methods exist for implementing each approximation into computer algorithms. As demonstrated in section 4.3.5, the vertical mixing model within ELCOM plays a significant role in determining water velocities within the MMP surface layer, and was the largest identified contributor of error to the modeled drifter paths. Refinements to the mixing model, or alternative mixing models (See §6.8), may produce more (or less) accurate drifter paths/results. Similarly, different algorithms for calculating free surface height, surface thermodynamics, or open boundary fluxes, for example, may lead to slightly different calculated velocities throughout the water column, and therefore to different predicted drifter paths. For this reason, the existing algorithms within the ELCOM model, while "state of the science," are continuously being improved, tested, and updated to obtain results more agreeable with both the theoretical concepts of fluid dynamics and with observed field data. Drifter modeling should be used in evaluating and testing such model improvements.

It is also possible that different hydrodynamic models applied to the MMP system will produce contrasting predictions of drifter motion. Direct comparisons of modeled drifter paths derived from alternative hydrodynamic models could then provide insight as to the potential benefits/detractors for using one model over another. In essence, drifter modeling results may be compared to evaluate the hydrodynamic models from which the results were derived. This process is underway at the Texas Water Development Board, where the relative capabilities of the ELCOM and ELCIRC (Zhang and Baptista, 2003) hydrodynamic models are being assessed. That assessment is being achieved through comparing the results presented herein with results from modeling the MMP drifter movement using ELCIRC, forced with identical boundary conditions as presented in this work.

The final recommended method for continuing research on model validation with drifter data is to conduct another field and modeling experiment similar to those presented herein but involving more extensive field data collections. The purposes of this second field experiment would be to: 1) develop another dataset for testing the GABI-F drifter modeling technique, and 2) reduce the amount of drifter path error attributed to uncertainty in the model boundary conditions. The field experiment would ideally be conducted within MMP so that model & field results could be compared with those obtained in this work. During this hypothetical field experiment, drifters should be deployed for a long as is practical to provide the greatest amount of drifter positional data. Along with the drifter data, traditional fixed-location current profilers should be used to record Eulerian velocity measurements. Upon modeling such a system, the

results of the Circle Analysis method could then be contrasted against the hydrodynamic model's ability to reproduce the velocities measured at the fixed location(s). In essence, this would be an attempt to first validate the hydrodynamic model using common Eulerian techniques and then re-validate the model using GABI-F drifter techniques. Results of each validation attempt could then be compared for consistency, potentially providing insight into the relative utility of either method.

Along with measuring currents with fixed-current meters and drifters, boundary condition data should be measured to reduce the uncertainty in the model forcing and therefore minimize the affects of this uncertainty on the predicted drifter paths. With respect to the MMP forcing data used in this project, numerous improvements are possible. For example, model bathymetry could be refined with high-resolution echosounder measurements. Temporary pressure transducers could be installed throughout the study area so that diurnal tidal oscillations and wave action are well documented during and preceding the drifter deployments. Differential or GPS land surveying techniques could be used to precisely determine the elevations of pressure transducers located throughout the domain, thus providing documentation on the actual water surface slopes typical of the MMP area. Acoustic Doppler Current Profilers (ADCPs) could be used to record the flows and water velocities along the perimeter of the MMP study area, thereby providing boundary information not included in this research. In addition, measurements of water temperature, salinity and buoyancy of the outfall plume could be made as the mixing and entrainment of plume water with the surrounding MMP water likely contributes to the surface currents in the vicinity of the sewage outfall.

As demonstrated in section 4.3, winds within MMP drive the circulation patterns for the area. Therefore to correctly model drifter movement due to wind-forced circulation, a sufficient number of wind sensors need to be used to properly determine the MMP wind field. The best option would be to equip each drifter with its own anemometer and compass so that the winds along the drifter paths were recorded and used in drifter modeling. Alternatively (or in addition), at least three weather stations (excluding the Whitfords station) should be installed, with one located west of the area of drifter deployment near the location of the LDS in this research (§3.3). The others should be located 1-2 km north and south of the sewage outfall. With such a wind station array, variations in wind forcing would be recorded, perhaps suggesting shear, divergence, or curl within the wind field. This information would be useful in further justifying/negating the assumption in this research that the MMP winds were uniform within the study area.

Appendix A:

Interpolation Methods for use in Particle Tracking

Lagrangian velocity interpolation from an Eulerian velocity field on a uniform grid may be carried out in numerous ways. In developing the particle tracking capability within ELCOM, six different horizontal interpolation schemes were tested for accuracy and applicability on various grid sizes and flow types. Each interpolation scheme applies a mathematical function to known velocities in the vicinity of the point to which the interpolation is made. The form of the mathematical function is referred to as the interpolation stencil; larger stencils may yield more accurate interpolated velocities, but at a greater computational cost. The schemes ranged in complexity and their ability to accurately reflect gradients within the flow field. The tested schemes were the following:

Linear Averaging (LA)

Bi-linear Interpolation (BLA)

Inverse Distance Weighting (IDW)

"Directional" Inverse Distance Weighting (DIDW)

1D Quadratic Lagrangian Interpolation (1DQ)

2D Quadratic Lagrangian Interpolation (2DQ)

A common numerical discretization technique within hydrodynamic models is the rectilinear Arakawa-C grid (Arakawa and Lamb, 1977), which has a single velocity calculated at each face of the grid cell. In implementing the various spatial interpolation functions for use on an Arakawa-C grid, each interpolation algorithm was designed to consider the velocities in the cells surrounding the cell containing the Lagrangian particle, known as the "particle cell." For display purposes in this document, the u-velocities are located on the positive-x face of each grid cell, and x is positive to the right. Similarly, the v-velocities are located on the positive-y face of the cell, with y positive toward the top of the page (See Figure A1). In demonstrating each of the interpolation schemes, an analytical velocity field is applied to a sample computational grid and used to calculate the u and v velocities at the grid cell faces. This analytical velocity field is given as:

$$\vec{u}(x,y) = \Psi(v_p, A)$$

$$\text{where} \begin{Bmatrix} r = \sqrt{(x-x_c)^2 + (y-y_c)^2} \\ v_p = 2\pi r + 3(x-x_c) + 3(y-y_c)^2 \\ A = \cos^{-1}\left(\frac{x-x_c}{r}\right) + \frac{\pi}{2} \end{Bmatrix} \qquad \text{(A.1)}$$

and where (x,y) are the coordinates of the velocity within the Cartesian grid, ψ is an operator converting from polar to Cartesian coordinates, V_p is the magnitude of the velocity vector at (x,y) and A is the direction of the velocity vector. The point (x_c, y_c) is the origin of the polar coordinate system, which need not coincide with the origin of the Cartesian coordinate system. For this discussion, the Cartesian origin is the lower left corner of the center grid cell (Figure A2) and polar coordinate origin is at the point (0.21, 0.89), where the unit is the grid cell length. With the drifter located at (0.71, 0.65), its analytical velocity from Eq. (A.1) is u = 2.23, v = 4.65.

Interpolation with Linear Averaging (LA)

The simplest of the spatial interpolation methods considered in this work is the linear averaging (LA) technique (Figure A2), which uses the velocities calculated at the particle cell faces to linearly interpolate the velocity of the particle at its location within the cell. This interpolation formula is:

$$u(d_X, d_Y) = \{u(1,0.5) - u(0,0.5)\} d_X + u(0) \qquad \text{(A.2)}$$

$$v(d_X, d_Y) = \{v(0.5,1) - v(0.5,0)\} d_Y + v(0) \qquad \text{(A.3)}$$

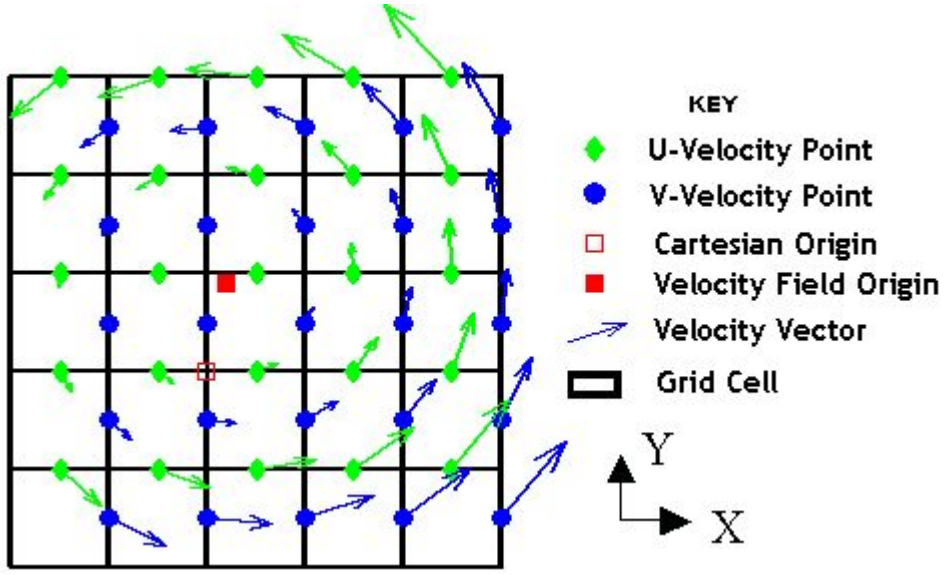

Figure A1 – Grid Setup for Horizontal Velocity Interpolation. In applying Eqn. 6.1, the origin (X,Y) = (0,0) is located at the lower left corner of the particle cell.

where the values in parentheses are the coordinates of the known velocities on the positive and negative cell faces in the direction of the interpolation, and d_X and d_Y are the fractional location of the particle relative to the cell length in the x and y directions, respectively. This method does not actually interpolate the velocity at the location of the particle, but rather at the location of the projection of the particle onto the line bisecting the cell in the direction of the velocity (Figure A2). Using the defined velocity field from Eq. (A.1), this method produces u = 3.29, v = 2.72. In this instance, the LA method over-predicts u, and under-predicts v.

The squares in Figure A2 represent the projection of the particle onto the bisecting centerlines of the grid cell. Velocities are interpolated at these locations. The linear interpolation method is suitable if the spatial velocity gradients in the domain are not strong, so that velocities at the middle of the grid cell are approximately equal to those velocities off the grid cell centerlines.

Interpolation with Bi-Linear Averaging (BLA)

The bi-linear Averaging (BLA) technique (Figure A3) attempts to improve upon the linear averaging (LA) interpolation scheme. It interpolates in both the principal directions (x,y) to obtain a velocity at the location of the particle rather than at the centerline of the grid cells. This method has been widely used in existing particle tracking schemes (e.g., Zhurbas and Oh, 2003).

In bilinear interpolation (Figure A3), three linear interpolations are performed for each velocity to be determined. When interpolating for the u-velocity, the first step is to perform the linear interpolation along the x-axis to estimate the velocity at the centerline of the

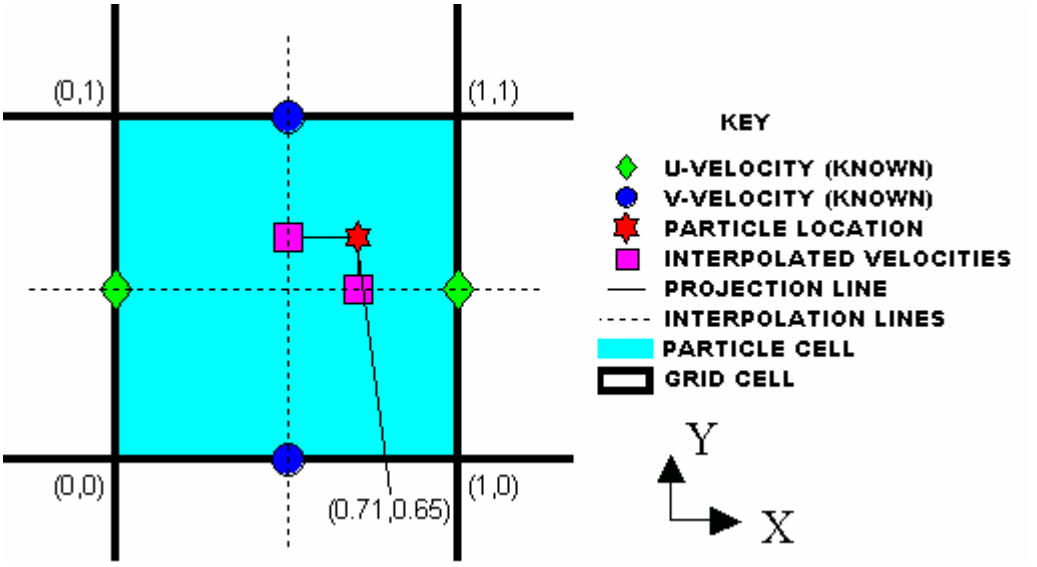

Figure A2 – Linear Interpolation of particle velocity at (0.71, 0.65)

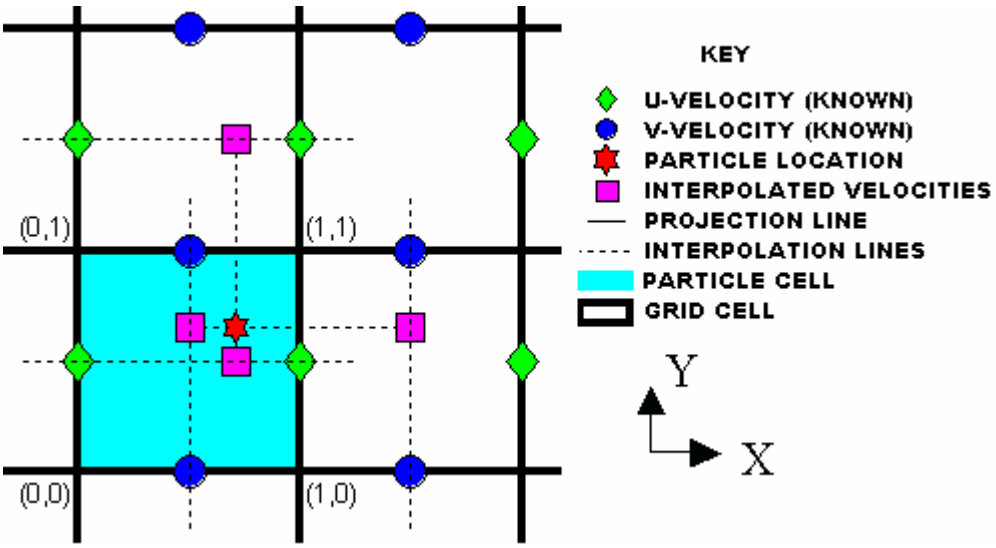

Figure A3 – Bilinear Averaging: Linear Averaging (LA) is applied in the particle cell and adjacent cells in the primary directions of the interpolation. The particle velocity is then interpolated by applying LA in the direction orthogonal to the previously interpolated velocities.

cell containing the particle. This step is referred to as interpolating in the "primary" direction, indicating that the interpolation is proceeding in the direction of the velocity specified in the interpolation (i.e., interpolating the **u**-velocity in the x-direction). The primary interpolation is repeated for the cell neighbor in the y-direction that is closest to the particle. The third interpolation is along the y-axis, using the values determined from the previous interpolations. This interpolation is referred to as "orthogonal" interpolation, indicating that the interpolation occurs in the direction perpendicular to the velocity interpolated (i.e., interpolating the u-velocity in the y-direction). This third (and final) interpolation yields a velocity interpolated to the particle location.

Using the velocities calculated from Eqn. (A.1), the BLA scheme predicts that u =1.98 and v = 4.76. These predicted velocities are improvements upon the LA predictions in that they are closer to the actual velocities. This form of interpolation is easy to implement, has a small interpolation stencil, and better represents spatial gradients than does the simpler LA technique.

Interpolation with Inverse Distance Weighting (IDW)

The Inverse Distance Weighting (IDW) method is a standard technique for interpolating randomly oriented data to a uniform structure (Shepard, 1968). IDW uses the distance between the known values and the interpolation location as a weighting parameter in assessing the influence of each known value on the interpolated result (Figure A4). The IDW formula used in this work is identical to that presented in Franke & Neilson (1980) and is used in the commercially available SMS software package (http://www.ems-i.com), given as:

$$\Phi(X,Y) = \sum_{i=1}^{n} w_i \Phi_i \qquad \text{(A.4)}$$

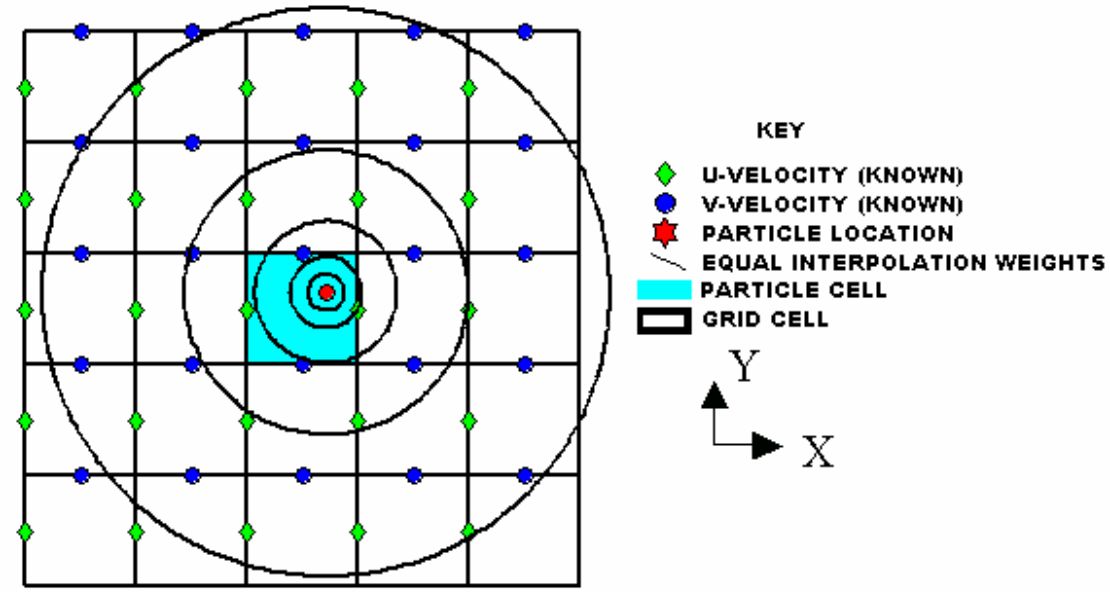

Figure A4 – IDW interpolation where weight is proportional to the distance from the particle (Circles show equal weight contours)

$$w_i = \frac{\left[\frac{R - h_i}{Rh_i}\right]^P}{\sum_{i=1}^{n}\left[\frac{R - h_i}{Rh_i}\right]^P} \quad (A.5)$$

$$h_i = \sqrt{(X_i - X)^2 + (Y_i - Y)^2} \quad (A.6)$$

$$R = \max(h_i) \quad (A.7)$$

where $\Phi(X,Y)$ is the velocity component (either **u** or **v**) to be interpolated to position (X,Y), and the **i**-subscript references one of the known velocity locations or values. The h_i terms are the shortest distances between the locations of the known velocities and the location of the velocity to be interpolated, and R is defined as the maximum of all of these terms. The parameter P determines the relative importance of the known values closer to the location of the value to be interpolated. In using this method in this work, the velocities in the 24 cells surrounding the drifter cell are considered. The user may select different values for P when attempting to determine which value produces the most accurate results. With this technique and P = 2, the predicted values of u and v at the drifter location are 3.19 and 4.23, respectively. The error in these predictions is due to the large gradients in the flow field over the 25 cells used in the interpolation and is likely to be reduced through use of higher values for P.

This IDW formulation provides more accurate results than Shepard's original (1968) IDW method if the known velocities are randomly oriented about the interpolation location (Franke & Neilson, 1980). Application on a uniform Arakawa-C grid, therefore, does not require the use of this method in favor of Shepard's. However, this method was employed in herein because of its widespread use in commercially available engineering and hydrology software packages, such as SMS and the GIS products produced by ESRI, Inc.

Interpolation with Directional Inverse Distance Weighting (DIDW)

The directional inverse-distance weighted (DIDW) technique is a modification of the IDW technique, similar to that proposed by Osting (2003). This method provides increased weight to the velocity locations either downstream or upstream of the particle location. In this approach, the approximate particle velocity is first estimated with the LA technique. Then the velocity locations upstream of the particle are defined, with the line of separation perpendicular to the estimated velocity vector. These upstream points are then given extra influence by a weighting factor W in Eqn.(A.5):

$$w_i = \frac{W\left[\frac{R - h_i}{Rh_i}\right]^P}{\sum_{i=1}^{n} W\left[\frac{R - h_i}{Rh_i}\right]^P} \quad (A.8)$$

The motivation behind this scheme is to simulate the fact that particles will be pushed by the water upstream of their location and will have momentum resulting from the upstream currents. The inclusion of weighting factor W provides a type of "Lagrangian Memory" to the interpolated velocity, as suggested as necessary by Addison (1997) when attempting to model field drifter movement. Implementation of this scheme results in weight contours that form half-circles on either side of the dividing line perpendicular to the LA velocity estimate (Figure A5). Using this scheme with W = 2 and P = 2, the predicted velocities at the particle location are: u = 3.85,, v = 2.71.

Interpolation with One Dimensional Quadratic Lagrange (1DQ)

The 5th scheme considered in this work is the one-dimensional Upwind Quadratic Lagrangian (1DQ) scheme. In this scheme, three velocities are used to generate a quadratic equation from which the value of the velocity at the particle location may be calculated (Figure A6). The 1DQ scheme is an upwind scheme in

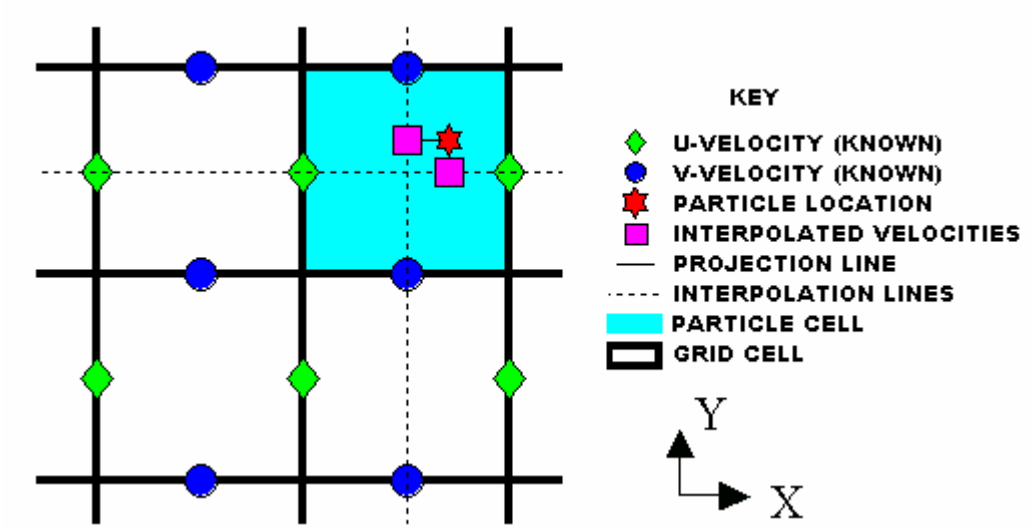

Figure A5 – 1DQ interpolation with the upstream direction estimated with the LA scheme.

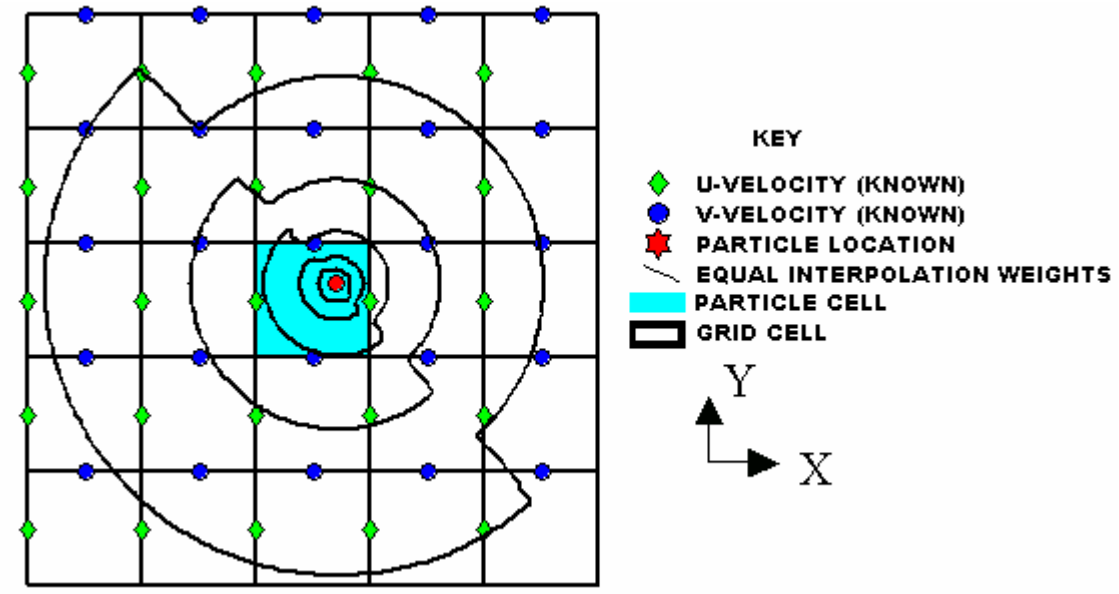

Figure A6 – DIDW interpolation – IDW interpolation with upstream velocities given greater weight than the downstream velocities. Arrow indicates velocity estimate from LA technique, used to determine upstream/downstream velocities. Contours emphasize greater weights located closer to particle position in the upstream direction.

that it uses two known velocities upstream and one velocity downstream of the particle location to form the interpolating stencil. As with the DIDW scheme, in considering flow direction the 1DQ scheme incorporates part of the "Lagrangian Memory" concept in estimating particle velocities.

The IDQ interpolation begins by using the LA scheme to estimate the upstream and downstream directions at the location of the particle. Once the upstream and downstream directions (and hence velocities) are known, the particle velocity $\overrightarrow{\Phi_p}$ is calculated as:

$$\overrightarrow{\Phi_p} = \frac{\Xi}{\Pi - \Gamma}\overrightarrow{\Phi_D} + \frac{(\Theta - \varsigma)}{\Pi - \Gamma}\overrightarrow{\Phi_U} + \frac{-\Omega}{\Pi - \Gamma}\overrightarrow{\Phi_{UU}} \qquad (A.9)$$

where the subscripts indicate the position of the velocity (D = downstream, U = upstream, UU = 2nd upstream, p = at the particle location), and

$$\Xi \equiv \frac{\left(X_U - X_p\right)^2}{\left(X_D - X_p\right)\left(X_U - X_p\right)^2 - \left(X_D - X_p\right)^2\left(X_U - X_p\right)} \qquad (A.10)$$

$$\Theta \equiv \frac{-\left(X_D - X_p\right)^2}{\left(X_D - X_p\right)\left(X_U - X_p\right)^2 - \left(X_D - X_p\right)^2\left(X_U - X_p\right)} \qquad (A.11)$$

$$\Gamma \equiv \frac{-\left[\left(X_U - X_p\right)^2 - \left(X_D - X_p\right)^2\right]}{\left(X_D - X_p\right)\left(X_U - X_p\right)^2 - \left(X_D - X_p\right)^2\left(X_U - X_p\right)} \qquad (A.12)$$

$$\Omega \equiv \frac{\left(X_U - X_p\right)^2}{\left(X_{UU} - X_p\right)\left(X_U - X_p\right)^2 - \left(X_U - X_p\right)\left(X_{UU} - X_p\right)^2} \qquad (A.13)$$

$$\varsigma \equiv \frac{-\left(X_{UU} - X_p\right)^2}{\left(X_{UU} - X_p\right)\left(X_U - X_p\right)^2 - \left(X_U - X_p\right)\left(X_{UU} - X_p\right)^2} \qquad (A.14)$$

$$\Pi \equiv \frac{-\left[\left(X_U - X_p\right)^2 - \left(X_{UU} - X_p\right)^2\right]}{\left(X_{UU} - X_p\right)\left(X_U - X_p\right)^2 - \left(X_U - X_p\right)\left(X_{UU} - X_p\right)^2} \qquad (A.15)$$

The X values in Eqs. (A.10)-(A.15) are measures of the position of the known velocities along the x-axis or y-axis for interpolating the **u** or **v** velocities, respectively. Using this scheme and velocities defined from Eqn. (A.1), the interpolated drifter velocities are: u = 3.23, v = 2.66.

The 1DQ scheme is similar to the LA scheme in that it does not predict the velocity at the particle location, but rather at the projection of the particle location along the cell centerline (squares in Figure A6). As such, this scheme does not take into account potential spatial gradients across the particle cell.

Interpolation with Two Dimensional Quadratic Lagrange (2DQ)

The 2DQ scheme implemented in this work for calculating Lagrangian particle velocities is a two dimensional application of quadratic interpolation one dimension (§6.1.5), similar to the quadratic interpolation used in solving the momentum transport equations in the hydrodynamic model ELCOM (Hodges et al, 2000). The difference in the scheme used in this work and in traditional quadratic Lagrangian interpolation lies in the flexibility of the scheme in selecting the upstream direction.

The 2-Dimensional Quadratic Lagrange (2DQ) interpolation scheme involves the application of the 1DQ scheme 4 times, using velocities calculated in 9 cells adjacent to (and including) the particle cell. Within each of the first three applications of the 1DQ scheme, three known velocities, each in the same row or column in the computational grid, are used in creating each interpolation polynomial. From these first 3 IDQ applications, three interpolated velocities are produced. These 3 velocities are then used in the 4th IDQ application, resulting in interpolated velocities at

the position of the particle. (Figure A7). This 4th interpolation occurs in a direction perpendicular to that of the first three 1DQ applications (Figure 3.4).

The application of the first three 1DQ schemes may occur in either the "primary" or "orthogonal" directions. "Primary" interpolation occurs in the direction of the velocity component to be interpolated; the u-velocity component interpolated in the x-direction. "Orthogonal" interpolation occurs in the direction perpendicular to the direction of the velocity component to be determined; the u-velocity component interpolated in the y-axis direction. In traditional numerical formulations of the 2DQ interpolation scheme (as in Hodges et al, 2000), the upwind direction is identical for each of the applications of the 1DQ technique. This constraint makes the choice of direction of the first applications of the 1DQ scheme irrelevant, because both primary and orthogonal interpolation produce identical results. For the 2DQ scheme presented here, the upwind direction is determined independently for each of the first three

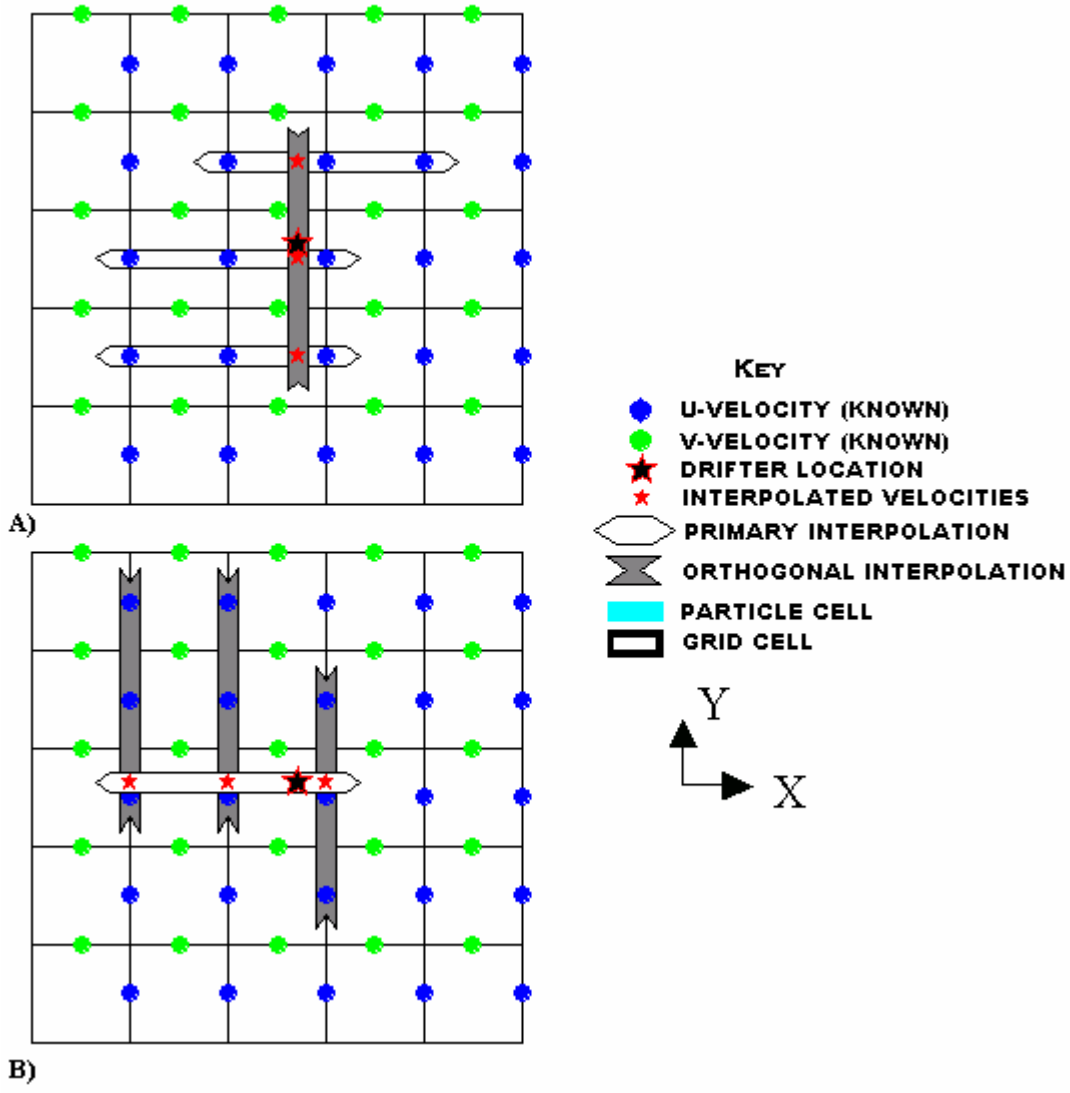

Figure A7 – 2DQ Interpolation – a) Primary Interpolation for u-velocity (2DQ1), b) Orthogonal interpolation for u-velocity (2DQ2).

1DQ applications based on the known velocities within the appropriate row or column of the computational grid. This relaxation of traditional 2DQ rules allows for a better representation of velocity gradients within the flow field in that the interpolated velocity is influenced to a greater extent by known velocities upstream of its position. The traditional approach allows for non-upwind velocities to influence the interpolated velocity if the spatial gradients within the velocity field are large relative to the computational grid size. The advantage of the 2DQ scheme presented in this dissertation is that it is better able to interpolate velocities when the velocity field contains large gradients relative to the grid size.

In primary (2DQ1) interpolation of the **u**-velocity (Figure A7a), the first row used is the row of cells containing the particle cell, where a row is defined as adjacent grid cells in the direction of the x-axis. The second and third rows are chosen to be upstream or downstream of the particle location, based on the **v**-velocity interpolated with the LA scheme. The 1DQ scheme is applied separately to the known **u** velocities in each of these rows, producing an interpolated velocity at the particle position in the x-direction of each of the rows. The final step is to apply the 1DQ scheme to these 3 interpolated velocities. This application occurs in the orthogonal direction, and produces an interpolated velocity at the exact location of the particle.

Figure A7b demonstrates orthogonal interpolation. In this approach, **u**-velocities aligned along the column boundaries are used in the 1DQ scheme to produce interpolated **u**-velocities at the y-position of the particle. Columns are defined as grid cells aligned along the y-axis. This interpolation is orthogonal because the **u**-velocities are being interpolated first along the y-axis. The final step is to use the 1DQ scheme in the primary direction with the interpolated velocities from the previous steps. This final 1DQ application produces an interpolated velocity at the exact location of the particle.

The 2DQ scheme has the ability to produce different interpolated velocities for the same position because it may use different sets of known velocities in the interpolation process. With the velocity field described by Eqn. (A.1) , the 2DQ1 and 2DQ2 schemes use different 9 known velocities in their interpolation (Figure A7). However, with velocity fields containing different spatial gradients than those implicit in Eqn. (A.1), the 2DQ1 and 2DQ2 schemes may use the same known values in their interpolation, and therefore produce the same interpolated velocity result. By re-defining the upstream/downstream relationship within each 1DQ application, the 2DQ method is more able to reflect the "Lagrangian memory" of a particle, as suggested as necessary by Addison (1997) when attempting to model field drifter movement.

Using the predefined analytical velocity field from Eqn. (A.1), the primary-direction 2DQ1 method predicts (**u,v)** = (1.69, 3.81), while the orthogonal-direction 2DQ2 method predicts (**u,v)** = (3.56, 4.61). Therefore, the direction of the interpolation clearly affects the outcome. The 2DQ1 scheme under-predicts the particle velocities, whereas the 2DQ2 over-predicts the **u**-velocity while only slightly under-predicting the **v**-velocity. A third method (2DQ3) is to use a weighted average of the velocities calculated by the primary and orthogonal interpolation schemes. Such an averaged result is likely to be more representative of the actual velocity at the particle location because it minimizes the bias derived from the interpolation directions. Giving each method an equal weight, the 2DQ3 method predicts (**u,v)** = (2.63,4.21), which is closer to the actual velocities than either the 2DQ1 or 2DQ2 results.

Spatial Interpolation Methods – Summary

The purpose of the preceding discussions of spatial interpolation schemes was to demonstrate how each scheme produces different results when applied to identical Eulerian velocity fields. While an exhaustive comparison between interpolation methods was not

conducted, the sample results presented in this section suggest that the bilinear averaging (BLA) and 2-D quadratic Lagrange interpolation schemes produce the most accurate results (Figure A8). As the 2DQ scheme incorporates more known velocities into its interpolation stencil, it was selected for use in this dissertation. The greater number of upstream known velocities provides a better "Lagrangian Memory" for the particle, which is required for drifter modeling (Addison, 1997).

Temporal Interpolation in Particle Tracking

With an Eulerian model velocities are defined at discrete times, and the velocity at one location can change from one time step to the next. In defining a representative particle velocity over a given time step, the Runga-Kutta 4th order (RK4) interpolation scheme has been found to reduce particle tracking errors when compared to the Euler Forward Step method, the Huen predictor-corrector method, the Robert filtered leapfrog method, and an Adams-Bashforth method (Ramsden and Holloway, 1991). The RK4 method is used in other drifter positioning programs (e.g., Chen et al, 2003) and is advantageous because it considers velocity gradients in space and time in order to produce a representative velocity.

To approximate the representative velocity, the RK4 integration scheme was applied to the known velocity fields at time steps n and n+1, separated in time by Δt. The basic RK4 algorithm is:

$$\vec{u}^{n+1/2} = \frac{1}{6}\left(k_1 + 2k_2 + 2k_3 + k_4\right) \quad \text{(A.16)}$$

$$k_1 = \vec{u}\left(t^n, \phi^n\right) \quad \text{(A.17)}$$

$$k_2 = \vec{u}\left(t^n + \frac{\Delta t}{2}, \phi^n + \frac{\Delta t}{2}k_1\right) \quad \text{(A.18)}$$

$$k_3 = \vec{u}\left(t^n + \frac{\Delta t}{2}, \phi^n + \frac{\Delta t}{2}k_2\right) \quad \text{(A.19)}$$

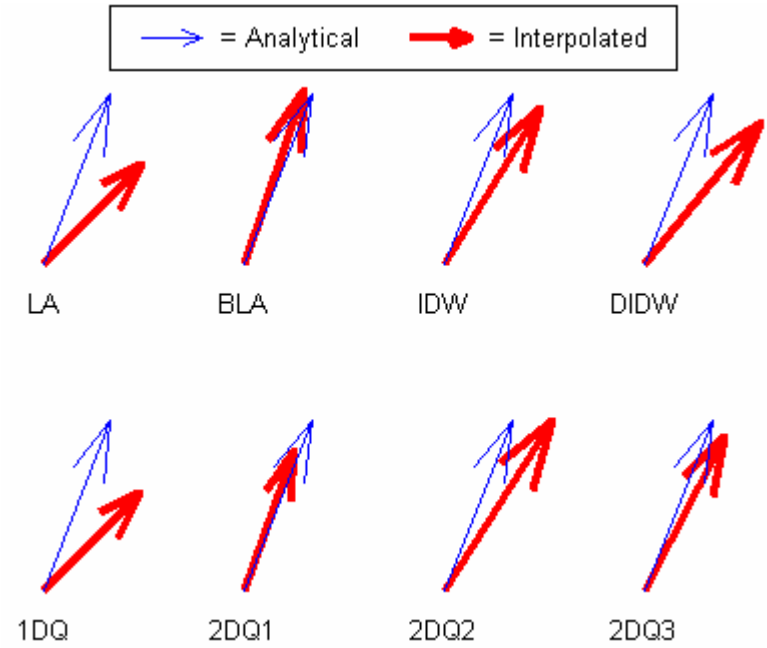

Figure A8 – Vector plot comparing interpolated velocities derived from each of the interpolation schemes considered in this work. The bilinear (BLA) and weighted 2-D quadratic Lagrange (2DQ3) produce the results most comparable to the analytical velocity.

$$k_4 = \vec{u}\left(t^{n+1}, \phi^n + \Delta t \cdot k_3\right) \qquad \text{(A.20)}$$

where ϕ is the position of the drifter and t is the time (Figure A9). The instantaneous value of velocities $\vec{u}^n$ and $\vec{u}^{n+1}$ at Eulerian grid points are calculated by the hydrodynamic model that approximates the function $\vec{u}(t,\varphi)$. Spatial interpolation is then needed to determine the velocity at the position ϕ based on the known velocities at the surrounding Eulerian grid points. An approximation of the velocity field at time $t^n + \Delta t/2$ is made by assuming a linear velocity change from the velocity fields calculated at t^n and t^{n+1}.

The effectiveness of the RK4 interpolation technique in capturing spatial gradients in the velocity field is demonstrated in Figure A10, where particle tracking using the RK4 scheme is presented within a tangential flow in a circular basin. Particles within this flow follow perfectly circular orbits, with their velocity proportional to the particle's distance from the basin center. This flow has constant spatial gradients in Cartesian coordinates, and if the spatial and temporal interpolation schemes overestimate the particle velocity, then the particle will artificially move onto a different orbit and experience an increase in speed.

Figure A10a demonstrates the inaccuracy of particle tracking using only the velocity at the particle's initial position over the entire timestep. This velocity (K1) would displace the particle off of its circular trajectory into a region of the flow with greater speed, forcing the particle to move off its correct trajectory. With the RK4 technique, this error in velocity (and therefore displacement error) is compensated for by the K2, K3, and K4 velocities, which are each calculated at intermediate locations along the particle's path as shown in Figure A10b-d. The summation of partial displacement vectors (Figure A10e,f) simulates the ever-changing velocity of the particle on the circular orbit, and allows the particle to be transported by different velocities over the model timestep. The final representative velocity yields a representative displacement which places the particle closer to its location along the circular trajectory than if the only K1 velocity were used in temporal interpolation.

Limitations to Temporal Interpolation Accuracy

Errors in temporal interpolation decrease as the spatial and temporal gradients in the flow field decrease. Smaller gradients reduce the possibility of the particle being displaced across flow streamlines, and smaller model time steps reduce the displacement error due to incorrectly interpolated velocities. In order to minimize the possibility of particle tracking error due to temporal

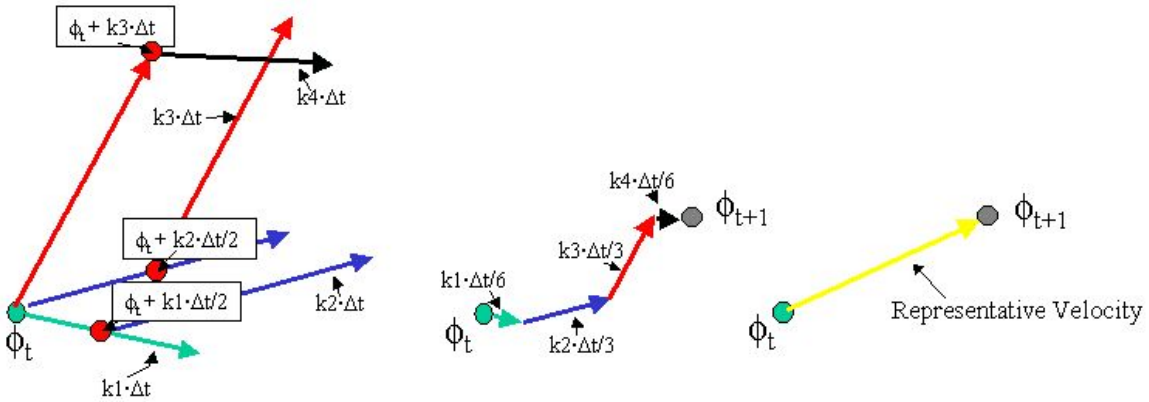

Figure A9 – Interpolating a representative velocity with RK4. Arrows are displacement vectors

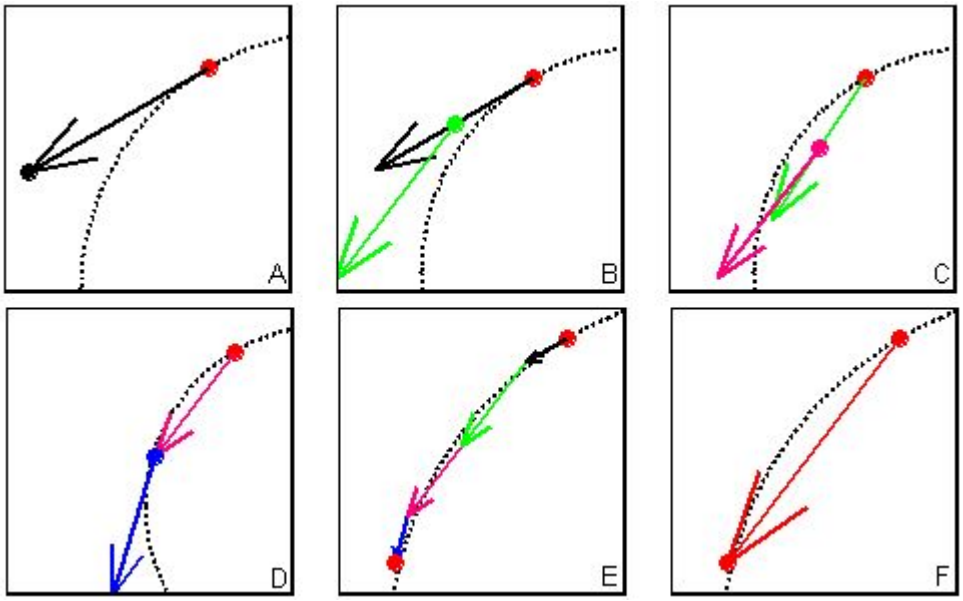

Figure A10 – Determining Displacement with the RK4 Method in a Tangential Flow Field. The particle (red dot) will travel in a circular path along the dotted line. A) Displacement due to K1 (Black Arrow), B) Displacement due to K2, C) Displacement due to K3, D) Displacement due to K4, E) Calculating the total displacement as the sum of the vectors, F) Total Displacement, with the particle nearly on its initial orbit.

interpolation, a time step limitation based on the model Courant-Fredricks-Levy (CFL) number is necessary (Eqn. (A.21)):

$$CFL_p \equiv \frac{u_P \Delta t}{\Delta x} \tag{A.21}$$

Within Eqn. (A.21), Δx is the model grid cell dimension (equivalent to the distance between adjacent calculated velocities), u_p is the speed of the particle within the flow, and Δt is the model timestep. The CFL_p value is therefore a measure of the number of grid cells through which a drifter particle may travel in any given time step. Larger CFL_p values mean the particle has the potential to experience greater variations in velocity over the time step, which will make interpolating the representative velocity less accurate. For this work, the maximum allowable CFL_p was 0.5, and in situations where the $CFL_p > 0.5$, sub-timesteps were used to reduce Δt until an acceptable CFL_p was obtained.

Appendix B:

Derivation of 3-level quadratic finite difference stencil

This appendix contains a mathematical derivation of the 3-level quadratic finite difference stencil used in the GABI-F drifter model (Eqns. (2.18)-(2.19)). The derivation involves using a quadratic equation to approximate drifter speeds at the current time based on known drifter speeds at two previous times (Figure B1):

In this derivation, the two known speeds occurred at times $-P\Delta T$ and $-Q\Delta T$ where P and Q are real numbers and ΔT is the model timestep. The derivation is presented in the general case for which P and Q may take on any value. The derivation is given as follows:

$$U_{drifter}(T) = aT^2 + bT + c \tag{B.1}$$

$$\frac{\partial U_{drifter}}{\partial T} = 2aT + b = b \quad \text{when } T = 0 \tag{B.2}$$

$$U(T=0) = c = U_{drifter} \tag{B.3}$$

$$\begin{aligned} U_{drifter}^{-1} &= a(-Q\Delta T)^2 + b(-Q\Delta T) + c \\ &= Q^2 a(\Delta T)^2 - Qb\Delta T + U_{drifter} \end{aligned} \tag{B.4}$$

$$\begin{aligned} U_{drifter}^{-2} &= a(-P\Delta T)^2 + b(-P\Delta T) + c \\ &= P^2 a(\Delta T)^2 - Pb\Delta T + U_{drifter} \end{aligned} \tag{B.5}$$

$$\begin{aligned} \Rightarrow Q^2 U_{drifter}^{-2} &= Q^2 P^2 a(\Delta T)^2 \\ &\quad - Q^2 Pb\Delta T + Q^2 U_{drifter} \end{aligned} \tag{B.6}$$

$$\begin{aligned} \Rightarrow P^2 U_{drifter}^{-1} &= P^2 Q^2 a(\Delta T)^2 \\ &\quad - P^2 Qb\Delta T + P^2 U_{drifter} \end{aligned} \tag{B.7}$$

$$\begin{aligned} \Rightarrow Q^2 U_{drifter}^{-2} - P^2 U_{drifter}^{-1} \\ = b\Delta T\left(P^2 Q - Q^2 P\right) + \left(Q^2 - P^2\right) U_{drifter} \end{aligned} \tag{B.8}$$

$$\Rightarrow b = \frac{Q^2 U_{drifter}^{-2} - P^2 U_{drifter}^{-1} - \left(Q^2 - P^2\right) U_{drifter}}{\Delta T\left(P^2 Q - Q^2 P\right)} \tag{B.9}$$

$$\begin{aligned} &\Rightarrow \frac{\partial U_{drifter}}{\partial T} \\ &= \frac{Q^2 U_{drifter}^{-2} - P^2 U_{drifter}^{-1} - \left(Q^2 - P^2\right) U_{drifter}}{\Delta T\left(P^2 Q - Q^2 P\right)} \end{aligned} \tag{B.10}$$

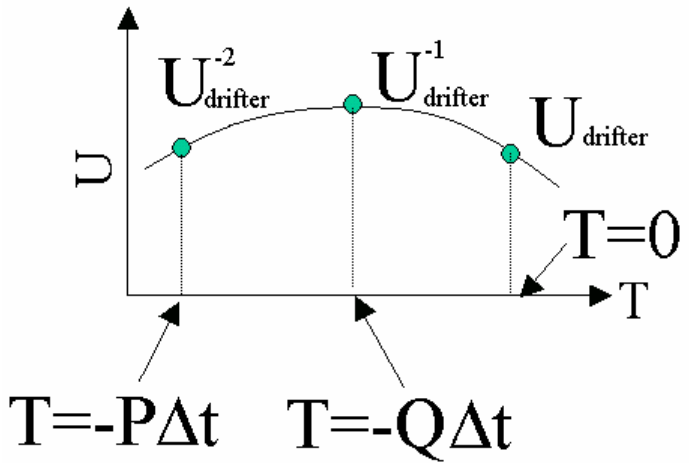

Figure B1 – Quadratic Approximation to temporal variations in drifter speed (U) using the speed at T = 0 (unknown) and speeds at two previous times (known).

Equation (B.10) is the general expression for the drifter acceleration at the current time (T=0). In the special case where the drifter speeds are calculated at each timestep and the timestep remains constant, Q = 1 and P = 2. Substituting these values into Eqn. (B.10) produces:

$$\Rightarrow \frac{\partial U_{drifter}}{\partial T} = \frac{U_{drifter}^{-2} - 4U_{drifter}^{-1} + 3U_{drifter}}{2\Delta T} \qquad \text{(B.11)}$$

which is identical to Eqn. (2.18) used in the GABI-F drifter model.

Appendix C:

Alternative GABI-F Solution methods

5.3.1. Introduction

This appendix contains descriptions of the alternative solution methods developed for the GABI-F drifter model as presented in section 2.5. Each alternative was never fully evaluated, and the method presented in section 2.5 was chosen as it best conformed to the theoretically important concepts of drifter and numerical modeling:

Higher-order methods will produce better results (but at high computational costs)

Drifter motion is controlled by the change in forcing with time.

For the following discussion, the GABI-F drifter model presented in Section 2.5 is referred to as the "existing" method. Each "alternative" method or method component presented in this section could be substituted for the corresponding existing method or method component. Further study is necessary to determine whether the existing method actually produces the best drifter model results.

The first alternatives to the existing method involve re-approximating the drifter acceleration term in Eq. (2.18). In a general sense, Eq. (2.18) may be re-written as:

$$\frac{\partial U_{drifter}}{\partial t} \approx \frac{R_1 U^n_{drifter} + R_2 U^{n-1}_{drifter} + R_3 U^{n-2}_{drifter}}{R_4 \Delta t} \quad \text{(C.1)}$$

where each R term is a coefficient with $R_1 + R_2 + R_3 = 1$ and $R_4 = 1$ or 2. The superscripts denote the time step, with the only unknown being the drifter velocity at time step n unknown. Substituting Eq. (C.1) into Eq. (2.9) yields:

$$R_4\lambda\Delta t\left(\vec{U}^n_{drifter}\right)^2 + \left(R_4\xi\Delta t - R_1\right)\left(\vec{U}^n_{drifter}\right) + R_4\varepsilon\Delta t - R_2 U^{n-1}_{drifter} - R_3 U^{n-2}_{drifter} = 0 \quad \text{(C.2)}$$

As with Eq. (2.19), Eq. (C.2) may not be solved using the quadratic formula because the coefficients λ, ξ, and ε are dependent upon $\vec{U}^n_{drifter}$. Each alternative GABI-F solution procedure incorporates differing methods for either defining the R_i values in Eq. (C.2) or for selecting the most appropriate drifter velocity out of numerous potential solutions to Eq. (C.2).

Approximation Methods for the Drifter Acceleration Term

Eq. (C.2) contains one unknown ($\vec{U}^n_{drifter}$) but also has unknown coefficients that are functions of $\vec{U}^n_{drifter}$ and the numerical approximation of the drifter acceleration (R_i coefficients). Three possible numerical approximations of acceleration were considered:

"SBE" – Simplified Backwards Euler (2nd order Accurate)

"CBE" – Complex Backwards Euler (2nd order Accurate)

"QPF" – Quadratic Polynomial Fitting (3rd order Accurate)

The backwards Euler scheme is generally given as:

$$\frac{du^n_{drifter,j}}{dt} = \frac{u^n_{drifter,j} - u^{n-1}_{drifter,j}}{\Delta t} \quad j = 1,2 \quad \text{(C.3)}$$

Substituting Eq. (C.3) into Eq. (2.9) produces:

$$\frac{u^n_{drifter,j} - u^{n-1}_{drifter,j}}{\Delta t} = \frac{\lambda_j}{m}\left(u^n_{drifter,j}\right)^2 + \frac{\xi_j}{m}\left(u^n_{drifter,j}\right) + \frac{\varepsilon_j}{m} \quad \text{(C.4)}$$
$$: \quad j = 1,2$$

The simplified Backwards Euler (SBE) scheme involves substituting $u^{n-1}_{drifter,j}$ into the right-hand side of Eq. (C.4), in place of $u^n_{drifter,j}$. This simplification is

reasonable when the drifter acceleration is small. With this simplification, $u^{n}_{drifter,j}$ is given as:

$$u^{n}_{drifter,j} = \frac{\lambda_j \Delta t}{m}\left(u^{n-1}_{drifter,j}\right)^2 + \left(\frac{\xi_j \Delta t}{m} + 1\right)\left(u^{n-1}_{drifter,j}\right) + \frac{\varepsilon_j \Delta t}{m} \quad : \quad j = 1,2 \tag{C.5}$$

This method produces a single value for $u^{n}_{drifter,j}$, which is calculable when coefficients λ, ξ, and ε are known. These drifter coefficients are determined from Eqns. (2.6) and (2.10)-(2.15) when $u^{n-1}_{drifter,j}$ is substituted for $u^{n}_{drifter,j}$.

The Complex Backwards Euler (CBE) scheme is derived by substituting Eqn. (C.3) directly into Eq. (2.9), yielding:

$$\frac{\lambda_j \Delta t}{m}\left(u^{n}_{drifter,j}\right)^2 + \left(\frac{\xi_j \Delta t}{m} - 1\right)\left(u^{n}_{drifter,j}\right) + \frac{\varepsilon_j \Delta t}{m} + u^{n-1}_{drifter,j} = 0 \quad : \quad j = 1,2 \tag{C.6}$$

With known coefficients λ, ξ, and ε, this scheme produces 0, 1 or 2 potential values for $u^{n}_{drifter,j}$. If 2 valid values are produced, selection criteria must be applied to select the appropriate drifter velocity. Alternatively, if 0 valid answers are produced, the coefficients λ, ξ, and ε must be re-determined.

The third method for approximating the drifter acceleration, namely the Quadratic Polynomial Fitting (QPF) method, was described fully in section 2.4 and was used in all GABI-F drifter modeling discussed in Chapter 4. Testing the GABI-F drifter model behavior using each of these three acceleration approximation methods provided insight into each method's applicability.

The SBE method, although simple, is favorable in that it produces a single value for the drifter velocity. It is a first order explicit numerical scheme, for which numerical approximation errors are expected to decrease linearly with decreasing model time step size. This method may become numerically unstable if the drifter velocity is too high or the model time step is too small. Method stability is often assured by requiring that the $CFL_{drifter}$ (See Eqn. (A.21)) be less than 1, although < 0.5 is preferable. The method also does not fully consider the influence of changing conditions within the water column from one time-step to the next. By using $u^{n-1}_{drifter,j}$ instead of $u^{n}_{drifter,j}$ in the right-hand side of Eqn. (C.4), the drifter velocity is largely influenced by water column conditions from the previous time step. The wind and water velocities at the current timestep may be substantially different from their past conditions if the modeled system is highly dynamic. The SBE approximation is not likely to produce stable or valid results in highly dynamic flows.

The CBE approximation, while still first-order accurate, is likely more appropriate than the SBE scheme because it is numerically stable for all $CFL_{drifter}$ drifter conditions. In further comparison with the SBE method, past environmental conditions are not as influential on the present drifter velocity because the CBE scheme only involves $u^{n-1}_{drifter,j}$ in one of the four terms in the Eqn. (C.6). The drawback of this method, however, is that it has the potential to produce multiple, mathematically valid values for the drifter velocity, and therefore requires the use of velocity selection criteria. This makes the method more computationally expensive (in terms of CPU time) than the SBE method, and model accuracy may decrease if inappropriate selection criteria are used.

The QPF method was expected to produce superior results than the SBE and CBE methods. Being second-order accurate, the method accuracy is to decrease with the square of the timestep decrease, thereby providing greater accuracy at smaller time steps. By incorporating drifter velocities from the previous two time steps into the solution for $u^{n}_{drifter,j}$, the "Lagrangian Memory" of the drifter is better represented; the temporal effects of drifter inertia are

given greater influence on the drifter velocity. This method is also unconditionally stable at all $CFL_{drifter}$ values, and like the CBE scheme places greater emphasis on present water column conditions in its solution. The method is more computationally expensive than both the SBE and CBE methods, however the greater accuracy is likely to make the method more appropriate for accurate and efficient particle tracking.

Estimation Methods for Drifter Coefficients

Solution of the GABI-F equations for drifter motion require defined values of the coefficients λ, ξ, and ε. These coefficients are determined from known properties of the drifter and the surrounding fluid (Eqns. (2.10)-(2.15)), and the unknown difference in velocity between the drifter and the surrounding fluid (Eq. (2.6)). However the term $\beta_{j,i}$ in Eq. (2.6) may take on only the values of ± 1, which limits the potential error in assuming values for this term. Two methods of estimating the value of $\beta_{j,i}$ (which is dependant upon the unknown value of $u^n_{drifter,j}$) were considered:

1. *"Steady-State" – Approximating* $u^n_{drifter,j}$ *with* $u^{n-1}_{drifter,j}$, *and*

2. *"All-Possible" - Using all possible combinations of signs on the* $\beta_{j,i}$ *terms making up the coefficients* λ, ξ, *and* ε.

The "Steady-State" method is the default method when using the SBE scheme for approximating drifter acceleration. With the CBE and QPF acceleration approximations, either the "Steady-State" or the "All-Possible" method potentially produces multiple numerically valid results for $u^n_{drifter,j}$. Use of these methods therefore requires that a selection criterion be applied.

With the "Steady-State" method, $\beta_{j,i}$ is determined assuming that the velocity difference between the water and the drifter is relatively constant in time. This steadiness, however, is not assured by the numerical methods for producing the drifter representative velocity. Upon solving for $\beta_{j,i}$ and applying one of the drifter acceleration methods, the calculated value for $u^n_{drifter,j}$ may be inconsistent with the "Steady-State" method. It must be used in Eq. (2.6) to produce new values for $\beta_{j,i}$, which must be identical to those used in calculating $u^n_{drifter,j}$ for the solution to be valid. If the calculated $u^n_{drifter,j}$ is invalid, then the solution procedure is repeated in an iterative manner, with the new $\beta_{j,i}$ values used to calculate a new $u^n_{drifter,j}$. This process continues until consistency is achieved between $u^n_{drifter,j}$ and the 5 values for $\beta_{j,i}$. This iterative process is more likely to be needed in highly stratified water columns, where significant horizontal velocity variation exists over the length of the drifter.

The "All-Possible" method is a variation on the iteration required in the "Steady-State" method in that it considers all possible combinations of values for $\beta_{j,i}$ in producing a representative velocity. This method was discussed in section 2.4.3 and was used for all GABI-F drifter modeling discussed in Chapter 4. The "All-Possible" method is more computationally expensive than the "Steady-State" method, but it may prove more accurate because it is not dependant upon the drifter velocity and water column conditions from the previous time step. For steady-flows, both methods are likely to produce the same results. However, for dynamic flows where changes in water column conditions are large over single model time-steps, the "All-Possible" method is likely superior. One drawback of both these methods is that their accuracy is dependant upon the selection criterion used in determining $u^n_{drifter,j}$, and it is probable that different selection criteria would favor one $\beta_{j,i}$ estimation method over another.

Drifter Velocity Selection Criteria

With the exception of the SBE scheme, each method for solving the drifter force balance equations has the potential to produce multiple, mathematically valid solutions for $u^n_{drifter,j}$. In selecting the most appropriate drifter velocity, the following five selection criteria were considered:

1. *"Max-Fluid" - using the value for* $u^n_{drifter,j}$ *that is closest to the calculated value* $u^n_{fluid-max,j}$, *where* $u^n_{fluid-max,j}$ *is the fluid velocity around the drifter section to which the greatest force is applied*

2. *"Equal Acceleration" - Using the value for* $u^n_{drifter,j}$ *which causes* $\frac{\partial u^n_{drifter,j}}{\partial t} \approx \frac{\partial u^n_{fluid-max,j}}{\partial t}$

3. *"Averaged Values" - Using an arithmetic mean of all possible solutions for* $u^n_{drifter,j}$.

4. *"Limited Acceleration" - Using the value for* $u^n_{drifter,j}$ *which causes* $\frac{\partial u^n_{drifter,j}}{\partial t} \approx \frac{\partial u^n_{fluid-max,j}}{\partial t}$ *such that* $\left|\frac{\partial u^n_{drifter,j}}{\partial t}\right| < \left|\frac{\partial u^n_{fluid-max,j}}{\partial t}\right|$, *and*

5. *"Absolute Averages" - Using an arithmetic mean of all possible solutions for* $\left|u^n_{drifter,j}\right|$ *with the direction of the drifter equal to the direction specified by.* $u^n_{fluid-max,j}$

These criteria allow the drifter to move independently of the surrounding fluid, but force the drifter to accelerate in the direction of the water acceleration and with approximately the same magnitude acceleration. An added benefit to modeling surface tethered drifters in these ways is that the affects of the wind on the surface float are considered. This is similar to the approach of Su (1991) in modeling the movement of spheres floating on the water surface, and is the first attempt at modeling GABI-F drifters in this manner.

While both water particles and field drifters are going to follow the fluid currents, drifters are likely to react more slowly to changes in fluid velocities. The five selection criteria investigated for use in GABI-F drifter movement attempt to reproduce this characteristic of field drifters. The following paragraphs describe the purpose for including each of the listed criteria for use in this study.

The "Max-Fluid" method recognizes that the drifter will be most affected by the fluid surrounding the drifter section to which the greatest force is applied. For drifters considered in this dissertation, the drogue section receives the greatest force. However, the GABI-F drifter methodology is sufficiently flexible to model the affects of surface sails or drifters with geometries other than that depicted in Figure 2.2, and therefore the drogue section nay not always be the section acted upon by $u^n_{fluid-max,j}$. With this criterion, the drifter is not constrained to move in the same direction as the fluid currents, and is not limited to speeds less than the prevailing currents. The drifter may move faster than $u^n_{fluid-max,j}$ if the forces on the other four drifter sections are sufficiently large and aligned in the same direction as the prevailing current. This situation is likely to occur if the drifter has a large surface float and antennae that are acted upon directly by the surface winds.

The "Equal-Acceleration" method forces the drifter to accelerate in manner comparable to that of water particles acting upon the drifter section receiving the greatest force. This method stresses that changes in the fluid velocities surrounding the drifter will affect the forces applied to the drifter, and therefore control the drifter's velocity. As with the "Max-Force" method, the drifter is allowed to accelerate faster or slower than the prevailing current, which allows the

surface winds and water column velocity stratification to influence the drifter velocity.

The "Averaged-Values" method is a simple method that assumes all of the potential drifter velocities are valid with each equally likely to be the true drifter velocity. This method is highly efficient in terms of computational time, but the averaging approach does not incorporate "Lagrangian Memory" or flow physics into the force balance solution procedure. This method was included to determine the necessity of complex criteria in estimating representative drifter velocities, and it was not expected to produce superior results.

The "Limited Acceleration" method is identical to the "Equal Acceleration" method except that the drifter is constrained to accelerate more slowly than the prevailing currents. This method stresses the importance of inertia on the movement of the field drifter, and limits the drifter's ability to move faster than $\overline{U}^{n}_{fluid-max}$. As this method was expected to produce the most accurate drifter velocities, it was used in all of the GABI-F drifter modeling presented in Chapter 4.

The "Absolute Averages" method is a variation of the "Averaged-Values" method, with the drifter's speed determined through absolute-value averaging but its direction equal to that of the prevailing current. This method is a likely improvement on the "Averaged-Values method because the drifter's direction is determined based on the physics behind fluid movement about the drifter. The averaging of the velocities is an attempt at recognizing that all methods are likely to produce slight errors in the drifter speed, and that these errors may cancel out through the averaging process.

With the possible exception of the "Averaged-Values" method, each of the criteria considered in this research will cause the modeled drifter to reach an equilibrium velocity in constant, uniform flows (*ff.* 6.6). The rate at which this equilibrium is established is one factor considered in determining which criteria is superior for use in SPLT. This rate, however, also depends upon the method of introducing the numerical drifter into the modeled flow field.

Drifter Deployment/Start-up Options

Each of the three methods for approximating the drifter acceleration (SBE,CBE, and QPF) involves knowledge of the drifter velocity at the previous model time step. Therefore inaccuracies in drifter velocity at previous time steps may be carried forward in time within the numerical solution procedure, and may lead to erroneous drifter trajectories and model results. Minimization of this error propagation in time requires careful consideration of the drifter velocity at the moment the simulation begins.

Immediately after deployment, a field drifter has a negligible velocity, and the forces acting upon it are greatest. The drifter accelerates in the direction of the surrounding fluid(s) motion, and the forces causing the acceleration diminish as the drifter's velocity approaches that of the prevailing currents. The time required for the drifter to reach equilibrium with the surrounding currents is an unknown function of the current's temporal fluctuation, the properties (drag, inertia) of the drifter, and the magnitude of the initial velocity difference between the drifter and current. To adequately model the movement of field drifters, then, the numerical drifter model must operate on a timescale comparable to the initial "set-up" time required to set the field drifter in motion with the prevailing current. Three initial conditions were considered in simulating the field drifter set-up time:

1. *"Zero Initial" - Deploying the numerical drifters as if they were initially at rest, and letting them equilibrate with the surrounding currents over multiple numerical model time steps*

2. *"Ramp Up" - Deploying the numerical drifters as if they were initially at rest, and applying the force balance technique over*

multiple model sub-time steps so that set-up occurs within a full single model time step

3. "Initial Current" - Deploying the numerical drifters as if they were initially moving with the prevailing currents (at $u^{n}_{fluid-max,j}$), thereby forcing the numerical drifter to decelerate to reach equilibrium.

These three methods differ in the amount of time required for the drifter to reach equilibrium with steady currents. The zero-initial method assumes the drifter requires forces from several model time steps in order to reach equilibrium. This situation is preferable if the model time step is short relative to the time required to "set-up" the field drifter. In contrast, the "Ramp-up" method assumes that the field drifter "set-up" time is shorter than a single model time step. By using sub-

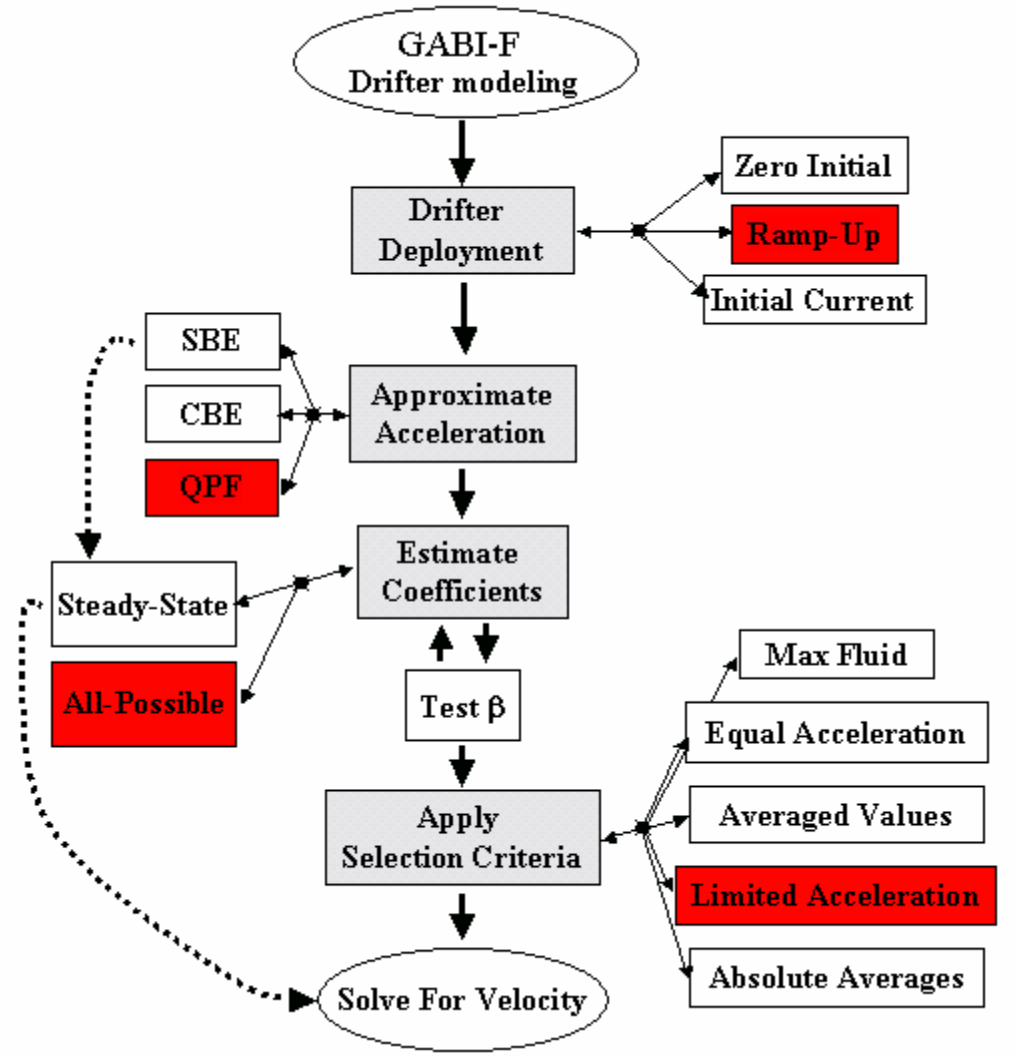

Figure C1 – Flow Diagram For determining drifter movement using the GABI-F drifter model. The four main solution steps are shown in gray, with their associated procedures off to the sides. Each solution method makes use of one of the procedures associated with each main step. Arrows indicate the sequence of the numerical solution procedure, with the dashed arrow distinguishing the SBE based scheme from those involving the CBE and QPF acceleration approximations. Red entries indicate those methods used in creating the results presented in Chapter 4.

time steps, this method subjects the drifter to a series of changing water column forces, and mimics the instantaneous forces applied to field drifters. This method is likely to provide the greatest accuracy if the fluid currents are dynamic on timescales shorter than the modeled time step. Finally, the "initial current" method uses a different approach to modeling the drifter deployment. By forcing the numerical drifter to initially move with the prevailing current, drag and inertia cause the drifter to decelerate over time. This method is better referred to as "set-down" rather than "set-up" because the modeled drifter initially has a speed greater than what it is likely to maintain due to the forces acting upon it. This method is not expected to produce superior results because it does not fully reflect the physical forces acting on the initially deployed field drifter.

All of the GABI-F drifter results presented in Chapter 4 were developed using the "Ramp-up" method.

GABI-F Drifter Simulation – Summary

This appendix presented possible variations to the GABI-F drifter method presented in Section 2.4. The GABI-F solution procedure (Figure C1) consists of four main sequential steps: 1) drifter deployment, 2) acceleration approximation, 3) coefficient estimation, and 4) velocity selection. With numerous methods proposed for mathematically describing each of the four solution steps, a total of 63 different GABI-F drifter procedures are possible. The determination of the relative merits of each solution option for the GABI-F particle tracking method should be included in further projects using the GABI-F drifter model.

Appendix D:

Effects of ELCOM Surface Thermodynamics

To assess the effects of surface thermodynamics on the modeled GABI-F drifter motion, 2 simulations were conducted for the D4 drifter deployment (§3.6.6). The first simulation was run using the surface thermodynamics subroutines within the ELCOM model, forced with the meteorological data collected with the LDS unit (§3.4.5). The second simulation was identical to the first except that it was conducted with the ELCOM surface thermodynamics subroutines turned off. Results from each of these simulations were compared using spaghetti diagrams, and the differences were indistinguishable with the naked eye. The maximum separation between drifters transported with and without the ELCOM surface thermodynamics subroutines was determined to be approximately 4m over nearly 9 hours of drifter deployment (Figure D1).

Based on the results presented in Figure D1, surface thermodynamics were considered to play a negligible role in determining the GABI-F drifter motion. All simulation results presented in Chapter 4 were derived from simulations using the surface thermodynamics subroutines, as their inclusion does not greatly diminish the duration of the ELCOM model runs. It should be noted that the water temperatures calculated by the ELCOM model were never checked against those measured in Marmion Marine Park during the field experiment.

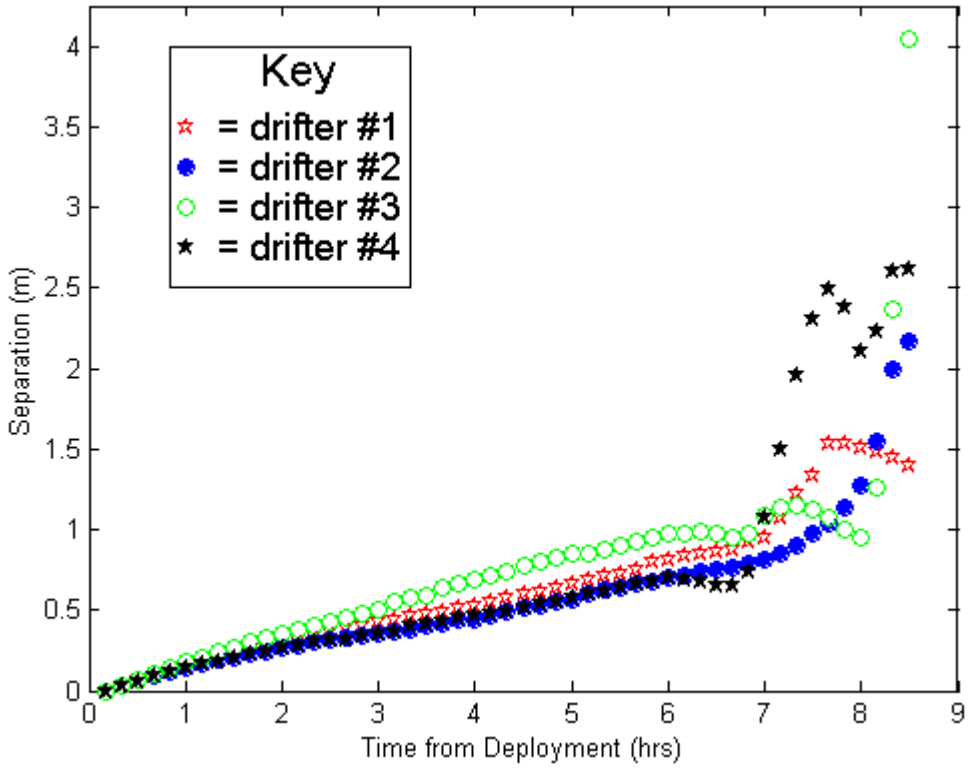

Figure D1 – Separation between drifters modeled with and without meteorological forcing implemented in ELCOM. Data from the D4 (March 26) simulations using the LDS winds and the northern tidal gradient.

Appendix E:

Verifying the ELCOM GABI-F Drifter Algorithm

The numerical implementation of the GABI-F drifter algorithm within the 3D hydrodynamic model ELCOM was verified by comparing results with those calculated within a Microsoft Excel spreadsheet. In both the ELCOM code and within the spreadsheet, drifters were placed in a uniform and constant flow field (U = 20 cm/s) with a constant wind forcing of 5 m/s in the same direction as the water flow. Table E1 contains the results from the ELCOM model and the spreadsheet.

As shown in Table E1, the ELCOM model and Microsoft Excel spreadsheet produce identical drifter velocities. The differences between the two results (ranging from 10^{-5} to 10^{-9} m/s) are outside of the numerical precision bounds set within the ELCOM model. Therefore the differences are not caused by errors in the GABI-F drifter model, but rather by differences in the number of digits afforded to each drifter speed by each tool (ELCOM or Excel). Based on this simple comparison, it was concluded that the GABI-F drifter algorithm is accurate. Comparisons between ELCOM and Excel under more complex forcing conditions (e.g., vertical stratification in water velocity) were not conducted

.

Table E1 – GABI-F Model Verification with data from Microsoft™ Excel

Timestep	ELCOM	Excel	Difference	Timestep	ELCOM	Excel	Difference
1	0.102849	0.102849	0.0000000	22	0.207138	0.207141	0.0000034
2	0.157419	0.157419	0.0000000	23	0.207265	0.207268	0.0000027
3	0.180414	0.180414	0.0000000	24	0.207366	0.207368	0.0000021
4	0.189846	0.189846	0.0000000	25	0.207445	0.207446	0.0000016
5	0.194025	0.194025	0.0000000	26	0.207506	0.207508	0.0000013
6	0.196221	0.196221	0.0000000	27	0.207554	0.207555	0.0000010
7	0.19766	0.19766	0.0000000	28	0.207592	0.207592	0.0000008
8	0.198803	0.198803	0.0000000	29	0.207621	0.207621	0.0000006
9	0.199832	0.199832	0.0000000	30	0.207643	0.207644	0.0000005
10	0.200814	0.200829	0.0000146	31	0.207661	0.207661	0.0000004
11	0.201755	0.201774	0.0000188	32	0.207674	0.207674	0.0000003
12	0.20264	0.202659	0.0000190	33	0.207685	0.207685	0.0000002
13	0.203453	0.20347	0.0000178	34	0.207693	0.207693	0.0000002
14	0.20418	0.204196	0.0000159	35	0.207699	0.207699	0.0000001
15	0.204818	0.204831	0.0000139	36	0.207704	0.207704	0.0000001
16	0.205364	0.205376	0.0000118	37	0.207707	0.207708	0.0000001
17	0.205825	0.205835	0.0000099	38	0.20771	0.20771	0.0000001
18	0.206207	0.206215	0.0000081	39	0.207713	0.207713	0.0000000
19	0.20652	0.206526	0.0000066	40	0.207714	0.207714	0.0000000
20	0.206773	0.206778	0.0000053	41	0.207716	0.207716	0.0000000
21	0.206976	0.20698	0.0000042	42	0.207717	0.207717	0.0000000

*** Data shown are velocities with units of m/s.

Appendix F:

Effects of Drag Coefficients on GABI-F Drifter Paths

As discussed in section 2.4 and section 5.3, the GABI-F drifter model requires specification of drag coefficients (c_d) for each drifter section. These coefficients must be provided as input by the ELCOM model user, and for this work the coefficients were assumed to be unity. This assumption was made based on work presented by Kundu and Cohen (2002). To discern effects of the drag coefficients on model-predicted drifter paths, comparative simulations using an Excel spreadsheet (Appendix E) were setup. The wind and water speeds within the Excel setup were 5 m/s and 0.2 cm/s. Results of one such comparison are presented in Figure F1 below.

Two key insights may be derived from Figure F1:

1 GABI-F drifters modeled in constant uniform flows will eventually achieve speeds in equilibrium with the surrounding fluids, and

2. the drag coefficients used in the GABI-F drifter model control the time required for the drifter to reach equilibrium.

For the example shown, the equilibrium drifter speed is 20.0772 cm/s, and this speed is achieved after timesteps 13, 16, and 49 for simulations using drag coefficients of 1.5, 1.0, and 0.3, respectively. The inverse relationship between drag coefficient and time required to reach equilibrium indicates that simulations with lower drag coefficients will not respond as quickly to changes in velocity of the surrounding fluids. Therefore correctly determining the drag coefficient for each drifter simulated is necessary for modeling the drifter's movement.

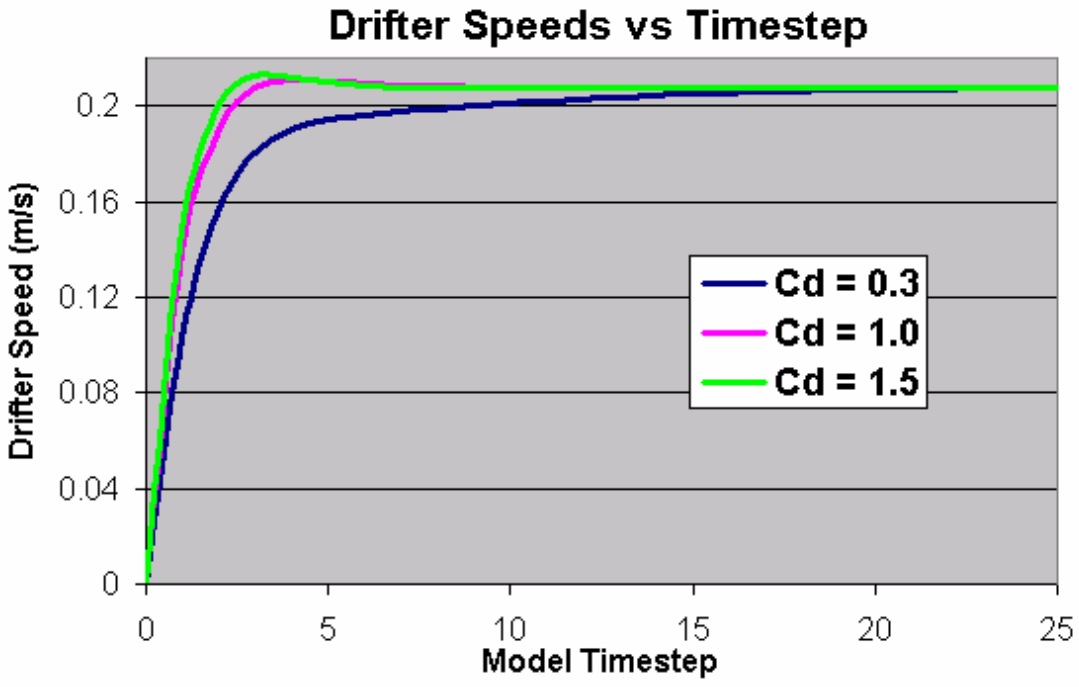

Figure F1 – GABI-F drifter speeds with variable drag coefficients. All model scenarios produce identical equilibrium velocities after sufficient timesteps. Lower drag coefficients require a greater number of timesteps to reach equilibrium.

Another interesting feature of the GABI-F method as shown in Figure F1 is that the model drifter reaches an equilibrium speed which is greater than the 20 cm/s speed of the surrounding water surrounding. The faster drifter speed than water speed occurs because the 5 m/s wind on the antennae and above surface buoy of the drifter provides enough forcing to push the drifter faster than the surrounding water currents.

Appendix G:

Drifter path sensitivity to alternative leeway factors

According to Thompson et al (2003), the leeway factor depends on the characteristics of the above-surface portions of the field drifter, and typical leeway factors are 0.036 for a life raft, 0.008 for a shallow-draft drifter with a short mast, and 0.0 for a completely submerged drogue. The drifters used in this work had very small above-surface components, and are likely to be closer to completely submerged drogues than to shallow draft drifters. Therefore based on Thompson et al (2003) and the characteristics of the drifters used in this work, suitable leeway factors should be less than 0.008. To determine the sensitivity of the model drifter results to variations in leeway factors, six simulations of the D2 deployment were conducted. For each simulation, drifters were modeled using the leeway method and a different leeway factor ranging from 0.001 to 0.008 (Figure G1). The spaghetti diagram results suggest that the field drifter movement is reasonably well reproduced with leeway factors between 0.001 and 0.004. Circle assessment results suggested that modeling with a leeway factor of 0.001 is successful for nearly 30% of all drifter timesteps (from the D2 simulation). However, as the leeway factor increases to 0.002, 0.003, and 0.004, the success probability decreases to 23%, 21% and 16%, respectively. This decease in success is attributed to the fact that higher leeway factors tend to cause the model drifters to travel with higher velocities, resulting in more speed-related model failures. As a result of the Circle assessment results, leeway drifter model results presented in Chapter 4 were all derived using a 0.001 leeway factor.

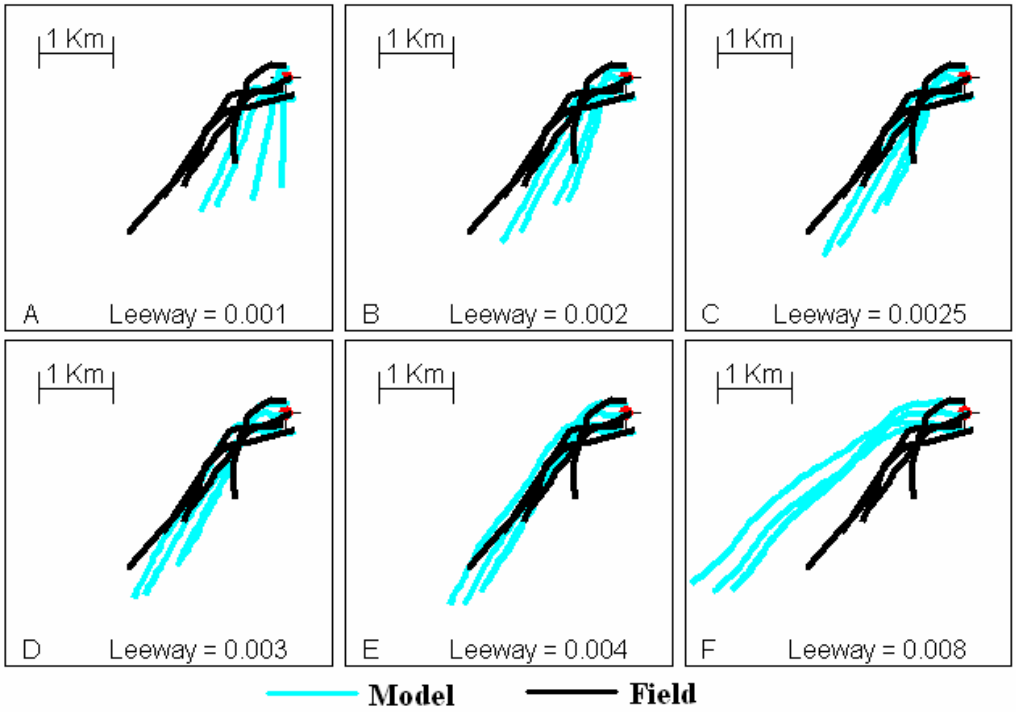

Figure G1 – D2 Simulation results using the leeway drifter model and leeway factors ranging from 0.001-0.008.

Appendix H:

Drifter paths derived with alternative mixing models

As discussed in Section 4.3, the ELCOM mixing model likely contributes the largest amount of error to the modeled drifter paths. This conclusion was based upon simulations using the current ELCOM mixing model described in Simanjuntak and Imberger (2006). Previous mixing models, like that used in Laval et al (2002) and Hodges et al (2000), involve alternative numerical approximations of mixing theory, and may therefore produce some benefits for use in drifter modeling. Figure H1 details the spaghetti diagrams created for each of the 5 drifter deployments using the present mixing model and that from Laval et al (2002). For the following discussion, ELCOM using with mixing model from Simanjuntak and Imberger (2006) is refered to as the "ELCOM-SI" model, and ELCOM using the Laval et al (2002) mixing model is referred to as the "ELCOM-L" model.

As shown in Figure H1, the spaghetti diagram plots suggest that the ELCOM-SI causes the model drifters to travel more slowly (and displace less distance) than the ELCOM-L model, especially during the D2 and D4 simulations. During the D2 and D4 simulations, the ELCOM-L model vastly over-predicts drifter speeds, causing model drifter displacements up to 2 km greater than the model drifters from the ELCOM-SI model and up to 3-4 km greater than the field drifter displacement. In section 3.4.4 and 4.3.2 it was reported that the winds during the D2 and D4 drifter deployments were the strongest winds observed over the course of the field experiment. This suggests that the ELCOM-L model does not perform well in high wind-speed conditions relative to the ELCOM-SI model. In contrast, winds during the D5 simulation were generally light and variable, and the ELCOM-L model was more successful at predicting D5 drifter transport than was the ELCOM-SI model. Results from both models were similar for the D1 and D3 drifter simulations.

Based on the drifter results presented in Figure H1 and Section 4.3.5, it is likely that improved drifter modeling will be achieved through an in-depth analysis of the vertical mixing model(s) used within ELCOM. Such an analysis was outside the scope of the research presented herein, but remains a point of consideration for future attempts at modeling drifter movement within Marmion Marine Park. The timestep dependence identified in section 4.3.5 is also apparent in the modeled drifter paths computed in ELCOM simulations of circulation within Lake Kinneret, Israel (Appendix J). This suggests that the open boundary conditions used in modeling Marmion Marine Park may not exert much influence on the drifter movement (Lake Kinneret is a land-locked lake modeled without open boundaries). The influence of the open boundary conditions on model drifter movement should also be investigated, however the improving the vertical mixing model should the first hurdle in any future work on this issue (at least if ELCOM remains the hydrodynamic model of choice).

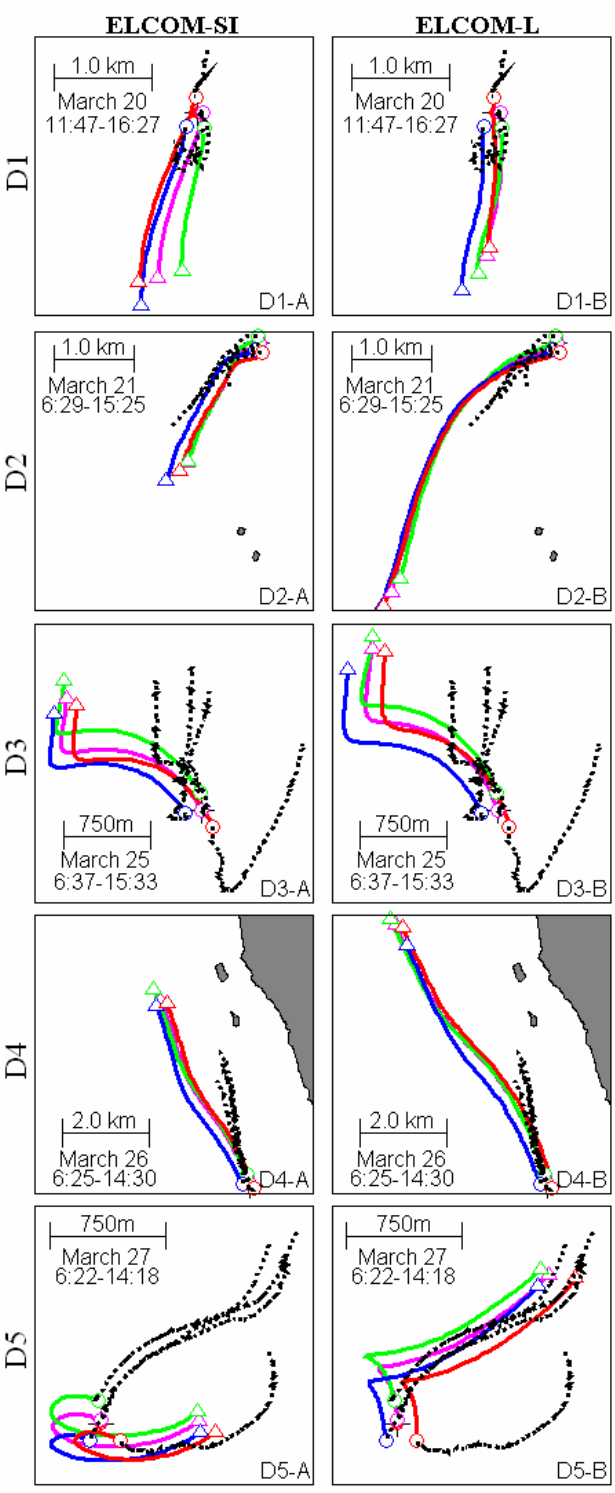

Figure H1 – Spaghetti Diagrams from simulations with alternative mixing models A) results from the ELCOM-SI model using the mixing model of Simanjuntak and Imberger (2006) and B)results from the ELCOM-L the model developed by Laval et al, 2002.

Appendix I:
Drifters in the Literature[1]

The use of particle tracking and field drifters to study water circulation is not new. Everyone who has ever thrown a stick into a river and watched it float downstream has realized (at least subconsciously) the potential for drifters to describe the transport properties of a water body. From this simple concept, entire industries and careers have been made. Researchers with interests in ocean outfall design, oil spill mitigation, aquatic species migration, and even climate change have all employed drifters and particle tracking technology in advancing their designs and theories. Even doctors have used models and chemical drifters to study arterial flow in advancing treatments for various diseases (Tambasco and Steinman, 2002).

This appendix strives to highlight the salient moments in the history of drifter development and modeling, as well as to distinguish the context into which this dissertation research fits. By no means is the following meant to be a complete discussion of drifter and particle tracking theory; to do so would require numerous volumes. For the sake of brevity, mention is given to the pioneering works within this field, while the discussion centers on the studies and developments from the late 1980's to the present time.

The following literature review is divided into related subsections, presenting particle-tracking methodologies before discussing previous drifter studies, drifter design, and drifter modeling.

Particle Tracking Methodology and Implementation

This section describes the evolution of numerical approaches to particle tracking within fluid flows described by an Eulerian model. The following discussion assumes the model is applied to describe fluid flow within a water body (lake, ocean, estuary, river, etc.), but is also suitable for describing atmospheric circulation or flows of particles within any type of fluid. Topics common to all particle tracking models are presented without citations, and citations are provided only for specific improvements or insights provided by each research project discussed.

Eulerian hydrodynamic models calculate velocities at a series of fixed points and times within the water body. Spatial interpolation from the Eulerian velocity field is needed to calculate the velocity at the location of a Lagrangian particle if the particle is not located at a point within the fluid where an Eulerian velocity is calculated. Temporal interpolation of the Lagrangian particle velocity is also needed even if the Eulerian velocity field is static; a Lagrangian particle moving within a heterogeneous static velocity field will experience different velocities over time as its position changes within the water body. Temporal interpolation is not needed in a static and homogeneous velocity field.

The accuracy of the spatial and temporal interpolation schemes directly affects the accuracy of the Lagrangian particle velocity and the particle's calculated trajectory through the water body. However, the interpolation accuracy must be appropriate for the complexity of the Eulerian velocity field as represented on the discretized representation of the water body. Inappropriate interpolation schemes will produce incorrect Lagrangian velocities and trajectories and will provide inaccurate insight into the physical transport mechanisms represented by the model.

While an in-depth discussion of the theory of numerical particle tracking as developed in this research is presented in §2, a brief review is needed here to put the evolution of particle tracking theory into context. A perfect Lagrangian particle will move in accord with the surrounding water, and its position given as:

[1] This appendix is an expansion of the discussion in §2.5.

$$\overrightarrow{x(t)} = \overrightarrow{x(t_0)} + \int_{t_0}^{t} \vec{u}\,dt \qquad (I.1)$$

where $\overrightarrow{x(t)}$ is the 3D position of the particle at time t, $\overrightarrow{x(t_0)}$ is the 3D position of the particle at some initial time, and $\vec{u}$ is the instantaneous 3D velocity vector of the water surrounding the particle. The velocity vector is continuous in time and potentially variable as a function of time and position of the particle. In an Eulerian velocity field, this continuous velocity vector is approximated by spatially and temporally discontinuous velocities defined at various locations within the water body. Therefore, a numerical Lagrangian particle-tracking model for use in an Eulerian velocity field must use a discrete form of Eq. (I.1), which may take the form of:

$$\vec{x}^{n+1} = \vec{x}^{n} + \vec{u}^{n+1/2}\Delta t \qquad (I.2)$$

where Δt is the time step from time n to time n+1, $\vec{x}^{n}$ and $\vec{x}^{n+1}$ are the positions of the particle at time n and n+1, respectively, and $\vec{u}^{n+1/2}$ is a velocity defined at the location of the particle over the discrete model time step. Eq. (I.2) is a simple forward Euler first-order method for creating Lagrangian particle trajectories. Other methods exist, and each method differs in its approach to considering the effect of spatial and temporal gradients within the modeled flow field.

The following discussion highlights three significant contributions to the development of numerical particle-tracking algorithms for use in hydrodynamic models. For clarity, each subsection heading is the citation for the work discussed, and all statements within a section (unless otherwise noted) refer to that citation.

Bennett and Clites (1987)

One of the first attempts to quantify and minimize interpolation errors in modeling particle trajectories was that of Bennett and Clites (1987). In order to predict oil spill movement within Lake Michigan, these researchers coupled their LPT scheme with the finite-difference Great Lakes spill model by Pickett (1981) and Schwabe et al (1984). Their numerical formulation incorporated the waterbody currents and direct effects of winds on particle movement, given as:

$$\frac{dx}{dt} = u(x,y,t) + au_a(x,y,t) \qquad (I.3)$$

$$\frac{dy}{dt} = v(x,y,t) + av_a(x,y,t) \qquad (I.4)$$

where the change in the particle's position (x,y) is a function of the waterbody currents (u,v) and the wind currents (u_a,v_a) at that position. The factor "a" is referred to as a "leeway" factor and determines the relative effect of the wind on the particle movement. The magnitude of the leeway factor is dependent upon the characteristics of the surface manifestation of the drifting "particle." This approach allowed them to distinguish between a "drifting life jacket and a drifting body," which was needed for studies of Lake Michigan. Under Eqs (I.3) and (I.4), the movement of a waterbody particle is calculated by setting "a" equal to zero.

One main concern addressed in their research was the prevention of particle beaching due to the stair-stepped grid approximation of the physical Lake Michigan shoreline. As such, they developed a 2nd-order Crank-Nicholson temporal interpolation scheme, coupled with a bilinear spatial interpolation scheme to transport the drifters. To test the accuracy of their numerical scheme, they used a rectilinear mesh applied to a circular basin and they defined velocities at the grid cell faces based on an exponential relationship involving the distance from the basin center. This velocity field forces particles to move in a circular orbit around the basin center (assuming the wind forcing is negligible). The error in their scheme was defined as the separation between a particle's initial position and its position after time T*, over which a particle that follows the perfectly circular trajectory completes one full orbit. In comparing results from the Crank-Nicholson scheme with those of the simpler forward

Euler 1st order schemes, they found that the second order time-stepping scheme reduces maximum separation error by nearly a factor of 10. The number of time steps required to obtain a separation error less than 10% of the basin radius was also reduced by half.

For testing their algorithm with both wind and water currents, they simulated drifter movement within Lake Michigan. The purpose of the simulations was to determine the effect of numerical grid size on the predicted drifter circulation patterns, not to match trajectories between field observed and modeled drifters. In numerical models differing only in the grid mesh size (10,5, and 2.5 km), the drifters each initially moved 1 km over the first day. However, the drifters simulated on the 10 km grid moved on a course approximately 45° from those on the 5 km and 2.5 km grids. After the first day, the drifter velocities diverged, with those on the 5 km and 2.5 km grid increasing to 2 times that of drifters on the 10km grid. Based on these results, Bennett and Clites (1987) concluded that variations in the hydrodynamic model setup were more influential on modeled drifter trajectories than on the spatial and temporal interpolation methods used within the Lagrangian particle tracking scheme. Their final conclusion was that the 14 km grids previously used in the Great Lakes Spill Model were insufficiently refined to capture the dynamics of the water body currents for particle-tracking purposes. Their study of modeled drifter trajectories led to the reduction in grid mesh size in future modeling efforts. This insight demonstrated the potential of Lagrangian particle tracking efforts to indicate model sensitivities and areas in which the model needs improvement.

Ramsden and Holloway (1991)

Ramsden and Holloway (1991) expanded upon Bennett and Clite's work by investigating the accuracy and computational speed of numerous temporal interpolation schemes for use in Lagrangian particle tracking. Their purpose was to determine the applicability of using Lagrangian particle tracking to estimate of water body diffusion and kinetic energy based on the statistical techniques developed by Freeland et al (1975) and Rossby et al (1983). By applying their particle tracking model to an analytically defined, static velocity field, they concluded that the 4th order Runga-Kutta scheme is superior to the forward Euler, Huen Predictor-Corrector, Robert Filtered Leapfrog, Adams-Bashforth, and Crank-Nicholson temporal interpolation schemes. This conclusion was not surprising given that the 4th order Runga-Kutta scheme was known to have a higher order of accuracy than the other schemes tested. One surprise from this work was that the Leapfrog method, which was (at the time of the publication) commonly used in integrating the Eulerian field equations within hydrodynamic models, was not suitable for modeling Lagrangian advection due to numerical stability concerns.

In considering Lagrangian particle tracking on temporally dynamic velocity fields, the principal contributor to error was found to be a lack of sufficient mesh resolution. Based on an analysis of vorticity balance as calculated with Lagrangian particle tracking on an analytical velocity field, they concluded that the choice of temporal interpolation scheme becomes irrelevant if the resolution of the Eulerian velocity dynamics is poor and the physics driving the water flows are not adequately represented. This conclusion was similar to that reached by Bennett and Clites (1987), yet all authors refrained from quantifying the mesh resolution required for a defined level of accuracy in particle tracking studies.

Yeung and Pope (1988)

Lagrangian statistics, including velocity autocorrelation functions and integral length scales, are of fundamental importance in quantifying and describing the characteristics of turbulent flows. Unfortunately, however, these statistics are also difficult to measure in laboratory experiments. This led Yeung and Pope (1988) to develop a particle tracking algorithm for extracting Lagrangian statistical quantities from simulated particle trajectories within any high-resolution velocity field. They used a direct numerical

simulation (DNS) model to generate statistically turbulent velocity fields from which they derived particle trajectories. These velocity fields were heterogeneous and contained temporal and spatial gradients. To accurately model trajectories within such fields, the resolution of the DNS model had to be sufficient to resolve the nonlinearly varying velocity field, and the spatial and temporal velocity interpolation techniques had to be of a high order of accuracy. Their first challenge was to develop and assess the relative adequacy of various spatial interpolation methods for use in precise particle tracking applications.

Yeung and Pope focused on improving spatial interpolation of velocities, arguing that errors due to inaccuracies in temporal interpolation were less important because of the generally greater spatial than temporal variability in turbulent flows. They employed a 2nd order Runga-Kutta temporal interpolation scheme because that scheme was incorporated into the numerical formulation of their DNS model. Increasing the accuracy of their particle tracking temporal interpolation to a 4th order scheme would have been fruitless because their model-generated temporal velocity field was of less accuracy. The use of a less accurate temporal interpolation method was also justified from their preliminary experiments, which indicated that spatial interpolation errors dominate solutions derived from coarsely resolved grids and less accurate interpolation schemes.

Each of the various spatial interpolation schemes considered by Yeung and Pope involved a weighted-averaging technique applied to the model-calculated velocities in the vicinity of the particle's position (Figure I1). The weights and contributing known velocities were determined based on the method of interpolation, with more accurate methods including more of the known velocities in the interpolation. They considered the linear interpolation scheme, a 3rd order Taylor series scheme, finite element interpolation functions, optimal schemes, and 4th order accurate cubic splines.

In assessing the accuracy of each method, they compared the interpolated values with those obtained by spectral (exact) interpolation, which provides highly

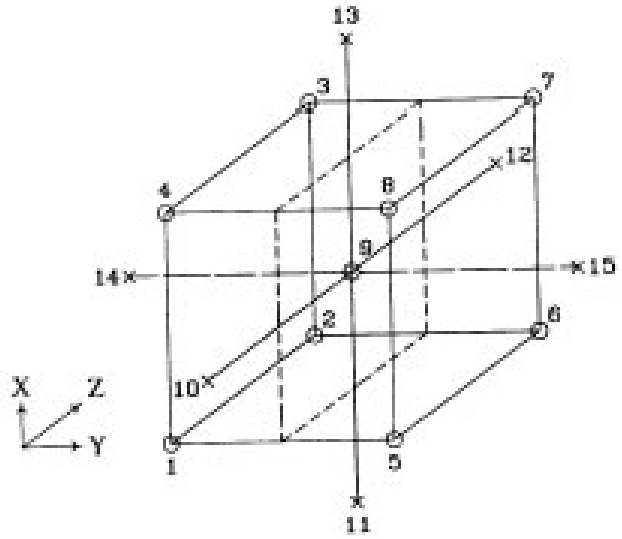

Figure I1 – Interpolation cell for particle tracking in a DNS model. Velocities are defined at the numbered nodes, and the particle is located within the volume bounded by nodes 1-8. (From Yeung and Pope, 1988)

accurate interpolated values but at prohibitively high computational costs. Interpolation methods were ranked based on their route-mean squared differences from the spectrally interpolated values, where the averaging occurred over an ensemble of particles located throughout the numerical grid. The interpolation schemes were also tested for accuracy on high-to-low resolution grids in order to assess the maximum grid size that permits acceptable levels of error in the particle tracking scheme.

From their series of numerical tests, Yeung and Pope concluded that cubic splines and a 13-point Taylor series expansion scheme provided superior interpolated velocities. Using these schemes, they were able to calculate Lagrangian statistics from both static and dynamic velocity fields. Their statistics agreed well with the classical turbulence theories described by Taylor (1921), which further supported their assertion that their particle tracking scheme was accurate. They also concluded that for accurate Lagrangian statistics, the model grid resolution must be sufficiently high so that the ratio of the smallest velocity scale in the flow (η) to the smallest scale resolved by the numerical grid ($1/\kappa_{max}$) is greater than unity (NOTE: κ_{max} is not as defined in Eq. (2.33)):

$$\kappa_{max}\eta \geq 1 \tag{I.5}$$

In summary, Yeung and Pope successfully used particle tracking to calculate characteristics of turbulent flows that are not easily measurable in the laboratory. In the process, they defined a model criterion for which particle tracking might be accurate and identified the most appropriate interpolation scheme for use in DNS models. One final conclusion they drew was that Eulerian velocity fields derived from Reynolds stress methods do not provide sufficient accuracy for calculating Lagrangian statistics.

While all of the conclusions made by Yeung and Pope were valid and useful in advancing the implementation of particle tracking into hydrodynamic models, they may not be applicable for modeling drifter movement within water bodies. DNS models produce highly accurate results for flows with low Reynold's numbers (Ferziger and Peric, 2002), and require a highly resolved numerical grid. In modeling circulation patterns in lakes and oceans where the water body dimensions are on the order of 10-100 km, highly resolved numerical grids are computationally impractical. Also, the flows in these water bodies have Reynold's numbers greater than the maximum Reynold's number limit for DNS applications (Ferziger and Peric, 2002).

The criterion given in Eq. (I.5) for determining the adequacy of the mesh resolution for particle tracking accuracy is not useful in hydrodynamic modeling of water body circulation unless some estimate of the smallest flow velocity scale (η) is made. Estimating the smallest velocity scales is often outside of the scope of water body hydrodynamic modeling, which focuses on general circulation patterns rather than on specific sub-grid scale velocity variations (Ferziger and Peric, 2002). The spatial extent of the modeled water bodies often precludes numerical resolution of the small-scale velocity fluctuations, due to the computational expense involved with increasing mesh resolution. As such, for waterbody modeling $1/\kappa_{max}$ is often considerably larger than any estimates for η which may be made, thereby making $\kappa_{max}\eta$ often less than unity. Therefore, based on Eqn.(I.5), particle tracking accuracy within models other than DNS is not sufficient for calculation of Lagrangian statistics. This conclusion is identical to that reached by Yeung and Pope, although they did not consider whether the tracking accuracy was sufficient for adequately describing the circulation patterns present in the modeled flow.

Given the stated accuracy limitations in the relatively low resolution mesh used in Reynold's stress-based hydrodynamic models, the use of highly accurate spatial interpolation schemes may not be warranted. For example, a cubic spline interpolation scheme involves at minimum 4 known velocities in the

direction of interpolation. These velocities are separated in space by three grid cells, which will limit the accuracy of the interpolation if the grid cell sizes are larger than the smallest velocity scales within the flow. With such a limited-resolution mesh, interpolation schemes involving fewer known velocities may more accurately represent the smaller-scale velocity gradients within the flow. This assertion is addressed in section 4, where less-accurate spatial interpolation schemes are evaluated for use in within a Reynold's stress based hydrodynamic model.

Drifter Use in Studying Water body Circulation

To date, drifters have been used in studying circulation in nearly every ocean basin. Their use in inland waterways and coastal areas is increasing as the technology involved in drifter design and drifter tracking steadily improves. This subsection provides a brief discussion of recent drifter studies in various water bodies, with emphasis given to the open ocean. Each of the studies discussed below used drifters to ascertain some characteristic of the circulation and current patterns within the subject water body. While many important studies are not addressed in this review, their citations are provided for reference purposes (Table I1).

Johnson et al (2004) used 14 profiling drifters to investigate the mean circulation and water properties of the Aleutian Basin in the Bering Sea. Their drifters were designed to follow the currents at 1000 dbar, and rise to the surface every ten days to transmit temperature and salinity profiles via satellite. The satellites fixed the drifters position while it was transmitting, thereby producing a time history of the drifter's location. Based on the drifter measurements, the researchers were able to resolve the northwestward flow of the deep Bering Slope Current, as well as cyclonic advection of warmer water from the southern part of the basin. This work provided insight into the

Table I1 Selected References for Drifter Studies in Various Water Bodies

Surface Ocean Studies:	Colin de Verdiere (1983)
	Poulain and Niiler (1989)
	Paduan and Niiler (1993)
	Sanderson (1995)
Deep Ocean Studies:	Freeland et al. (1975)
	Krauss and Bfoning (1987)
	Poulain et al (1996)
	Richez (1998)
Great Lakes Studies:	Csanady (1963)
	Murthy (1975)
	Murthy (1976)
	Sanderson and Okubo (1986)
	Palmer et al. (1987)
	Sanderson (1987)
	Muzzi and McCormick (1994)
	Okumura and Endoh (1995)
	Pal et al. (1998)
Channels Studies:	Dever et al. (1998)
Coastal Zone Studies:	List et al. (1990)
	Haynes and Barton (1991)
Lakes:	Manley et al, 1999
	Stocker and Imberger (2003)

transport mechanisms of salinity, temperature, and potentially nutrients within the Aleutian Basin.

Centurioni et al (2004) also used satellite-tracked drifters to study circulation, focusing on the influx of the Philippine Sea surface water into the South China Sea through the Luzon Strait. Based on 13 years of velocity data derived from surface drifters, they concluded that Philippine Sea water enters the South China sea only between October and January with a mean velocity of 0.7±0.4 m/s. Anomalies to the observed mean drifter circulation patterns were attributed to anticyclonic and cyclonic eddies west of the Luzon Strait. The anomalous drifter velocities were greater than expected for currents driven by the northeast monsoon, which lead Centurioni et al (2004) to suggest that a deeper westward current system was influencing circulation in the region. This region between the Philippine Sea, the South China Sea, Taiwan, and the Kuroshio Extension has been the subject of numerous other Lagrangian drifter studies, notably Niiler et al (2003), Tseng and Shen (2003), and Kim and Sugimoto (2002).

Smith et al (2003) used drifters to investigate the nutrient exchange between the Scotian Shelf waters and Georges Bank, and important North Atlantic fishing ground. Four of their drifters crossed into the Georges Bank area, indicating that the prevailing currents likely deliver nutrients and particles from the Scotian Shelf to the gadoid spawning grounds on the Georges Bank. The drifter data also lead Smith et al (2003) to estimate the depth of the nutrient-transporting currents, as well as the residence time for the Scotian Shelf waters within the Georges Bank region. The causes of the nutrient exchange were suggested to be mesoscale baroclinic features within the Scotian Shelf as well as possible offshore fronts related to the North Atlantic Oscillation index.

The North Atlantic Oscillation Index is also cited as a cause of the circulation patterns observed in the Nordic Seas, as reported by Jakobsen et al (2003). They used Lagrangian drifters to discern large-scale circulation patterns (gyres and interconnected jets), and concluded that the Nordic Sea circulation cells are tightly linked to bottom topography. They also found that instabilities within these current structures led to the stirring and mixing of Polar and Atlantic water masses.

In an attempt to model global sea levels, Niiler et al (2003) used surface velocity data derived from drifters in calculating a near surface momentum balance of the global ocean. With drifter velocity data, satellite altimetry (for calculating pressure gradients), and available wind data, they were able to compute a global sea level that agreed within uncertainties with that produced by a geostrophic, hydrostatic momentum balance

Drifter studies have also been conducted in direct support of biological analyses of the global ocean. Luschi et al (2003) used satellites to track the movement of sea turtles within the Indian Ocean, and compared their movement with currents derived from surface drifter data. They found that the turtles traveled within the currents, and therefore their long-term migratory patterns were linked to ocean circulation. Natunewicz et al (2001) used satellite-tracked drifters to follow the migration of blue crab larvae near the mouth of Delaware Bay, USA. They found that larvae within the coastal plume discharge from Delaware Bay traveled further southward than larvae in the water adjacent to the plume. They also found that the wind forcing on the larval transport became dominant when the river inflow to Delaware Bay diminished. Therefore from drifter movement, they were able determine the factors affecting the larvae transport, which then correlates to the survival rate of the blue crabs.

Aside from supporting biological studies and quantifying water body circulation, drifter studies have also been used to calculate and quantify turbulent statistics for water body flows. Zhang et al (2001) used

100 drifters in the Newfoundland Basin to calculate integral time and length scales for turbulent flow. They found that the turbulent scales observed with the drifter data agreed well with Taylor's dispersion theory (1921), and that isopycnal drifters are more accurate representations of Lagrangian particles than surface drifters. McClean et al (2002) compared Lagrangian statistics from drifter observations to those derived from model simulations of circulation in the North Atlantic. They found that the modeled statistics were in good agreement with the observed statistics when the model was run under simplified conditions (forced stability without eddy fluctuation modeling).

Addison (1997) used fractal statistics to simulate the "Lagrangian Memory" of drifter particles. The "Lagrangian Memory" concept states that a drifter's future trajectory is linked to the dynamics of the currents that transported the drifter to its current location (Yvergniaux and Chollet, 1989). This dependence on previous current characteristics allowed Addison to separate mean and turbulent flow velocities out of velocities implied by ocean drifter data and then use the turbulent flow velocities to calculate ocean dispersion coefficients. One conclusion to be drawn from this work is that accurate predictions of ocean drifter trajectories should include knowledge of the drifter's velocity at previous times and locations. This approach deviates from the use of the Runga-Kutta 4th order temporal interpolation scheme for drifter movement and attempts to incorporate the momentum and inertia of physical drifters in drifter trajectory simulation. These concepts form the basis for the GABI-F particle tracking method described in §2.4.

Despite the prevalent use of drifters in studying ocean circulation, only recently have drifters been used in determining the circulations in lakes, estuaries, and coastal zones. Due to the relative sizes of the water bodies being studied, the lake and estuarine drifters are often smaller and set at shallower depths than the ocean drifters. Researchers at the Centre for Water Research at The University of Western Australia have deployed surface drifters in their studies of Lake Kinneret (Israel), San Roque Reservoir (Argentina), Brownlee Reservoir (USA), Lake Burragorang (Australia), and Marmion Marine Park off the coast of Western Australia (Jörg Imberger – pers. comm.). With the exception of Lake Kinneret, results from these experiments have yet to be published. (Discussion of the Lake Kinneret experiment and results is given in section 6 and 8). American researchers have used drifters in studies of Lake Champlain (Manly et al, 1999).

Drifter Design & Technology Improvements

As introduced previously, a Lagrangian particle is a mass less water particle that passively advects with the water currents. A Lagrangian "drifter" (or "drifter" for this discussion) is a physical entity designed to approximate a Lagrangian particle. Tracking drifter motion with time provides direct evidence of the currents within the waterbody. Free-floating drifters may follow the 3-dimensional currents (Harcourt et al, 2002) or may be tethered to surface floats (Johnson et al, 2003) and follow only the horizontal currents at a given depth. As such, surface-tethered drifters cannot capture spreading induced by vertical shear and therefore are not able to describe the total fate of a diffusive substance (Peeters, 1994). Nevertheless, surface-tethered drifters are representative of diffusive substances when vertical shear dispersion is small compared to horizontal shear dispersion – a common condition in the well-mixed surface layer of the near-coastal zone (Alongi, 1998). Surface-tethered drifters are also advantageous when compared to free-floating drifters in that less detail (and expense) is involved in their design (D'Asaro et al 1996; Johnson et al 2003). This section presents the current state of drifter design and technology. For clarity, each subsection heading is the citation for the work discussed, and all statements within a section (unless otherwise noted) refer to that citation.

Poulain (1999)

In a field experiment from 1994 to 1996, Poulain (1999) used satellite tracked drifters to monitor circulation patterns within the Adriatic Sea. These drifters were designed in accordance with the designs put forth by Davis (1985), consisting of a 1-m-long negatively buoyant tube with four drag-producing vanes extending radially from the tube over its entire length (Figure I2). Floats attached to the top of each vane assured neutral buoyancy, and the satellite tracking signals were transmitted via a surface antennae. The drifter unit's light weight allowed for easy handling and deployment.

Data comparisons from drifters, fixed current meters, and dispersive dye studies suggested that the drifter velocities were accurate to within 3 cm/s relative to the water velocity. The drifter positions were fixed by measuring the Doppler frequency shift in signals emitted by the drifter and received by the Argos Data Collection and Location System (DCLS) carried by NOAA polar orbiting satellites. Positions were assumed accurate to within 200-300m, which was sufficient accuracy for quantifying the Adriatic Sea circulation. This level of accuracy, for both the drifter velocity and the position determination, represented the "industry standard" for the time of the study.

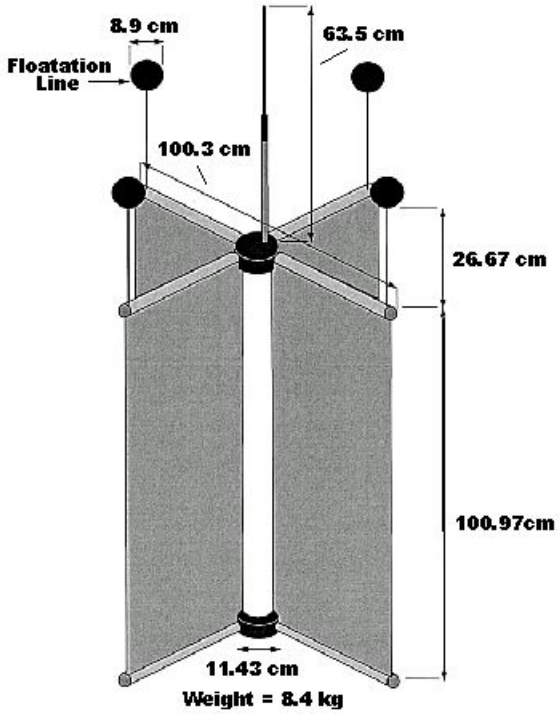

Figure I2 – Schematic diagram of drifters used in Poulain (1999). Modified for clarity.

D'Asaro et al (1996) and Harcourt et al. (2000)

In their 1996 publication, D'Asaro et al. describes a neutrally buoyant drifter designed to track the three-dimensional motion of water parcels in highly turbulent regions of the ocean. These drifters have high drag, a compressibility that nearly matches that of seawater, rapid (1 Hz) sampling, and short-range, high precision acoustic tracking (Figure I3). The relatively large drag screen (compared to the drifter hull) assures that the drifter has large rotational drag, which allows for accurate measurements of water column vorticity based on the spin rate of the drifter. Sensors on the drifter measure and record pressure, temperature, and direction of spin. Upon experiment termination, the drifter ascends to the surface by modifying its buoyancy. Once at the surface, their VHF radio beacon transmits a signal to the boat in charge of instrument retrieval.

The purpose of the work of D'Asaro et al (1996) was to document the abilities of the drifter and to estimate the degree to which it represents a "Lagrangian" particle in that it moves in exact accord with the surrounding fluid. Their analysis indicated that these drifters follow the motion of the surrounding water to better than 0.01 m/s, which is a 2 cm/s improvement on the drifters reported by Poulain (1999). The error between the drifter and water velocities was due to the net buoyancy of the float and its finite size. The drifter size prevented it from responding to velocity fluctuations at scales smaller than itself, and the slight difference in drifter buoyancy caused deviation of drifter and water particle motion. The drifter's buoyancy was controlled by making its

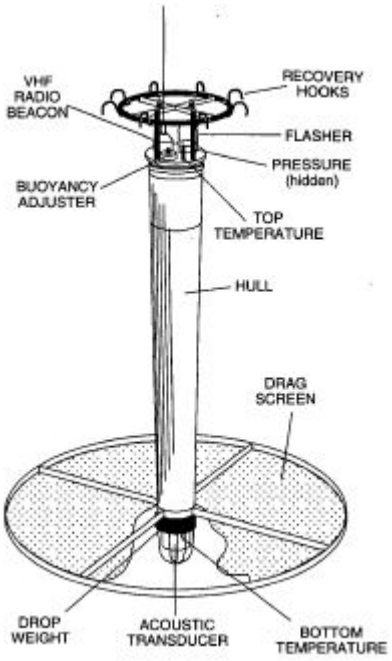

Figure I3 – Three-dimensional current following drifter design. Reproduced from Figure 1 of D'Asaro et al. (1996).

compressibility very close to that of seawater, by making its drag large, by reducing air pockets and bubbles on the drifter, and by carefully controlling variations in the float's mass and volume between deployments. Proper drifter ballasting was also needed for neutral buoyancy, and is determined through a "trial-and-error" type process when deploying the drifters.

Harcourt et al. (2000) used a variation of the D'Asaro et al. (1996) drifter design in their field/modeling experiment to measured convection in the Labrador Sea. Their drifter was designed to remain at a depth of 2 km, and the drifter's horizontal position was tracked with the low-frequency acoustic (RAFOS) tracking system described by Rossby et al. (1986). While their experiment was successful at capturing vertical water velocities and convection, they found that maintaining neutral buoyancy of the drifter was difficult. This difficulty was due in part to chemical reactions between the drifter hull and the surrounding seawater, which caused the overall drifter mass to change over the course of the drifter deployment. Based on this change in mass, Harcourt et al. (2000) estimated that the drifters maintained an average vertical velocity of 7 mm/s, which was corrected during the post-processing of the drifter data.

Implicit in D'Asaro et al. (1996) and Harcourt et al. (2000) is that technical skill is needed in creating and deploying accurate three-dimensional current following drifters. The 0.01 m/s error in velocity measured with these drifters may represent a 10-20% error in velocity (see section 5 for velocities calculated in Marmion Marine Park, Australia) and could also lead to a separation between the drifter and water particle of up to 864 m over a one day deployment. This separation may not be significant for large-scale oceanic studies of circulation, but it may be too large for using Lagrangian particle tracking for hydrodynamic model verification. The effort put into creating such an accurate "Lagrangian" drifter may therefore not be necessary if the purpose of the drifter experiment is to test a hydrodynamic model.

Johnson et al (2003)

The drifters described in Johnson et al (2003) were designed for use in the shallow surf zones and coastal embayments of the world's oceans (Figure I4). The drifters were designed to be compact, of minimal cost, easy to deploy, and to use "off the shelf" GPS receivers in tracking their position. Unlike the drifters of D'Asaro et al (1996), these drifters designed to be within the manufacturing capabilities of most research groups, and to cost less than US$750 per unit.

As shown in Figure I4, slightly different designs were employed for drifters used in different water body types. All drifters consisted of a cylindrical canister that housed the GPS recorder, battery, and data logger. This canister was attached to a series of cone shaped stabilizers (for the surf zone drifters) or to a cross-sail design drogue (for the coastal embayment drifters).

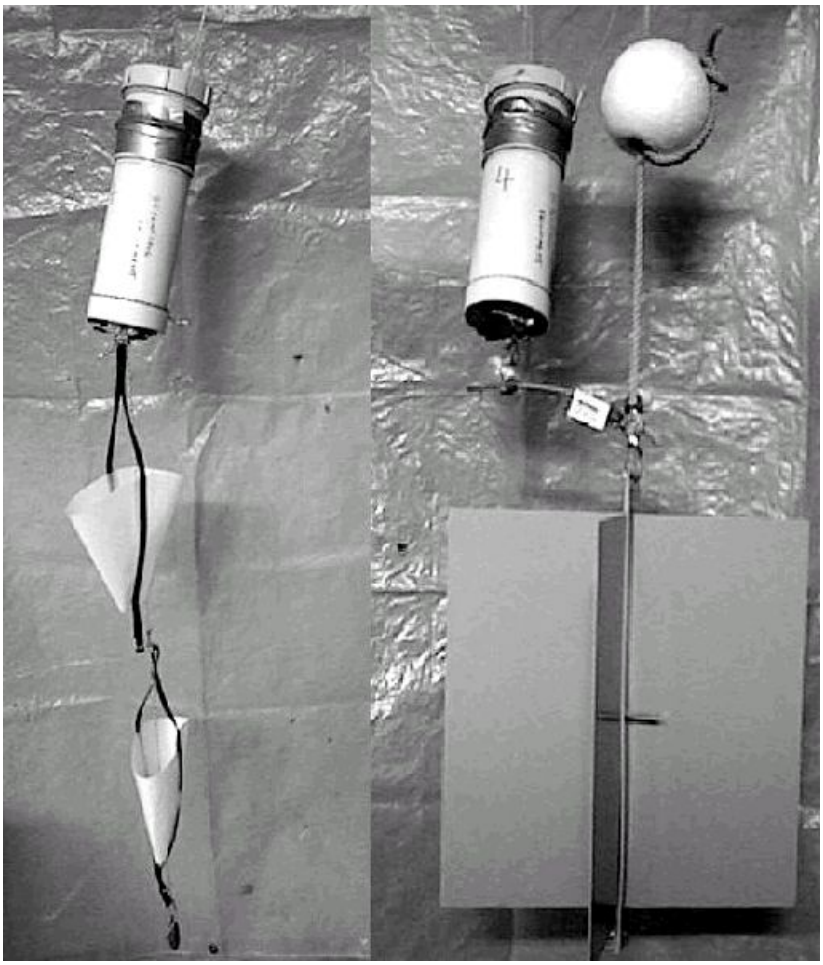

Figure I4 – GPS-tracked drifters for use in the surf zone (left) and coastal embayments (right). From Johnson et al. (2003)

Neutral buoyancy was achieved through the addition of synthetic floats. The authors recognized that these drifters were "*quasi-Lagrangian*" in that they would not behave exactly like water particles due to their finite size, wind slippage, and drag on the tether. They hoped, however, that the ease of use and low cost of the drifters would make up for the lack of accuracy in the measured trajectory.

Positional accuracy of the Johnson et al (2003) drifters was greatly improved over those used by Poulian (1999), due to the world-wide removal of Selective Availability (SA) on GPS signals in 2000. This removal increased horizontal accuracy from 300 m to less than 10 m for non-differentially corrected GPS signals, thereby decreasing the scales of motion that could be resolved with drifters. The removal of SA from GPS signals essentially allowed for accurate GPS tracking of drifters within water bodies with larger spatial velocity gradients than the open ocean.

Trajectories from the drifters described by Johnson et al (2003) were successfully used to estimate dispersion within the surface layer of Lake Kinneret, Israel (Stocker and Imberger, 2003). The simple drifters developed by Johnson et al. (2003) have also

proven for useful for researchers at The University of Western Australia, who have deployed similar surface drifters in their studies of San Roque Reservoir in Argentina, Brownlee Reservoir in the USA, and Lake Burragorang in Australia (J. Imberger – pers. comm.).

Applications of LPT in Field & Modeling Experiments

Many particle tracking algorithms are being used in modeling circulation within fluids. While some published research involves drawing conclusions without validation of the LPT results with field drifter data, attempts have been made at comparing modeled and observed drifter trajectories. Studies which included verification of the simulated Lagrangian trajectories stressed the accuracy of the modeling techniques, whereas studies without verification focused on the implications of the simulated trajectories. This section provides a brief discussion of examples of the studies using LPT modeling without field drifter data and details studies in which model and field data comparisons were made. For clarity, each subsection heading is the citation for the work discussed, and all statements within a section (unless otherwise noted) refer to that citation.

Recent examples of drifter modeling without field drifter validation focus on assessing water circulation in relatively large water bodies with nearly constant environmental forcing conditions. For example, Chen et al (2003) used bi-linear spatial interpolation in combination with a fourth-order Runga-Kutta (RK4) time interpolation technique to transport particles in a numerical model of the North Atlantic Ocean near Georges Bank. They used particle tracking to determine water exchange pathways across the spring density front and also to discover how these pathways might influence the exchange of nutrients and biological productivity. Fuentes and Marinone (1999) used a bilinear spatial interpolation scheme in conjunction with a 2nd order Runga-Kutta temporal interpolation scheme to predict circulation within the Gulf of California. They focused on the effect of differing wind forcing on the predicted circulation and used the modeled drifters to demonstrate this circulation difference.

A second order Runga-Kutta scheme in combination with linear interpolation of velocities in space was used by Garraffo et al (2001) to study North Atlantic drifter movement as predicted by the MICOM oceanic model. In that study, a comparison between field and numerical drifter trajectories was made, while recognizing such comparisons are difficult due to errors in field drifter location reports, model forcing, numerical discretization, and turbulence modeling. Lagrangian velocity integral time scales from their field and numerical drifters showed "reasonable agreement." Garraffo et al (2001) assumed (but did not show) that their drifter transport scheme was not a significant source of error relative to the other model errors.

Nairn and Kawase (1991) deployed drifters in Puget Sound in order to assess the predictability of the estuarine currents with a derivative of the Princeton Ocean Model (POM). They compared Lagrangian velocities interpolated from their modeled Eulerian velocity field with the velocities observed with the field drifters. Modeled drifter speeds were consistently less than the observed velocities, and no apparent biases were observed in the direction of the drifter modeling. They attributed some of the discrepancy between modeled and observed data to the omission of tidal harmonics in the model forcing conditions, and did not specify their interpolation methods in generating modeled Lagrangian velocities. Also, they did not attempt to match field and modeled drifter trajectories, and as such did not require temporal interpolation. The conclusion from this work was that comparing field and modeled drifters is useful for a more detailed characterization of the water body currents than is provided through the deployment of a limited number of stationary current meters.

Simpson and Gobat (1994)

In developing their maximum cross-correlation (MCC) method for deriving velocities from satellite imagery, Simpson and Gobat (1994) compared modeled Lagrangian velocities with those from field drifter measurements. They modeled the Lagrangian velocities with a Runga-Kutta 4th order scheme applied to the velocity field generated from their MCC analysis. The "good overall" agreement between field drifter and numerical drifter trajectories indicated that the MCC technique was able to correctly interpret velocities from the satellite data. This work demonstrates the potential for using modeled and field Lagrangian drifters to support results and conclusions derived from different instruments or techniques. The study's authors came to the following conclusion regarding the usefulness of modeling drifters:

> "The technique of simulating drifters may prove useful in calibrating the pattern and search tile sizes used in computing velocities from satellite data with the MCC methods. Furthermore, simulated drifters could provide an inexpensive supplement and/or alternative to *in situ* data in cases were funding or other considerations preclude *in situ* data collection." (Simpson and Gobat, 1994)

While this potential is certainly warranted, Simpson and Gobat (1994) did not qualify their conclusion with a discussion on the sensitivity of drifter modeling to small-scale variations in the velocity field. They modeled drifters over 300-500 hours with 0.5-1.0 hour time steps. Therefore a drifter moving at 5 cm/s (typical slow speeds in the coastal ocean) would travel 90-180 meters over a single timestep and 54 – 90 kilometers over the model duration. Consistent deviations of 1° and 1 cm/s between the field drifter and modeled drifter velocities would then produce separation distances of nearly 18 meters and 2.4 kilometers over a single timestep and the model duration, respectively. Clearly only general comparisons between modeled and observed drifter trajectories may be made at these scales of separation, unless the simulated drifter velocities are interpolated accurately.

Simpson and Gobat (1994) did not include spatial interpolation between the locations of MCC-derived water velocities and the locations of the simulated drifters. Spatial interpolation was not necessary because of the spatial averaging within the MCC method, which produces a generalized velocity value that is then attributed to an area of the waterbody surface. Spatial interpolation is also not as crucial in drifter modeling in oceanic environments where horizontal velocity gradients are generally weak and currents are driven by large-scale (O(100km)) size eddies (Poulain, 1999). As implied by Yeung and Pope (1991) accurate spatial interpolation of simulated velocities is important if Lagrangian trajectories are to be used for describing characteristics of the waterbody currents. This also implies that accurate spatial interpolation is not crucial if less accurate simulated Lagrangian trajectories are suitable for the purposes of the analysis.

Carey and Shen (1995)

In modeling fluid mixing between parallel oscillating plates, Carey and Shen (1994) incorporated particle tracking with a Heun Predictor-Corrector technique into a finite element model. Using 30,000 numerical drifter particles, they assessed mixing by tracking particle movement over time steps of 0.06 seconds and calculating particle spatial densities over time (Figure I5). To assess their model's validity, they compared their results with previously published laboratory mixing experiments from Ottino (1989).

Carey and Shen's model results showed remarkable agreement between the mixing simulation and the laboratory study, indicating that the numerical mixing and transport models were accurate. They also reported similar results when modeling with a 0.3 second and 3.3second timestep, and found that significant accumulated integration error occurred after 3000 seconds were modeled (Carey and Shen, 1995). Mesh size/resolution was not reported in this work, and it was not considered as a variable against which to test

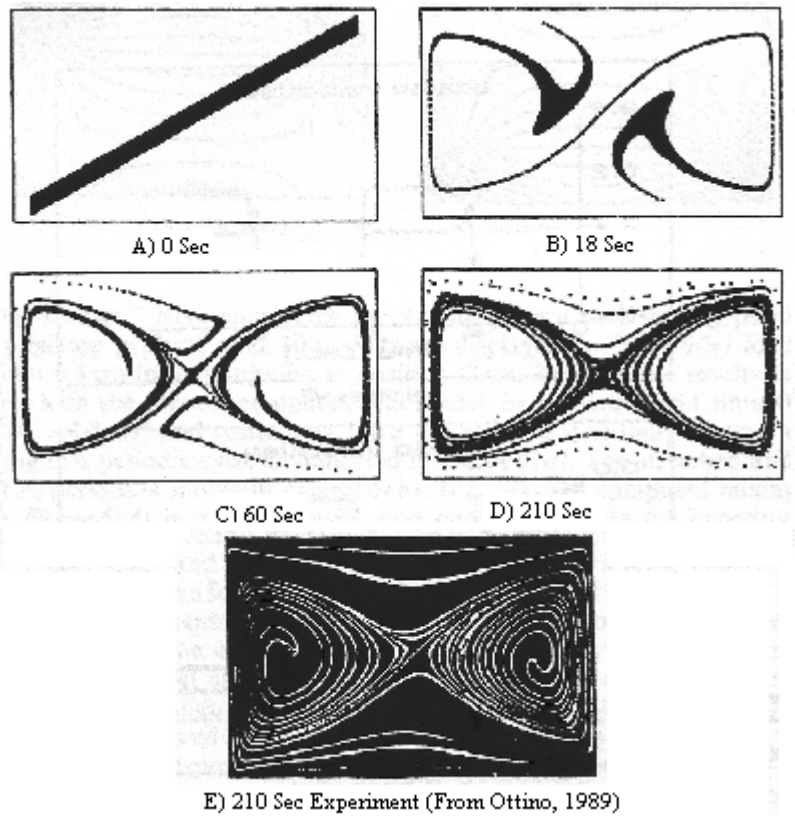

Figure I5 – LPT Simulation of mixing from Carey and Shen (1995). Figure modified for clarity only. Sections A-D are numerical mixing experiments; Section E is a laboratory experiment from Ottino (1989).

the accuracy of the mixing or particle tracking model. The final conclusion from this work was that highly-accurate numerical modeling using particle tracking is preferable to laboratory mixing experiments because a greater number of mixing scenarios may be analyzed during the same time period. This increase in temporal efficiency in conducting experiments extends researchers the greater possibility of determining the optimal mixing frequency based on numerous (and repeatable) simulations (Carey and Shen, 1995).

Harcourt et al (2000)

Another attempt at modeling the movement of field drifters was conducted by Harcourt et al (2000), in which they used 3D Lagrangian floats to assess deep water convection in the Labrador Sea. They compared the field measurements from the floats to "measurements" made by numerical floats embedded into a 3D Large Eddy Simulation (LES) model of the same waterbody. The focus of this work was on the vertical distribution kinetic energy, heating, and acceleration rates, and emphasis was not given to horizontal advection.

In their modeling of Lagrangian drifters, Harcourt et al (2000) eliminated the need for spatial interpolation by assigning the drifter a velocity equal to the volume-averaged velocity of the LES mesh element containing the drifter. The Adams-Bashforth method of temporal interpolation was used because it was incorporated into the solution procedure for the LES model. The vertical velocity of the drifter was obtained through the application of a force balance similar in approach to that developed in section 2.5. Comparisons

between modeled and observed drifter measurements were favorable, providing the authors with confidence that their LES model was able to correctly simulate deep-water convection. The authors prefaced their conclusions, however, with this statement regarding the difficulty of such comparisons:

> "Comparing LES time-averaged Eulerian statistics with the ensemble-averaged modeled drifter measurements can elucidate the response of drifters to convection. But comparing real drifters to model drifters embedded in the LES simultaneously compares both the response of real versus modeled drifters and the dynamics of real versus modeled convection. Consequently, statistically significant differences between observed and modeled quantities derived from drifter time series may arise from several distinct sources: 1) the suitability of the computational problem posed in the LES model as a representation of convection in the Labrador Sea, 2) the suitability of the drifter model as a representation of the float response to ambient conditions, 3) the numerical accuracy of the LES and embedded model drifters in simulating the given physical problem, and 4) uncertainty pertaining to the field experiment due to incomplete knowledge of environmental conditions and equipment characteristics" (Harcourt et al, 2000)

The above statement reiterates the concepts discussed by Garraffo et al (2001), and highlights the potential difficulties associated with drifter modeling. However it also implies that accurate drifter modeling requires accurate hydrodynamic models. Therefore by obtaining agreement between field-observed and numerically modeled drifter measurements, the hydrodynamic model is necessarily accurate.

Summary

Drifter use in determining circulation patterns is perhaps the most basic, and first considered, method for assessing the transport and mixing properties of currents. In studies ranging from sewage outfall plumes in the coastal ocean, to large scale mixing within ocean basins, to transport in lakes and estuaries, drifter data has often been collected and analyzed. Advancements in drifter design and GPS technology have caused increases in the accuracy of field drifter measurements. Similar advancements in computing and numerical simulation have recently allowed researchers to simulate the movement of Lagrangian particles and thereby create the potential for merging knowledge gained from Lagrangian observations with that from Lagrangian simulation. However, modeling of Lagrangian particles is still in its relative infancy, and improvements to both hydrodynamic models and Lagrangian particle tracking techniques are needed.

As stated repeatedly in this literature review, Lagrangian particle tracking is difficult due to the uncertainties in model boundary conditions, numerical methods, and field data. The ultimate goal of those interested in Lagrangian particle tracking is the reduction of these uncertainties so that credible engineering results are obtained. The research presented in the remaining sections strives to reduce errors in existing Lagrangian particle tracking theory, first by developing a new, GABI-F particle tracking technique. This new technique builds upon the ideas of "Lagrangian memory" suggested by Addison et al (1997), as well as the force balance approach discussed by Harcourt et al (2000) and the concept behind the use of leeway factors in Bennett and Clites (1987) and Thompson et al (2004). The GABI-F method also incorporates aspects of the existing particle tracking techniques discussed in this section and reflects the "*quasi-Lagrangian*" nature of field drifters (Johnson et al, 2003). The second innovation presented in this work is the development of a new methodology for determining model skill at predicting drifter trajectories. This methodology improves upon the used of field-model drifter displacement and spaghetti diagrams as analysis tools, and strives to quantify model skill.

Validation of the GABI-F technique and analysis methodology is provided by comparing modeled and

field observed drifter trajectories from Marmion Marine Park, Australia. Aside from validating the new techniques, this case study points out potential errors within the numerical model and field experiment setup, which may then be planned for and eliminated in future field and modeling experiments. In this way, the results of this research will hopefully provide continued insight to other researchers in this developing field.

Appendix J:

Lake Kinneret Surface Drifters and Model Particle Tracking[2]

Abstract

Horizontal circulation within the surface layer of Lake Kinneret was modeled using a 3D hydrodynamic model (ELCOM) in conjunction with a numerical particle tracking algorithm. Differences in circulation predicted by changing model spatial and temporal resolution, wind forcing, and spin-up time were assessed. Comparisons of field and modeled drifter trajectories demonstrate model sensitivity to small changes in model setup and the difficulty in obtaining good agreement. Integration of numerical error when using a coarse model grid and time step appears to dominate the prediction of particle tracks, an effect compounded by uncertainties in spatial gradients of wind forcing.

Introduction

This paper compares field-observed and modeled surface layer drifter tracks in Lake Kinneret, Israel. The primary objective of this research was to assess the ability of the ELCOM hydrodynamic model and a coupled particle tracking model to reproduce the tracks of observed field drifters. Secondary objectives were to estimate the model sensitivity to uncertainties in boundary conditions (wind forcing), domain discretization (temporal and spatial), and model spin-up time.

ELCOM (Estuary and Lake COmputer Model, created by researchers at the Centre for Water Research at the University of Western Australia) is a three-dimensional hydrodynamic model for lakes, reservoirs, and estuaries. ELCOM solves the unsteady 3D-Reynolds-averaged Navier-Stokes equations using a semi-implicit method with quadratic Euler-Lagrange discretizations (Hodges et al., 2000). The free-surface evolution is governed by vertical integration of the continuity equation for incompressible flow in the water column applied to the kinematic boundary condition (e.g., Kowalik and Murty, 1993). The fundamental numerical scheme is adapted from the TRIM approach of Casulli and Cheng (1992) with modifications for scalar conservation, numerical diffusion, and implementation of a mixed-layer turbulence closure.

Lake Kinneret (Israel, 32°50' N, 35°35' E) has an elliptical shape, and extends 20 km in length by 10km in width (Figure J1). The lake is highly temperature stratified during the summer months, and is forced by a daily westerly sea breeze (Assouline and Mahrer, 1996). This periodic forcing produces basin-scale

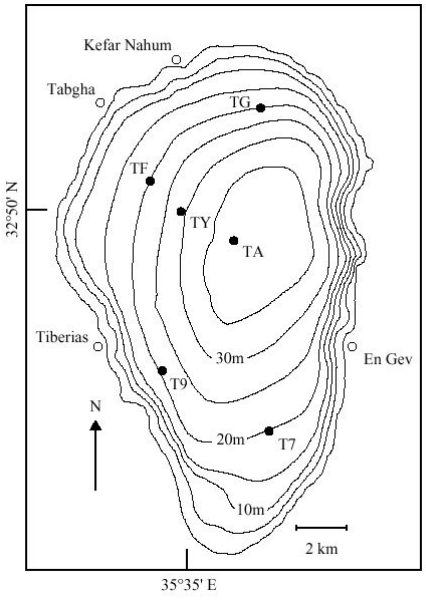

FIG. J1 – Bathymetric Map of Lake Kinneret, showing locations of wind measurement stations (From Stocker and Imberger, 2003 – with permission)

[2] Note: this text was presented at the 17th ASCE Engineering Mechanics Conference, June 13-16, 2004 at the University of Delaware, Newark, DE. under the authorship of Jordan E. Furnans, Ben R. Hodges, and Jörg Imberger. It is presented here to provide a more accessible reference.

internal seiches dominated by a vertical mode 1, 24-h-period Kelvin wave and by 12-and 20-h Poincaré waves with vertical modes 1 and 2 (Laval et al, 2003; Antenucci et al, 2000).

Field studies of the lake suggest that the mean surface circulation is counter-clockwise when winds are greater than 3-4 m/s, regardless of the wind direction (Serruya, 1975). Ou and Bennet's (1979) analytical and numerical modeling of the lake dynamics suggested that this mean cyclonic surface-layer circulation could be explained as a residual Kelvin-wave circulation associated with a uniform wind. More recent studies using a coupled atmospheric and hydrodynamic model (Pan et al., 2002) show that the curl of the wind stress accounts for the depth averaged vorticity in the surface layer, implying the mean surface circulation is directly forced and requires knowledge of spatial wind gradients to accurately model. Laval et al. (2003) reinforced this latter conclusion while studying the effects of wind spatial and temporal variations on the lake internal wave field. Laval et al. (2003) used model results of isotherm displacement and the surface vorticity balance to conclude: 1) spatially varying wind forcing is required to predict the dynamic density field observed in the lake; and 2) results could be improved with a more accurate representation of the spatial wind distribution. Stocker and Imberger (2003) used surface drifters to quantify the surface circulation, and found the surface currents are highly dynamic, changing from clockwise in May 2001 to predominantly counter-clockwise in June 2001.

The present work attempts to use the previously validated ELCOM model of Lake Kinneret to model surface drifters introduced by Stocker and Imberger in the June 20-23, 2001 drifter experiment. The drifters are modeled with trajectories derived from semi-Lagrangian[3] particle tracking (Furnans et al, 2004; Furnans, 2004). Comparisons between the modeled and observed drifter trajectories provide insight into the difficulty of matching field and model results given the uncertainties in spatial wind patterns and time integration of model error. The latter leads to dramatic divergence of drifter paths as a function of model spatial and temporal discretization..

Methodology

Following Laval et al. (2003), Lake Kinneret was discretized with a 400-m resolution in the horizontal and 1 m in the vertical direction. During the simulation period (June 20-23,2001) the inflow from the Jordan River was negligible and the impact of the outflow was approximated as well-diffused so the lake was considered closed with only meteorological forcing acting on the surface. No-slip boundaries conditions were used for horizontal bottom boundaries and free-slip boundary conditions were used for vertical land boundaries. Stress at the free surface due to wind was modeled as a momentum source distributed vertically over the surface wind mixed layer (Hodges et al., 2000). The bottom drag coefficient was 3×10^{-3}, appropriate for a mud/sand bottom (Soulsby 1983).

The model was run for a variety of wind and discretization conditions outlined in Table J1. The base wind field was Run2_VW from Laval et al. (2003), which provides a temporally and spatially-varying wind field obtained through bilinear interpolation from eight wind stations. To test the sensitivity of the results to a small change in the wind field, run #2 applied a 1 degree increase in the wind direction, which is within the accuracy range of the Lake Diagnostic (LDS) systems used in measuring the lake wind field (J. Imberger, pers. comm., 2004). Model runs incorporating spin-up times of 24 hr and 96 hr were conducted to examine the model sensitivity to initial conditions. The 24 hr spin-up is equivalent to the forcing period of the dominant mode-1 internal Kelvin wave within the lake (Hodges et al, 2000; Laval

[3] The "semi-Lagrangian" drifter model referred to herein is equivalent to the GABI-F model presented in this technical report.

TABLE J1. Field and Numerical Drifter Comparisons

Run	Wind Field	Discretization	Timestep	Spin-up Time
#1	Run2_VW	400m	450s	24 hrs
#2	Run2_VW+1°	400m	450s	24 hrs
#3	Run2_VW	400m	450s	96 hrs
#4	Run2_VW	400m	225s	24 hrs
#5	Run2_VW	400m	45s	24 hrs
#6	Run2_VW	200m	45s	24 hrs
#7	Run2_VW	100m	45s	24 hrs

et al, 2003), while the 96 hr suggested by Imberger (pers. comm. 2004) is based on recent unpublished studies.

Simulations using the base wind field and the 24 hr spin-up were run at three model time steps (run #3, 4 and 5) to examine the model sensitivity to time step refinement. Using a fine time step and three horizontal grid resolutions (run #5, 6 and 7) provides a basis for analyzing the sensitivity to spatial discretization.

Results and Discussion

Over the 3-day simulation, the modeled drifters in runs #1 and #2 traveled approximately 1/3 of the distance traveled by the field drifters (Figure J2). Each modeled drifter from run #1 (Figure J2a) had a trajectory with the same general characteristics of the field drifters for the first day. Errors in both drifter position and modeled velocity accumulate with time, causing a divergence in the field and modeled trajectories. Comparing the two panels of Figure J2, it can be seen that a small change in the wind direction (+1° in Fig. 2b) causes changes of 0.5-4.0 km in the drifter position at the end of the simulations.

The importance of model timestep is evident in Figure J3, which shows trajectories from model runs #3, 4 and 5, differing in only their timestep. Over smaller time steps, numerical drifter displacements will

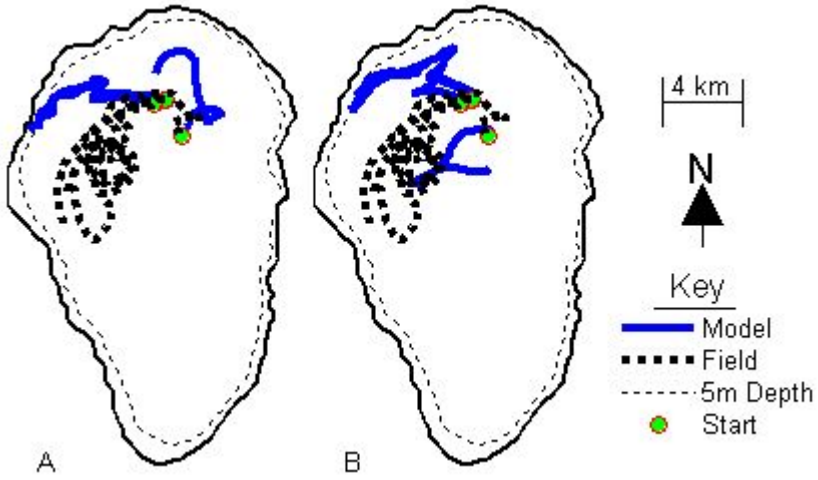

FIG. J2 – Field & Lagrangian trajectories derived from modeling with 1° difference in wind fields a) run #1, b) run #2. Field and modeled trajectories are shown as dashed are solid lines, respectively.

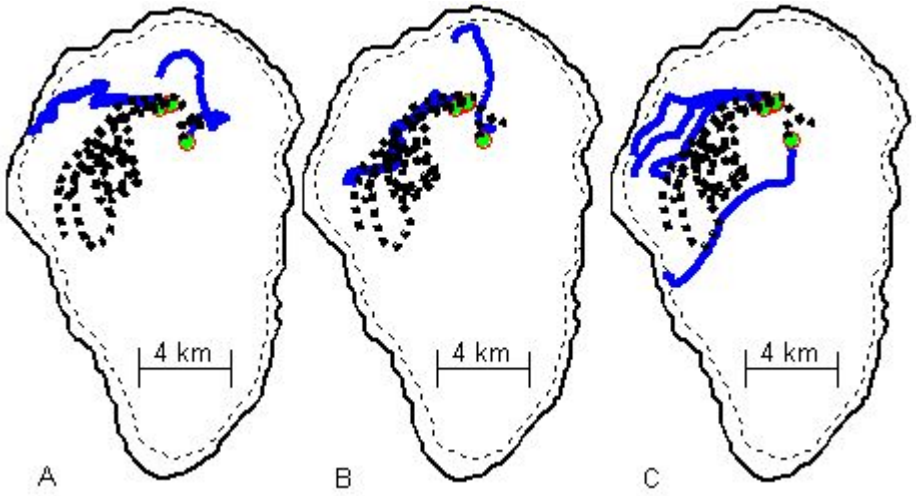

FIG. J3 –Modeled Lagrangian trajectories under differing model timesteps. a) 450s (run #1), b) 225s (run #4), and c) 45s (run #5). Symbols as in FIG. 2.

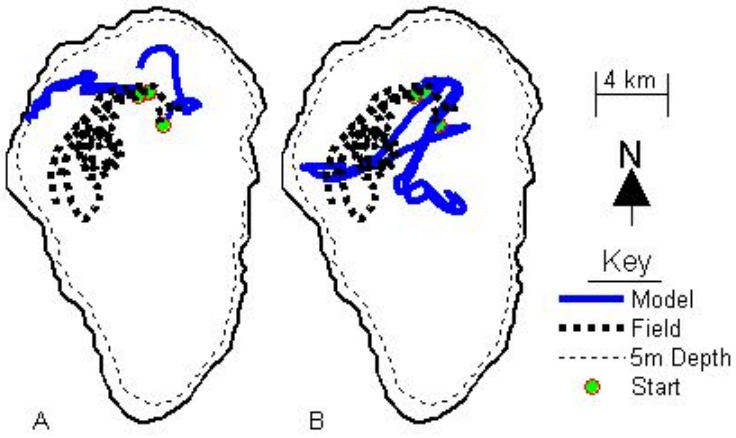

FIG. J4 – Field & Lagrangian trajectories derived from modeling with different spin-up times, a) run #1, b) run #3. Field and modeled trajectories are shown as dashed are solid lines, respectively.

be proportionately smaller, and the temporal integration error associated with drifter movement is reduced. When modeled with a 450s timestep (Run #1, Figure 3a), three drifters traveled west, whereas these same drifters traveled more to the southwest at the smaller timesteps (Runs #4 & #5, Figure J3B,C). The movement of the drifter initially located closer to the lake center shows a reversal of direction when modeled at the three different time steps, from a northward course at 450s and 225s to a southward course at 45s. This variation indicates divergence in the velocity field in the center of the lake, at horizontal scales approximated by the drifter displacement over a single 225 second time step (approximately 10-15m).

The impact of initial conditions on modeled drifters is demonstrated in comparing the results from runs #1 and #3, which differ in the amount of time allotted to model spin-up (Figure J4). The spin-up time is the time required for sufficient energy from environmental forcings to enter the mathematical representation of the lake, and for the lake to achieve a

relatively stable circulation and internal wave oscillation pattern. Unfortunately, data for the spatial distribution of wind prior to the drifter experiment of Stocker and Imberger (2003) is not available; thus in run #3, the extra 3-days spin-up time consisted of repeating the first three days of wind data used in model run #1. While the details of this wind field are unlikely to exactly replicate the actual wind, the reliability and repeating characteristics of the Lake Kinneret summer sea breeze are well documented (Stocker and Imberger, 2003), so the large scale forcings of the actual wind should be reasonably represented. From Figure 4, it is clear that the spin-up time has a significant impact on the predicted drifter paths; the 96-hr spin-up time provided velocities up to twice those with a 24 hr spin up, and modeled trajectories were closer to the center of lake.

The modeled trajectories are also sensitive to the model grid resolution (Figure J5) while the time step is held small (45 s). Reducing numerical grid size theoretically increases the agreement between the modeled and field drifter trajectories (Ramsden and Holloway, 1991), however this did not occur. The changes seen as the grid is refined may have several possible sources, which require further investigation. Firstly, it is possible that the flow fields at 200 m and 100 m are still too coarsely refined to capture the spatial scales of the surface layer eddies that are affecting field drifter position. However, given the field drifters show path oscillations on the order of 1-2 km, it would seem that the both these grid scales should be sufficient. A second possibility is that the reduction of error in the particle tracking spatial interpolation, combined with the finer representation of the velocity field at smaller grid resolutions, leads to model drifters being routed into significantly different eddy structures. A third possibility is that the changes in imposed wind field associated with interpolation to the finer grid scale leads to development of different eddy structures in the surface layer. Finally, it is possible that initial conditions (i.e., the surface velocity field after spin-up) are the principle cause of the divergence. Numerical dissipation is reduced on the finer grids, which may affect the necessary spin-up time to obtain a good representation of drifter tracks.

Conclusions

This research examines the sensitivity of a 3D hydrodynamic model with coupled particle tracking for reproducing field drifter trajectories in the surface layer of Lake Kinneret. This task is inherently difficult as errors in particle position lead to errors in future particle velocities, so that the total error will accumulate with time. The ELCOM model, used

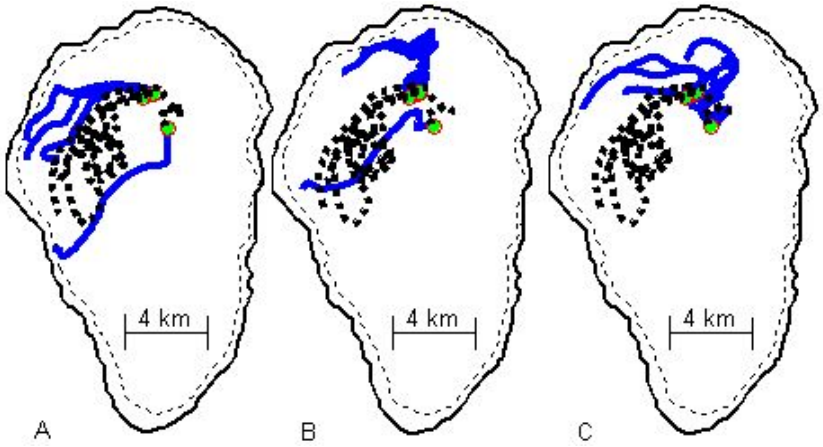

FIG. J5 –Modeled Lagrangian trajectories under differing horizontal domain discretizations. a) 400m (run #5), b) 200m (run #6), and c) 100m (run #7). Symbols as in FIG. 4.

herein, has previously been shown to model the motion of internal waves within the lake (Laval et al, 2003, Hodges et al., 2000). However, this paper shows that the surface currents predicted under identical modeling conditions did not agree with the currents suggested by field drifters. The sensitivity of the surface currents to variations in wind forcing, spin-up time, model timestep, and grid resolution suggest that accurate modeling of drifter trajectories requires a highly resolved grid and precise knowledge of the spatial and temporal characteristics of the wind field. Even with such data, it appears that there is likely a short temporal horizon over which model drifters can reasonably predict the field drifter location. Given the variations in predicted surface circulation patterns from each of the model runs, it is clear that comparing field and modeled trajectories may be used as a qualitative rather than qualitative check of model accuracy.

Acknowledgments

The authors would like to acknowledge researchers at the Centre for Water Research at the University of Western Australia for their assistance in developing the Lake Kinneret models. Specific thanks are given to Roman Stocker and Jason Antenucci who (in part) provided the field data and impetus for this project. Funding for this project was provided by the Australian-American Fulbright Association as well as the Texas Water Research Institute.

References

Addison PS. (1996) “A method for modeling dispersion dynamics in coastal waters using fractional Brownian motion”. IAHR Journal of Hydraulic Research 1996; 34: 549–561.

Aldrige, J.N,. Kershaw, P., Brown, J., McCubbin, D., Leonard, K.S., Young, E.F. (2003) “Transport of plutonium (239/240Pu) and caesium (137Cs) in the Irish Sea: comparison between observations and results from sediment and contaminant transport modeling.” Continental Shelf Research. 23, 869-899. Elsevier Science Ltd.

Alongi, D.M. (1998) “Coastal Ecosystem Processes” CRC Press

Amorocho, J., and DeVries, J.J. (1980) “A New evaluation of the wind stress coefficient over water surfaces” Journal of Geophysical Research. 85, 433-442.

Antenucci, J. P., Imberger, J., and Saggio, A., (2000). “Seasonal evolution of the basin-scale internal wave field in a large, stratified lake. Limnology and Oceanography. 45. 1621-1638.

Arakawa and V. Lamb. Computational design of the basic dynamical processes of the ucla general circulation model. In Methods in Computational Physics, volume 17, pages 174-267. Academic Press, 1977.

Assouline, S., and Mahrer, Y., (1996) “Spatial and temporal variability in microclimate and evaporation over Lake Kinneret: Experimental evaluation. Journal of Applied Meteorology. 35: 1076-1084.

Batchelor, G.K., (1952) “Diffusion in a field of homogeneous turbulence II: The Relative motion of particles”, Proc. Cambridge Philos. Soc. 48, 345-362.

Bennett, John. R., and Clites, Anne Hutchinson. (1987). “Accuracy of Trajectory Calculation in a Finite-Difference Circulation Model”. Journal of Computational Physics 68, 272-282.

Bergeson, L. (2001) “One Hot Issue: TMDL Litigation”., Pollution Engineering. February/March 2001.

Borsuk, M.E., Stow, C.A., and Reckhow, K.H., (2003). “An Integrated approach to TMDL development for the Neuse River estuary using a Bayesian probability network model (Neu-BERN).” Journal of Water Resources Planning and Management. 129, 283-294.

Borsuk, M., Stow, C., and Reckhow, K., (2004)“Confounding Effect of Flow on Estuarine Response to Nitrogen Loading” Journal of Enivronmental Engineering., Vol. 130., No. 6 June 1.ASCE

Bowen, J.D., (2003) “ A CE-Qual-W2 Model of the Neuse Estuary for TMDL development” Journal of Water Resources Planning and Management Vol 129, No 4. July

Caissie, D., Satish, M., El-Jabi, N. (2005) “Predicting river water temperatures using the equilibrium temperature concept with application on Miramichi River catchments (new Brunswick, Canada)” Hydrological Processes 19 (11) 2137-2159.

Carey, G., and Shen, Y. (1995) “Simulation of fluid mixing using least0squares finite elements and particle tracing” International Journal for Numerical Methods in Heat and Fluid Flow. Volume 5, 549-573.

Casulli, V., and Cheng, R.T., (1992) “Semi-implicit finite difference methods for three-dimensional shallow water flow.” International Journal for Numerical Methods in Fluids, 15(6), 629-648

Chen, Changsheng, Xu, Qichun, Beardsley, Robert C., Franks, Peter J.S.,(2003) “Model study of the cross-frontal water exchange on Georges Bank: A three-dimensional Lagrangian experiment.” Journal of Geophysical Research, vol 108, No. C5.

Colin De Verdiere, A. (1983) “Lagrangian eddy statistics from surface drifters in the eastern North Atlantic”. Journal of Marine Research. V. 41, 375-398

Csanady, G.T. (1963) "Turbulent diffusion in Lake Huron", *Journal of Fluid Mechanics*. 17, 360-384.

CWR#1, 2003 – LDS User's Guide – Centre for Water Research, The University of Western Australia.

D'Asaro, E.A., Farmer, D.M., Osse, J.T., and Dairiki, G.T. (1996) "A Lagrangian Float." Journal of Atmospheric and Oceanic Technology. 13, 1230-1246.

Deng, Q., and Fang, G. (2001) "Numerical visualization of mass and heat transport for conjugate natural convection/heat conduction by streamline and heatline". International Journal of Heat and Mass Transfer 45 2373-2385.

Dever, E.P., Hendershott, M.C., and Winant, C.D. (1998) tatistical aspects of the surface drifter observations of circulation in the Santa Barbara Channel" Journal of Geophysical Research 103, 24781-24797.

Fischer, H.B., List, E.J., Koh, R.C.Y, Imberger, J., and Brooks, N.H., (1979) "Mixing in inland and coastal waters" Academic Press

Franke R., and Nielsen, G.M. (1980), "Scattered data interpolation of large sets of scattered data." International Journal of Numerical Methods in Engineering, 15, 1691-1704.

Freeland, H., Rhines, P., and Rossby, T. (1975) "Statistical observations of the trajectories of neutrally buoyant floats in the North Atlantic. Journal of Marine Research. V. 33m 383-404.

Fuentes O., Marinone S. (1999) "A numerical Study of the Lagrangian Circulation in the Gulf of California" Journal of Marine Systems 22, 1-12.

Garraffo, Zulema D., Mariano, Arthur J., Griffa, Annalisa, Veneziani, Carmela, Chassignet, Eric P. (2001). "Lagrangian data in a high-resolution numerical simulation of the North Atlantic. 1. Comparison with in situ drifter data"., Journal of Marine Systems, 29 pg 157-176.

Godfrey, J.S., Ridgway, K.R., (1985) "The large scale environment of the poleward-flowing Leeuwin Current, Western Australia: Longshore steric height gradients, wind stresses, and geostrophic flow. Journal of Physical Oceanography, 15, 481-495.

Harcourt, Ramsey R., Steffen, Elizabeth L., Garwood, Roland W., D'Asaro, Eric A., (2002)"Fully Lagrangian Floats in Labrador Sea Deep Convection: Comparison of Numerical and Experimental results." Journal of Physical Oceanography 32, pg 493-510.

Havens, K.E., and Walker, WW. (2002) "Development of a total phosphorous concentration goal in the TMDL process for Lake Okeechobee, Florida (USA)." Lake and Reservoir Management. 19 (3) 227-238.

Haynes, R., and Barton, E.D., (1991) "Lagrangian observations in the Iberian coastal transition zone" Journal of Geophysical Research 96, 14731-14741

Hillmer, I, and Imberger, J (2005) "Influence of advection on time and space scales of ecological variables in a coastal equilibrium flow" (Submitted)

Hodges, B.R. (1998), Heat Budget and *Thermodynamics at a Free Surface: Some Theory and Numerical Implementation.* Centre for Water Research, University of Western Australia, Technical Report ED1300BH, 14 pgs.

Hodges, B. R. (2000). "Numerical techniques in CWR-ELCOM". Technical report, Centre for Water Research, University of Western Australia, Nedlands, Western Australia, 6907. Reference WP 1422-BH.

Hodges, B.R., Imberger, J., Saggio, A., Winters, K., (2000). "Modeling basin-scale internal waves in a stratified lake." Limnol. Oceanogr. 45: 1603-1620.

Hodges, B.R., Imberger, J. (2001). "Simple Curvilinear Method for Numerical Methods of Open Channels". Journal of Hydraulic Engineering. Vol 127, No. 11.

Hodgkin, E.P., and DiLollo, V. (1958) "The tides of south-western Australia". Journal of the Royal Society of Western Australia, 41, 42-54.

Holt, JT, Allen, JI, Proctor, R, Gilbert, F. "Error Quantification of a high-resolution coupled hydrodynamic-ecosystem coastal ocean model: Part 1 model overview and assessment of the hydrodynamics." Journal of Marine Systems 57 (1-2): 167-188. AUG 2005.

Hughes, C.E., Aierey, P.L., Duran, E.B., Miller, B.M., Sombrito, E., (2004) "Using Radiotracer techniques for coastal hydrodynamic model evaluation" Journal of Environmental Radioactivity. 76 195-206. Elsevier Science Ltd

Jiang, D., Liu, H., Wang, W. (2001) "Test a modified surface wind interpolation scheme for complex terrain in a stable atmosphere". Atmospheric Environment 35, 4877-4885. Elsevier Science, Ltd.

Johnson, Billy H., Kim, Keu W, Heath, Ronald E., Hsieh, Bernard B., and Butler, H. Lee (1993). "Validation of Three-Dimensional Hydrodynamic Model of Chesapeake Bay." Journal of Hydraulic Engineering. V. 119, no. 1. pg 2-20.

Johnson, D., Stocker, R., Head, R., Imberger, J., and Pattiaratchi, C. (2003) "A compact, low-cost gps drifter for use in the Oceanic Nearshore Zone, Lakes, and Estuaries". Journal of Atmospheric and Oceanic Technologies (Submitted).

Klein, P., and Hua, B.L. (1990) "The mesosacale variability of the sea surface temperature: an analytical and numerical model". *Journal of Marine Research*. 48, 729-763.

Kowalik, Z., and Murty, T. S. (1993). Numerical modeling of ocean dynamics. World Scientific.

Krauss, W. and Boning, C.W. (1987) "Lagrangian properties of eddy fields in the Northern Atlantic as deduced from satellite tracked buoys. Journal of Marine Research., V 45, 249-291.

Kundu, P, and Cohen, I., (2002) Fluid Mechanics, 2nd edition.

Lacorata, G, Aurell, E., Vulpiani, A.(2001) "Drifter Dispersion in the Adriatic Sea: Lagrangian data and chaotic model" Annales Geophysicae 19: 121-129.

Laval B, Imberger, J., Hodges, B.R., and Stocker, R., (2003) "Modeling circulation in lakes: Spatial and temporal variations", Limnol. Oceanogr. 48(3) 983-994.

Lawrence, G.A., Ashley, K.I., Yonemitsu, N, and Ellis, J.R. (1995) "Natural dispersion in a small lake". *Limnol. Oceanogr.* 40. 1519-1526.

Lee, J., and Neville-Jones,P. (1987) "Initial Dilution of horizontal jet in crossflow". Journal of Hydraulic Engineering/ V. 109, No. 2. 199-219.

Lewis, E. (1988) Principles of Naval Architecture. The Society of Naval Architects and Marine Engineers.

List, E.J., Gartrell, G. and Winant, C.D. (1990) "Diffusion and dispersion in coastal waters." Journal of Hydraulic Engineering 11, 1158-1179.

Lord, D.A, and Hillman, K. (eds.) (1995). Perth Coastal Waters Study – Summary Report. Water Authority of Western Australia.

Mankin, K.R., Wang, S.H., Koeliker, JK, Huggins, DG., and deNoyelles, F.,(2003) "Watershed-lake water quality modeling: Verification and application". Journals of Soil and Water Conservation 58 (4): 188-197. Jul-AuG.

Manley, T.O., K. Hunkins, J. Saylor, G. Miller and P. Manley.(1999) "Aspects of summertime and wintertime hydrodynamics of Lake Champlain". Water Resources Monograph No. 14, American Geophysical Union, pp. 67-115

Marti, C., and Imberger, J. (2004) "Connectivity provided by residual circulation in a stratified lake: Lake Kinneret, Israel". Centre for Water Research Reference ED 1617-CM. In press.

Murthy, C.R. (1975) "Dispersion of floatables in lake currents" Journal of Physical Oceanography., 5 193-195.

Murthy, C.R (1976) "Horizontal diffusion characteristics in Lake Ontario" Journal of Physical Oceanography. 6, 76-84.

Muzzi, R.W., and McCormick, M. (1994) "A new glopal positioning system drifter buoy". Journal of Great Lakes Research. 3, 1-4

Nairn, B., Kawase, M. (2001) "Comparison of Observed Circulation Patterns and Numerical Model Predictions in Puget Sound, WA." Proceedings of Puget Sound Research 2001 (http://www.psat.wa.gov on 11/5/2005).

Okubo, A. (1971) "Oceanic diffusion diagrams" Deep Sea Research. 18, 789-802.

Okumura, Y, and Endoh, S. (1995) "Telemetry Lagrangian measurements of water movement in lake using GPS and MCA." Trans. Soc. Instrument and Control Eng. 31, 1324-1328

Okubo, A., and Ebbesmeyer, C.C. (1976) "Determination of vorticity, divergence and deformation rates from analysis of drogue observations" Deep Sea Research 23, 345-352.

Ou, H.W., and Bennett, J.R., (1979) "A theory of the mean flow driven by long internal wavers in a rotating basin, with application to Lake Kinneret" Journal of Physical Oceanography. 9. 1112-1125.

Paduan, J.D., and Niiler, P.P. (1993) "Structure of velocity and temperature in the Northeast Pacific as measured with Lagrangian drifters in Fall 1987", Journal of Physical Oceanography 23, 585-600.

Pal, K.P., Murthy, R., and Thomson, R.E. (1998) "Lagrangian measurements in Lake Ontario" Journal of Great Lakes Research. 24, 681-697

Palmer, M.D., Jarvis, R., and Thompson, L. (1987) "Drogue cluster and dye-dispersion measurements" Canadian Journal of Civil Engineering 14. 320-326

Pan, H., Avissar, R., and Haidvogel, D.B., (2002). "Summer circulation and temperature structure of Lake Kinneret" Journal of Physical Oceanogrphy 32, 295-313.

Paldor, N, Dvorkin, Y., Mariano, A., Ozgokmen, T., Ryan, E. (2004) "A practical, hybrid model for predicting the trajectories of near-surface ocean drifters" Journal of Atmospheric and Oceanic Technology. Volume 21.

Pickett, P.J., 1997 "Pollutant Loading Capacity for the Black River, Chehalis River System, Washington". Journal fo the American Water Resources Association. 33 (2). 465-480. April.

Poulain, P.-M., and Niiler, P.P.(1989), "Statistical analysis of the surface circulation in the California current system using satellite tracked-drifters.", Journal of Physical Oceanography, 19, 1588-1603

Poulain, P.-M., Warn-Varnas,A., and Niiler, P.P.(1996), "Near-surface circulation of the Nordic seas as measured by Lagrangian drifters", J. Geophysical Research., 101(C8), 18237-18258

Poulain, P (1999) "Drifter observations of surface circulation in the Adriatic Sea between December 1994 and March 1996" Journal of Marine Systems 20, 231-253.

Provenzale, A. (1999) "Transport by coherent barotropic vortices". *Annu. Rev. Fluid Mech. 31, 55-93.*

Ramsden, Dave., Holloway, Greg. (1991) "Timestepping Lagrangian Particles in Two Dimensional Eulerian Flow Fields", Journal of Computational Physics 95. 101-119

Richez, C. (1998) "The West Spitzbergen Current as seen by SOFAR floats during the ARCTEMIZ 88 Experiment: Statistics, differential kinematic properties, and potential vorticity balance." Journal of Geophysical Research 103, 15539-15565.

Roberts, P., Snyder, W., and Baumgartner, D. (1989) "Ocean outfalls I: Submerged waterfield formation" Journal of Hydraulic Engineering, Vol. 115, No. 1, 1-25.

Roulund, A., Sumer, B, Fredsoe, J., Michelson, J. (2005) "Numerical and experimental investigation of flow and scour around a circular pile" Journal of Fluid Mechanics 534, 351-401.

Sahin, I., Crane, J., Watson, K. (1993) "Added mass coefficients for submerged bodies by a low-order panel method". AIAA 31st Aerospace Sciences Meeting and Exhibit, Reno NV, Jan 11-14. 9 pages.

Sanderson, B.G., & Okubo, A. (1986) "An analytical calculation of two dimensional dispersion. J. Oceanogr. Soc. Japan. 42 139-153.

Sanderson, B.G., (1987) "An analysis of Lagrangian kinematics in Lake Erie." Journal of Great Lakes Research. 13, 559-567

Sanderson, B.G. (1995) Structure of an eddy measured with drifters" Journal of Geophysical Research 100, 6761-6776

Serruya, S. (1975) "Wind, water temperature and motions in Lake Kinneret: general pattern." Verh. Internat. Verein. Limnol. 42, 139-153.

Shepard, D. (1968) A Two-dimensional function for irregularly spaced data. In Proc. ACM Nat. Conf., Pages 517--524, 1968

Siddorn, J.R., Allen, J.I., and Uncles, R.J. (2003) "Heat, Salt and Tracer Transport in the Plymouth Sound Coastal region: a 3-D modeling study". J. Mar. Biol. Ass. UK. 83, 673-682.

Simanjuntak, A, Imberger, J (2006) – Ongoing research at the Centre for Water Research at the University of Western Australia. Publications pending.

Simpson, J.J., and J.I. Gobat, 1994: Robust velocity estimates, stream

functions and simulated Lagrangian drifters from sequential spacecraft data.

IEEE Trans. on Geosci. Rem. Sens., 32: 479-493.

Smith R.L., Huyer, A., Godfrey, J.S., Church, J.A., (1991). The Leeuwin Current off Western Australia. Journal of Physical Oceanography, 14, 623-628.

Stacey, M.T., Cowen, E. A., Powell, T.M., Dobbins, E., Monismith, S.G., and Koseff, J.R. (2000). "Plume dispersion in a stratified, near-coastal flow: measurements and modeling" Continental Shelf Research. 20, 637-663.

Stocker , R., and Imberger, J. (2003) "Horizontal transport and dispersion in the surface layer of a medium-sized lake" Limnology and Oceanography 48 (3), 971-982.

Stow, A.C., Roessler, C., Borsuk, M., Bowen, J., and Reckhow, K., (2003). "Comparison of Estuarine Water Quality Models for Total Maximum Daily Load Development in Neuse River Estuary." Journal of Water Resources Planning and Management. 129, No. 4. ASCE.

Su, Y. (1991) Model for Transport of Floating Debris in the Ocean. Ph.D. Dissertation, The University of Texas at Austin.

Tambasco, M., Steinman, D. (2002)"On Assessing the Quality of Particle Tracking through Computational Fluid Dynamic Models" Journal of Biomechanical Engineering Vol 124. 166-175.

Thompson, K., Sheng, J, Smith, P, Cong, L (2003) "Prediction of surface currents and drifter trajectories on the inner Scotian Shelf" Journal of Geophysical Research, Vol. 108. No C9, 3287.

Thompson, R.O.R.Y., (1984). "Observations of the Leeuwin Current off Western Australia" Journal of Physical Oceanography, 14, 623-628.

Thorpe, S., Heywood, K., Stevens, D., Brandon, M. (2004) "Tracking passinve drifters in a high resolution ocean model: implications for interannual variability of larval krill transport to South Georgia" Deep Sea Research I 52, 909-920.

Toner, M., Kirwan Jr., A., Kantha, L, Choi, J. (2001) "Can general circulation models be assessed and their output enhanced with drifter data?" Journal of Geophysical Research, Vol. 106. No C9. 19,563-19579.

Truesdell, C. (1954) The Kinematics of Vorticity. Indiana University Press.

Umgiesser, G., and Zampato, L. (2001) "Hydrodynamic and salinity modeling of the Venice channel network with coupled 1D-2D mathematical models" Ecological Modelling 138, 75-85.

US EPA #1 – 10/22/05 CERCLA-02-2003-2027, www.epa.gov/hudson/

Wang, P.F. (2001) "Dispersion resulting from aggregating hydrodynamic properties in water quality modeling". International Journal of Engineering Science 39, 95-112

Willgoose, G., (1997) "A hydrodynamic particle tracking algorithm for simulating settling of sediment" Mathematics and Computers in Simulation 43., 343-349.

Wool, T., Davie, S., and Rodriguez, H. (2003) "Development of Three-Dimensional Hydrodynamic and Water Quality Models to Support Total Maximum Daily Load Decision Process for the Neuse River Estuary, North Carolina". Journal of Water Resources Planning and Management. Vol 129, No. 4. ASCE.

Yeung, P.K., and Pope, S.B., (1988) "An Algorithm for Tracking Fluid Particles in Numerical Simulations of Homogeneous Turbulence," Journal of Computational Physics vol. 79, 373-416.

Yvergniaux, P, Chollet, J. (1989) "Particle Trajectories modeling based on a Lagrangian memory effect" XXIIIth IAHR Conference – Hydraulics and the Environment. Ottawa, Canada 21-25 August.

Zaker, N., Imberger, J., and Pattiaratchi, C.,(2001) "Dispersion of an effluent plume in a shallow coastal area". Journal of Marine Environmental Engineering. Vol. 6, 83-108.

Zaker, N., Imberger, J., and Pattiaratchi, C.,(2002) "Numerical Simulation of the Coastal Boundary Layer off Perth, Western Australia". Journal of Coastal Research. Vol. 18, n. 3 470-485.

Zhenquan, Li., "A mass conservative streamline tracking method for two dimensional CFD velocity fields." Journal of Flow Visualization and Image Processing., v 9, n 1, 2002. 75-87.

Zhurbas, V., and I.S. Oh, (2003) "Lateral diffusivity and Lagrangian scales in the Pacific Ocean as derived from drifter data. Journal of Geophysical Research, 108(C5) 3141.